Tailoring Covalent Organic Frameworks as Efficient Heterogeneous Catalysts for Electrochemical Ammonia Generation

विद्या वाचस्पति की
उपाधि की अपेक्षाओं की आंशिक पूर्ति में प्रस्तुत शोध प्रबंध

A thesis submitted in partial fulfillment of the requirements of the degree of Doctor of Philosophy

द्वारा / By
प्रगल्भ शेखर / Pragalbh Shekhar

पंजीकरण सं. / Registration No.:20183596

शोध प्रबंध पर्यवेक्षक / Thesis Supervisor: Prof. R. Vaidhyanathan

भारतीय विज्ञान शिक्षा एवं अनुसंधान संस्थान पुणे
INDIAN INSTITUTE OF SCIENCE EDUCATION AND RESEARCH PUNE

2024

Dedicated to
My parent and family members

Certified that the work incorporated in the thesis entitled "***Tailoring Covalent Organic Frameworks as Efficient Heterogeneous Catalysts for Electrochemical Ammonia Generation***" submitted by **Mr. Pragalbh Shekhar** carried out by the candidate at the Indian Institute of Science Education and Research (IISER), Pune, under my supervision. The work presented here or any part of it has not been included in any other thesis submitted previously for the award of any degree or diploma from any other University or Institution.

Date: 15 August 2024

Dr. R. Vaidhyanathan
(Research Supervisor)
Professor, IISER-Pune
Pune-411008, India

Name of Student: Pragalbh Shekhar

Reg. No.: 20183596

Thesis Supervisor(s): Prof. R. Vaidhyanathan

Department: Chemistry

Date of joining program: 01/08/2018

Date of Pre-Synopsis Seminar: 17/01/2024

Title of Thesis: ***Tailoring Covalent Organic Frameworks as Efficient Heterogeneous Catalysts for Electrochemical Ammonia Generation***

I declare that this written submission represents my idea in my own words and where others' ideas have been included; I have adequately cited and referenced the original sources. I declare that I have acknowledged collaborative work and discussions wherever such work has been included. I also declare that I have adhered to all principles of academic honesty and integrity and have not misrepresented or fabricated or falsified any idea/data/fact/source in my submission. I understand that violation of the above will be cause for disciplinary action by the Institute and can also evoke penal action from the sources which have thus not been properly cited or from whom proper permission has not been taken when needed.

The work reported in this thesis is the original work done by me under the guidance of ***Prof. R. Vaidhyanathan***

Date: 16/08/2024 ***Pragalbh Shekhar***

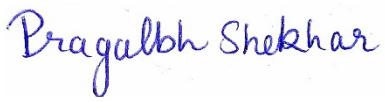

First and foremost, I wish to express my deepest gratitude to my research supervisor, Prof. R. Vaidhyanathan, for his unwavering encouragement and guidance over the last five years. His mentorship has been invaluable, especially in helping me understand the intricacies of scientific project design and execution in a structured and thoughtful manner. His dedication and passion for research have deeply inspired me, and I am truly thankful for all I have learned from him. I would also like to extend my sincere thanks to the Indian Institute of Science Education and Research (IISER), Pune, and our former director, Prof. Jayant B. Udgaonkar, for providing state-of-the-art research facilities, financial support, and a vibrant research atmosphere. I am equally thankful to our current director, Prof. Sunil S. Bhagwat, for seamlessly continuing this tradition of excellence. I am deeply grateful to my Research Advisory Committee (RAC) members, Prof. R. Nandini Devi (NCL Pune) and Dr. Muhammed Musthafa (IISER Pune), whose invaluable suggestions greatly shaped my projects during my PhD journey. I also appreciate the collaborative insights provided by Dr. Vinod C. Prabhakaran (NCL Pune). A special thanks to Prof. Shigeyuki Masaoka (Osaka University), Prof. Mio Kondo (Tokyo Tech), and Dr. Kento Kosugi (Tokyo Tech) for inviting me to collaborate at Osaka University, which was a transformative experience. I would also like to extend my gratitude to all the faculty members at IISER Pune, especially Prof. Nirmalya Ballav (Chair of Chemistry), for their continuous support. I owe a special thank you to my lab mates—Shyamapada, Shalini, Dinesh, Debanjan, Rahul, Sattwick, Rinku, Himan, Deepak, Piyush, Liya, Chitvan, and Augustas—for their constant help and camaraderie. I also acknowledge the former group project fellows—Chandana, Aleena, Ankit, Deep, Reshma, Akshara, and Yashraj—for their contributions and support during my PhD. I would also like to express my heartfelt thanks to my B.Sc. and M.Sc. teachers, with special mentions to Prof. Ram Dulare Ram and Prof. Vinay Sanguri, for imparting knowledge and life lessons, both academic and beyond. To my friends, both at IISER and beyond— Umashakar, Pranjal, Ajad, Amrit, Rishu, Vikas, Aman, Manjeet, Kamesh, Ravi, Prajjwal, Dhruv, Darshan, Akanksha, Habib, Souvik, Sanchayita, Ardhra, and others—thank you for your friendship and support. My gratitude also extends to my school, college, and master's friends—Mukesh, Aman, Rajesh, Sushil, Satis, Anjani, Ashish, and Anuj—who have been a part of this journey. I must acknowledge Dr. Umeshareddy Kacherki (Deputy Librarian), along with Shivashankar, Anuradha, and the entire library staff, for their invaluable

assistance. My appreciation also goes to the instrumental operators—Mr. Parveen Nasa, Mr. Sandeep, Mr. Ravinder, Mr. Nilesh Dumbre, Ms. Swati, Mr. Anil, Mr. Mahesh, Mr. Yatish, Mr. Nitin, Mrs. Megha, and many more—for their technical support. I am deeply thankful to the IISER Pune non-teaching staff, particularly Mr. Mayuresh, Mr. Tushar, Ms. Vrushali, Mr. Prabhas, Mr. Ranjan, and Mrs. Sayalee, for their continuous assistance over the years. Finally, I owe everything to my family. My heartfelt gratitude goes to my parents and elder brother and sister for their unwavering belief in me and their unconditional support throughout my academic journey. I also extend my thanks to other family members for their continued encouragement. Additionally, I am grateful to the American Chemical Society (ACS), the Royal Society of Chemistry (RSC), and John Wiley & Sons (Wiley-VCH) for publishing several of my research articles produced during my PhD at IISER Pune. I am extremely thankful to CSIR for the fellowship that made this work possible.

Pragalbh Shekhar

Chapter 1: Introduction to Ammonia Production, Covalent Organic Frameworks (COFs), and Electrochemical Ammonia Production

Ammonia (NH_3) plays a pivotal role in modern industry, primarily as a key component in agricultural fertilizers. Its synthesis, predominantly achieved through the Haber-Bosch process, is critical to meeting global food production needs. However, this conventional method requires high operational temperatures (400-500°C) and pressures (15-25 MPa), making it both energy-intensive and a significant contributor to greenhouse gas emissions. To mitigate the environmental impact of traditional ammonia synthesis, there is increasing interest in alternative methods that leverage renewable energy sources. Electrochemical ammonia production offers a promising solution by directly converting nitrogen (N_2) into ammonia (NH_3) through the nitrogen reduction reaction (NRR). This process operates under milder conditions compared to the Haber-Bosch process, potentially reducing energy consumption and CO_2 emissions. Nonetheless, achieving high performance and selectivity in electrochemical ammonia synthesis remains a challenge due to the inherent stability of N_2 and competition with hydrogen evolution reactions.

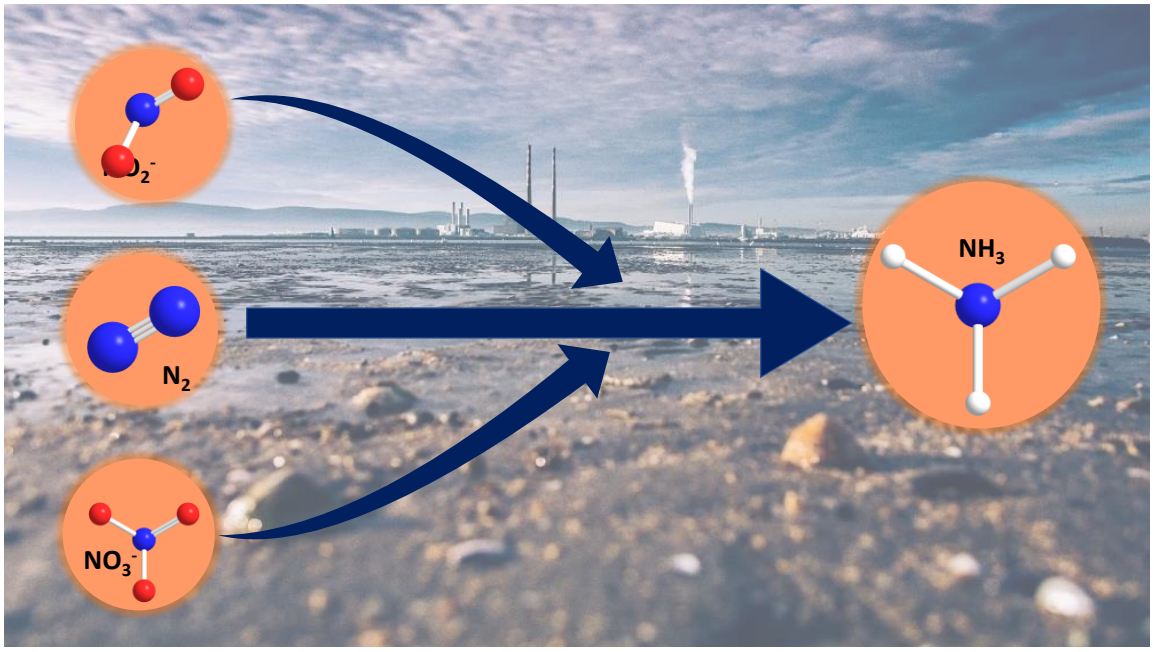

Figure 1. Overview of Advanced Electrocatalytic Pathways for Ammonia Synthesis

Covalent Organic Frameworks (COFs) have emerged as a transformative class of materials in the field of catalysis, gas storage, and separation. COFs are characterized by their well-defined, porous structures formed through covalent bonding between organic units. This

structural design allows for precise control over their physical and chemical properties, including surface area, pore size, and functionalization. The ability to engineer COFs at the molecular level makes them ideal candidates for applications in electrocatalysis. In recent years, COFs have been increasingly utilized as supports for catalysts in electrochemical reactions, including the NRR. By incorporating metal complexes or nanoparticles into COFs, researchers aim to enhance catalytic activity and selectivity for ammonia production. The unique properties of COFs-such as their high surface area and ability to stabilize active sites make them advantageous for these applications. Furthermore, the modularity of COFs allows for the integration of multiple catalytic sites within a single framework, which can improve overall catalytic performance.

This chapter provides an overview of the traditional and alternative methods for ammonia production, with a focus on the potential of electrochemical approaches powered by renewable energy. It introduces the concept of COFs, emphasizing their role in advancing catalytic processes. The subsequent chapters will build upon this foundation, presenting novel COF-based catalysts for ammonia synthesis through NRR, as well as their applications in nitrate and nitrite reduction reactions.

Chapter 2: Resorcinol-Azodianiline Covalent Organic Framework Supported FeOOH Quantum Dots Catalyzed Electrochemical Ammonia Synthesis under Ambient Conditions

In this chapter, a novel COF system supported by FeOOH quantum dots (QDs) was synthesized and employed for electrochemical nitrogen reduction reaction (NRR) under ambient conditions. The hybrid material (COF@FeOOH) was systematically characterized, and its performance was evaluated for NRR. The optimized system achieved a notable ammonia yield of 77.4 $\mu g h^{-1} m g^{-1}_{cat}$, with a Faradaic efficiency of 46.4% in a 0.1 M $LiClO_4$ electrolyte at -0.4 V versus the reversible hydrogen electrode (RHE). The integration of FeOOH QDs into the COF matrix enhanced the catalytic sites, leading to increased activity and stability for the NRR, showcasing the potential of these hybrid materials in sustainable ammonia production.

Chapter 3: Pentanuclear Metal Complex-Anchored Covalent Organic Framework for Electrocatalytic Nitrate Reduction Reaction

This chapter focuses on the design and synthesis of a COF with a pentanuclear metal complex (M_5, where M = Fe, Co, or Zn) anchored within its framework. The COF was evaluated for its

electrocatalytic activity in the nitrate reduction reaction (NO_3RR). A systematic study revealed that the iron-based system exhibited the highest catalytic performance, with a superior ammonia yield of 13.5 $mgh^{-1}mg^{-1}_{cat}$ and an impressive Faradaic efficiency of 88% at -1.1 V versus RHE. The performance hierarchy of the metal centers was established as Fe > Co > Zn, demonstrating the versatility of the pentanuclear complex in tuning the catalytic activity for NO_3RR. The structural integrity and stability of the catalyst were validated through extensive characterization, including HRTEM, PXRD, IR spectroscopy, and adsorption studies.

Chapter 4: Pentanuclear Metal Complex-Anchored Covalent Organic Framework for Electrocatalytic Nitrite Reduction Reaction

In this chapter, the pentanuclear metal complex-anchored COF system was further explored for its efficacy in the nitrite reduction reaction (NO_2RR). The COF framework was synthesized with Fe, Co, and Zn as central metals in the pentanuclear complex. The electrocatalytic study indicated that the cobalt-based COF demonstrated the highest performance, achieving a nitrite reduction rate of 3.9 $mgh^{-1}mg^{-1}_{cat}$ and a Faradaic efficiency of 99.3% at -0.9 V versus RHE. The performance order for the NO_2RR was established as Co > Fe > Zn. This study further underscores the tunable nature of the COF systems and their capacity to selectively reduce nitrite ions with high efficiency, offering insights into the role of metal centers in catalysis.

Materials related	
COF:	Covalent Organic Frameworks
CON:	Covalent Organic Nanosheets
MOF:	Metal Framework
ZIF:	Zeolite Imidazole Frameworks
DFT	Density Functional Theory
GCMC	Grand Canonical Monte-Carlo
BTC	Breakthrough Curve
TON	Turnover Number
BE	Binding Energy
UFF	Universal Force Field
PAF	Polymeric Aromatic Framework
LDFT:	Non Local Density Functional Theory
AFM:	Atomic Force Microscopy
TOF	Turnover Frequency
TGA	Thermogravimetric Analysis
np.	Nano particles
MAS:	Magic Angle Spuning
MOF:	Metal Organic Framework
CP:	Coordination Polymer
HCPs:	Hyper-crosslinked polymers
POPs:	porous organic polymers
FE-SEM:	Field Emission-Scanning Electron
HR-TEM:	High Resolution Transmission Electron Microscopy
SAED:	Selected Area Electron Diffraction
BET	Brunauer Emmett Teller
HOA:	Heat of Adsorption
TGA:	Thermogravimetric analysis
PXRD:	Powder X-Ray Diffraction
SCXRD:	Single Crystal X-ray diffraction
AFM:	Atomic Force Microscopy
BET:	Brunauer Emmett Teller
GCD:	Galvanostatic charge-discharge
GCD:	Galvanostatic charge-discharge
EDLC:	Electrical Double Layer Capacitance
CE:	Counter Electrode
FE:	Faradic Efficiency
WE:	Working Electrode
RE:	Reference Electrode
CV:	Cyclic Voltammogram
Chemicals related	
DMF:	N, N-Dimethyl formamide
DMSO:	Dimethyl sulfoxide
NMP:	N-Methyl-2-pyrrolidone

ACN:	Acetonitrile
O-DBC:	Ortho-Dichlorobenzene
FE-SEM:	Field Emission-Scanning Electron Microscopy
FT-IR:	Fourier Transform Infra-red-spectra
NMR.	Nuclear Magnetic Resonance
CDCI	Deuterated Chloroform
Units	
°C:	Degree Celsius
K.	Kelvin
mmol:	Milli moles
hrs:	hours
µl:	Microliter
um:	micrometer
mL:	Milliliter
nm:	nanometer
min:	Minutes
mol:	moles
gm:	Gram
Å	Angstrom
MHz:	Megahertz
V:	volts
mV:	Millivolts
M:	Molar
A:	Ampere
mA:	Milliampere
F:	Faraday
mg:	Milligram
K:	Kelvin
mA/g:	milliampere/gram
mAh/g	milliampere hour/gram
CC:	Cubic Centimeter
RH:	Relative Humidity
RT:	Room Temperature
S/cm:	Siemen per Centimeter
σ:	Ionic conductivity
°C:	Degree Celsius
Å	Angstrom
A:	Ampere
ACN:	Acetonitrile
AFM:	Atomic Force Microscopy
AFM:	Atomic Force Microscopy
BE	Binding Energy
BET	Brunauer Emmett Teller
BTC	Breakthrough Curve
CC:	Cubic Centimeter

CDCI	Deuterated Chloroform
CE:	Counter Electrode
COF:	Covalent Organic Frameworks
CON:	Covalent Organic Nanosheets
CP:	Coordination Polymer
Csp:	specific capacitance
CV:	Cyclic Voltammogram
DFT	Density Functional Theory
DMF:	N, N-Dimethyl formamide
DMSO:	Dimethyl sulfoxide
EDLC:	Electrical Double Layer Capacitance
F:	Faraday
FE-SEM:	Field Emission-Scanning Electron Microscopy
FE-SEM:	Field Emission-Scanning Electron
FT-IR:	Fourier Transform Infra-red-spectra
GCD:	Galvanostatic charge-discharge
GCD:	Galvanostatic charge-discharge
GCMC	Grand Canonical Monte-Carlo
gm:	Gram
HCPs:	Hyper-crosslinked polymers
HOA:	Heat of Adsorption
hrs:	hours
HR-TEM:	High Resolution Transmission Electron Microscopy
K.	Kelvin
K:	Kelvin
LDFT:	Non Local Density Functional Theory
M:	Molar
mA/g:	milliampere/gram
mA:	Milliampere
ENRR	Electrocatalytic Nitrogen Reaction
ENO_3RR	Electrocatalytic Nitrate Reaction
ENO_2RR	Electrocatalytic Nitrite Reaction
mAh/g	milliampere hour/gram
MAS:	Magic Angle Spuning
mg:	Milligram
MHz:	Megahertz
min:	Minutes
mL:	Milliliter
mmol:	Milli moles
MOF:	Metal Framework
MOF:	Metal Organic Framework
mol:	Moles

mV:	Millivolts
nm:	nanometer
NMP:	N-Methyl-2-pyrrolidone
NMR.	Nuclear Magnetic Resonance
np.	Nano particles
O-DBC:	Ortho-Dichlorobenzene
PAF	Polymeric Aromatic Framework
POPs:	porous organic polymers
PXRD:	Powder X-Ray Diffraction
RE:	Reference Electrode
RH:	Relative Humidity
RT:	Room Temperature
SAED:	Selected Area Electron Diffraction
SCXRD:	Single Crystal X-ray diffraction
TGA	Thermogravimetric Analysis
TGA:	Thermogravimetric analysis
TOF	Turnover Frequency
TON	Turnover Number
UFF	Universal Force Field
um:	micrometer
V:	volts
WE:	Working Electrode
ZIF:	Zeolite Imidazole Frameworks
µl:	Microliter

List of Publications

1. **Shekhar, P.**; Kosugi, K.; Singh, H. D.; Kushwaha, R.; Rase, D.; Matsuzaki, T.; Jain, C.; Singh, P.; Singh, Y.; Vinod, C. P., Resorcinol–Azodianiline Covalent Organic Framework Supported FeOOH Quantum Dot-Catalyzed Electrochemical Ammonia Synthesis under Ambient Conditions. *Chemistry of Materials* **2024,** *36* (17), 8229-8238.
2. **Shekhar, P**.; Devulapalli, V. S. D.; Reji, R.; Singh, H. D.; Jose, A.; Singh, P.; Torris, A.; Vinod, C. P.; Tokarz III, J. A.; Mahle, J. J., COF-supported zirconium oxyhydroxide as a versatile heterogeneous catalyst for Knoevenagel condensation and nerve agent hydrolysis. *Iscience* **2023,** *26* (11), 108088.
3. Chakraborty, D.; **Shekhar, P.**; Singh, H. D.; Kushwaha, R.; Vinod, C.; Vaidhyanathan, R., Ag Nanoparticles Supported on a Resorcinol-Phenylenediamine-Based Covalent Organic Framework for Chemical Fixation of CO2. *Chem. Asian J.* **2019,** *14* (24), 4767-4773.
4. Kushwaha, R.; Haldar, S.; **Shekhar, P.**; Krishnan, A.; Saha, J.; Hui, P.; Vinod, C. P.; Subramaniam, C.; Vaidhyanathan, R., Exceptional Capacitance Enhancement of a Non-Conducting COF through Potential-Driven Chemical Modulation by Redox Electrolyte. *Adv. Energy Mater.* **2021,** *11* (13), 2003626.
5. Chandran, C.; Singh, H. D.; Leo, L. S.; **Shekhar, P.**; Rase, D.; Chakraborty, D.; Vinod, C. P.; Vaidhyanathan, R., A covalent organic framework with electrodeposited copper nanoparticles–a desirable catalyst for the Ullmann coupling reaction. *J. Mater. Chem. A* **2022,** *10* (29), 15647-15656.
6. Haldar, S.; Rase, D.; **Shekhar, P.**; Jain, C.; Vinod, C. P.; Zhang, E.; Shupletsov, L.; Kaskel, S.; Vaidhyanathan, R., Incorporating Conducting Polypyrrole into a Polyimide COF for Carbon-Free Ultra-High Energy Supercapacitor. *Adv. Energy Mater.* **2022,** *12* (34), 2200754.
7. Devulapalli, V. S. D.; Kushwaha, R.; Ovalle, E.; Singh, H. D.; **Shekhar, P.**; Chakraborty, D.; Vinod, C. P.; Vaidhyanathan, R.; Borguet, E., Synergistic electronic effects in AuCo nanoparticles stabilized in a triazine-based covalent organic framework: a catalyst for methyl orange and methylene blue reduction. *ACS Applied Nano Materials* **2022,** *5* (4), 4744-4753.
8. Rase, D.; Illathvalappil, R.; Singh, H. D.; **Shekhar, P.**; Leo, L. S.; Chakraborty, D.; Haldar, S.; Shelke, A.; Ajithkumar, T. G.; Vaidhyanathan, R., Hydroxide ion-conducting viologen–bakelite organic frameworks for flexible solid-state zinc–air battery applications. *Nanoscale Horizons* **2023,** *8* (2), 224-234.
9. Kushwaha, R.; Jain, C.; **Shekhar, P.**; Rase, D.; Illathvalappil, R.; Mekan, D.; Camellus, A.; Vinod, C. P.; Vaidhyanathan, R., Made to Measure Squaramide COF Cathode for Zinc Dual-Ion Battery with Enriched Storage via Redox Electrolyte. *Adv. Energy Mater.* **2023,** *13* (34), 2301049.

10. Singh, H. D.; Singh, P.; Vysyaraju, R.; Balasubramaniam, B. M.; Rase, D.; **Shekhar, P.**; Jose, A.; Rajendran, A.; Vaidhyanathan, R., Unlocking the Separation Capacities of a 3D-Iron-Based Metal Organic Framework Built from Scarce Fe4O2 Core for Upgrading Natural Gas. *Chemistry of Materials* **2023,** *35* (19), 8261-8271.
11. Jain, C.; Kushwaha, R.; Rase, D.; **Shekhar, P.**; Shelke, A.; Sonwani, D.; Ajithkumar, T. G.; Vinod, C. P.; Vaidhyanathan, R., Tailoring COFs: Transforming Nonconducting 2D Layered COF into a Conducting Quasi-3D Architecture via Interlayer Knitting with Polypyrrole. *J. Am. Chem. Soc.* **2023,** *146* (1), 487-499.
12. Nandi, S.; Singh, H. D.; **Shekhar, P.**; Chakraborty, D.; Kushwaha, R.; Vaidhyanathan, R., An intrinsically zwitter-ionic COF: a carboxylic acid and pseudo-tetrahedral sp 3 nitrogen functionalized covalent organic framework with potential for humidity sensing. *J. Mater. Chem. A* **2024,** *12* (5), 2839-2847.
13. Singh, P.; Singh, H. D.; **Shekhar, P.**; Jain, C.; Song, P.; Loloei, M.; Edwin, M.; Gao, Y.; Masoumifard, N.; Vaidhyanathan, R., Ultra-Microporous Zinc-Diaminotriazolate-Oxalate Metal Organic Framework with Nonlayered-Pillared Structure Showing High Carbon Dioxide Uptakes at Low Partial Pressures. *Chemistry of Materials* **2025.**
14. Singh, P.; Singh, H. D.; **Shekhar, P.**; Nasa, P.; Rase, D.; Jain, C.; Singh, Y. K.; Vaidhyanathan, R., CO2-Specific Gate Opening Transforms a Dense Cation-Filled Zinc-Aminotriazolato-Oxalate Framework into an Ultramicroporous MOF. *Crystal Growth & Design* **2024,** *24* (21), 8838-8846.
15. Rase, D.; Manna, N.; Kushwaha, R.; Jain, C.; Singh, H. D.; **Shekhar, P.**; Singh, P.; Singh, Y. K.; Vaidhyanathan, R., Design enhancement in hydroxide ion conductivity of viologen–bakelite organic frameworks for a flexible rechargeable zinc–air battery. *Chem. Sci.* **2024,** *15* (18), 6949-6957.

Table of Contents

Chapter 1

Introduction To Ammonia Production, Covalent Organic Frameworks (COFs) And Electrochemical Ammonia Production

1.1. Introduction

The chemical ammonia (NH_3) is utilized extensively in a variety of industries. Its primary application is in agriculture as fertilizer, contributing up around 80% of the world's ammonia usage (Figure 1.1 & 1.2)[1]. Ammonia-based fertilizers are essential for improving crop yields, especially in crops like corn, wheat, and soybeans[2]. Ammonia is also utilized in the manufacturing of polymers, insecticides, fertilizers, explosives, dyes, and pharmaceuticals[3].

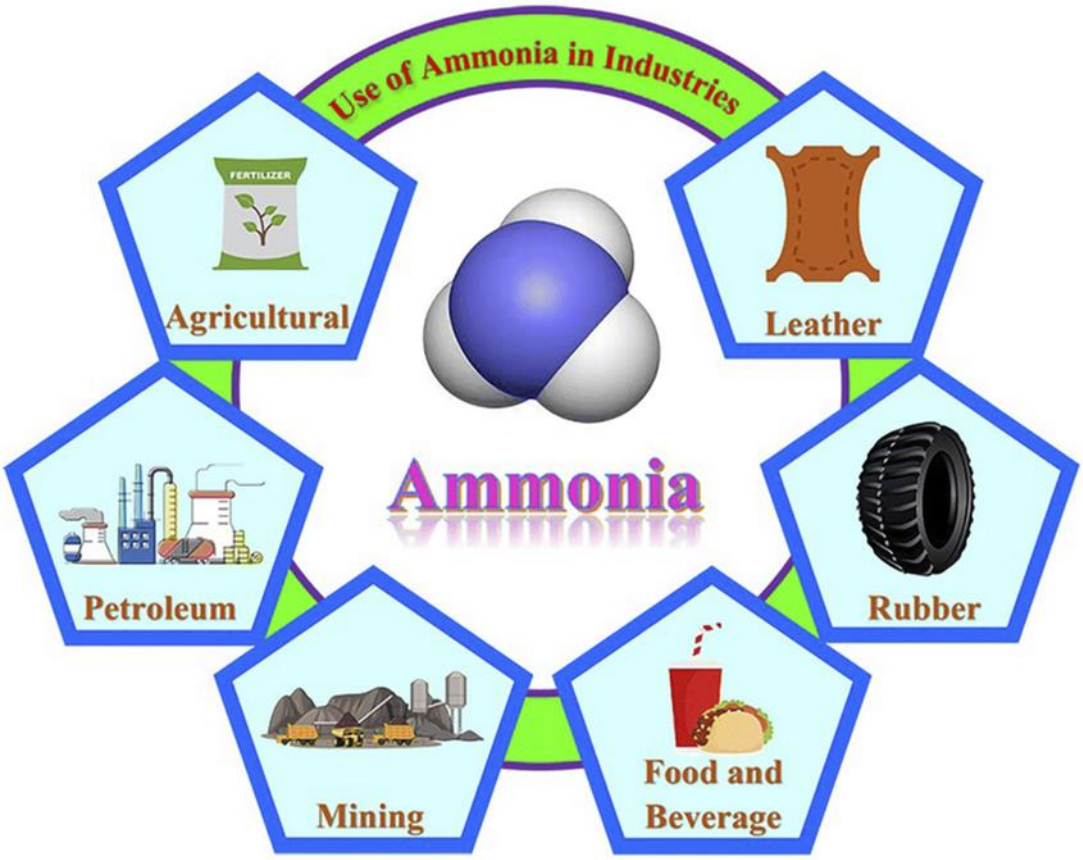

Figure 1.1. Various applications of ammonia in industries. *(Adopted from Ref 3)*

1.2. Ammonia in Agriculture

Ammonia plays a vital role in agriculture, significantly influencing crop production and soil management. Its primary applications include fertilizer production, which boosts crop yields, and its environmental impact, which poses challenges for sustainable agricultural practices. The following sections detail the key aspects of ammonia's role in agriculture, highlighting its benefits and the associated challenges, including potential soil degradation and substantial energy consumption in its production.

1.2.1. Fertilizer Production

Ammonia is the primary nitrogen source in fertilizers, such as urea and diammonium phosphate, which are essential for crop growth and development (Figure 1.2)[4]. Nitrogen fertilizers enhance N_2O production by providing substrates for microbial processes such as nitrification and denitrification, which convert nitrogen into various forms.[5]. The global annual consumption of nitrogen fertilizer is approximately 110.4 teragrams (Tg). Since 1961, when fertilizer usage data became available at the country level, nitrogen utilization has roughly increased by eightfold[6-8].

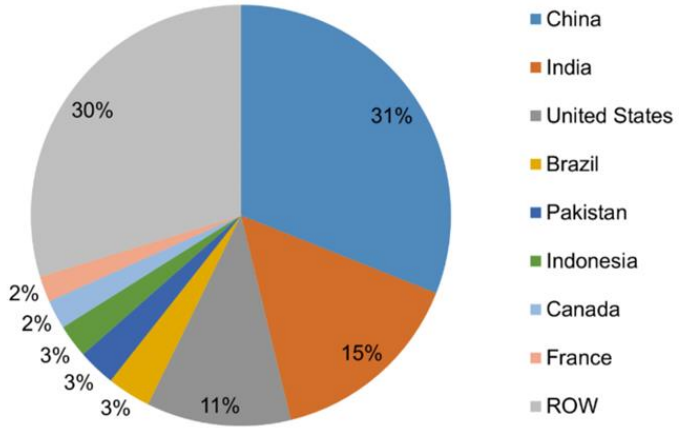

Figure 1.2. Country-wise consumption of nitrogen-based fertilizers. (*Adopted from Ref 10*)

* ROW Rest of world

1.2.2. Crop Yields

The use of ammonia-based fertilizers has resulted in significant increases in agricultural productivity and crop yields worldwide. According to studies, nitrogen fertilizers can significantly increase crop yields when compared to unfertilized crops[9]. This increase in yield has been critical in feeding a growing world population and ensuring food security. Nitrogen fertilizers, including those derived from ammonia, have been a major driver of the "Green Revolution", dramatically increasing cereal production in developing countries since the 1960s[8]. As per an analysis published by the International Fertilizer Association (IFA), cereals are expected to account for nearly half (46%) of the future increase in global nitrogen (N) fertilizer demand. Fruits and vegetables are expected to be the second-largest contributor, accounting for an extra 16% increase (Figure 1.3)[10].

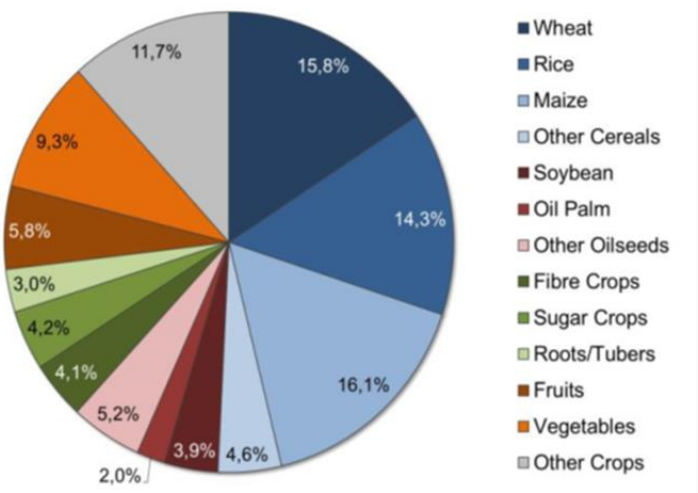

Figure 1.3. Crop-wise consumption of nitrogen-based fertilizers. (*Adopted from Ref 10*)

used to process this dry stream of CO_2 and N_2, where the sorbent selectively removes CO_2 while leaving behind a pure stream of N_2 (Figure 1.1). Adsorbed CO_2 must be recycled and geo-sequestered after complete adsorption.[12, 23] Since the concentration of CO_2 in the flue gas is only 10-15%, the post combustion CO_2 capture is quite challenging. There are many materials known with high CO_2 capacity at higher pressures but Since there is relatively little partial pressure of CO_2 in the effluent gas, they are not the most suitable for post-combustion CO_2 capture..[24, 25] Hence materials displaying abrupt CO_2 uptake at low pressures could be best suited for the post combustion process.[26] But high CO_2 uptake at lower pressures also reflects the robust interaction between molecules of CO_2 and the adsorbent which implies to the high heat of adsorption and hence a potentially high regeneration cost.[17] However, for the initial screening, CO_2/N_2 comparisons at the area of low pressure may provide an impression of the performance of the material and if the CO_2 adsorption is physisorptive generally it is not an issue. Although the most popular approach for post-combustion CO_2 capture uses aqueous amine (where the separation takes place via a chemical absorption method),[27] because of its high regeneration cost, corrosiveness, poor stability and large footprints, it is neither energy efficient nor economically sustainable.[28, 29.] In contrast, porous solid sorbent-based CO_2 capture involves passing the flue gas through a solid sorbent bed that selectively captures CO_2. Because significantly less regeneration energy is required as to the weaker interactions between the sorbent and sorbate, which makes it both cost-effective and energy-efficient.[30] Solid sorbents have number of other benefits over the aqueous amines. For instance amines are known to decompose and lose their capacity over time, corrode the

bed in the long run, and difficulty in handling liquids.[17] On the other hand, solid sorbents have good capacity, selectivity, does not corrode the bed and most importantly easy to handle compared to the former. Given all these particulars, solid sorbents are definitely the front runners for the post combustion CO_2 capture. There are different classes of sorbents among the solid sorbents itself. Zeolites, like 13X, are already employed as CO_2 scrubbers in large PSA systems.[31] However, they struggle in humid environments; their high water-adsorption, requires their operation and activation under high temperatures, which makes the overall capture economy unattractive.[32]

1.2.3 Environmental Impact

Ammonia is a naturally occurring chemical, but its use in agriculture has serious environmental consequences. It helps to replenish nitrogen in the soil, which is quickly depleted during the growing season. Nitrogen fertilizers can cause soil acidification over time, reducing soil health and microbial activity. Acidic soils can limit the amount of vital nutrients that are available to plants, lowering overall soil fertility.[11-12] The Haber-Bosch process is primarily utilized in the energy-intensive process of synthesizing ammonia. This process uses a catalyst made of iron to react ambient nitrogen with hydrogen at high temperatures and pressures to create ammonia. The energy requirements for this process are substantial; it is estimated that producing one metric ton of anhydrous ammonia requires approximately 1090-1250 cubic meters of natural gas.[13] The reliance on fossil fuels for ammonia production raises concerns about greenhouse gas emissions and the carbon footprint of its use in agriculture.

1.3. Ammonia in industry

Ammonia is an essential chemical that finds many uses in industry, reflecting its versatility and significance in various sectors. Its unique chemical properties and reactivity make it indispensable for synthesizing a diverse array of products and processes, from everyday goods to advanced technological solutions. The following sections outline the key industrial uses of ammonia, demonstrating its critical role in enhancing efficiency, productivity, and innovation across different fields.

1.3.1 Plastics Production

Ammonia is a primary precursor for the production of various plastics, especially acrylonitrile, which is vital for producing synthetic fiber like nylon. The production process typically involves the catalytic reaction of ammonia with propylene and air, resulting in acrylonitrile formation.[14-15]

1.3.2 Explosives Manufacturing

Ammonia plays a critical role in producing ammonium nitrate, a widely utilized explosive in mining and construction industries. Its nitrogen-rich composition contributes to the stability and effectiveness of explosive formulations.[16-17]

1.3.3 Dye Production

In the dye industry, ammonia is utilized in synthesizing various dyes essential for colouring textiles and paints. Its involvement in dye chemistry is crucial for creating stable and vibrant colour compounds.[14,18]

1.3.4 Pesticide Formulation

A crucial component of some pesticide formulations is ammonia, enhancing agricultural productivity by providing effective pest control solutions. Its application in pesticide synthesis is crucial for developing compounds that target specific pests.[16]

1.3.5 Pharmaceutical Applications

In pharmaceuticals, ammonia is involved in synthesizing various medications, including antibiotics and vitamins. Its role as a precursor in drug synthesis is essential for producing therapeutic agents.[14-15]

1.3.6 Metal Treatment Processes

Ammonia is utilized in nitriding processes, enhancing the hardness and wear resistance of metal surfaces. This treatment is critical for improving the durability of tools and machinery.[14,17]

1.3.7 Cleaning and Degreasing Agents

Ammonia's ability to dissolve grease and oils makes it a valuable component in industrial cleaning solutions. Its effectiveness in removing contaminants from machinery is well established.[14,19]

1.3.8 Refrigeration Systems

Ammonia has historically been used as a refrigerant due to its high energy efficiency and favourable thermodynamic properties. It continues to be utilized in large-scale industrial refrigeration systems.[14,21]

1.3.9 Food Production

Ammonia is employed as a food additive in the production of baked goods and processed meats, serving as both a leavening agent and a preservative. Additionally, it is used in the beverage industry, including in beer and soft drinks, to control pH levels and improve the flavour and overall quality of the final product.[14,21]

1.3.10 Hydrogen Production

Ammonia is being investigated as a hydrogen carrier for clean energy applications. Through thermal decomposition, ammonia can be converted into hydrogen, which is a clean-burning fuel with potential applications in both energy storage and transportation.[14-15]

1.4 Ammonia's Global Economic Importance

Ammonia holds substantial economic importance globally, influencing job creation, international trade, and energy markets. Its production and use impact economic development and resource efficiency, with significant implications for both local and global economies. The following sections outline the key economic aspects of ammonia, emphasizing its role in job creation, trade, and energy resource management.

1.4.1 Job Creation and Economic Development

The ammonia industry serves a predominant role in job creation across several sectors, including production, transportation, and application. This industry stimulates economic

growth, particularly in regions hosting ammonia production facilities, thereby contributing to both local and national economies (Figure 1.4).[22]

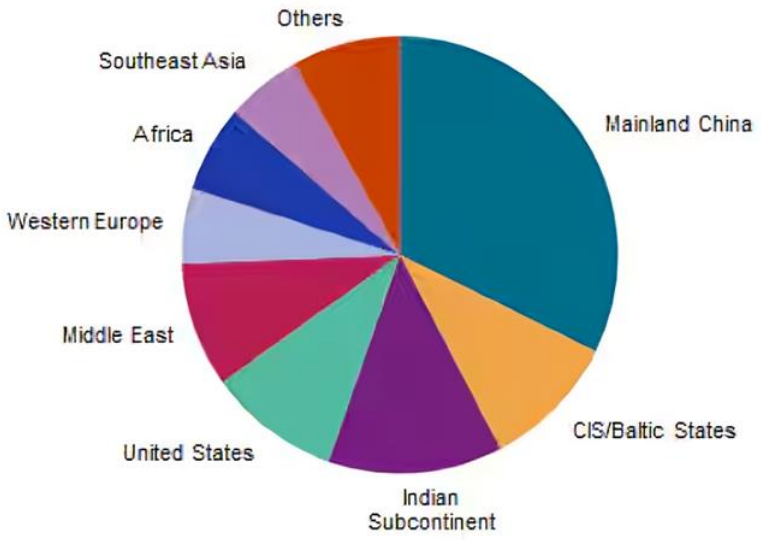

Figure 1.4. Country-wise global consumption of ammonia

1.4.2 International Trade

Ammonia is a vital commodity in international trade, with countries rich in natural gas its primary feedstock often exporting ammonia and ammonia-based fertilizers. This trade is essential for enhancing agricultural productivity on a global scale.[22-23]

1.4.3. Energy and Resource Efficiency

The production of ammonia is closely linked to global energy markets due to its heavy reliance on natural gas. This dependence makes ammonia production sensitive to fluctuations in energy prices, highlighting the need for more efficient production methods to reduce economic vulnerabilities associated with energy market instability.[23-24]

1.5. Ammonia Production Methods

Ammonia production methods have evolved significantly, ranging from biological processes to advanced industrial techniques (Figure 1.5). These methods are critical for meeting global ammonia demand and are characterized by their diverse approaches, each with its own advantages and limitations. Biological methods leverage natural processes and microorganisms to convert atmospheric nitrogen into ammonia, offering sustainable

alternatives but with inherent efficiency limitations. In contrast, industrial techniques, including advanced catalytic processes, have been developed to meet large-scale production needs with high efficiency and scalability. This broad spectrum of production methods underscores the importance of innovation and optimization in ammonia synthesis to support agricultural, industrial, and environmental applications. The following sections detail the various methods of ammonia production, highlighting both biological and industrial approaches.

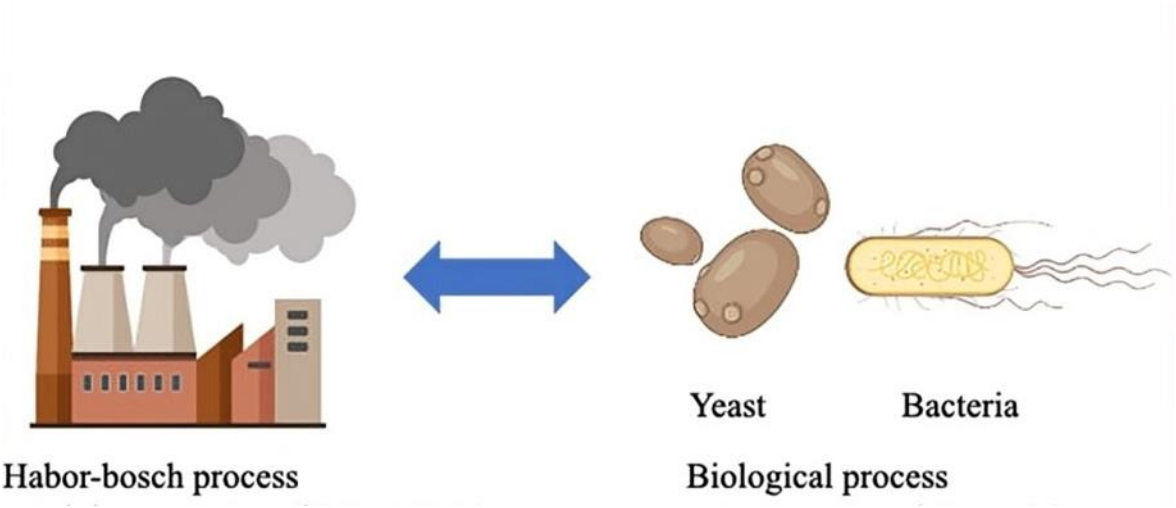

Figure 1.5. Methods of ammonia production *(Adopted from Ref 24)*.

1.5.1 Biological Ammonia Production

Several biological approaches to ammonia production exist, including:

a) Nitrogen fixation. The primary method where atmospheric nitrogen is converted into ammonia. Nitrification: The microbial conversion of ammonia into nitrates.

b) NO_x reduction: The reduction of NO_x ammonia.

c) Urea hydrolysis: Breakdown of urea to release ammonia.

d) Metabolic engineering of microorganisms: Genetic modifications to enhance ammonia production capabilities.

e) In vitro ruminal microbial fermentation: A newer approach utilizing rumen bacteria to ferment protein biomass into ammonia.

Among these methods, biological fixation of nitrogen and fermentation in microorganisms are the most extensively studied and reported. For instance, *Rhizobium* bacteria form symbiotic associations by inhabiting legume root nodules, while blue-green algae can independently fix nitrogen through photosynthesis.[25]

Biological nitrogen fixation (BNF) is an important natural mechanism conducted by various microorganisms, including bacteria, algae that is blue-green, and aquatic fern. These organisms can used in atmospheric nitrogen (N_2) fixation into ammonia (NH_3), either independently or in symbiotic relationships with host plants.[26] This process was first documented in 1888 and has significant implications for agriculture and ecosystem health.[27-28] The key enzyme responsible for ammonia synthesis in these organisms is nitrogenase, which is encoded by the NIF gene, a family of proteins found nitrogen-fixing algae and bacteria. Nitrogenase catalyzes atmospheric nitrogen is converted to ammonia under ambient circumstances., making it essential for plant growth.[26,29]

There are three main kinds of nitrogenases:

a) Mo nitrogenase: The most common form, containing molybdenum.

b) V nitrogenase: Contains vanadium.

c) Fe nitrogenase: Composed solely of iron.

These enzymes stabilize the transition states necessary to produce ammonia, enabling the process to occur at near-ambient conditions. The enzyme's active location of Mo nitrogenase is known as $MoFe_7S_9N$ cluster (or FeMo-cofactor), facilitates the hydrogenation of nitrogen, leading to ammonia production through an associative mechanism rather than nitrogen dissociation followed by hydrogenation.[30-33] The general reaction for nitrogen fixation can be represented as follows:

$$N_2 + 8H^+ + 8e^- \rightarrow 2\ NH_3 + H_2$$

This reaction highlights the competition between ammonia synthesis and hydrogen evolution, which is an area of ongoing research in electrocatalysis inspired by biological nitrogen fixation (Figure 1.6).

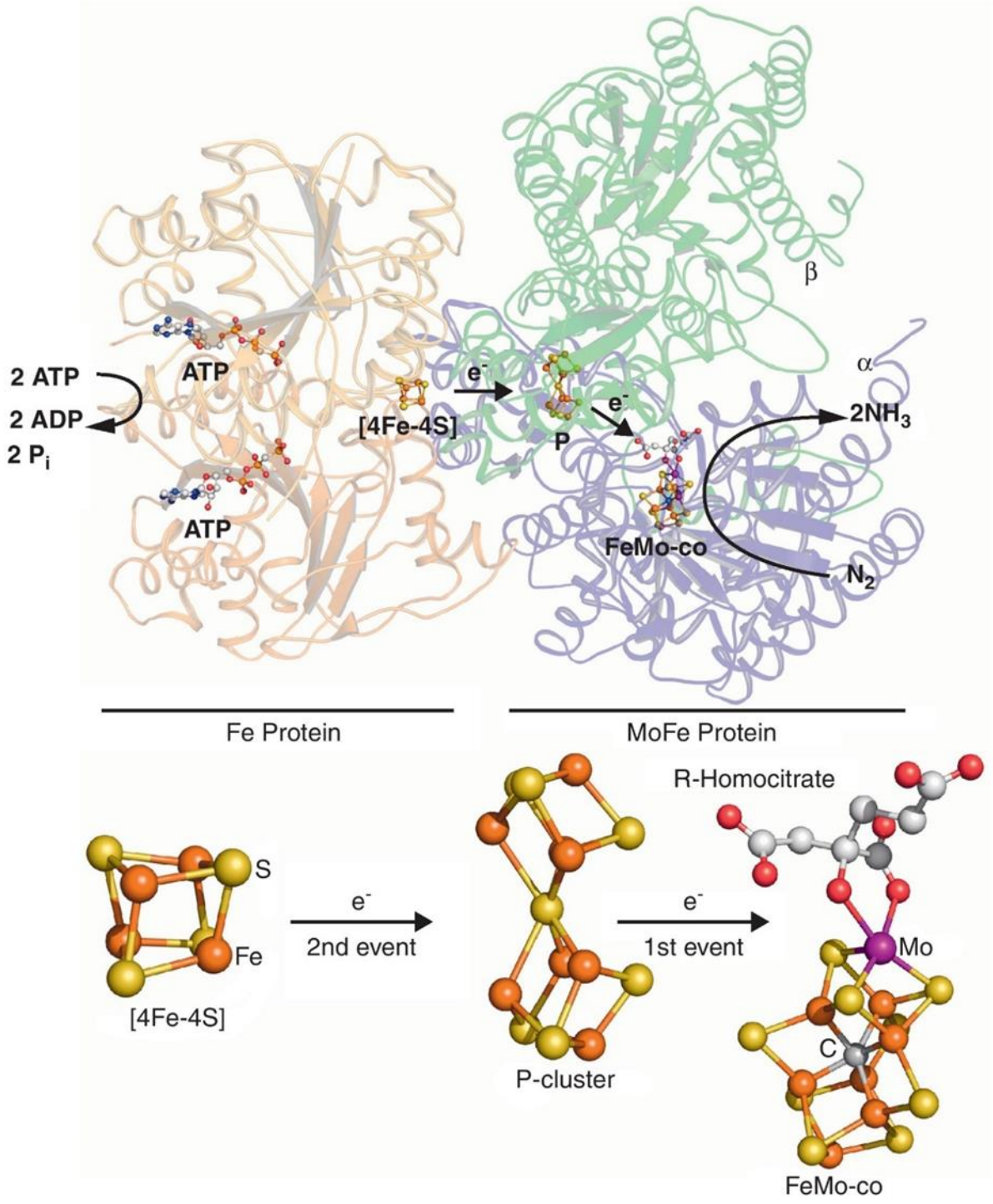

Figure 1.6: Schematic Diagram of Ammonia Formation in Nitrogenase. (*Adopted from Ref 31*)

Despite nitrogenase's effectiveness, biological nitrogen fixation alone is insufficient to satisfy the global ammonia demand. The enzyme nitrogenase achieves an estimated maximum efficiency of roughly 10-15%, which is reduced further when considering the entire bacterial

system. As a result, synthetic ammonia synthesis methods are required to augment natural processes.[26] Current research is investigating bio-inspired catalysts for localized fertilizer production on plant seeds, emulating the functionality of the nitrogenase enzyme.

Metabolic engineering involves modifying the genetic and metabolic pathways of microorganisms to enhance their ability to produce ammonia. This approach leverages the natural ammonia production capabilities of certain bacteria and algae, optimizing their metabolic processes for industrial applications.[34-35] Biological ammonia generation by rumen bacteria fermentation of protein biomass is a novel strategy that has the potential to supplement established ammonia bioproduction methods.[36] This process involves the in-vitro fermentation of protein-rich biomass by rumen bacteria, which can convert the biomass into ammonia under controlled conditions. The fermentation process typically operates at near-ambient temperatures, making it an energy-efficient and sustainable method for ammonia production.[37]

1.5.2 Industrial Ammonia Synthesis

Industrial ammonia production has evolved significantly over the past century, driven by advancements in various industrial processes. Initially, nitrogen fixation was achieved through methods such as the Birkeland-Eyde and Frank-Caro processes, alongside the thermochemical synthesis process discovered by Carl Bosch and Fritz Haber, called as the Haber-Bosch process[39]. Birkeland-Eyde and Frank-Caro processes were well-documented elsewhere[40], but from the late 1920s, The Haber-Bosch process became prevalent because to its cheap energy usage and scalability benefits.[40] The Haber-Bosch process was first published and patented by Haber and Le Rossignol in 1913 and 1916, respectively (Figure 1.7) [41-43]. This process demonstrated feasibility with system operating at 500-550 °C and 100-200 atm pressure, producing approximately 2 kg of NH_3 per day. Despite initial scepticism from Nernst, who deemed ammonia synthesis unfeasible[44], Haber and Le Rossignol's approach proved successful, eventually revolutionizing synthetic ammonia production.

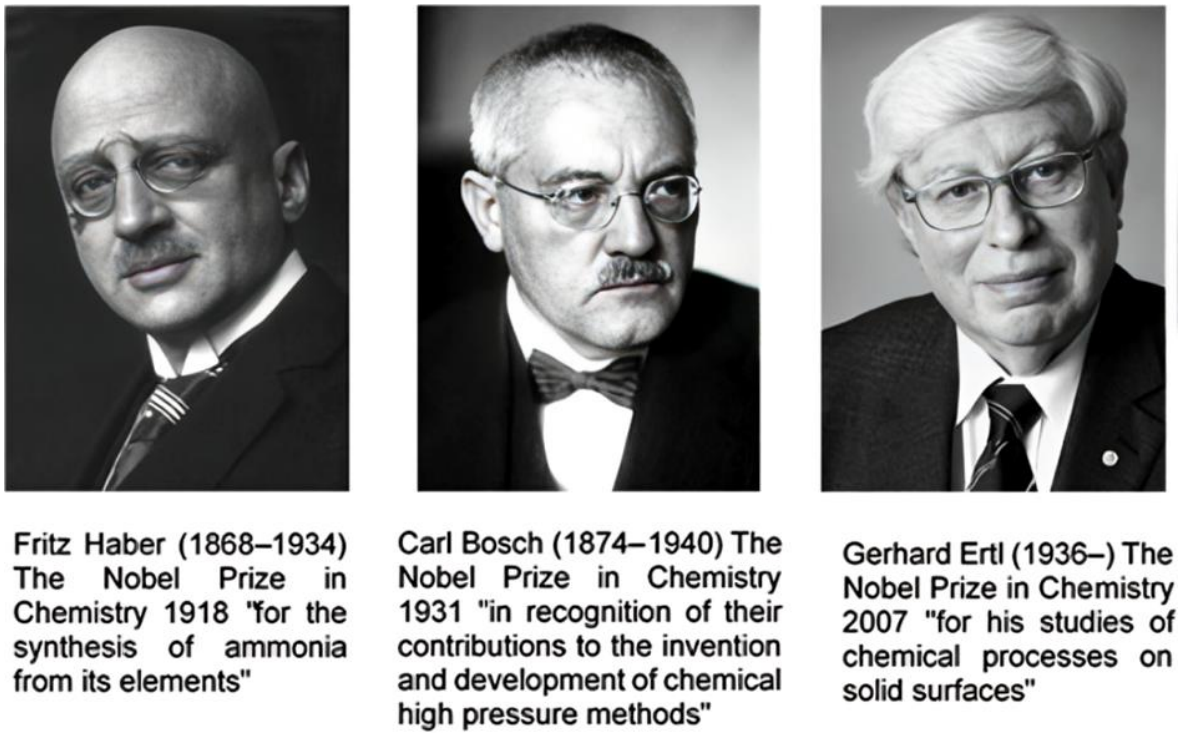

Figure 1.7. Renowned Nobel Laureates in the Development of Industrial Ammonia Synthesis. (*Adopted from Ref 42*)

In the early 20th century, Mittasch et al. developed an iron catalyst with many components as a more plentiful substitute for osmium in ammonia synthesis[45-46]. Extensive research in subsequent decades resolved the surface mechanisms of these catalysts, culminating in Ertl et al.'s work in the 1970s[47]. Engineering challenges, such as developing burst-proof converters, were addressed by Bosch et al. in the 1910s[48], marking a significant technological advancement in high-pressure chemical processes. The combustion of coal and lignite was the main technique used to produce hydrogen at first. Nonetheless, the accessibility of inexpensive methane with reduced sulfur and chlorine content, became the preferred method due to its efficiency with active catalysts[49]. The methane reforming process, which produces hydrogen, nitrogen, and carbon oxides, became a key component of the Haber-Bosch process[50]. During the 1920s to 1950s, alternative process designs, such as the Claude process, were proposed. The Claude process, operating at 900-1000 pressure, with numerous reactors and condensers in series, the goal was to remove the need for recycling within the synthesis cycle. However, practical issues like as heat loss and temperature swings rendered it is less energy efficient than the Haber-Bosch process. (Figure 1.8).[51-52]

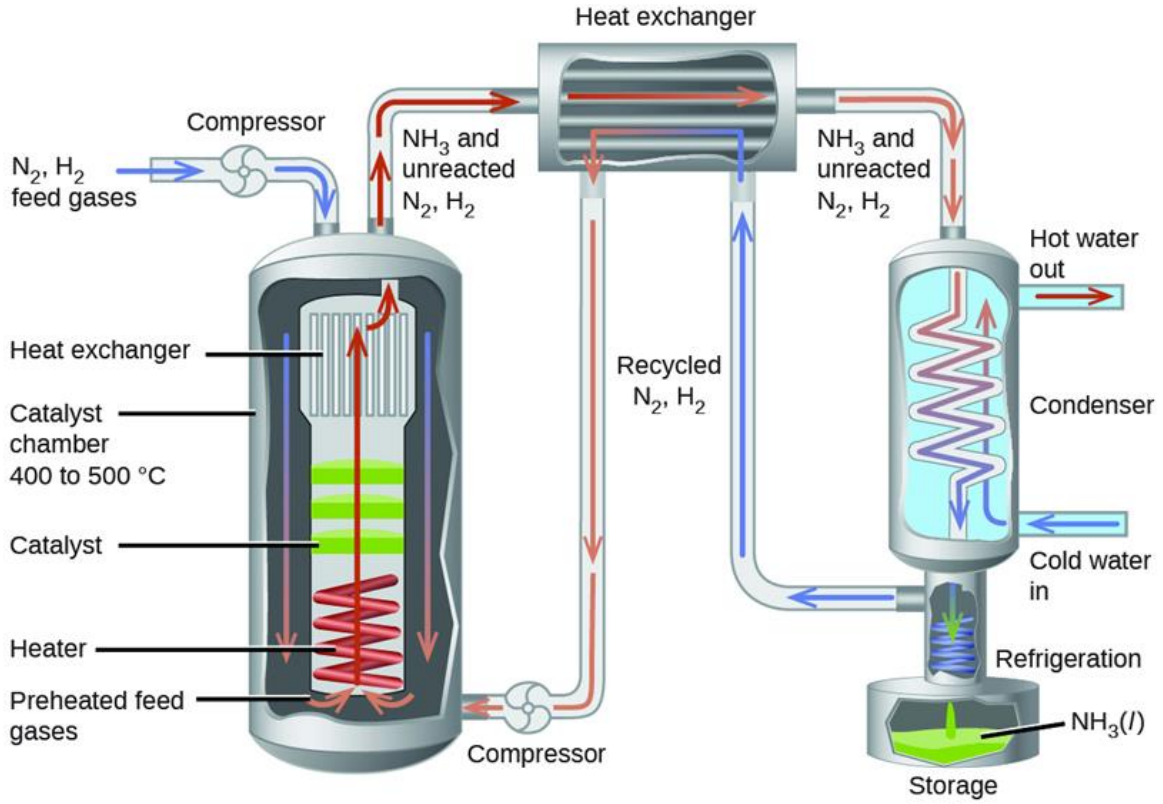

Figure 1.8. Schematic diagram of the Haber- Bosch Process for Industrial Ammonia Synthesis. (*Adopted from Ref 51*)

Over the last century, the goal of ammonia production has been to improve energy efficiency. Historical developments include transitioning from coal or lignite gasification (90-100 GJ/tNH_3) and steam methane reforming (50-55 GJ/tNH_3)[53]. Introduction of centrifugal compressors, process optimization, and improved catalyst stability have contributed to reducing energy consumption to 27 GJ/tNH_3 [39,53-56]. Modern plants, with capacities up to 3300 tNH_3/d and potential future expansions to 5000-6000 tNH_3/d, demonstrate the significant scale-up in ammonia synthesis[49,54]. The iron catalyst applied in the Haber-Bosch process has remained largely unchanged, focusing initially on stability against chemical poisons and later on catalytic activity[47,58,59]. Innovations include the introduction of cobalt to lower reduction temperatures and the use of wüstite ($Fe_{1-x}O$) for enhanced performance[56,60]. More recent advancements involve the addition of rare earth metals, iron nanoparticles, and developments in Ru-based catalysts. Ru-catalysts, active at lower pressures and large

conversions, have been used in processes like the Kellogg Advanced Ammonia Process (KAAP), though their higher cost and scarcity limit their widespread use[56,61,62].

While the Haber Bosch process is effective producing ammonia, it is also extremely energy-intensive and largely dependent on fossil fuels. This process consumes around 1% of the world's energy supply and contributes to almost 1.2% of global CO_2 emissions. The environmental impact of the Haber Bosch process is significant, contribute to greenhouse gas emissions and climate change. The dependence on fossil fuels for hydrogen production, primarily through steam methane reforming, results in substantial CO_2 emissions—about 1.6 tons of CO_2 are emitted for every ton of ammonia generated.[63] These factors underscore the urgent need for more sustainable ammonia production methods that could mitigate the environmental impact associated with traditional processes. Future developments in ammonia synthesis may involve new catalyst formulations to reduce operating pressures and temperatures, potentially lowering energy consumption further[63]. Innovations in process designs and equipment, such as the Uhde process and autothermal reforming, continue to drive improvements in efficiency and scalability[57]. As research progresses, the focus remains on enhancing catalytic performance and reducing energy inputs to meet evolving industrial demands.

1.5.3 Sustainable and Energy-Efficient Alternatives

To address these challenges, research is focused on developing sustainable and energy-efficient alternatives for ammonia production. One promising approach is electrocatalytic ammonia synthesis, which leverages renewable energy sources and function under ambient conditions. This process involves the reduction of nitrogen to ammonia using electrocatalysts, offering a potentially more environmentally friendly and energy-efficient solution. For example, Wang et al. (2017) discuss using renewable power to drive nitrogen reduction reactions, emphasizing the potential of this strategy to reduce the carbon footprint of ammonia manufacturing.

Electrocatalytic technologies for ammonia generation provide various benefits over conventional systems, particularly the Haber Bosch process. These benefits include a

significant reduction in carbon footprints, the potential for decentralized production, and the ability to operate under milder conditions.

a) Reduction of Carbon Footprint:

Electrocatalytic methods can significantly lower the carbon footprints associated with ammonia production by utilizing electricity from renewable sources such as solar, wind, and hydropower. This shift reduces reliance on fossil fuels, which are integral to the Haber-Bosch process. By harnessing renewable energy, electrocatalytic ammonia synthesis can produce ammonia with a much lower environmental impact. Research by Licht et al. (2014) demonstrated that using solar energy to power nitrogen reduction reactions could yield ammonia while minimizing carbon emissions compared to conventional methods[65]. Similarly, Zhang et al. (2020) highlighted the feasibility and environmental benefits of wind-powered ammonia synthesis, indicating a promising direction for sustainable ammonia production.[66]

b) Decentralized Production:

Electrocatalytic methods facilitate localized ammonia production, minimizing the need for extensive transportation networks and associated emissions. This decentralized approach allows ammonia to be produced closer to where it is required, lowering transportation costs and the carbon impact associated along-distance delivery. The ability to produce ammonia on-site can also enhance food security by providing fertilizers directly to agricultural regions, thereby decreasing reliance on centralized production facilities.

c) Milder Operating Conditions:

Electrocatalytic technologies usually function at lower temperatures and pressures than the Haber-Bosch process, which demands large energy inputs (about 400-600 °C and 100-200 atm). Operating under milder conditions not only decreases energy requirements but also enhances the sustainability of ammonia production. Shipman and Symes show electrocatalytic nitrogen reduction can be performed at standard temperature and pressure, making it a significant advantage over traditional methods.[67]

1.5.4 Challenges and Future Directions

Despite their potential, electrocatalytic methods face several challenges, including achieving high efficiency, selectivity, and stability of electrocatalysts. Ongoing research is focused on

developing advanced materials and optimizing reaction conditions to overcome these obstacles. Integrating renewable energy sources with electrocatalytic systems also requires significant advancements in energy storage and grid management.

a) Efficiency and Selectivity: Achieving high efficiency and selectivity in electrocatalytic ammonia production is tough due to the competing reactions and the inert nature of nitrogen molecules. Researchers are exploring various strategies, such as the development of novel catalyst materials and reaction environments that favour nitrogen reduction over hydrogen evolution. For instance, Montoya et al. highlight the importance of tuning the catalyst's electronic properties to enhance NRR selectivity.[68]
b) Stability of Electrocatalysts: The stability of electrocatalysts over prolonged periods of operation is another significant challenge. Many catalysts suffer from deactivation due to poisoning, sintering, or structural degradation under reaction conditions. Developing robust materials that can maintain high activity and selectivity over long periods is crucial. Research by Seh et al. has focused on identifying and engineering catalysts with enhanced durability and resistance to degradation.[69]
c) Integration with Renewable Energy Sources: Integrating renewable energy sources with electrocatalytic systems presents additional challenges, particularly in terms of energy storage and grid management. Renewable sources of energy like solar and wind are intermittent, necessitating advanced energy storage solutions to make sure a stable and continuous supply of power for ammonia production. Studies such as those by Turner et al. emphasize the need for innovations in energy storage technology and smart grid management can effectively utilize renewable energy for electrocatalytic ammonia production.[70]

1.6 An Introduction Covalent Organic Framework: Design and Synthesis

Synthetic linear polymers, designed with repeating monomer units linked by covalent bonds to form long and unbranched chains, plays a important role in many modern applications like packaging, textiles, adhesives, coatings, biomedical applications, and electrical insulation.[71-72]. However, their limited porous volume restricts their use in gas storage, separation, catalysis, and charge storage.[73] To address these issues, hyper-crosslinked and porous organic polymers (POPs) offer a viable alternative. These materials, built from aromatic or aliphatic

monomers, form highly interconnected greater surface area and porosity in two- or three-dimensional structures when compared to linear polymers. (Figure 1.9-10) Synthesized through methods such as Friedel-Crafts alkylation and Friedel-Crafts condensation polymerization, HCPs and POPs offer exceptional chemical stability and are used in environmental cleanup, energy storage, gas storage, separation, catalysis, and sensing.[74-76] Despite their advantages, the lack of crystallinity in HCPs and POPs poses challenges in understanding their structure-property relationships. The goal is to utilize their full potential, it's essential to control their topology, morphology, and directional growth, which helps in understanding their structure-property relationships.[73] Both experimental and computational methods are essential to achieving this control, leading to significant technological advancements. High degrees of polymerization with controlled directionality and structural periodicity require precise integration of building units and predictable topological evolution. However, maintaining proper geometry, porosity, and molecular-level properties during polymer growth remains challenging.[77] Covalent Organic Frameworks (COFs) are a breakthrough in polymer research that has gained worldwide attention (Figure 1.11).[78] Unlike traditional polymers, COFs allow for molecular-level design, enabling unprecedented manipulation of primary and higher-order arrangements. These polymers grow in a reticular manner, creating 2D or 3D porous crystalline formations linked together by strong covalent connections. This structure allows for predictable composition and properties. The templated synthesis of COFs creates confined void spaces and exposed surfaces that interact photons, excitons, electrons, holes, ions, and molecules, giving a molecular platform for diverse applications spanning materials chemistry, physics, and technology.[79-80] COFs are used in gas separation[81], electrocatalysis[82], chemical sensing[83], optoelectronics[84], energy conversion[85], and energy storage[86].

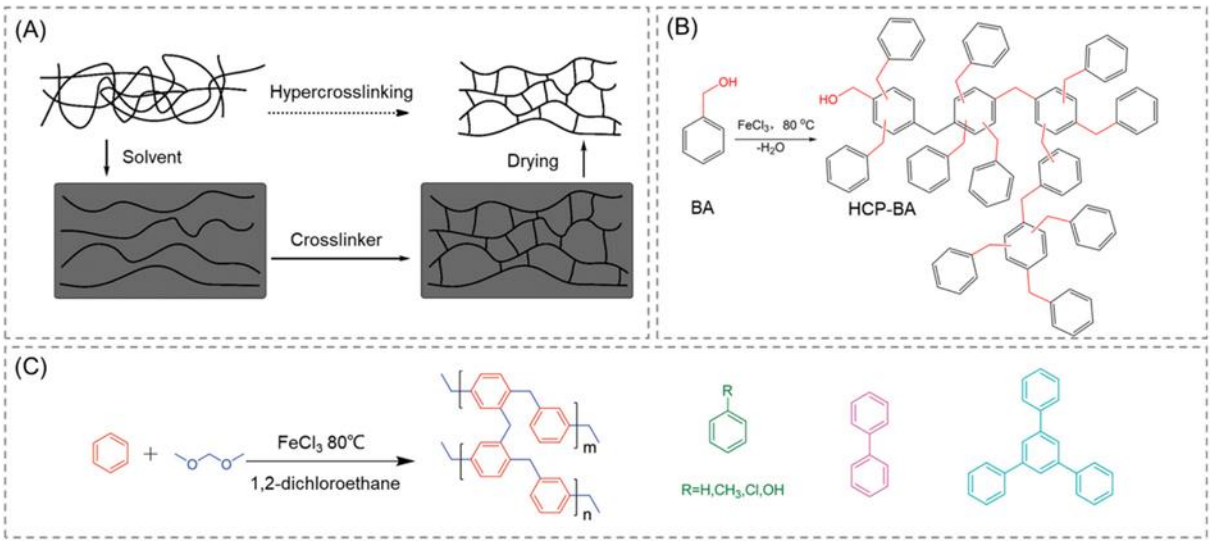

Figure 1.9: (A) Schematic mechanism of the post-crosslinking strategy (B) The self-condensation synthesis of hyper-crosslinked polymer-1,4-benzenedimethanol (HCP-BDM) is illustrated in the scheme. (C) Scheme depicting the usual synthetic road to network structure using the knitting method. (*Adopted from Ref 74*)

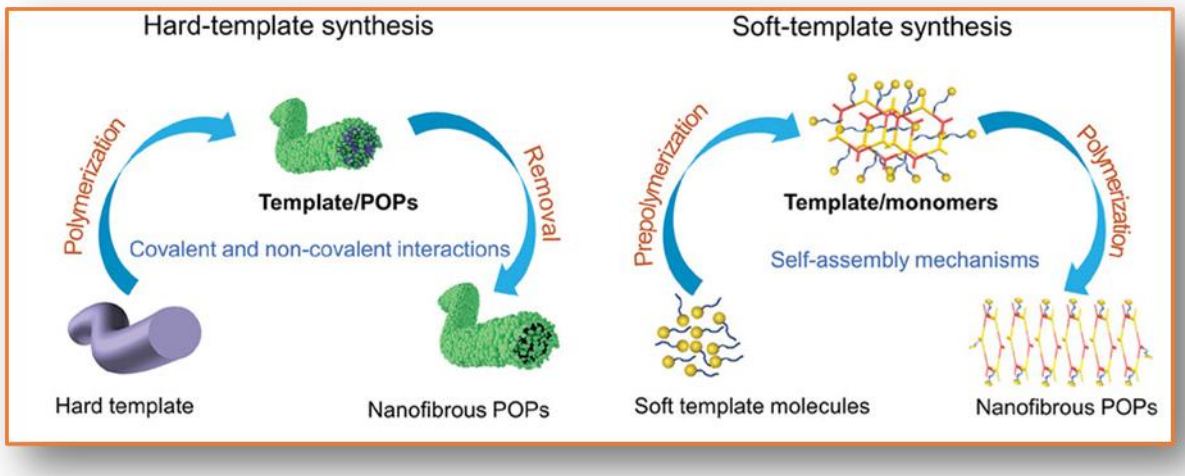

Figure 1.10. Synthesis strategy for preparation of nanofibrous POPs. (*Adopted from Ref 75*)

explored over the years (Figure 1.12-13). Compared to earlier boronate ester linkages, reversible imine bond formation offers improved structural stability against solvents and chemicals.[86]

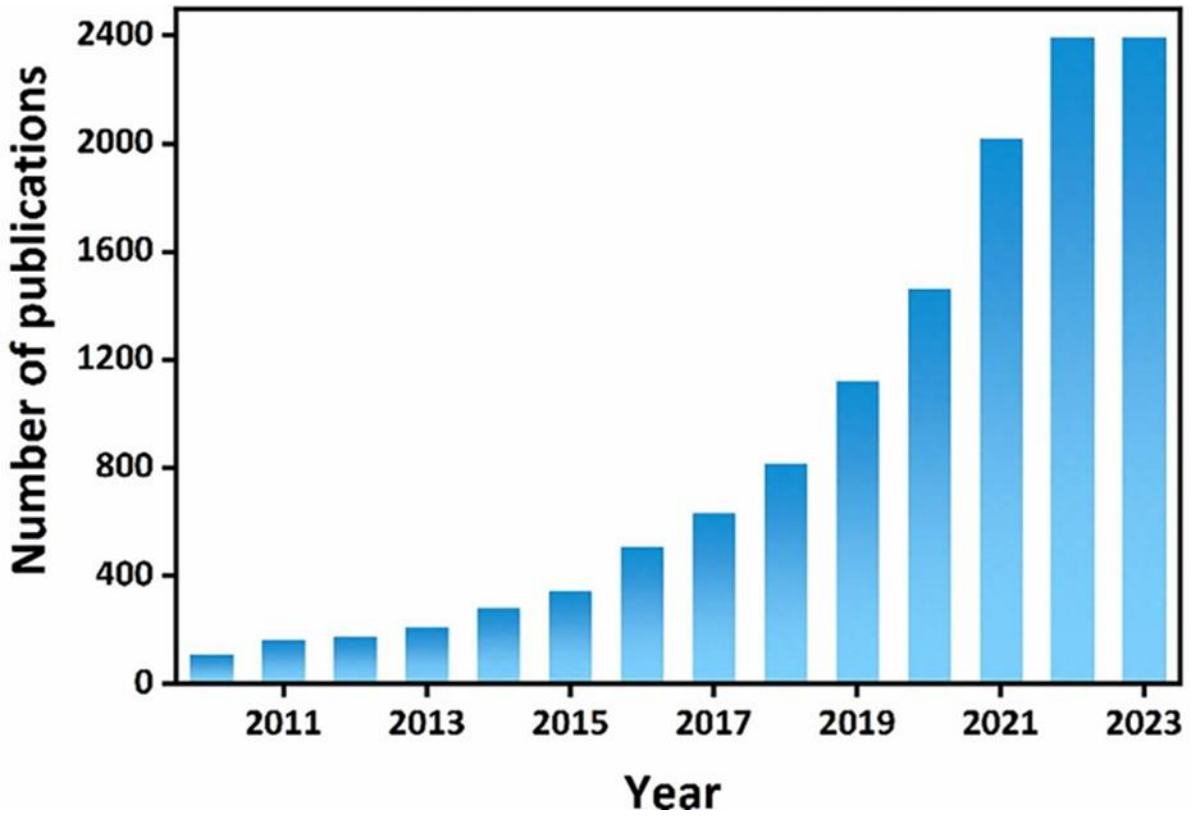

Figure 1.11: Recent literature reported on COFs over the years. (*Adopted from Ref 86*)

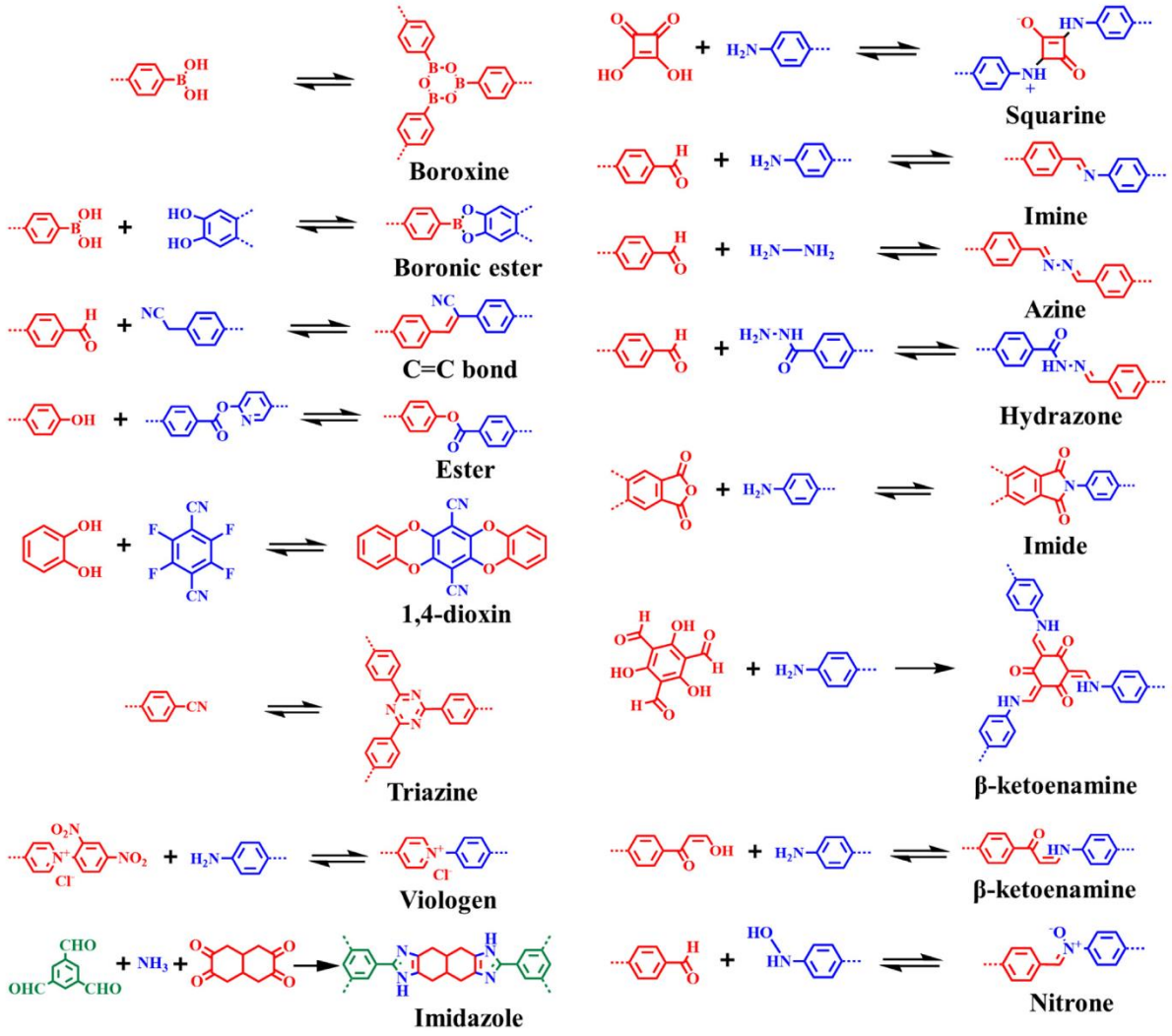

Figure 1.12. Various types of linkages for formation of COF. (*Adopted from Ref 82*)

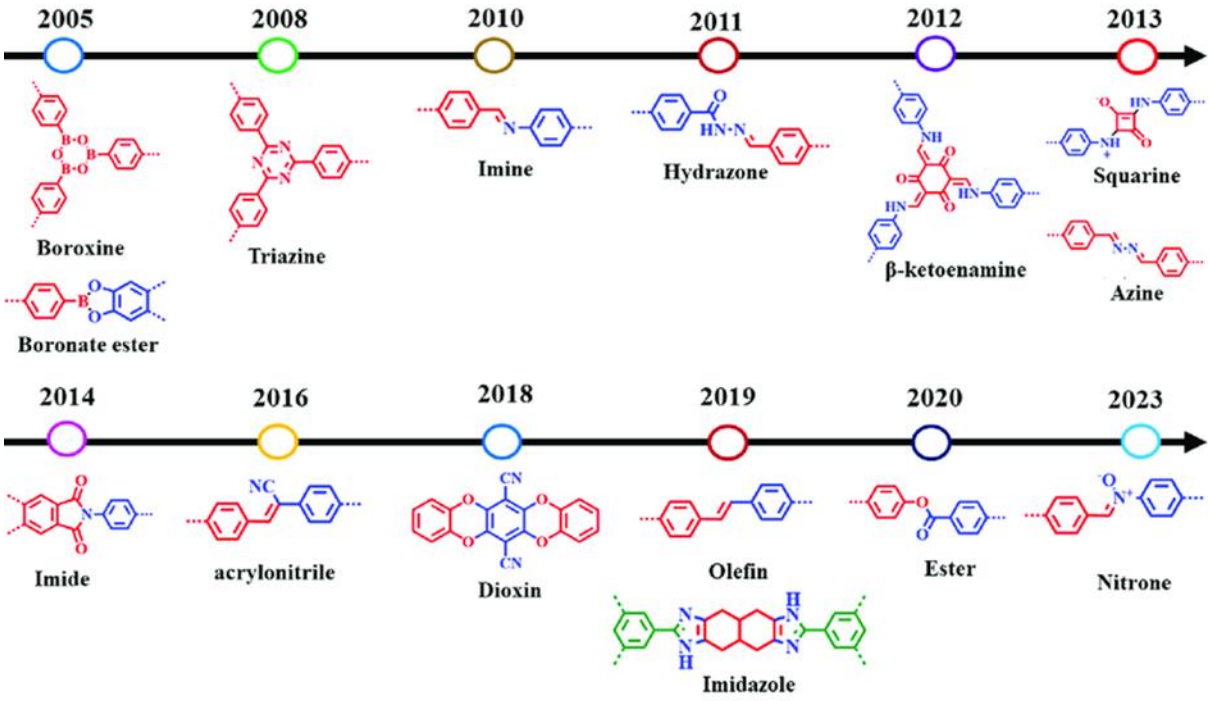

Figure 1.13. Development of COF linkages over years. (*Adopted from Ref 82*)

Yaghi and his coworkers developed the first general synthesis strategy for single crystal of a COF using dynamic chemistry with a modulator approach. In their method, they used aniline as a modulator, along with another modulator of the same type to promote crystallization.[88] However, this process was not widely applicable to general crystals and was very slow, often requiring more than 2-4 weeks to form a single crystal due to the use of a weak acid and the modulator approach. Due to these limitations this method still faces challenges. (Figure 1.14)

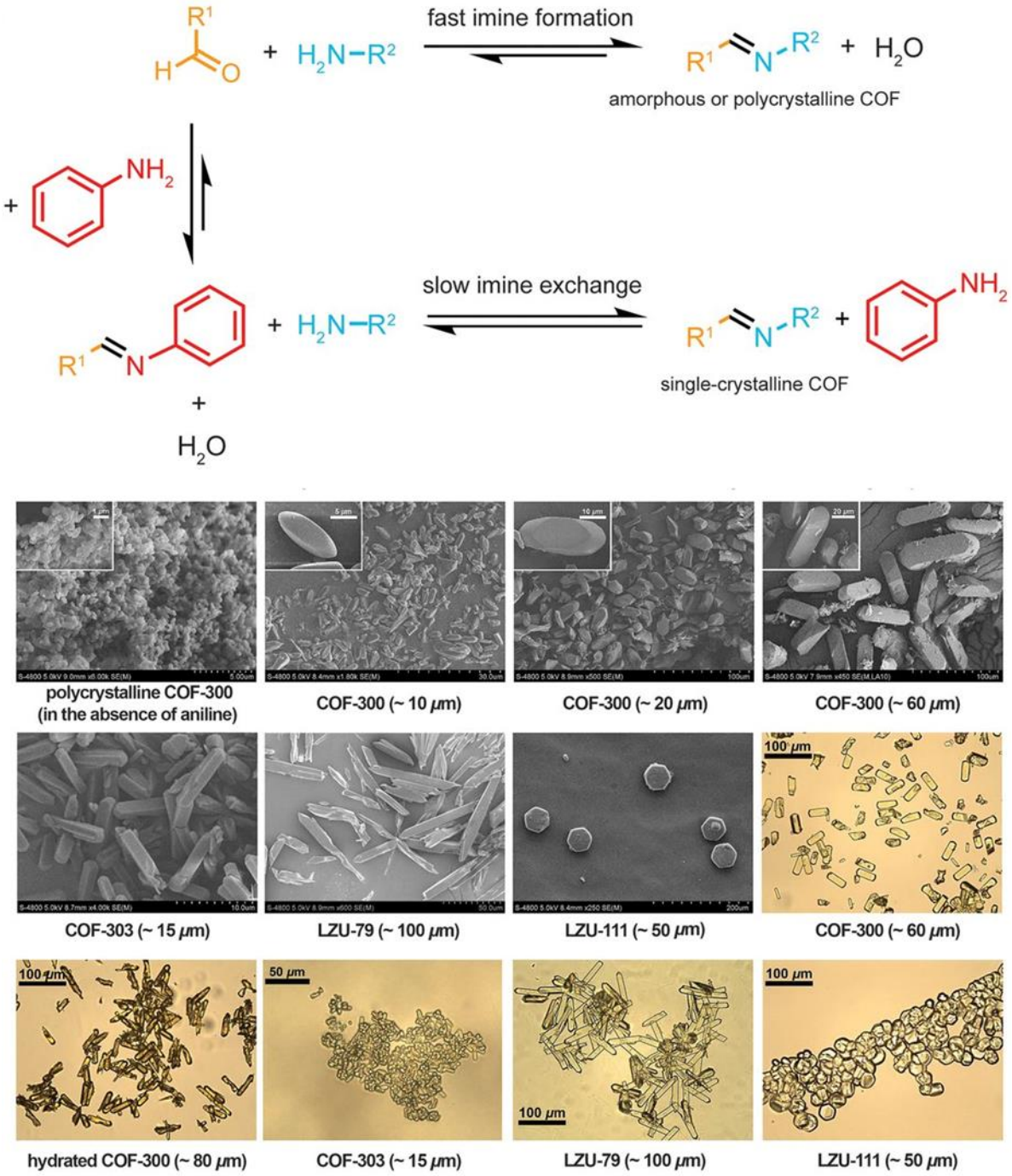

Figure 1.14. Crystal development of massive imine-based COFs regulated by aniline and Scanning electron microscopy (SEM) and optical microscope photographs of single-crystalline COFs (*Adopted from Ref 88*)

To overcome these challenges, Wang et al. introduced a more efficient method using CF_3COOH as a stronger catalyst and $CF_3CH_2NH_2$ as a compatible modulator. This innovative combination significantly accelerated the reaction kinetics, allowing for the formation of COF crystals within 1-2 days. These crystals were suitable for analysis by single-crystal X-ray

diffraction (SCXRD). The growth rates of single-crystal COFs were markedly enhanced, achieving an 83-fold increase for COF-300 and a 57-fold increase for LZU-306. Furthermore, this approach provided a versatile framework for COF synthesis, successfully synthesizing 16 different COFs using this method.[89] (Figure 1.15)

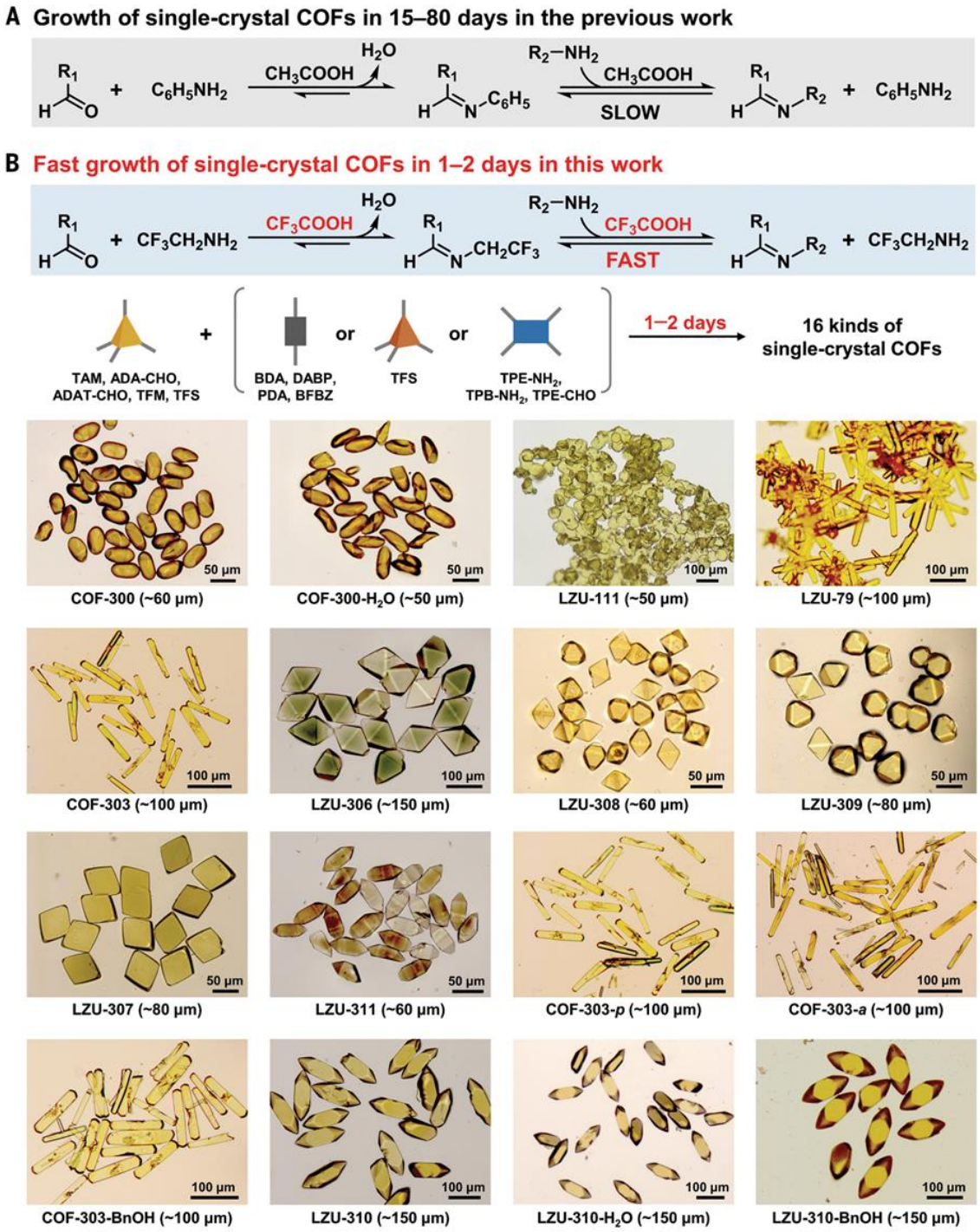

Figure 1.15. Rapid development of large-sized single-crystal COFs. (*Adopted from Ref 89*)

Additionally, interlayer hydrogen bonding stabilization in β-ketoenamine-connected frameworks enhances the chemical robustness of COFs.[90] The sp^2-hybridized Schiff bond formation guides the spatial orientation of the skeleton in 2D or 3D, directing chain growth according to a predesigned topology diagram. The complementary geometry of aldehydes and amines, along with van der Waals forces and hydrogen bonding are examples of non-covalent interactions, determine COF topology (Figure 1.16-18). Planar monomers typically control the propagation of polymer backbones in a polygonal space on 2D x-y planes, leading to a layered structure. Substantial π-π stacking interactions of aromatic building blocks enable alignment of 2D covalent sheets along the z-direction results in fully ordered π-arrays and 1D nano-porous channels.[91]

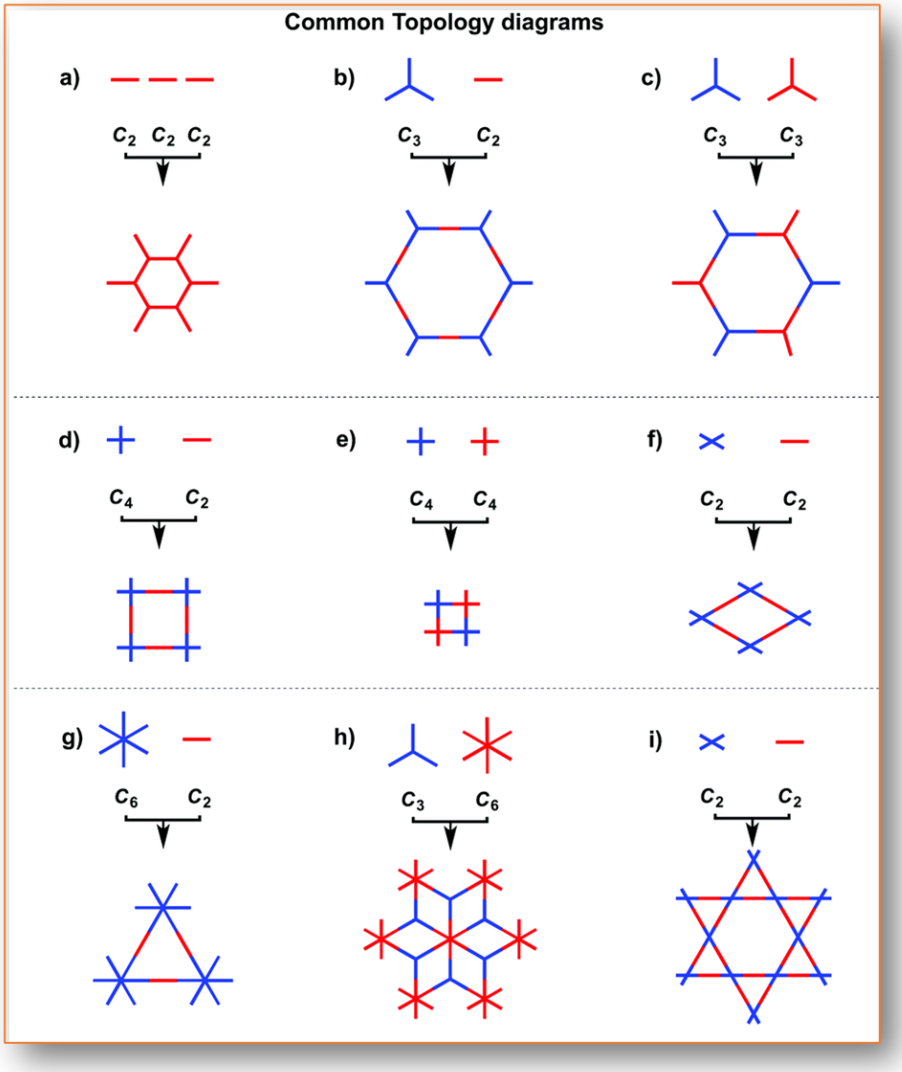

Figure 1.16. Common single stage topologies for COF synthesis. (*Adopted from Ref 91*)

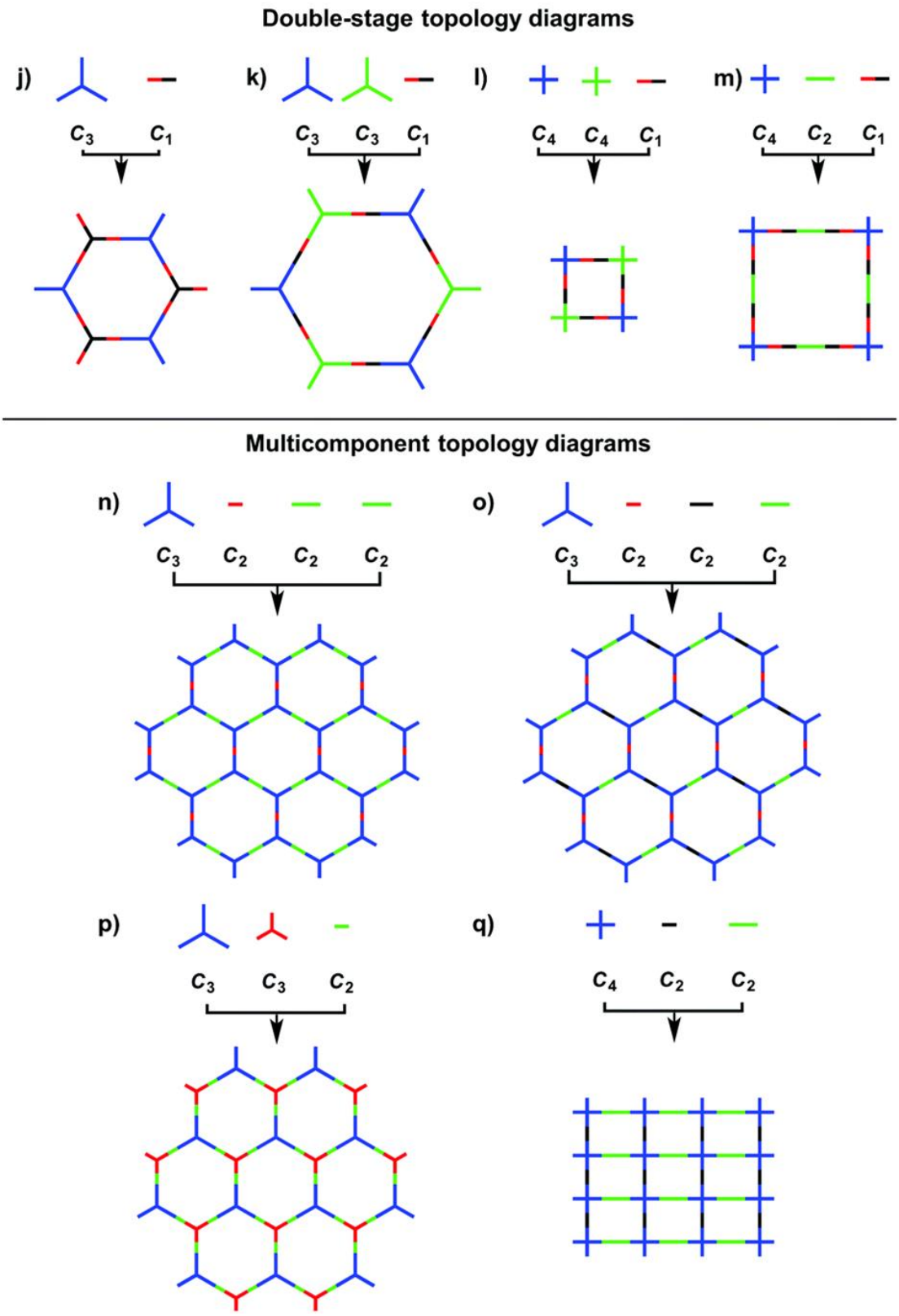

Figure 1.17. Common double stage and multi-component topologies for COF synthesis. (*Adopted from Ref 91*)

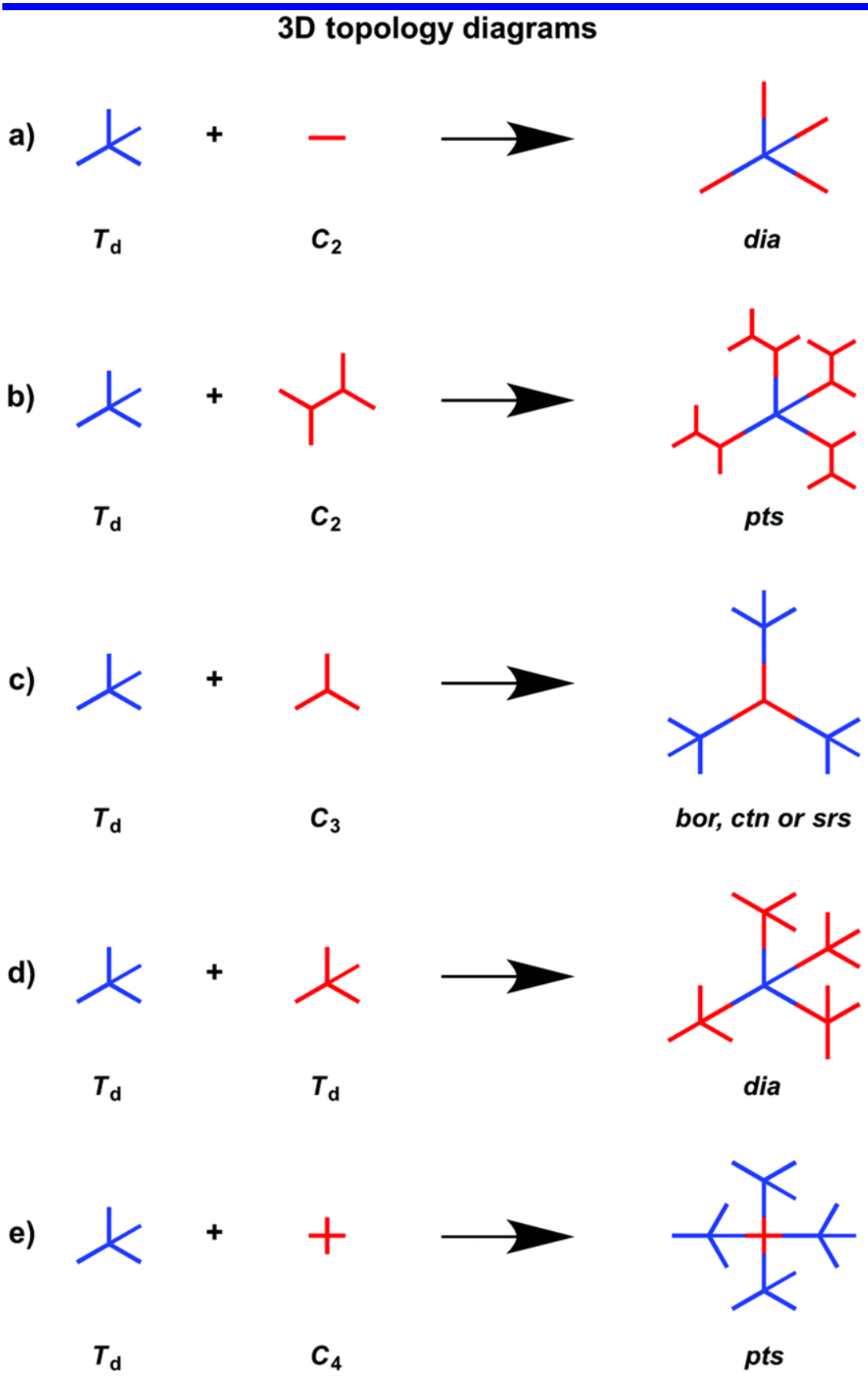

Figure 1.18. Common 3D topologies for COF synthesis. (*Adopted from Ref 91*)

Research on COF and COF-derived materials for various applications has rapidly expanded, offering controllable surface areas and stable frameworks for heterogenous catalysis. Enhancing performance involves chemically tuning the electronic activity of the framework by increasing the number of electron-donating heteroatoms (N and O) per unit cell. COFs, with their conjugated skeletons and anchoring sites, provide efficient pathways for catalytic surface area, charge carrier transport, including electrons, holes, and ions. The synthesis of COFs (Covalent Organic Frameworks) has advanced significantly since their inception, primarily because of the fundamentals of dynamic covalent chemistry. These dynamic connections enable the reversible creation of covalent bonds, enabling error correction during the assembly process and resulting in highly ordered structures. Various synthesis methods have been developed, each presenting distinct advantages and challenges that alter the characteristics of the produced COFs, such as porosity, stability, and crystallinity (Figure 1.19).[92] Solvothermal synthesis involves heating monomers in a sealed environment,[93] while ionothermal synthesis utilizes ionic liquids to facilitate reactions at elevated temperatures.[94] Microwave synthesis offers rapid reaction times and improved porosity,[95] and mechanochemical methods leverage mechanical energy to induce solvent-free reactions.[96] Sonochemical synthesis uses ultrasonic waves to promote reactions, and light-promoted synthesis is driven by light to enable precise control over reaction conditions. Schiff bond-based COFs are generated by condensation reactions of aldehydes and amines, allowing for efficient and scalable production. The dynamic nature of Schiff bonds enables responsiveness to external stimuli, positioning these materials for potential applications in self-healing technologies.[97] The choice of synthesis method is critical for tailoring COFs to specific applications, highlighting the importance of understanding the underlying chemistry involved in their formation. By leveraging these diverse synthesis strategies, researchers can design COFs with tailored properties for an extensive variety of applications, including catalysis, gas storage, and more.

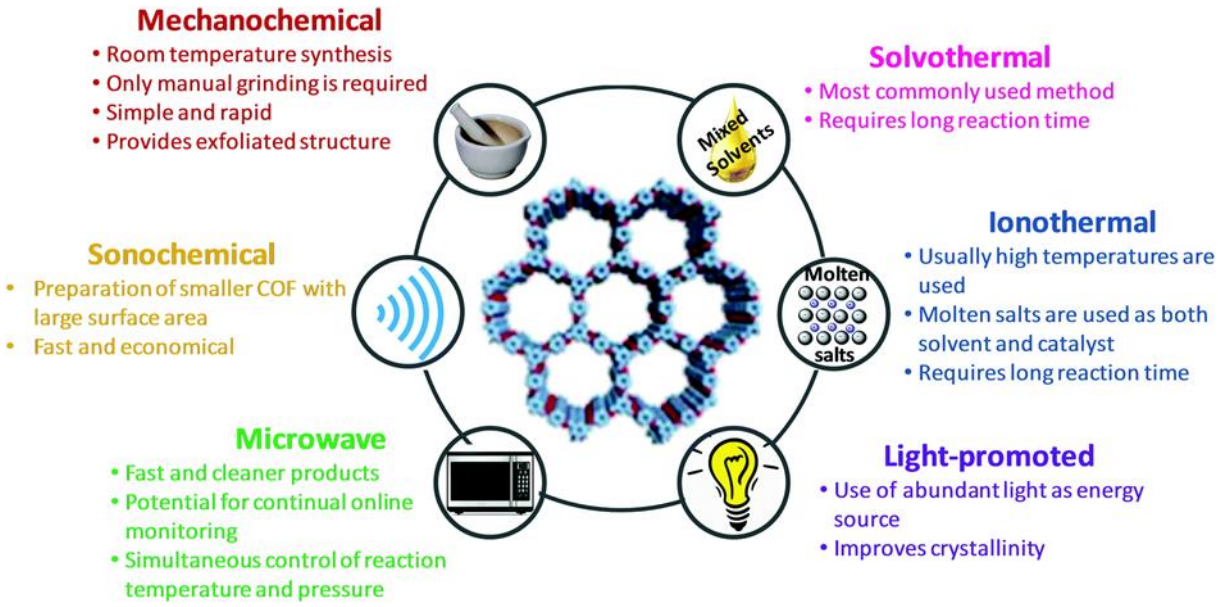

Figure 1.19. Various synthesis methods of COFs, such as Synthesis methods include mechanochemical, solvothermal, ionothermal, sonochemical, microwave, and light-promoted. (*Adopted from Ref 92*)

COFs have various benefits over other classic catalytic materials like metal-organic frameworks (MOFs) and zeolites:

a) Structural Regularity:

COFs provide a higher degree of structural regularity than zeolites, leading to more predictable catalytic behaviour. The ability to design COFs with specific pore sizes enhances selectivity in catalytic reactions, a challenge often faced by zeolites due to their complex structures.

b) Organic Composition:

Unlike MOFs, which often include metal centers, COFs are composed entirely of organic materials. This characteristic simplifies synthesis and reduces the risk of metal leaching during catalytic processes, a significant concern with MOFs.

c) Post-Synthetic Modification:

COFs can be readily modified after synthesis to introduce additional functionalities, enhancing their catalytic properties. This flexibility is less common in traditional materials, where modifications can be more challenging.[98]

d) Recyclability:

COFs have demonstrated potential for reusability in catalytic applications, as their organic nature allows for easier recovery and recycling compared to metal-based catalysts, which can suffer from leaching and loss of activity over time.[99]

COFs' unique features and benefits make them a very promising family of materials for catalysis and other applications. Their capability to synthesized with high precision, combined with their tunable properties and stability, opens new avenues for research and development in materials science and catalysis. As research continues to expand the understanding of COFs, their potential applications will likely broaden, making them a focal focus in the search for effective and long-lasting catalytic systems.

1.7 Applications of COFs

1.7.1 Gas Storage and Separation

One of the key features of COF is their ability to tune functional groups and pore sizes, making them ideal candidate for gas storage and separation. In last decade, gas capture has gained a lot attention due to the large amounts of pollutant gases, such as H_2, CO_2, and CH_4 emitted by industries. This has brought up a serious attention to develop material to capture these gases effictvitly.[100] Three-dimensional COFs have better storage capacities than two-dimensional layered structures due to their increased surface area and pore volumes. For example, a three-dimensional COF-102 with a Langmuir dimension of 4650 m^2/g has a greater methane storage capacity of 25 wt% at 298 K and 80 pressures. Furthermore, COF-102 and COF-103 have strong hydrogen uptake, with 72.4 and 70.5 mg/g respectively.[101] 3D COF comprising C-O single bonds in the skeleton of the structure demonstrates an S-shaped isotherm for diverse gases such as CO_2, C_2, and C_3 hydrocarbons; moreover, they show special selectivity towards C_3H_4 from C_3H_4/C_3H_6 combinations.[102]

1.7.2 Sensing

The building blocks of COFs can be varied to enhance their electrochemical or chemical sensitivity to light, enabling their use as sensors. Sensitive binding groups can be incorporated either directly into the monomers during synthesis or through post-synthetic modifications, thereby creating stable sensors suitable for various applications. In recent years several reports have been publish on COFs based sensors. COFs have been employed in sensor technology to detect gases like volatile organic compounds (VOCs) and toxic gases. Chen et al. created fluorescent hydrazine connected COF (XB-COF) for selective detection of Pd^{2+} ions, obtaining a limit of detection (or LOD) of 0.29 µM. Additionally, incorporated the COF into a filter to create a practical sensor for visual detection of Pd^{2+} ions (Figure 1.20).[103]

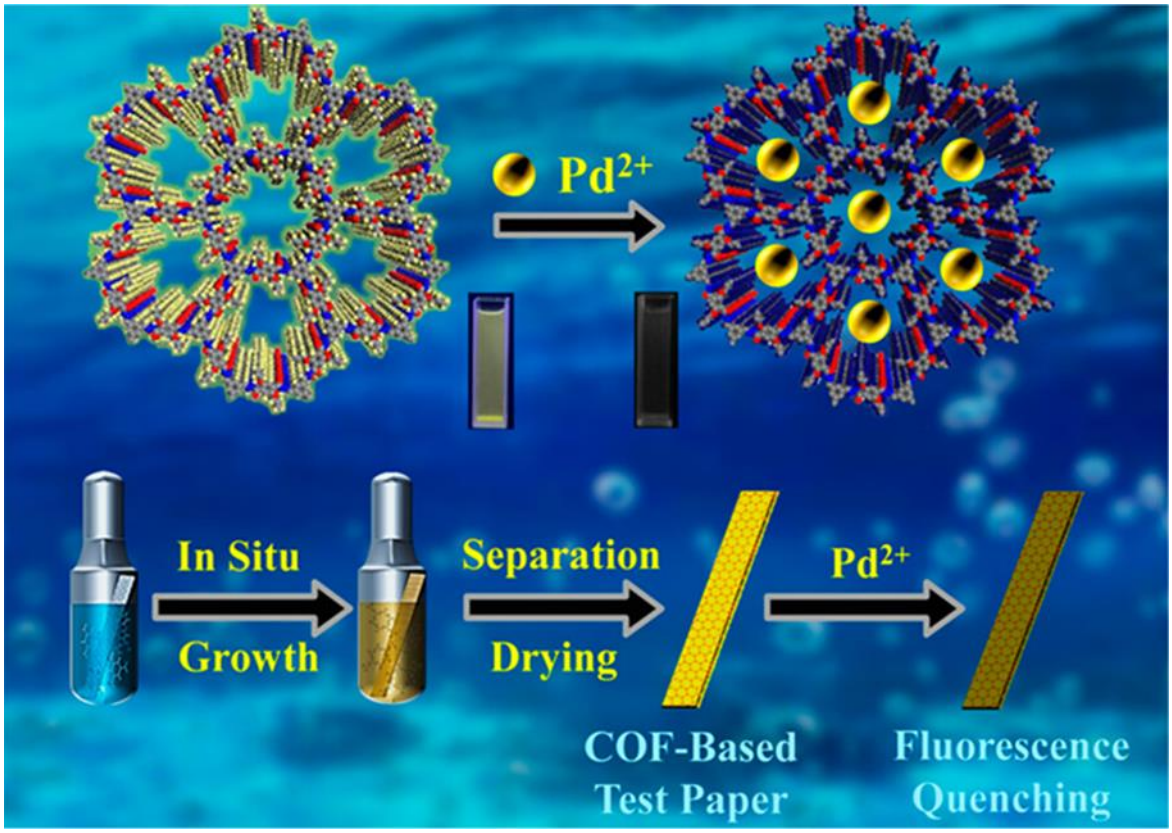

Figure 1.20. Fluorescent quenching of XB-COF, and the production and fluorescence quenching of XB-COF-based test paper. (*Adopted from Ref 103*)

1.7.3 Drug Delivery

COFs are less explored in drug delivery compared to MOFs. However, in recently, substantial research efforts were focused to investigating and expanding potential applications for the COFs in this area. In several studies, COFs have been utilized as delivery vehicles for anti-

cancer drugs or photosensitizers. Feng and co-workers have synthesized Cage-COF-TT for drug delivery applications, demonstrating a high drug loading capacity along with an effective medication release profile in a simulated bodily fluid environment.[104] Jiang et al. synthesized a light activated and The COFs were hypoxia-responsive azo bond-containing and nano in size, with photosensitive substances chlorin e6 (Ce6) and the hypoxia-activated medication tirapazamine (TPZ) immobilised. When administered to tumor locations, the Schiff base-containing COF degrades, resulting in the release of TPZ. During laser irradiation, Ce6 produces reactive oxygen species (ROS), which contribute to the selective death of cancer cells, enhance tumor hypoxia, and induce the creation of reductase (Figure 1.21).[105]

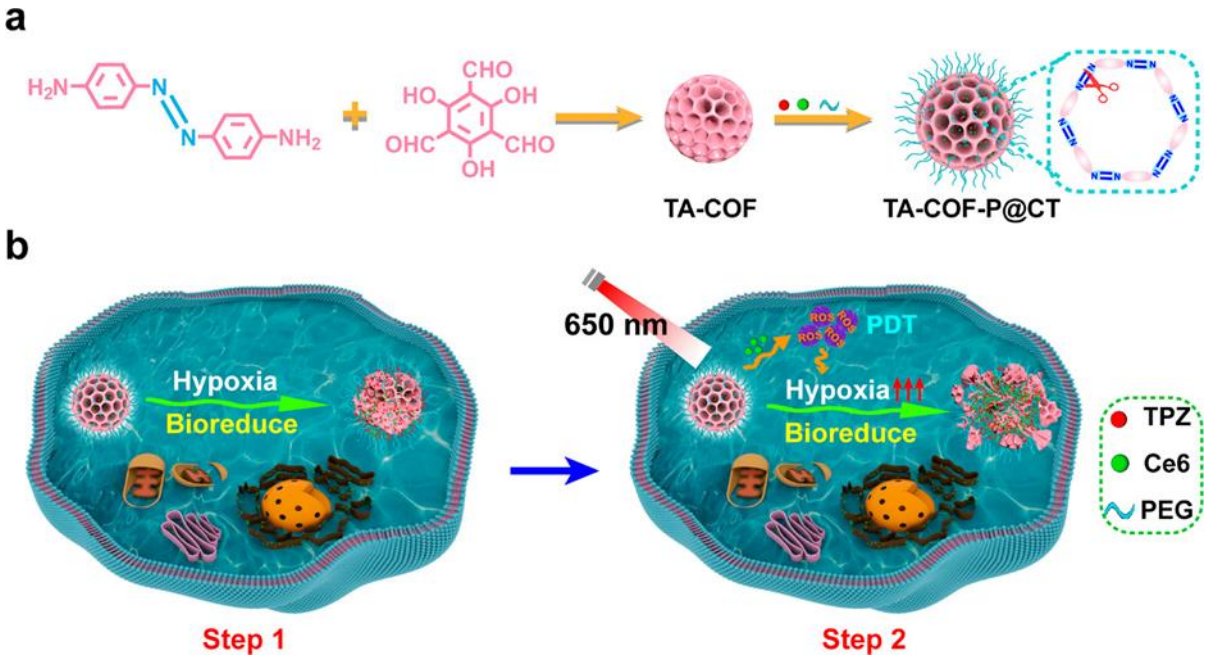

Figure 1.21: (a) Illustration of the synthesis of TA-COF and TA-COF-P@CT for combination cancer treatment. (b) Schematic depicting the two-step light-activated hypoxia-sensitive medication delivery for cancer therapy. (*Adopted from Ref 105*)

1.7.4 Energy storage

Covalent Organic Frameworks are developing as attractive energy storage materials due to their large surface area and configurable pore geometries. In batteries, COFs enhance electrode performance by increasing charge storage and transfer efficiency. For supercapacitors, their large surface area and tailored chemical properties improve energy and power density, enabling rapid charge and discharge. COFs' unique attributes make them

valuable for advancing energy storage technologies. Vaidhyanathan and coworkers investigated the supercapacitor performance of three Schiff base-based COFs with pyridyl-hydroxyl groups. These IISERP-COFs, stabilized by keto enol tautomerism and H-bonding, feature abundant triazine and pyridyl groups that enable fast and substantial storage of charge through reversible H^+ interactions. High surface area contributes to electric double-layer capacitance (EDLC), while redox-active sites enhance pseudocapacitive energy storage. In a three-electrode configuration, IISERP-COF-10 had the highest specific capacitance of 546 F/g at 500 mA/g, then followed by IISERP-COF12 at 400 F/g and IISERP-COF11 at 310 F/g, which corresponded to the corresponding surface areas (IISERP-COF10: 1233 m^2/g; IISERP-COF11: 921 m^2/g; IISERP-COF12: 1067 m^2/g). IISERP-COF12 has a greater OH group the material's composition, adopting the keto form, showed greater affinity for protic electrolytes, resulting in the highest pseudocapacitive contribution [106]

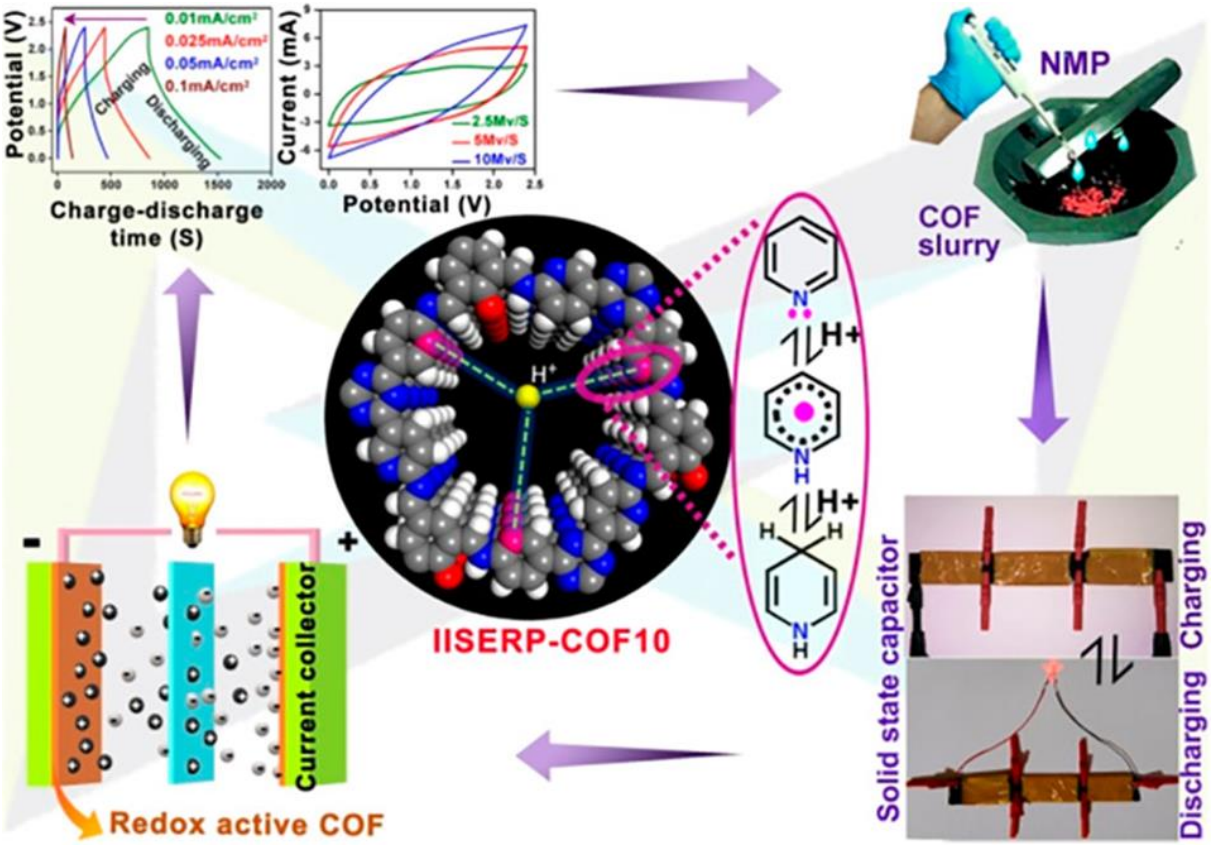

Figure 1.22: Photographic depiction of the electrode, solid-state apparatus, mechanism, and performance. (*Adopted from Ref 106*)

1.7.5 Heterogeneous Catalysis

Heterogeneous catalysis involves reactions where the catalyst and reactants are in different phases, such as gas-solid or liquid-solid systems. This type of catalysis is favored in industrial processes due to its stability and ease of catalyst recovery through methods like filtration or centrifugation. The ability to recover and reuse catalysts is a significant advantage in large-scale manufacturing, where catalyst recyclability is crucial.[107] However, classical heterogeneous catalysis frequently suffers from problems such as low selectivity, slower reaction kinetics, and longer reaction times compared to homogeneous catalysis.[108] Despite these challenges, recent advancements have shown that these limitations can be mitigated by employing heterogeneous nanocatalysts, which offer enhanced efficiency and selectivity.

The use of highly porous materials such as COFs, in heterogeneous catalysis has garnered significant interest. COFs are particularly promising due to their periodic framework structure, high porosity, and large effective surface area, which offer many and easily accessible active sites for catalytic reactions. These properties enable COFs to overcome some of the traditional limitations of heterogeneous catalysis, making them a viable option for efficient and selective transformations.[109-111] Despite these benefits, the use of COFs in catalysis is currently underexplored when compared to other porous materials, presenting a fertile area for further research and development. COF-based heterogeneous catalysts may be produced by carefully leveraging the unique qualities of COFs, such as their variable pore size, large surface area, and customizable chemical activity. These properties allow for the precise modification of COFs to enhance their catalytic activity, selectivity, and stability, making them highly effective for various catalytic processes (Figure 1.23).[109] The development of COF-based electrocatalysts typically involves strategies such as heteroatom incorporation, metalation, encapsulation of active sites, and the use of COF-derived materials (Figure 1.24). In this thesis, we will employ encapsulation of active sites within COFs and metalation strategies. These approaches allow for the precise tuning of COF properties to optimize their activity, selectivity, and stability in various electrocatalytic applications.[111]

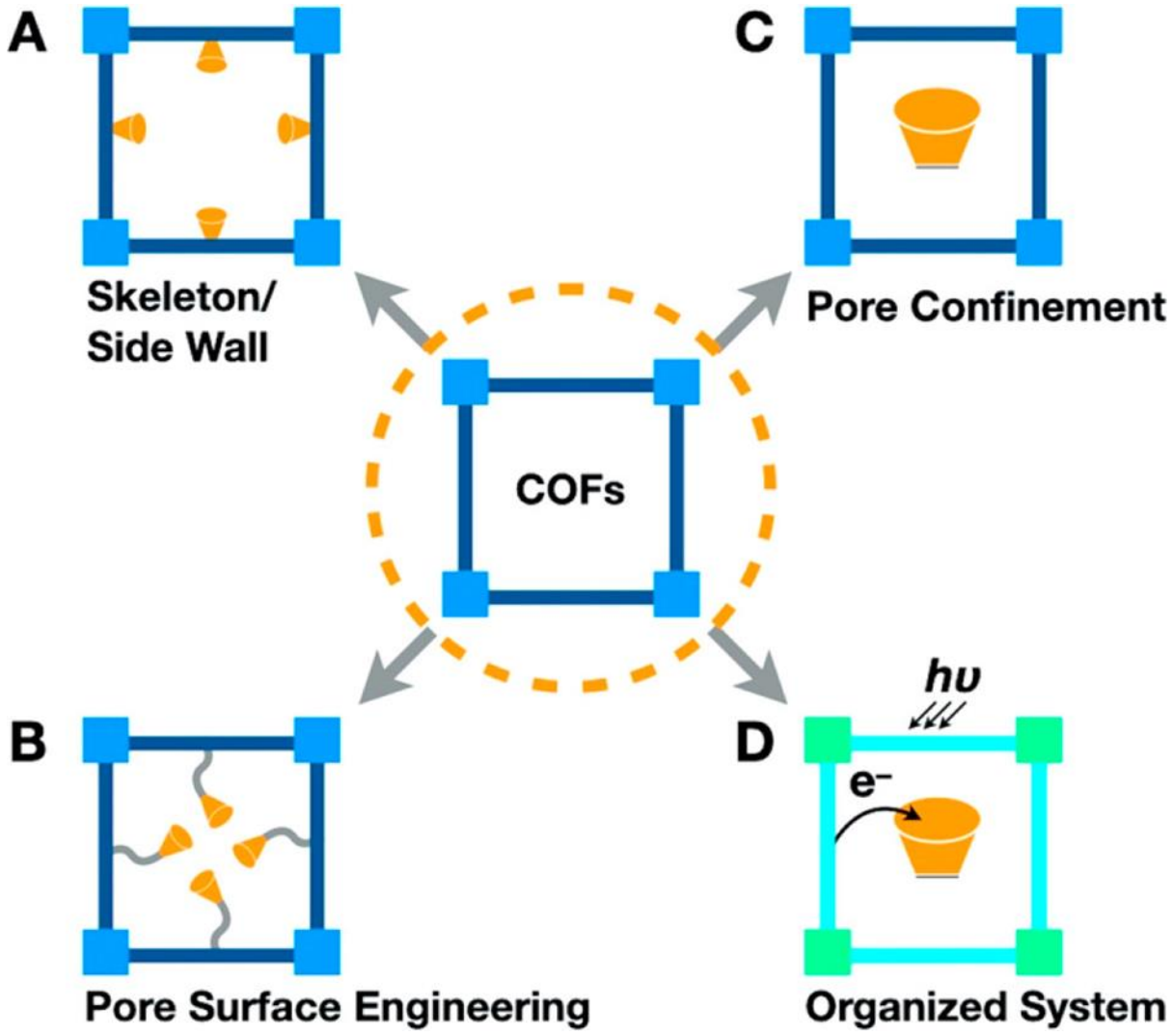

Figure 1.23: Designing COFs for heterogeneous catalysis using (A) skeleton and side wall, (B) pore surface engineering, (C) pore confinement, and (D) systematically structured systems. (*Adopted from Ref 109*)

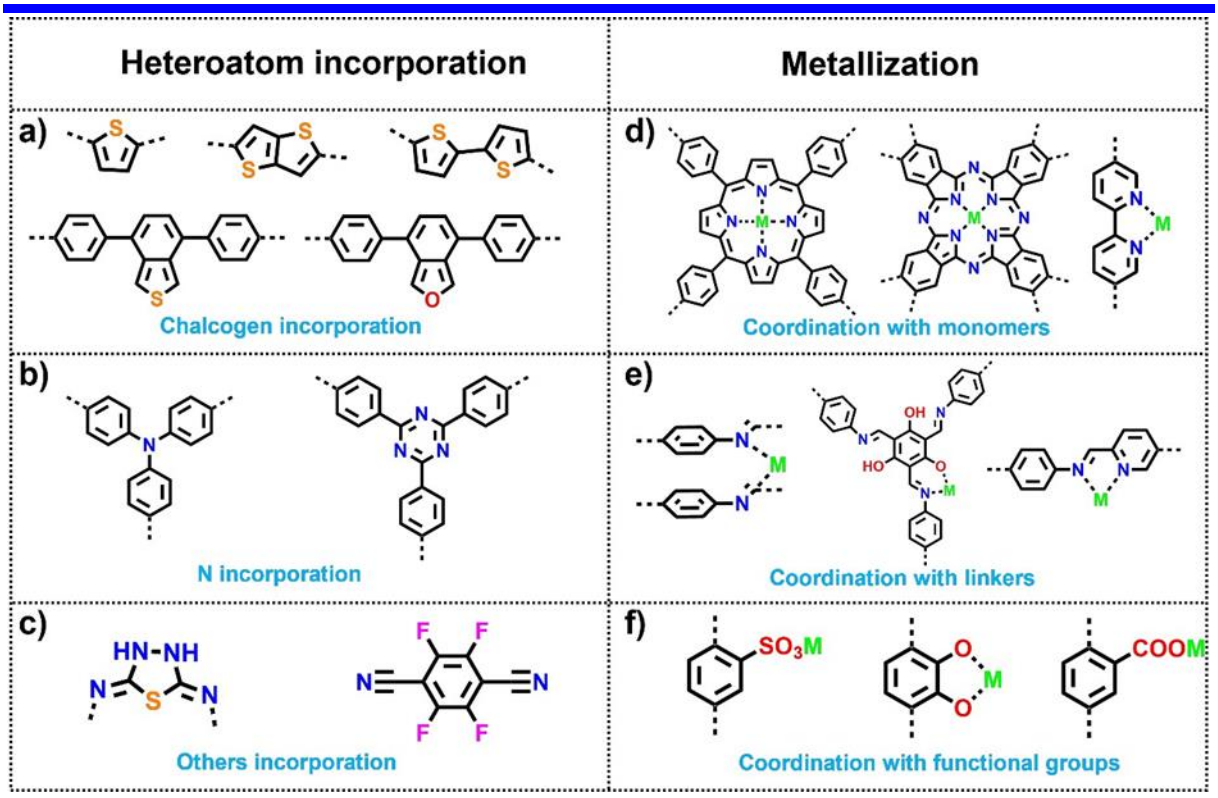

Figure 1.24: Heteroatom doping and metalation strategies for preparation of COF-based catalysts. (a) Chalcogen incorporation. (b) N element incorporation. (c) Other elements incorporation. (d). Metal coordination with monomers. (e). Metal coordination with linkers. (f). Metal coordination with functional groups (*Adopted from Ref 111*)

1.8 Electrochemical ammonia synthesis

Electrochemical ammonia synthesis is a potential method for generating ammonia directly from nitrogen and water using electrical energy, providing a more environmentally friendly alternative to the conventional HB process. This method involves three primary reactions: the electrochemical nitrogen reduction (NRR), electrochemical nitrate reduction (NO_3RR), and electrochemical nitrite reduction (NO_2RR). The NRR process is central to this approach, where N_2 gas is converted to ammonia (NH_3) at the cathode in the presence of an appropriate catalyst, such as transition metals or metal complexes. This reaction is highly significant because of its potential to directly used in renewable energy and reduce reliance on energy-intensive ammonia production methods. Recent advancements in catalyst design, include the discovery of innovative materials and the adjustment of reaction conditions, have improved the efficiency and selection of the NRR. Challenges remain, such as enhancing catalyst stability

and selectivity while managing reaction kinetics and minimizing hydrogen evolution side reactions. Nonetheless, ongoing research into new catalysts and reaction strategies continues to advance the field, making electrochemical ammonia synthesis a compelling area of study for sustainable chemical production. A detailed flowchart outlining the systematic protocol for catalyst design and ammonia production in electrochemical synthesis is proposed (Figure 1.25).[112]

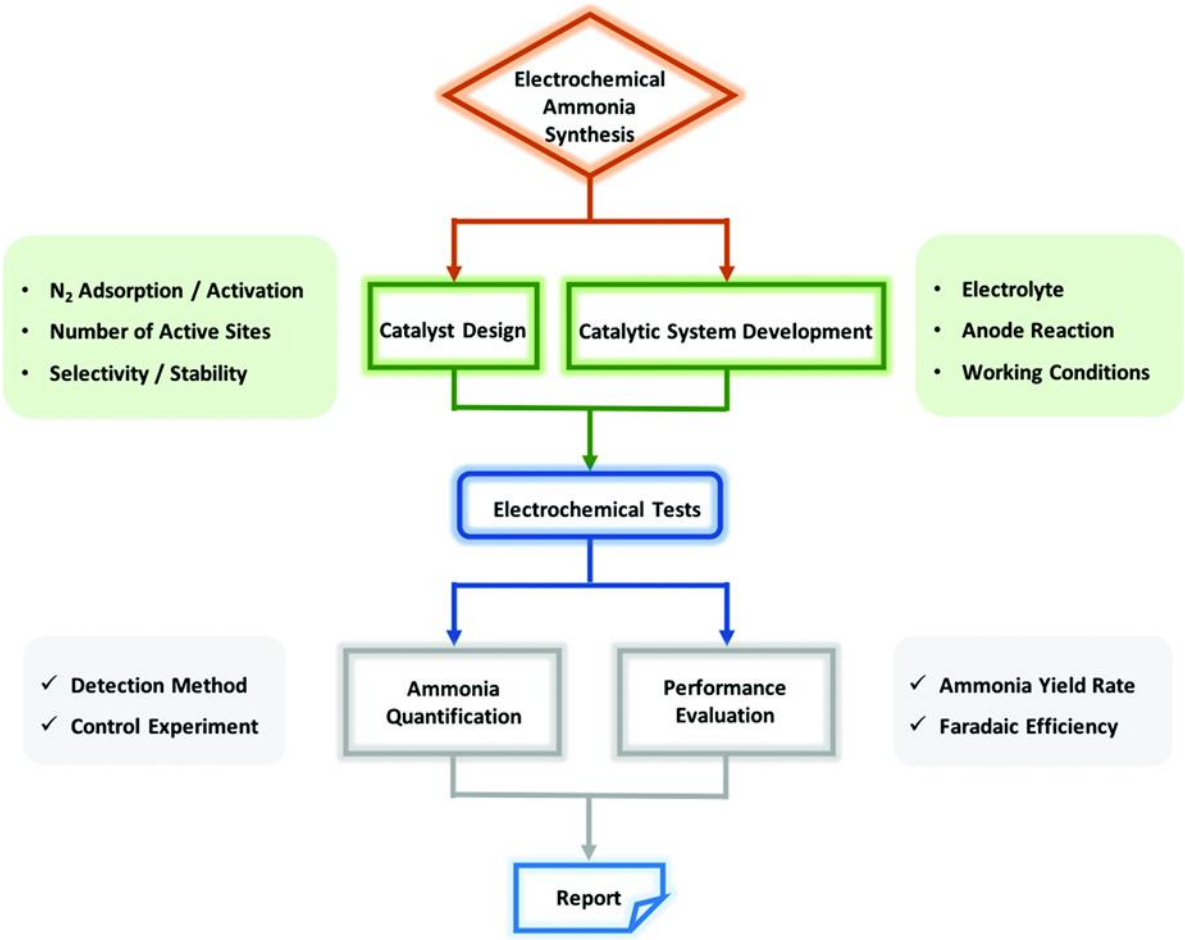

Figure 1.25: A Flowchart for electrochemical NH_3 synthesis. (*Adopted from Ref 112*)

1.8.1 Electrochemical Nitrogen Reduction Reaction (NRR)

The electrochemical nitrogen reduction process (NRR) converts N2 to NH_3 directly, utilizing water as a hydrogen source and energy as a driving force. The total reaction can be described as:

N_2 (g) + 6 H_2O (l) + 6e^- → 2NH_3 + 6OH^- (aq) E^o = 0.092V vs RHE

NRR is significant because it offers a potential alternative to the energy-intensive HB process for ammonia production, which requires extremely high temperatures (400-500°C) and pressures (150-300 atm). Electrocatalytic NRR can operate under ambient conditions, making it a more sustainable and energy-efficient approach.[113-114] The mechanism of NRR includes the adsorption of N_2 on the catalyst surface, followed by stepwise reduction of nitrogen to NH_3 through the formation of various intermediates, such as NH_x (x = 1-3) species. The rate is generally determined by the first N_2 activation and cleavage of the N≡N triple bond.[115](Figure 1.26) Efficient catalysts should facilitate this step while minimizing the competing hydrogen conversion reaction.

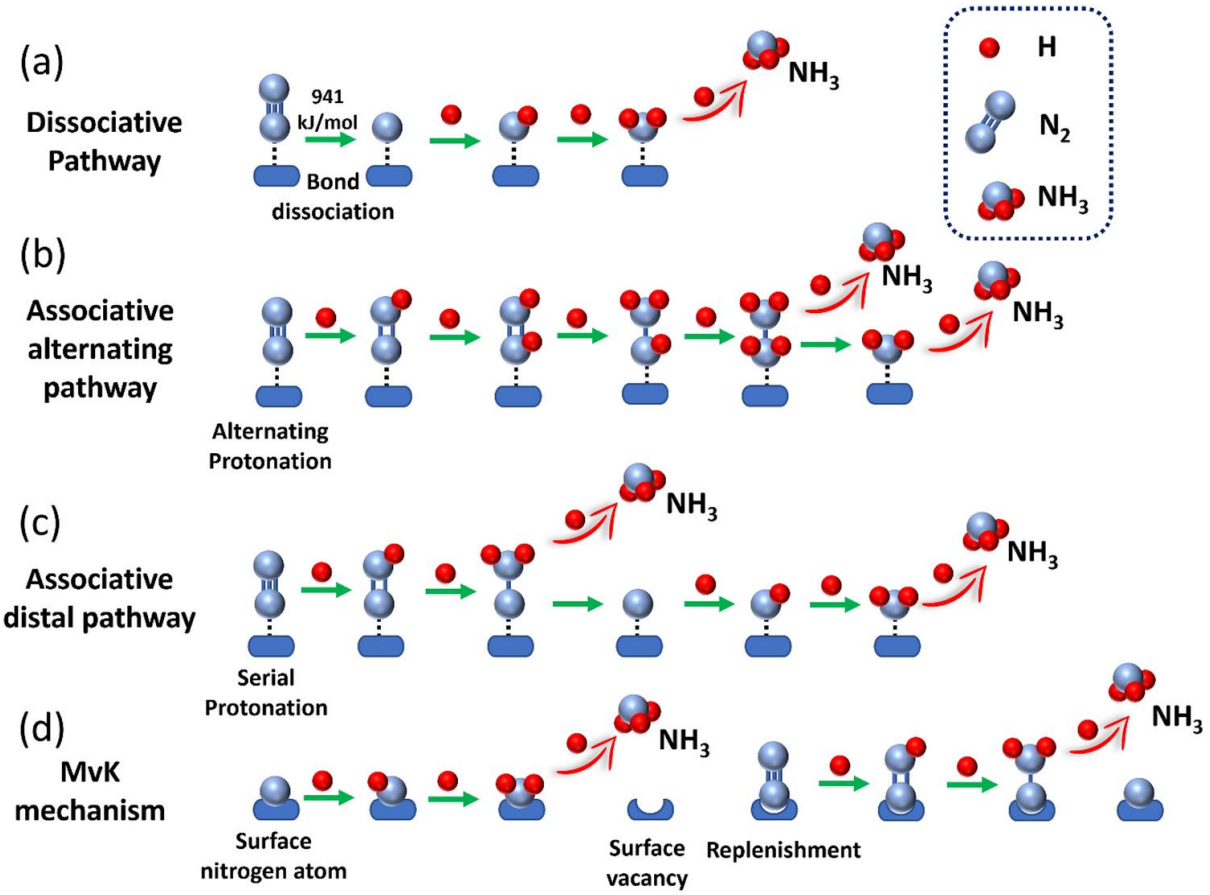

Figure 1.26: The proposed response mechanisms in the literature are illustrated as a dissociative, b alternating associative, c distal associative, and d MvK mechanism. (*Adopted from Ref 115*)

1.8.2 Electrochemical Nitrate Reduction Reaction (NO_3RR)

The electrochemical nitrate conversion reaction (NO_3RR) involves the reduction of nitrate (NO_3^-) to NH_3 using electricity and water as the hydrogen source. The overall reaction can give as follows:

$NO_3^- + 6H_2O + 8e^- \rightarrow NH_3 + 9OH^-$ $E^o = -0.12V$ vs RHE

NO_3RR is significant because it allows for the removal of nitrate, a common water pollutant, while simultaneously producing ammonia, a valuable chemical feedstock. This process can be particularly useful for treating nitrate-contaminated water and wastewater. NO_3RR operates through two primary mechanisms: direct and indirect. At low NO_3^- concentrations, the direct reaction mechanism is dominant, while at high concentrations, the indirect mechanism may become more relevant.[116] However, most NO_3RR typically follows the direct reaction pathway. The mechanism of NO_3RR includes the adsorption of nitrate ions on the catalyst surface, followed by a series of reduction steps. The reaction route is dependent on the catalyst material and operation circumstances, but it typically proceeds through the formation of nitrite (NO_2^-), nitric oxide (NO), and N intermediates before reaching the final product, ammonia (Figure 1.27).[117-119]

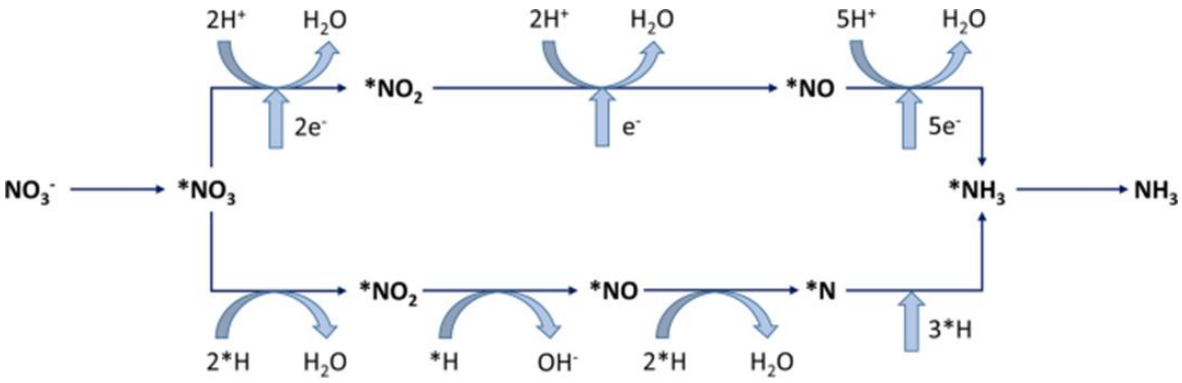

Figure 1.27: Electrochemical NO_3RR mechanism pathways (*Adopted from Ref 119*)

1.8.3 Electrochemical Nitrite Reduction Reaction (NO_2RR)

The electrocatalytic nitrite reduction reaction (NO_2RR) involves the conversion of nitrite (NO_2^-) to NH_3 ammonia using electricity and water as the hydrogen source. The overall reaction can be represented as:

$NO_2^- + 7H^+ + 6e^- \rightarrow NH_3 + 2H_2O$

NO_2RR is significant because it allows for the removal of nitrite, another common water pollutant, while producing ammonia. This process can be used in conjunction with NO_3RR for the comprehensive treatment of nitrate and nitrite-contaminated water.[120] The mechanism of NO_2RR is like that of NO_3RR, involving three key processes: (1) Adsorption of nitrite ions (NO_2^-) onto active sites of electrocatalysts, (2) a sequence of hydrogenation step, and (3) desorption of NH_3 (ammonia) from the catalyst surface. Initially, adsorbed NO_2^- is reduced to nitric oxide (NO), which cleaves the N=O link and hydrogenates to generate HNO. Further hydrogenation lowers HNO to H_2NO, which gains an electron and produces hydroxylamine (NH_2OH). Finally, the adsorbed hydroxylamine is fully reduced and converted into ammonia. (Figure 1.28).[121-122]

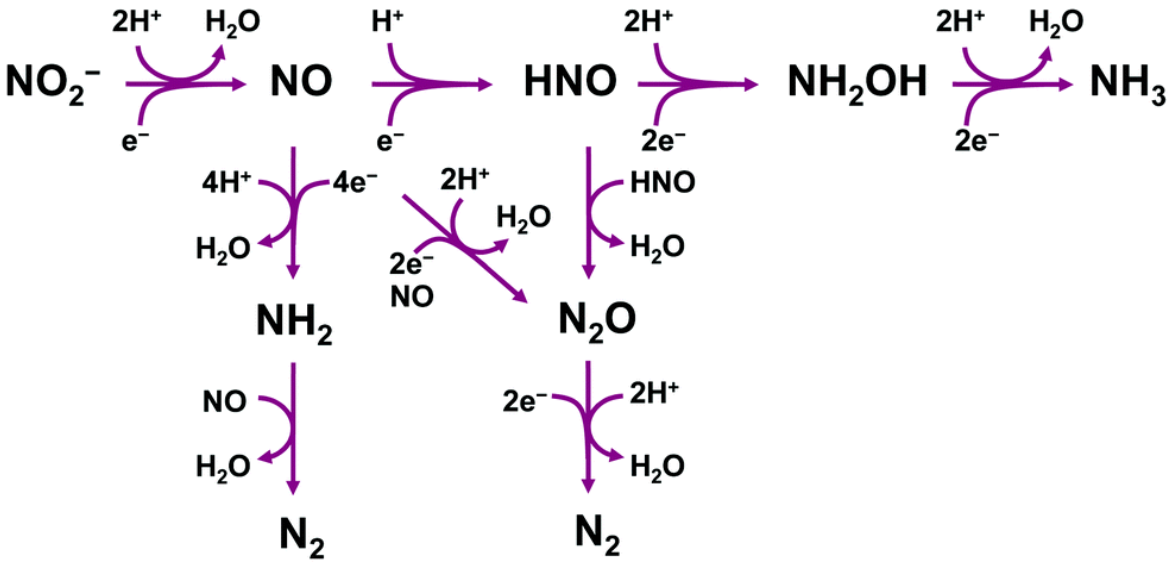

Figure 1.28. Electrochemical NO_2RR mechanism pathways (*Adopted from Ref 122*)

1.9 Covalent Organic Frameworks for electrochemical ammonia synthesis – Recent literature

The incorporation of metal nanoparticles or metalated monomers into Covalent organic frameworks have develop as a promising area of research for developing heterogeneous catalysts for ammonia synthesis. The intrinsic heterogeneity of COFs contributes to their exceptional stability and recyclability, while their porous architecture provides a high surface area, facilitating enhanced catalytic activity. Although COFs have tremendous potential in ammonia synthesis, there are little studies on their function in this process.[123-124]

In 2021, Feng and coworkers investigated the use of a covalent organic framework (MPc-pz) constructed with pyrazine linkers and incorporating M-N_4-C centers derived from metal-phthalocyanine units (Figure 1.29).[125] They systematically varied the metals (Fe, Ni, Co, Cu, Zn and Mn) within the framework and evaluated their performance in electrochemical nitrogen conversion reaction (ENRR). The FePc-pz framework with Fe-N4-C core shown better activity for ENRR, reaching an ammonia production rate of 33.6 µg h^{-1} $mgcat^{-1}$ and a Faradaic efficiency of 31.9% at -0.1 V against RHE. This study provided critical insights into the selection of metal centers for optimizing electrochemical nitrogen reduction reactions.

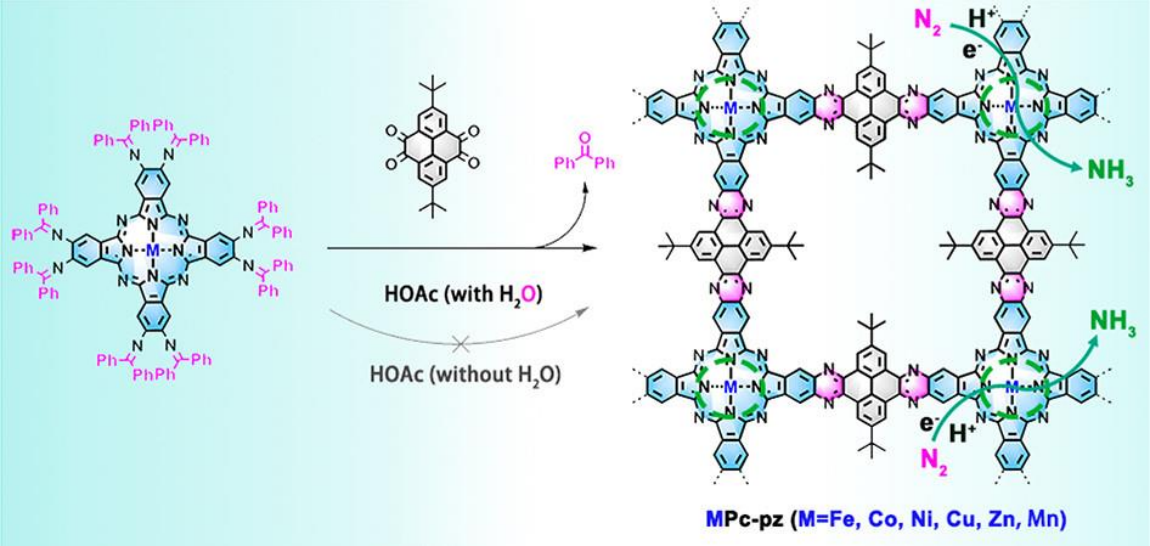

Figure 1.29. Schematic diagram of the synthetic process for MPc-pz (M = Fe, Ni, Co, Cu, Zn).(*Adopted from Ref 125*)

Jin and coworkers (2021) synthesized a conjugated covalent organic framework (COF) featuring quasi-phthalocyanine units coordinated with transition metal centers (Ti, Cu, and Co) (Figure 1.30).[126] The nitrogen reduction reaction (NRR) experiments revealed that the Ti-COF demonstrated superior NRR activity compared to Cu-COF and Co-COF counter parts. Ti metal centre activated inert N_2 molecules and suppressed the hydrogen evolution process, resulting in improved performance. The Ti-COF electrocatalyst has a Faradaic efficiency of 34.62% and an ammonia production of 26.89 µgh^{-1} $mg^{-1}_{cat.}$, making it a promising option for NRR.

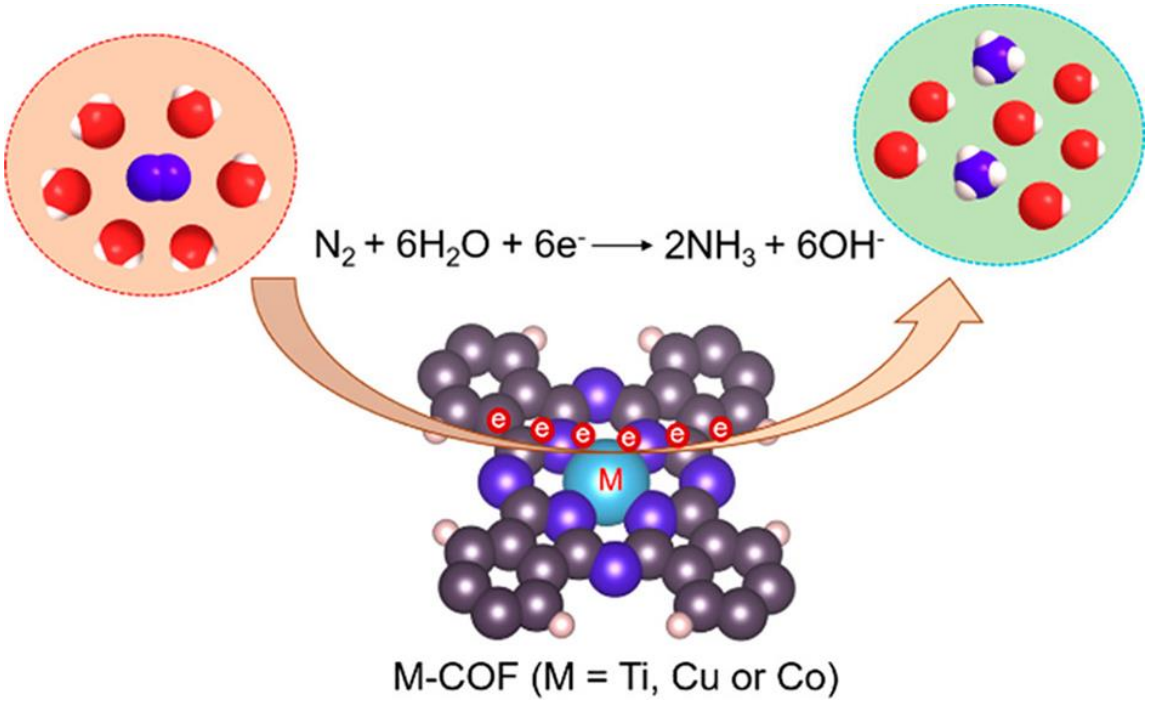

Figure 1.29. Scheme presentation of ENRR of M-COF (M = Fe, Co, Cu,). (*Adopted from Ref 126*)

Later in 2023, Du and co-workers synthesized COF-Fe/MXene nanosheets are 2D ferric covalent organic frameworks through a postmodification process.[128] By varying the hydrophobicity of the COF, The Fe/MXene composite displayed improved NRR activity, efficiently repelling water molecules to prevent the hydrogen evolution process (HER), and therefore improving NRR performance. Among the modified COF-MXene composites, the perfluorodecanethiol-modified COF-Fe/MXene hybrid exhibited the best performance, achieving an ammonia yield of 41.8 $\mu g h^{-1} mg^{-1}_{cat.}$ and a Faradaic efficiency of 43.1% at −0.5 V versus RHE in a 0.1 M Na_2SO_4 water solution (Figure 1.30). This observation provides a promising strategy for designing and synthesizing molecules to enhance NRR by suppressing HER.

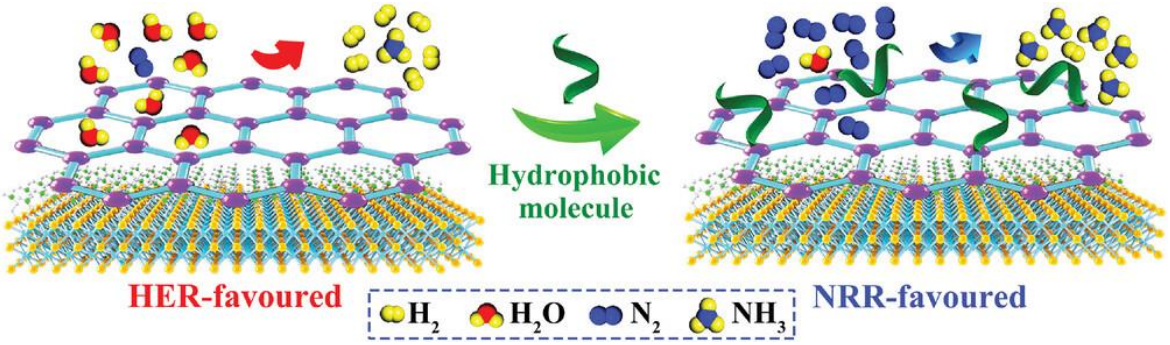

Figure 1.30. Schematic presentation of ENRR of the hydrophobic COF/MXene nanosheets. (*Adopted from Ref 127*)

In addition to NRR some other studies have done to explore nitrate reduction reaction at ambient temperature and pressure. As compared to NRR NO_3RR is easier because N=O is relatively easier to break. In recent years few groups have shown remarkable performance and selectivity for NO_3RR. In 2023, Li and coworkers synthesized a two-dimensional in nature nickel porphyrin-based covalent organic framework (COF) designed specifically for the electrocatalytic nitrate conversion process (NO_3RR).[128] The highly ordered porous architecture of COF facilitated superior catalytic performance, achieving a selectivity of approximately 90% under mild overpotential conditions, with an ammonia conversion rate increasing up to 2.5 $mgh^{-1}cm^{-2}$. Furthermore, comprehensive full-cell NO_3-OER electrolysis tests were done to examine the practical performance of this COF in reducing nitrate, showing its potential for scale applications (Figure 1.31).

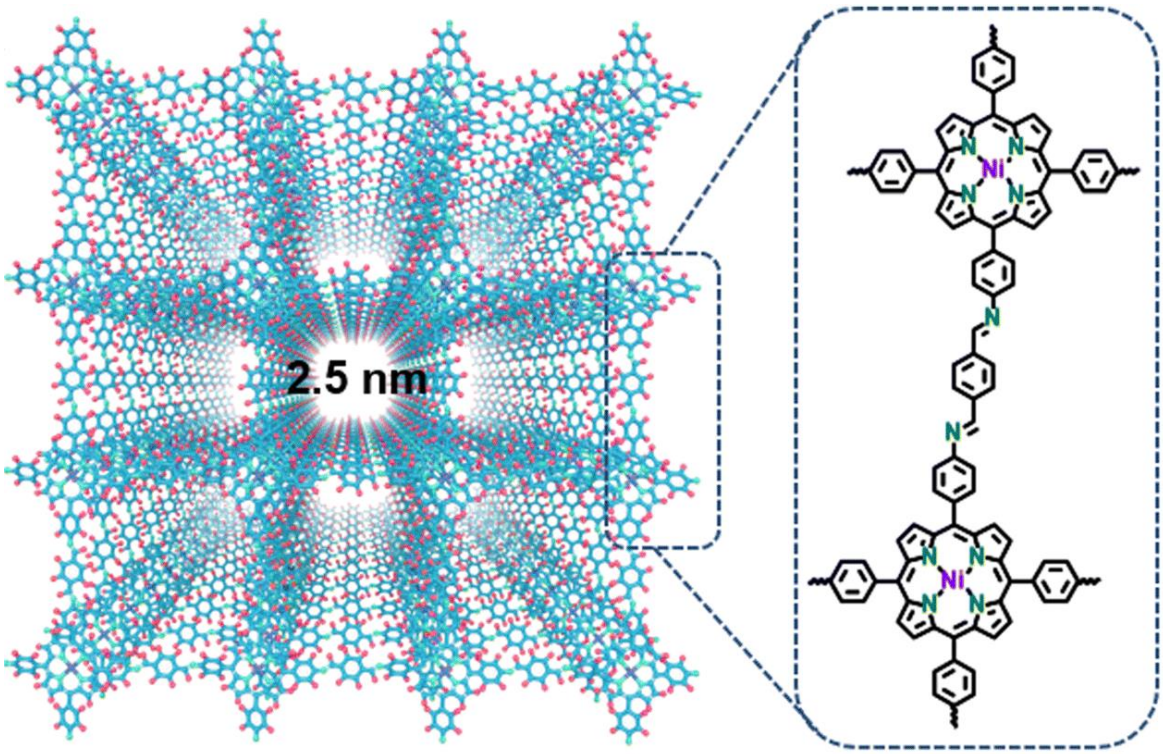

Figure 1.31. Schematic structure of NiPr-TPA-COF and its monomer units. (*Adopted from Ref 128*)

Furthermore, Lu and co-workers engineered a 2D metal porphyrin-type COF (M = Fe, Co, Ni) for targeted enhancement of electrocatalytic nitrate reduction reaction (NO_3RR).[129] By systematically varying the metal centres and linkers, they elucidated the impact of these modifications on NO_3^-RR performance. The Fe-porphyrin-based COF emerged as the most effective catalyst, with a performance hierarchy of Fe > Cu > Ni > Co. Specifically, the Fe-porphyrin COF achieved a Faradaic efficiency for ammonia of 85.4% and a notable ammonia yield rate of 1883.6 µmol h^{-1} mg^{-1}_{COF}. Furthermore, the substitution of the benzene linker with thieno [3,2- b] thiophene was found to increase the charge density at the active site of Fe, thereby modulating the reduction potential of the COF. Additionally, a Zn–NO_3^- battery using the COF-366-Fe as the cathode electrode showed outstanding ammonia selectivity, with a sharp peak $FENH_3$ of 83.7% and a yield rate of 130.1 µmolh^{-1} mg^{-1}_{cat} at 3 $mAcm^{-2}$(Figure 1.32).

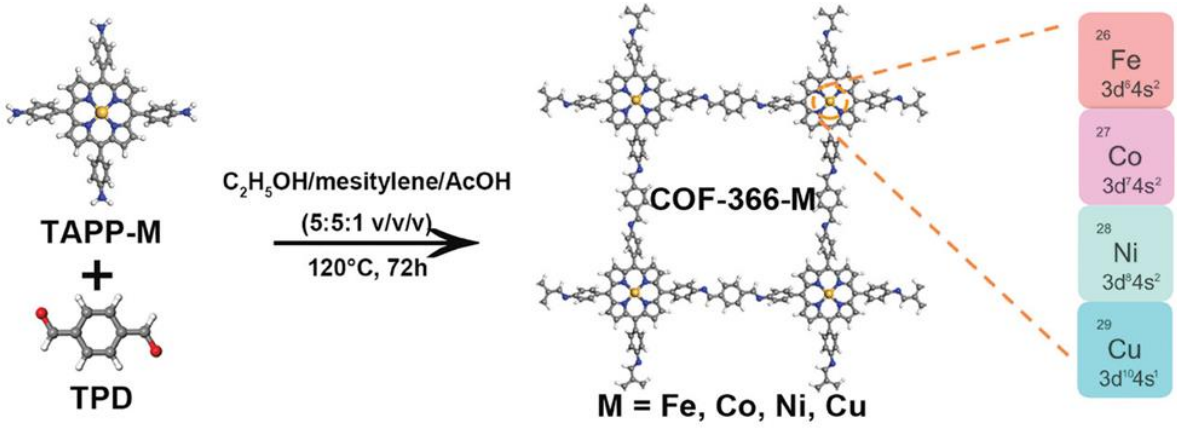

Figure 1.32. Conjugated porphyrin-based COFs with optional metal centres and optional linkers toward NO_3RR. (*Adopted from Ref 129*)

Future research will benefit from further exploration of COF designs and metal configurations to enhance efficiency, selectivity, and stability, aiming for scalable and practical applications in ammonia synthesis and other critical electrochemical processes.

Despite these challenges, ongoing research efforts focused on understanding the fundamental principles governing MOF stability and developing innovative strategies to address their limitations. Overcoming issues related to chemical and mechanical instability, is critical for MOFs role as versatile materials with widespread utility across diverse sectors, ranging from energy and environmental remediation to pharmaceuticals and beyond.

1.10 References

1. https://www.spglobal.com/commodityinsights/en/ci/products/ammonia-chemical-economics-handbook.html#:~:text=Ammonia%20is%20the%20basic%20building,to%2060%25%20of%20all%20fertilizers).
2. https://www.acs.org/molecule-of-the-week/archive/a/ammonia.html).
3. Hosseini, H. Dielectric barrier discharge plasma catalysis as an alternative approach for the synthesis of ammonia: a review. *RSC advances* **2023,** *13* (40), 28211.
4. https://www.thyssenkrupp.com/en/stories/sustainability-and-climate-protection/ammonia-in-agriculture:-the-engine-of-plant-growth).
5. Venterea, R. T.; Burger, M.; Spokas, K. A. Nitrogen oxide and methane emissions under varying tillage and fertilizer management. Journal of environmental quality 2005, 34 (5), 1467.
6. Erisman, J. W.; Sutton, M. A.; Galloway, J.; Klimont, Z.; Winiwarter, W. How a century of ammonia synthesis changed the world. *Nature geoscience* **2008,** *1* (10), 636.
7. Lu, C.; Tian, H. Global nitrogen and phosphorus fertilizer use for agriculture production in the past half century: shifted hot spots and nutrient imbalance. *Earth System Science Data* **2017,** *9* (1), 181
8. Heffer, P.; Prud'homme, M. Global Nitrogen Fertiliser Demand and Supply: Trend. *Current Level and Outlook* **2016**, 4
9. https://youmatter.world/en/definitions/what-haber-bosch-process-ecological-impact/).
10. Heffer, P.; Gruère, A.; Roberts, T. Assessment of fertilizer use by crop at the global level. *International Fertilizer Industry Association, Paris* **2013**
11. Galloway, J. N.; Townsend, A. R.; Erisman, J. W.; Bekunda, M.; Cai, Z.; Freney, J. R.; Martinelli, L. A.; Seitzinger, S. P.; Sutton, M. A. Transformation of the nitrogen cycle: recent trends, questions, and potential solutions. *Science* **2008,** *320* (5878), 889.
12. Sutton, M. A.; Oenema, O.; Erisman, J. W.; Leip, A.; Van Grinsven, H.; Winiwarter, W. Too much of a good thing. *Nature* **2011,** *472* (7342), 159.
13. Chataut, G.; Bhatta, B.; Joshi, D.; Subedi, K.; Kafle, K. Greenhouse gases emission from agricultural soil: A review. *Journal of Agriculture and Food Research* **2023,** *11*, 100533.
14. Yüzbaşıoğlu, A. E.; Avşar, C.; Gezerman, A. O. The current situation in the use of ammonia as a sustainable energy source and its industrial potential. *Current Research in Green and Sustainable Chemistry* **2022,** *5*, 100307.
15. Lucentini, I.; Garcia, X.; Vendrell, X.; Llorca, J. Review of the decomposition of ammonia to generate hydrogen. *Industrial & Engineering Chemistry Research* **2021,** *60* (51), 18560.
16. Wyer, K. E.; Kelleghan, D. B.; Blanes-Vidal, V.; Schauberger, G.; Curran, T. P. Ammonia emissions from agriculture and their contribution to fine particulate matter: A review of implications for human health. *Journal of Environmental Management* **2022,** *323*, 116285.
17. Oommen, C.; Jain, S., Ammonium nitrate: a promising rocket propellant oxidizer. *Journal of hazardous materials* **1999,** *67* (3), 253-281.
18. Shang, X.; Wang, Q.; Jiang, Z.; Ma, H.; Zhang, D. Liquid-Ammonia-Mediated Dyeing Process of Wool at a Lower Temperature. *Processes* **2022,** *10* (11), 2172.
19. Fedoruk, M. J.; Bronstein, R.; Kerger, B. D. Ammonia exposure and hazard assessment for selected household cleaning product uses. *Journal of Exposure Science & Environmental Epidemiology* **2005,** *15* (6), 534.
20. Wang, L.; Cardwell, T. J.; Cattrall, R. W.; de Castro, M. D. L.; Kolev, S. D., Determination of ammonia in beers by pervaporation flow injection analysis and spectrophotometric detection. *Talanta* **2003,** *60* (6), 1269-1275.
21. Pearson, A. Refrigeration with ammonia. *International journal of refrigeration* **2008,** *31* (4), 545.
22. https://www.iea.org/reports/ammonia-technology-roadmap/executive-summary).
23. MacFarlane, D. R.; Cherepanov, P. V.; Choi, J.; Suryanto, B. H.; Hodgetts, R. Y.; Bakker, J. M.; Vallana, F. M. F.; Simonov, A. N. A roadmap to the ammonia economy. *Joule* **2020,** *4* (6), 1186.
24. Watanabe, Y.; Aoki, W.; Ueda, M. Ammonia production using bacteria and yeast toward a sustainable society. *Bioengineering* **2023,** *10* (1), 82.
25. Adeniyi, A.; Bello, I.; Mukaila, T.; Sarker, N. C.; Hammed, A. Trends in biological ammonia production. *BioTech* **2023,** *12* (2), 41.
26. Appl M. Ammonia: principles and industrial practice. 1st ed. Weinheim (Germany): WileyVCH Verlag GmbH; **1999**

27. Rouwenhorst, K. H. R.; Krzywda, P. M.; Benes, N. E.; Mul, G.; Lefferts, L. Ammonia production technologies. *Techno-Economic Challenges of Green Ammonia as an Energy Vector* **2021**, 41.
28. Bazhenova, c. T.; Shilov, A. Nitrogen fixation in solution. *Coordination chemistry reviews* **1995,** *144*, 69.
29. Cherkasov, N.; Ibhadon, A.; Fitzpatrick, P. A review of the existing and alternative methods for greener nitrogen fixation. *Chemical Engineering and Processing: Process Intensification* **2015,** *90*, 24.
30. Foster, S. L.; Bakovic, S. I. P.; Duda, R. D.; Maheshwari, S.; Milton, R. D.; Minteer, S. D.; Janik, M. J.; Renner, J. N.; Greenlee, L. F. Catalysts for nitrogen reduction to ammonia. *Nature Catalysis* **2018,** *1* (7), 490.
31. Seefeldt, L. C.; Hoffman, B. M.; Dean, D. R. Electron transfer in nitrogenase catalysis. *Current opinion in chemical biology* **2012,** *16* (1-2), 19.
32. Burgess, B. K.; Lowe, D. J. Mechanism of molybdenum nitrogenase. *Chemical reviews* **1996,** *96* (7), 2983.
33. Skulason, E.; Bligaard, T.; Gudmundsdóttir, S.; Studt, F.; Rossmeisl, J.; Abild-Pedersen, F.; Vegge, T.; Jónsson, H.; Nørskov, J. K. A theoretical evaluation of possible transition metal electro-catalysts for N 2 reduction. *Physical Chemistry Chemical Physics* **2012,** *14* (3), 1235.
34. Ueda, M. Establishment of cell surface engineering and its development. *Bioscience, biotechnology, and biochemistry* **2016,** *80* (7), 1243.
35. Watanabe, Y.; Kuroda, K.; Tatemichi, Y.; Nakahara, T.; Aoki, W.; Ueda, M. Construction of engineered yeast producing ammonia from glutamine and soybean residues (okara). *AMB Express* **2020,** *10*, 1.
36. Pengpeng, W.; Tan, Z. Ammonia assimilation in rumen bacteria: a review. *Animal biotechnology* **2013,** *24* (2), 107.
37. Bach, A.; Calsamiglia, S.; Stern, M. D. Nitrogen metabolism in the rumen. *Journal of dairy science* **2005,** *88*, E9.
38. Ernst, F. A. *Fixation of atmospheric nitrogen*; D. Van Nostrand Company, 1928.
39. Elvers, B., *Ullmann's encyclopedia of industrial chemistry*. Verlag Chemie Hoboken, NJ: 1991; Vol. 17.
40. Travis, A. S.; Travis, A. S.; Costa *Nitrogen capture*; Springer, 2018.
41. Haber, F.; Rossignol, R. L. The Production of Synthetic Ammonia. *Industrial & Engineering Chemistry* **1913,** *5* (4), 328.
42. Albonetti, S.; Perathoner, S.; Quadrelli, E. A. *Horizons in sustainable industrial chemistry and catalysis*; Elsevier, 2019.
43. Sheppard, D. Robert Le Rossignol, 1884–1976: engineer of the 'Haber'process. *Notes and Records: the Royal Society Journal of the History of Science* **2017,** *71* (3), 263.
44. Nernst, W. Über das Ammoniakgleichgewicht. *Zeitschrift für Elektrochemie und angewandte physikalische Chemie* **1907,** *13* (32), 521.
45. Farber, E. From Chemistry to Philosophy: The Way of Alwin Mittasch (1869-1953). *Chymia* **1966,** *11*, 157.
46. Mittasch, A.; Frankenburg, W. In *Advances in catalysis*; Elsevier, 1950; Vol. 2.
47. Ertl, G. Surface science and catalysis—studies on the mechanism of ammonia synthesis: the PH Emmett award address. *Catalysis Reviews Science and Engineering* **1980,** *21* (2), 201.
48. Prieto, G.; Schüth, F. The Yin and Yang in the development of catalytic processes: Catalysis research and reaction engineering. *Angewandte Chemie International Edition* **2015,** *54* (11), 3222.
49. Brightling, J. Ammonia and the fertiliser industry: The development of ammonia at Billingham. *Johnson Matthey Technology Review* **2018,** *62* (1), 32.
50. Rostrup-Nielsen, J. R. In *Catalysis: Science and Technology Volume 5*; Springer, 1984.
51. (https://wisc.pb.unizin.org/chem109fall2021ver02/chapter/haber-bosch-process/)
52. West, J. The Claude synthetic ammonia process and plant. *Journal of the Society of Chemical Industry* **1921,** *40* (22), R420.
53. Philibert, C. Renewable energy for industry. *Paris: International Energy Agency* **2017,** *65*.
54. Rouwenhorst, K. H. R.; Krzywda, P. M.; Benes, N. E.; Mul, G.; Lefferts, L. Ammonia production technologies. *Techno-Economic Challenges of Green Ammonia as an Energy Vector* **2021**, 41.
55. Patil, B.; Wang, Q.; Hessel, V.; Lang, J. Plasma N2-fixation: 1900–2014. *Catalysis today* **2015,** *256*, 49.
56. Liu, H. *Ammonia synthesis catalysts: innovation and practice*; World Scientific, 2013.
57. Kirk, R.; Othmer, D. *Kirk-Othmer encyclopedia of chemical technology*; Wiley, 1978.
58. Hellman, A.; Honkala, K.; Dahl, S.; Christensen, C.; Nørskov, J. In *Comprehensive Inorganic Chemistry II (Second Edition): From Elements to Applications*; Elsevier, 2013.
59. Ozaki, A.; Taylor, H. S.; Boudart, M. Kinetics and mechanism of the ammonia synthesis. *Proceedings of the Royal Society of London. Series A. Mathematical and Physical Sciences* **1960,** *258* (1292), 47.
60. Liu, H.; Han, W. Wüstite-based catalyst for ammonia synthesis: Structure, property and performance. *Catalysis Today* **2017,** *297*, 276.

61. Jacobsen, C. J.; Dahl, S.; Boisen, A.; Clausen, B. S.; Topsøe, H.; Logadottir, A.; Nørskov, J. K. Optimal catalyst curves: Connecting density functional theory calculations with industrial reactor design and catalyst selection. *Journal of Catalysis* **2002,** *205* (2), 382.
62. Hinrichsen, O.; Rosowski, F.; Muhler, M.; Ertl, G. The microkinetics of ammonia synthesis catalyzed by cesium-promoted supported ruthenium. *Chemical engineering science* **1996,** *51* (10), 1683.
63. Erisman, J. W.; Sutton, M. A.; Galloway, J.; Klimont, Z.; Winiwarter, W. How a century of ammonia synthesis changed the world. *Nature geoscience* **2008,** *1* (10), 636.
64. Rouwenhorst, K. H.; Van der Ham, A. G.; Mul, G.; Kersten, S. R. Islanded ammonia power systems: Technology review & conceptual process design. *Renewable and Sustainable Energy Reviews* **2019,** *114*, 109339.
65. Wilson, R.; Cahill, D. G. Anisotropic failure of Fourier theory in time-domain thermoreflectance experiments. *Nature communications* **2014,** *5* (1), 5075.
66. Song, Z.; Ren, Z.; Deng, Q.; Kang, X.; Zhou, M.; Liu, D.; Chen, X. General models for estimating daily and monthly mean daily diffuse solar radiation in China's subtropical monsoon climatic zone. *Renewable Energy* **2020,** *145*, 318.
67. Shipman, J., & Symes, M. D. (2017). Electrocatalytic Nitrogen Reduction: A Sustainable Approach to Ammonia Synthesis. Nature Chemistry, 9, 1-10. DOI: 10.1038/nchem.2797.
68. Montoya, J. H.; Tsai, C.; Vojvodic, A.; Nørskov, J. K. The challenge of electrochemical ammonia synthesis: a new perspective on the role of nitrogen scaling relations. *ChemSusChem* **2015,** *8* (13), 2180.
69. Seh, Z. W.; Kibsgaard, J.; Dickens, C. F.; Chorkendorff, I.; Nørskov, J. K.; Jaramillo, T. F. Combining theory and experiment in electrocatalysis: Insights into materials design. *Science* **2017,** *355* (6321), eaad4998.
70. Turner, J.; Sverdrup, G.; Mann, M. K.; Maness, P. C.; Kroposki, B.; Ghirardi, M.; Evans, R. J.; Blake, D. Renewable hydrogen production. *International journal of energy research* **2008,** *32* (5), 379.
71. Gunatillake, P.; Mayadunne, R.; Adhikari, R. Recent developments in biodegradable synthetic polymers. *Biotechnology annual review* **2006,** *12*, 301.
72. Feldman, D.; Barbalata, A. *Synthetic polymers: technology, properties, applications*; Springer Science & Business Media, 1996.
73. Das, S.; Heasman, P.; Ben, T.; Qiu, S. Porous organic materials: strategic design and structure–function correlation. *Chemical Reviews* **2017,** *117* (3), 1515.
74. Liao, Q.; Kim, E. J.; Tang, Y.; Xu, H.; Yu, D. G.; Song, W.; Kim, B. J. Rational design of hyper-crosslinked polymers for biomedical applications. *Journal of Polymer Science* **2024,** *62* (8), 1517.
75. Yang, C.; Wang, K.; Lyu, W.; Liu, H.; Li, J.; Wang, Y.; Jiang, R.; Yuan, J.; Liao, Y. Nanofibrous Porous Organic Polymers and Their Derivatives: From Synthesis to Applications. *Advanced Science* **2024,** *11* (19), 2400626.
76. Mohamed, M. G.; EL-Mahdy, A. F.; Kotp, M. G.; Kuo, S.-W. Advances in porous organic polymers: Syntheses, structures, and diverse applications. *Materials Advances* **2022,** *3* (2), 707.
77. Cote, A. P.; Benin, A. I.; Ockwig, N. W.; O'Keeffe, M.; Matzger, A. J.; Yaghi, O. M. Porous, crystalline, covalent organic frameworks. *science* **2005,** *310* (5751), 1166.
78. Huang, N.; Zhai, L.; Coupry, D. E.; Addicoat, M. A.; Okushita, K.; Nishimura, K.; Heine, T.; Jiang, D. Multiple-component covalent organic frameworks. *Nature communications* **2016,** *7* (1), 1232.
79. Colson, J. W.; Dichtel, W. R. Rationally synthesized two-dimensional polymers. *Nature chemistry* **2013,** *5* (6), 453.
80. Alahakoon, S. B.; Thompson, C. M.; Occhialini, G.; Smaldone, R. A. Design principles for covalent organic frameworks in energy storage applications. *ChemSusChem* **2017,** *10* (10), 2116.
81. Ding, S.-Y.; Wang, W. Covalent organic frameworks (COFs): from design to applications. *Chemical Society Reviews* **2013,** *42* (2), 548.
82. Vardhan, H.; Rummer, G.; Deng, A.; Ma, S. Large-scale synthesis of covalent organic frameworks: challenges and opportunities. *Membranes* **2023,** *13* (8), 696.
83. Mullangi, D.; Dhavale, V.; Shalini, S.; Nandi, S.; Collins, S.; Woo, T.; Kurungot, S.; Vaidhyanathan, R. Low-Overpotential Electrocatalytic Water Splitting with Noble-Metal-Free Nanoparticles Supported in a sp3 N-Rich Flexible COF. *Advanced Energy Materials* **2016,** *6* (13), 1600110.
84. Nandi, S.; Singh, S. K.; Mullangi, D.; Illathvalappil, R.; George, L.; Vinod, C. P.; Kurungot, S.; Vaidhyanathan, R. Low band gap benzimidazole COF supported Ni3N as highly active OER catalyst. *Advanced Energy Materials* **2016,** *6* (24), 1601189.
85. Furukawa, H.; Yaghi, O. M. Storage of hydrogen, methane, and carbon dioxide in highly porous covalent organic frameworks for clean energy applications. *Journal of the American Chemical Society* **2009,** *131* (25), 8875.

86. Ben, H.; Du, W.; Zhao, J.; Wang, Y.; Wu, Y.; Lin, F.; Lei, Y.; Zhou, S.; Pu, J.; Ye, M. Ionic covalent organic frameworks: From synthetic strategies to advanced electro-, photo-, and thermo-energy functionalities. *Coordination Chemistry Reviews* **2024,** *517*, 216003.
87. Vyas, V. S.; Haase, F.; Stegbauer, L.; Savasci, G.; Podjaski, F.; Ochsenfeld, C.; Lotsch, B. V. A tunable azine covalent organic framework platform for visible light-induced hydrogen generation. *Nature communications* **2015,** *6* (1), 8508.
88. Ma, T.; Kapustin, E. A.; Yin, S. X.; Liang, L.; Zhou, Z.; Niu, J.; Li, L.-H.; Wang, Y.; Su, J.; Li, J. Single-crystal x-ray diffraction structures of covalent organic frameworks. *Science* **2018,** *361* (6397), 48.
89. Han, J.; Feng, J.; Kang, J.; Chen, J.-M.; Du, X.-Y.; Ding, S.-Y.; Liang, L.; Wang, W. Fast growth of single-crystal covalent organic frameworks for laboratory x-ray diffraction. *Science* **2024,** *383* (6686), 1014.
90. Kandambeth, S.; Mallick, A.; Lukose, B.; Mane, M. V.; Heine, T.; Banerjee, R. Construction of crystalline 2D covalent organic frameworks with remarkable chemical (acid/base) stability via a combined reversible and irreversible route. *Journal of the American Chemical Society* **2012,** *134* (48), 19524.
91. Liu, R.; Tan, K. T.; Gong, Y.; Chen, Y.; Li, Z.; Xie, S.; He, T.; Lu, Z.; Yang, H.; Jiang, D. Covalent organic frameworks: an ideal platform for designing ordered materials and advanced applications. *Chemical Society Reviews* **2021,** *50* (1), 120.
92. Sharma, R. K.; Yadav, P.; Yadav, M.; Gupta, R.; Rana, P.; Srivastava, A.; Zbořil, R.; Varma, R. S.; Antonietti, M.; Gawande, M. B. Recent development of covalent organic frameworks (COFs): synthesis and catalytic (organic-electro-photo) applications. *Materials Horizons* **2020,** *7* (2), 411.
93. Yang, S.-T.; Kim, J.; Cho, H.-Y.; Kim, S.; Ahn, W.-S. Facile synthesis of covalent organic frameworks COF-1 and COF-5 by sonochemical method. *RSC advances* **2012,** *2* (27), 10179.
94. Maschita, J.; Banerjee, T.; Savasci, G.; Haase, F.; Ochsenfeld, C.; Lotsch, B. V. Ionothermal synthesis of imide-linked covalent organic frameworks. *Angewandte Chemie International Edition* **2020,** *59* (36), 15750.
95. Dey, A.; Chakraborty, S.; Singh, A.; Rahimi, F. A.; Biswas, S.; Mandal, T.; Maji, T. K. Microwave Assisted Fast Synthesis of a Donor-Acceptor COF Towards Photooxidative Amidation Catalysis. *Angewandte Chemie International Edition* **2024**, e202403093.
96. Zhang, X.; Xue, S.; Yan, Y.; Liu, S.; Ye, Q.; Zhou, F. Mechanochemical Synthesis of Thiadiazole Functionalized COF as Oil-Based Lubricant Additive for Reducing Friction and Wear. *Langmuir* **2024,** *40* (8), 4373.
97. Deng, Y.; Wang, Y.; Wang, J.; Wei, Z.; Xin, C.; Liu, J.; Zhao, C.; Zhang, Z. Dynamic covalent chemistry concept toward preparing crystalline covalent organic frameworks for dual-mode acidochromic responses. *Materials Today Chemistry* **2022,** *26*, 101027.
98. Post-synthetic modifications of covalent organic frameworks (COFs) for diverse applications.
99. Sarkar, S.; Ghosh, S.; Islam, S. M. A Zn (ii)-functionalized COF as a recyclable catalyst for the sustainable synthesis of cyclic carbonates and cyclic carbamates from atmospheric CO 2. *Organic & Biomolecular Chemistry* **2022,** *20* (8), 1707.
100. Furukawa, H.; Yaghi, O. M. Storage of hydrogen, methane, and carbon dioxide in highly porous covalent organic frameworks for clean energy applications. *Journal of the American Chemical Society* **2009,** *131* (25), 8875.
101. Waller, P. J.; Gándara, F.; Yaghi, O. M. Chemistry of covalent organic frameworks. *Accounts of chemical research* **2015,** *48* (12), 3053.
102. Liu, X.; Wang, Z.; Zhang, Y.; Yang, N.; Gui, B.; Sun, J.; Wang, C. Gas-Triggered Gate-Opening in a Flexible Three-Dimensional Covalent Organic Framework. *Journal of the American Chemical Society* **2024,** *146* (16), 11411.
103. Lu, Y.; Liang, Y.; Zhao, Y.; Xia, M.; Liu, X.; Shen, T.; Feng, L.; Yuan, N.; Chen, Q. Fluorescent test paper via the in situ growth of COFs for rapid and convenient detection of Pd (II) ions. *ACS applied materials & interfaces* **2021,** *13* (1), 1644.
104. Li, M.; Peng, Y.; Yan, F.; Li, C.; He, Y.; Lou, Y.; Ma, D.; Li, Y.; Shi, Z.; Feng, S. A cage-based covalent organic framework for drug delivery. *New Journal of Chemistry* **2021,** *45* (6), 3343.
105. Ge, L.; Qiao, C.; Tang, Y.; Zhang, X.; Jiang, X. Light-activated hypoxia-sensitive covalent organic framework for tandem-responsive drug delivery. *Nano Letters* **2021,** *21* (7), 3218.
106. Haldar, S.; Kushwaha, R.; Maity, R.; Vaidhyanathan, R. Pyridine-rich covalent organic frameworks as high-performance solid-state supercapacitors. *ACS Materials Letters* **2019,** *1* (4), 490.
107. Ross, J. R. *Heterogeneous catalysis: fundamentals and applications*; Elsevier, 2011.
108. Ranga, S. Comparative Analysis of Homogeneous and Heterogeneous Catalysis IJETSR, Volume 4, Issue 9, 2017 2394 – 3386.
109. Guo, J.; Jiang, D. Covalent organic frameworks for heterogeneous catalysis: principle, current status, and challenges. *ACS Central Science* **2020,** *6* (6), 869.

110. Alsudairy, Z.; Brown, N.; Campbell, A.; Ambus, A.; Brown, B.; Smith-Petty, K.; Li, X. Covalent organic frameworks in heterogeneous catalysis: Recent advances and future perspective. *Materials Chemistry Frontiers* **2023,** *7* (16), 3298.
111. Feng, J.-D.; Zhang, W.-D.; Gu, Z.-G. Covalent Organic Frameworks for Electrocatalysis: Design, Applications, and Perspectives. *ChemPlusChem*, e202400069.
112. Yang, B.; Ding, W.; Zhang, H.; Zhang, S. Recent progress in electrochemical synthesis of ammonia from nitrogen: strategies to improve the catalytic activity and selectivity. *Energy & Environmental Science* **2021,** *14* (2), 672.
113. Qing, G.; Ghazfar, R.; Jackowski, S. T.; Habibzadeh, F.; Ashtiani, M. M.; Chen, C.-P.; Smith III, M. R.; Hamann, T. W. Recent advances and challenges of electrocatalytic N2 reduction to ammonia. *Chemical reviews* **2020,** *120* (12), 5437.
114. Martín, A. J.; Shinagawa, T.; Pérez-Ramírez, J. Electrocatalytic reduction of nitrogen: from Haber-Bosch to ammonia artificial leaf. *Chem* **2019,** *5* (2), 263.
115. Jesudass, S. C.; Surendran, S.; Kim, J. Y.; An, T.-Y.; Janani, G.; Kim, T.-H.; Kim, J. K.; Sim, U. Pathways of the electrochemical nitrogen reduction reaction: from ammonia synthesis to metal-N2 batteries. *Electrochemical Energy Reviews* **2023,** *6* (1), 27.
116. Jeon, K.-W.; Huo, S.; Espinosa, B. I.; Wang, X. Recent Development of Catalysts for the Nitrate Reduction Reaction: Electrochemical Solution to Produce Ammonia. *Topics in Catalysis* **2024**, 1-12.
117. Lu, X.; Song, H.; Cai, J.; Lu, S. Recent development of electrochemical nitrate reduction to ammonia: A mini review. *Electrochemistry Communications* **2021,** *129*, 107094.
118. Theerthagiri, J.; Park, J.; Das, H. T.; Rahamathulla, N.; Cardoso, E. S.; Murthy, A. P.; Maia, G.; Vo, D. V. N.; Choi, M. Y. Electrocatalytic conversion of nitrate waste into ammonia: a review. *Environmental Chemistry Letters* **2022,** *20* (5), 2929.
119. Santhosh, C.; Chinnam, S.; Madhu, G.; Kottam, N.; Chigurupati, S.; Sankannavar, R. Review on electrocatalytic nitrate reduction to ammonia: advances, challenges and future prospects. *Ionics* **2024**, 1-9.
120. Liang, J.; Li, Z.; Zhang, L.; He, X.; Luo, Y.; Zheng, D.; Wang, Y.; Li, T.; Yan, H.; Ying, B. Advances in ammonia electrosynthesis from ambient nitrate/nitrite reduction. *Chem* **2023,** *9* (7), 1768.
121. Zhang, X.; Wang, Y.; Wang, Y.; Guo, Y.; Xie, X.; Yu, Y.; Zhang, B. Recent advances in electrocatalytic nitrite reduction. *Chemical Communications* **2022,** *58* (17), 2777.
122. Yue, L.; Song, W.; Zhang, L.; Luo, Y.; Wang, Y.; Li, T.; Ying, B.; Sun, S.; Zheng, D.; Liu, Q. Recent advance in heterogenous electrocatalysts for highly selective nitrite reduction to ammonia under ambient condition. *Small Structures* **2023,** *4* (11), 2300168.
123. Dolla, T. H.; Zhang, B.; Matthews, T.; Chabalala, M. P.; Ajayi, S. O.; Sikeyi, L. L.; Liu, X.; Mathe, M. K. Metal/covalent-organic framework-based electrocatalysts for electrochemical reduction of nitrate to ammonia. *Coordination Chemistry Reviews* **2024,** *518*, 216061.
124. Chowdhury, I. H.; Gupta, S.; Rao, V. G. Covalent organic framework: an emerging catalyst for renewable ammonia production. *ChemCatChem* **2023,** *15* (11), e202300243.
125. Zhong, H.; Wang, M.; Ghorbani-Asl, M.; Zhang, J.; Ly, K. H.; Liao, Z.; Chen, G.; Wei, Y.; Biswal, B. P.; Zschech, E. Boosting the electrocatalytic conversion of nitrogen to ammonia on metal-phthalocyanine-based two-dimensional conjugated covalent organic frameworks. *Journal of the American Chemical Society* **2021,** *143* (47), 19992.
126. Jiang, M.; Han, L.; Peng, P.; Hu, Y.; Xiong, Y.; Mi, C.; Tie, Z.; Xiang, Z.; Jin, Z. Quasi-phthalocyanine conjugated covalent organic frameworks with nitrogen-coordinated transition metal centers for high-efficiency electrocatalytic ammonia synthesis. *Nano Letters* **2021,** *22* (1), 372.
127. He, H.; Wen, H. M.; Li, H. K.; Li, P.; Wang, J.; Yang, Y.; Li, C. P.; Zhang, Z.; Du, M. Hydrophobicity tailoring of ferric covalent organic framework/MXene nanosheets for high-efficiency nitrogen electroreduction to ammonia. *Advanced Science* **2023,** *10* (15), 2206933.
128. Lv, F.; Sun, M.; Hu, Y.; Xu, J.; Huang, W.; Han, N.; Huang, B.; Li, Y. Near-unity electrochemical conversion of nitrate to ammonia on crystalline nickel porphyrin-based covalent organic frameworks. *Energy & Environmental Science* **2023,** *16* (1), 201.
129. Hu, H.; Miao, R.; Yang, F.; Duan, F.; Zhu, H.; Hu, Y.; Du, M.; Lu, S. Intrinsic Activity of Metalized Porphyrin-based Covalent Organic Frameworks for Electrocatalytic Nitrate Reduction. *Advanced Energy Materials* **2024,** *14* (6), 2302608.. A. Lashof and D. R. Ahuja, *Nature*, 1990, **344**, 529-531.

Chapter 2

Resorcinol-Azodianiline Covalent Organic Framework Supported FeOOH Quantum Dots Catalyzed Electrochemical Ammonia Synthesis Under Ambient Conditions

2.1. Introduction

Since the 19th century, ammonia (NH_3) has been an essential feedstock for nitrogen-based fertilizers and pharmaceuticals.[1] However, the conventional Haber-Bosch process for NH_3 synthesis is associated with sustainability challenges, including significant energy use and CO_2 emissions.[2] These drawbacks stem from the inert nature of nitrogen, necessitating harsh reaction conditions (400°C-450 °C and 15 MPa-25 MPa). As a result, creating ecologically friendly and sustainable methods for NH_3 production under ambient settings becomes required.[3] In recent years, the electrocatalytic nitrogen reduction process (ENRR) is a promising and energy-efficient approach for ammonia production.[4-5] The ENRR offers the potential for NH_3 production under milder reaction conditions, providing cost effective and economical alternative to the H-B process.[2] However, The ENRR suffers slow kinetics and low selectivity problems, owing to the high energy barriers associated with N_2 activation and the competing hydrogen evolution reaction (HER), which occur in comparable potential ranges.[6-7] Extensive research has focused on developing efficient electrocatalysts to enhance NRR efficiency.[8] Several electrocatalyst materials, including noble metals, non-noble metals, alloys, and non-metallic materials, have been studied to increase ENRR performance.[9-10] Despite these efforts, achieving high catalytic performance remains a challenge. Therefore, the development of high-performance NRR electrocatalysts is crucial to meet the requirements for efficient and sustainable NH_3 synthesis.[11-15]

A covalent organic framework (COF) represents a porous, polymeric assemblage generated through the covalent cross-linking of functionalized monomers.[16-18] Its exceptional characteristics include a notable surface area, well-organized pore structure, and low density. Given the broad spectrum of composition, structure, and properties exhibited by COFs, they find utility across a diverse array of applications. These include electrocatalysis, charge storage, dye degradation, water remediation, proton conduction, sensing, gas sorption, storage, and separation.[19-22] An effective strategy for developing active catalysts/electrocatalysts has been to disperse or deposit catalytically active metal compounds in the form of nanoparticles (NPs).[23-27] COFs have been made from predesigned monomers that possess advantages such as conjugated π-clouds, charge-transfer moieties, and electron-rich functional groups that make them behave like conducting or semiconducting materials; when these redox-active sites in COF are coupled with the metal-based nanoparticles, a synergy can be expected, and the activation energy for specific

catalysis can be lowered.[19] The intrinsic porosity of these supports aid minimize the catalysis sluggishness.

Noble metal-based catalysts have demonstrated effective performance in the nitrogen reduction reaction (NRR). However, their widespread utilization is impeded by scarcity and high-cost issues.[28] First-row transition metal oxides (TMOs) have emerged as promising candidates due to their ease of large-scale preparation and increasing attention in various applications.[29] For us, Iron (Fe) fits the bill and plays a crucial role in biological nitrogenases as Fe-protein and MoFe-protein involved in N_2 fixation.[30] Inspired by this, the Fe oxides have been extensively investigated for N_2 reduction electrocatalysis.[31-34] FeOOH has garnered significant attention due to its unique tunnel-type structure and sustained redox action.[35-36] Encouraged by our recent success with oxy-hydroxide to act as a catalyst with simultaneous Bronsted-Lewis acidity and the ability of N-ligated transition metal to serve as Bronsted acid sites,[37] we chose FeOOH for this study.[38] FeOOH QDs (bandgap of 2.02 eV) have been surface activated with Pt to make catalysts.[39] We realize this activation can be achieved via electrochemical methods too. When these semiconducting FeOOH QDs are grown as amorphous high surface area particles, they can also have many defective sites, which would improve their catalytic efficiency.[39-40] COF can provide the right confinement to grow FeOOH QDs. Recent studies have demonstrated the efficient electrocatalytic performance of FeOOH nanorods in N_2 fixation, and its catalytic activity can be further enhanced through fluorine doping.[33] However, the intrinsic low electronic conductivity and poor catalytic surface area of FeOOH pose challenges to its catalytic activity. To overcome these issues, we have synthesized FeOOH QDs anchored on COF pores decorated with keto groups in a nano-sized and homogenous manner. This heterogeneous catalyst is well characterized, and its electroactivity towards nitrogen fixation has been studied. This catalyst showed the NRR yield of 77.4 $\mu g h^{-1} mg_{cat}^{-1}$ and Faradic efficiency of 46.4 % in 0.1 M $LiClO_4$ under −0.4 V vs. RHE. The incorporation of FeOOH, a potential Lewis-Bronsted acid, into this porous high surface area COF support delivers a high performance recyclable heterogeneous catalyst.

2.2. Experimental details

2.2.1 Synthesis of IISERP-COF33:

A solvothermal technique was used to manufacture IISERP-COF in a Pyrex tube. First, 2,4,6-triformylresorcinol (58 mg, 0.3 mmol) and 4,4'-azodianiline (96 mg, 0.45 mmol) were

measured into a Pyrex tube and dissolved in a combination of DMA (1.0 mL), ethanol (3.0 mL), and o-DCB (3.0 mL the solution was agitated until a consistent greenish colour emerged. Next, 0.5 mL of 6 M aqueous acetic acid was added. The tube and its contents were then frozen in a liquid nitrogen bath and sealed. It was baked at 120°C for 3 days and progressively cooled to room temperature over 12 hours. The resultant product was a maroon precipitate that was washed with methanol. The yield was 89%, with the chemical formula $C_{54}N_{12}O_4H_{36}$ and a molecular weight of 916.96 g/mol.

2.2.2 Synthesis of FeOOH QDs:

FeOOH QDs were produced using previously published processes with modest modifications.[35] For the synthesis technique, 1.0 mmol $FeCl_3 \cdot 6H_2O$ and 3.0 mmol $KHCO_3$ were dissolved in 40 mL of ethanol. The resultant solution was exposed to magnetic stirring for 8 hours to achieve complete mixing and reaction. The reaction products were then separated by centrifugation and rinsed multiple times with distilled water. Finally, the filtered products were dried in a vacuum oven at 40 °C to eliminate any leftover solvent and moisture.

2.2.3 Synthesis of FeOOH@COF:

FeOOH@COF were produced using a process like that of FeOOH QDs, with minor differences. About 1.0 mmol of $FeCl_3 \cdot 6H_2O$ was dissolved in 20 mL of ethanol. Separately, dissolve 200 mg of COF in 20 mL of ethanol and mix the two solutions together. After that, 3.0 mmol of $KHCO_3$ was added and left to stir for 8 hours. The reaction products were then separated by centrifugation and rinsed multiple times with distilled water. Finally, the filtered products were dried at 40 °C in a vacuum oven to eliminate any residual solvent and moisture.

2.2.4 Working electrode preparation:

To create homogeneous ink, 1 mg of FeOOH@COF electrocatalyst was added to 360 µL of ethanol, followed by 40 µL of Nafion solution (10 wt.% in ethanol) and ultrasonically treated for 15 mins. The catalyst ink was drop casted onto carbon fabric at a loading of 0.5 mg cm^{-2}.

2.2.5 Electrochemical measurements:

After first purging the Ar gas to get rid of any dissolved oxygen and oxygen-based contaminants, N_2 was used to purge it for a duration of 30 minutes. The electrocatalytic process was carried out using the electrochemical H-cell with Nafion 117 membrane. Nafion membrane was pre-treated before measurement by immersing it in ultrapure milliQ water and soaking it in an H_2O_2 (5 weight percent) aqueous solution for five hours at 80°C. At room temperature and pressure, electrochemical experiments were carried out in a 9 mL aqueous

solution containing 0.1 M $LiClO_4$. Ag/AgCl (NaCl 3.0 M) served as the reference electrode, Pt wire served as the counter electrode, and a carbon cloth covered with the catalyst served as the working electrode. Under continuous stirring, the constant potential electrolysis was carried out at −0.4 V vs. RHE. The RHE reference scale is applied to all reference electrodes by utilizing the formula

E (vs. RHE) = E (vs. Ag/AgCl) + 0.222 + 0.0591 × pH.

2.2.6 Determination of NH_3:

Using the indophenol blue technique, colorimetry was used to quantify the concentration of NH_3 in the solution after diluting the resultant electrolyte ten times. Following the reaction, 2 mL of the solution was combined with 2 mL of a 1 M NaOH coloring solution that included 10% $C_7H_5NaO_3$ and 10% $C_6H_5Na_3O_7{\cdot}2H_2O$ in element. Next, the solution was mixed with 0.2 mL of the catalyst solution of nitroprusside disodium dihydrate, $C_5FeN_6Na_2O$ (1 wt%), and 1 mL of an oxidizing solution comprising 0.05 M $NaClO_4$. The UV-vis absorption spectra were obtained following a two-hour period of darkness. The absorbance at a wavelength of 655 nm was used to determine the quantity of NH_3. Using the standard NH_4Cl solution and NH_3 concentrations of 0, 50, 100, 150, 200, and 250 ppm in 0.1 M $LiClO_4$ solution, the concentration-absorbance curve was calibrated. The fitting curve, which has an R2 of 0.996 and y = 0.00429x + 0.029, indicates a strong linear relationship between absorbance and NH_3 concentration.

2.2.7 Determination of N_2H_4:

The Watt and Chrisp technique were used to estimate the N_2H_4. The color reagent was a mixture of HCl and C_2H_5OH (V/V: 1/10) with 18.15 mg mL^{-1} of para-(dimethylamino) benzaldehyde, $C_9H_{11}NO$, as the solvent. To be more precise, 2 mL of electrolyte was stirred for 15 minutes after being introduced to 2 mL of color reagent. The hydrazine yields were quantified by measuring the absorbance of the solution using the hydrazine standard curve (y = 0.01648 x + 0.000232, R^2 = 0.999).

2.2.8 Determination of NH_3 yield and FE:

FE = (n$F * C * V$) / Q

$YR_{NH3} = (17C * V)/(t * m)$

where F is the Faradaic constant (96500 C mol^{-1}), M is the molar mass of products, Q is the total amount of applied electricity, t is the electrolysis time, m is the mass of catalyst, and n is the number of electrons transferred during NRR. V is the volume of cathodic electrolyte (9 mL).

2.2.9 Isotope-labelled experiments:

The feeding gases for the isotope labeling tests were $^{14}N_2$ and $^{15}N_2$, which were provided by Cambridge Isotope Laboratories, Inc. and had a purity of 98%. Before the experiment began, all possible N contamination was eliminated from the labeled $^{15}N_2$ gas by passing it through dual alkaline solutions (1 M KOH aqueous solution) and acid solutions (1 M H_2SO_4 aqueous solution) before purging it into the electrolyte solution. Prior to the $^{15}N_2$ gas flow, 30 minutes of Ar gas ran through the whole setup to eliminate any $^{14}N_2$ gas that could have been left in the system. After that, $^{15}N_2$ gas flowed for 15 minutes. The NRR experiment was carried out in a circulation setup in 9 mL of 0.1 M $LiClO_4$ aqueous solution for 2 hours at −0.4 V vs. RHE. Then, for 1H nuclear magnetic resonance (NMR) spectroscopy measurement (JEOL 400 MHz), 0.5 mL of the solution was combined with 0.1 mL of d6-DMSO and 0.1 mL of 1 M HCl.

2.2.10 Crystallographic structure modeling:

The Accelrys system was used for all atomic manipulations, crystallographic modeling, and simulations. (Materials Studio V 8.0) software.

To solve the structure of the COF, an initial structure was modeled via atomic-simulation using Materials Studio V.8.0. The initial model was tried in P6 or P3 as the possible high symmetry space groups; however, a satisfactory structure with acceptable bond lengths could not be obtained to match the experimental PXRD. Following this, symmetry was lowered to monoclinic and a satisfactory obtained space group was *P2/m*. Both the eclipsed and staggered configurations were simulated. The eclipsed one had lower energy and matched the experimental PXRD much better. Using this eclipsed model, we carried out Pawley refinement and the final lattice parameters and profile parameters were extracted (Figure 2.2A). The structure in *P*2/m had the following parameters *a* =33.65, *b* = 33.65, *c* = 3.3889 Å;

β = 120.0; R_p = 3.76%; R_{wp} = 6.84%. Formula sum: $C_{54}N_{12}O_4H_{34}$; Formula weight 914.94 g/mol. In the final modeled structure, the azo-linker results in a large pore of 28 Å (factors the Vander Waal radius of atoms) in this eclipsed model (Figure A2.1), which is well suitable with the experimental pore size (~27 Å). An excellent Pawley fit was obtained with prominent h00 reflections and the 001 reflection, indicating high degree of crystallinity. Importantly, the 001-reflection occurring at 2θ = 27.4° matches well with the interlayer separation of the modeled structure, suggestive of strong π-stacking. This Pawley refined structure was used in the optimization of the FeOOH@COF structure described in the A2.

2.2.11 XPS measurements:

Thermo K Alpha spectrometer was utilized to perform XPS measurements utilizing micro focused, monochromates Al Kα radiation with an energy of 1486.6 eV. During the spectral collection, the spectrometer's base pressure was greater than 10-8 mbar. For each core level, the pass energy used for spectral collection was maintained at 50 eV. During the data collecting process, charge correction was provided by the electron flood cannon. XPS peak software with a Shirley type backdrop was used to suit the peaks of each core-level.

2.2.12 Powder X-ray diffraction:

Utilizing a Rigaku Miniflex-600 apparatus, powder XRDs were processed with PDXL software.

2.2.13 Thermo-gravimetric Analysis:

Utilizing the NETSZCH TGA-DSC equipment, thermogravimetric analysis was performed. The samples were heated from 25 °C to 600 °C at 5 K/min during the TGAs, which were conducted under N_2 gas flow (20 ml/min) (purge + protection).

2.2.14 Nuclear Magnetic Resonance spectroscopy (NMR):

NMR spectra of the catalytic products were obtained using a 400 MHz Bruker 400 MHz Jeol ECS-400.

2.2.15 UV-visible spectroscopy:

Equipped with a Shimadzu UV-3600 UV-vis-near-IR spectrophotometer, solution state and diffuse-reflectance UV-visible spectra were captured. Spectroscopic measurements of diffuse-reflectance were performed using a white standard of $BaSO_4$.

2.2.16 IR spectroscopy:

A Bruker Optics ALPHA-E spectrometer equipped with a universal Zn-Se ATR (attenuated total reflection) accessory was used to get the infrared spectra.

2.2.17 Field Emission-Scanning Electron Microscopy:

Electron microscope including embedded AsB and EsB detectors and an integrated charge compensator. Instruments Oxford Xmax 80 mm^2. (Carl Zeiss NTS, Gmbh), Imaging parameters: Inlens detector, 200 kX, WD = 2 mm, and 2 kV. The materials were first carefully pulverized, bathed in ethanol for 30 minutes, and sonicated for two hours to prepare them for SEM imaging. These evenly distributed samples were vacuum-dried for 12 hours after being drop-casted onto the silicon wafer.

2.2.18 HR-Transmission electron microscopy:

The TEM pictures were taken using an FEI (Jeol FEG 2100F is the type) high-resolution transmission electron microscope (HR-TEM) that was outfitted with a field emission source running at 300 KeV. On a Cu grid, the evenly distributed sample was drop cast.

2.2.19 Adsorption analysis:

A 3-FLEX pore and surface area analyzer and, in certain instances, Micromeritics ASAP 2020 were used for all the adsorptions.

2.2.20 Computational details:

Accelrys (Materials Studio V8.0) was the program used for all software computations and simulations.

2.3. Results and discussion

2.3.1 Characterization:

Triformyl-resorcinol and azodianiline were used in a simple Schiff base synthesis under solvothermal conditions to create IISERP-COF33. The wet chemical technique was used to produce FeOOH@COF. Using this procedure, 20 mL of ethanol were mixed with 200 mg of IISERP-COF33, and the mixture was agitated for 10 minutes. 20 mL of 1.0 mmol $FeCl_3.6H_2O$ and 3.0 mmol of $KHCO_3$ were added to this distributed solution, respectively. In the experimental part, a thorough synthesis of IISERP-COF33 and FeOOH@COF has been described (Fig. 2.1, Scheme A2.1 and A2.2).

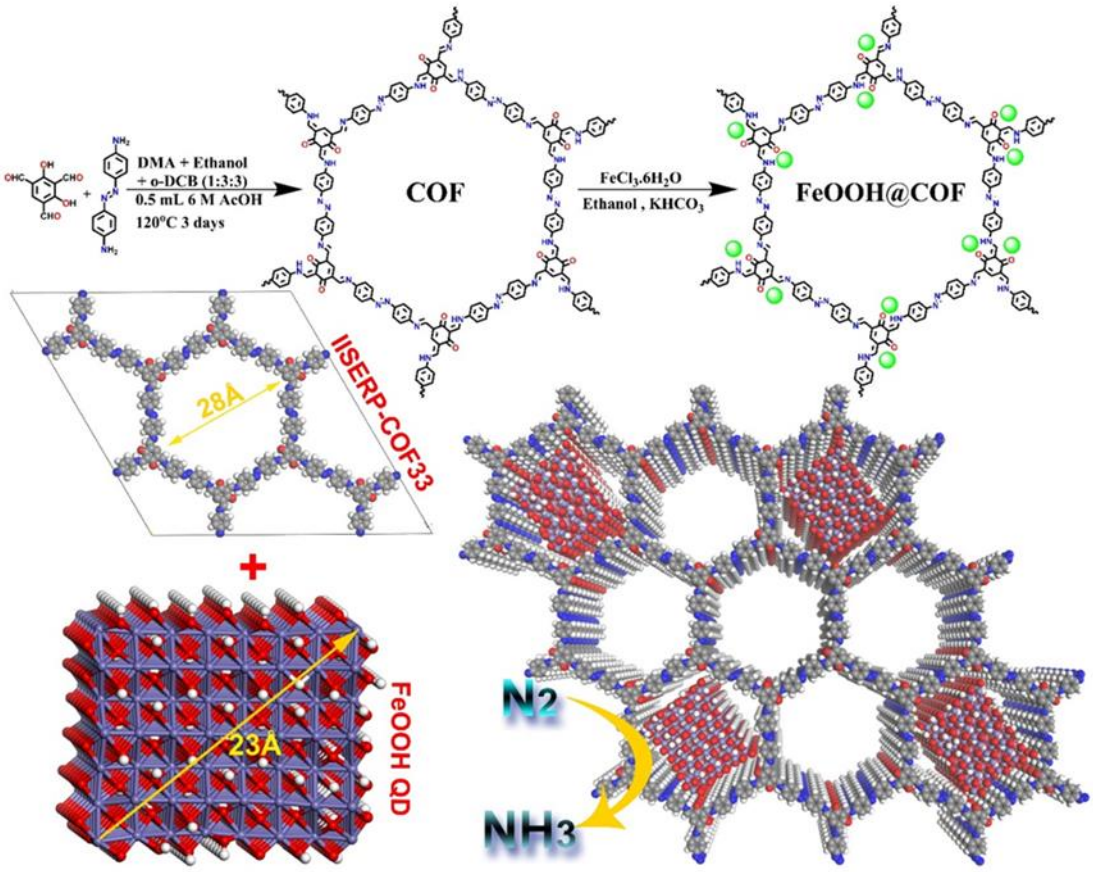

Figure 2.1. Schematic presentation of IISERP-COF33 and FeOOH@COF synthesis, and the DFT optimized structures of the IISERP-COF33 and the FeOOHODs – Schematic structural representation representation of nitrogen reduction reaction catalyst.

The structure of the IISERP-COF33 was crystallographically modeled using Materials Studio. For this, an initial structure was generated via atomic-simulation. The initial model was

constructed in P6 or P3; however, a satisfactory structure with acceptable bond lengths could not be obtained. Following this, space group P2/m, symmetry was reduced to monoclinic, and a workable solution was found. Both the eclipsed and staggered configurations were simulated. The eclipsed one had lower energy and matched the experimental PXRD much better. Using this eclipsed model, we carried out Pawley refinement and the final lattice parameters and profile parameters were extracted (Fig. 2.2A). The structure in *P*2/m had the following parameters *a* =33.65, *b* = 33.65, *c* = 3.3889 Å; *β* = 120 °; R_p = 3.76 %; R_{wp} = 6.84 %.

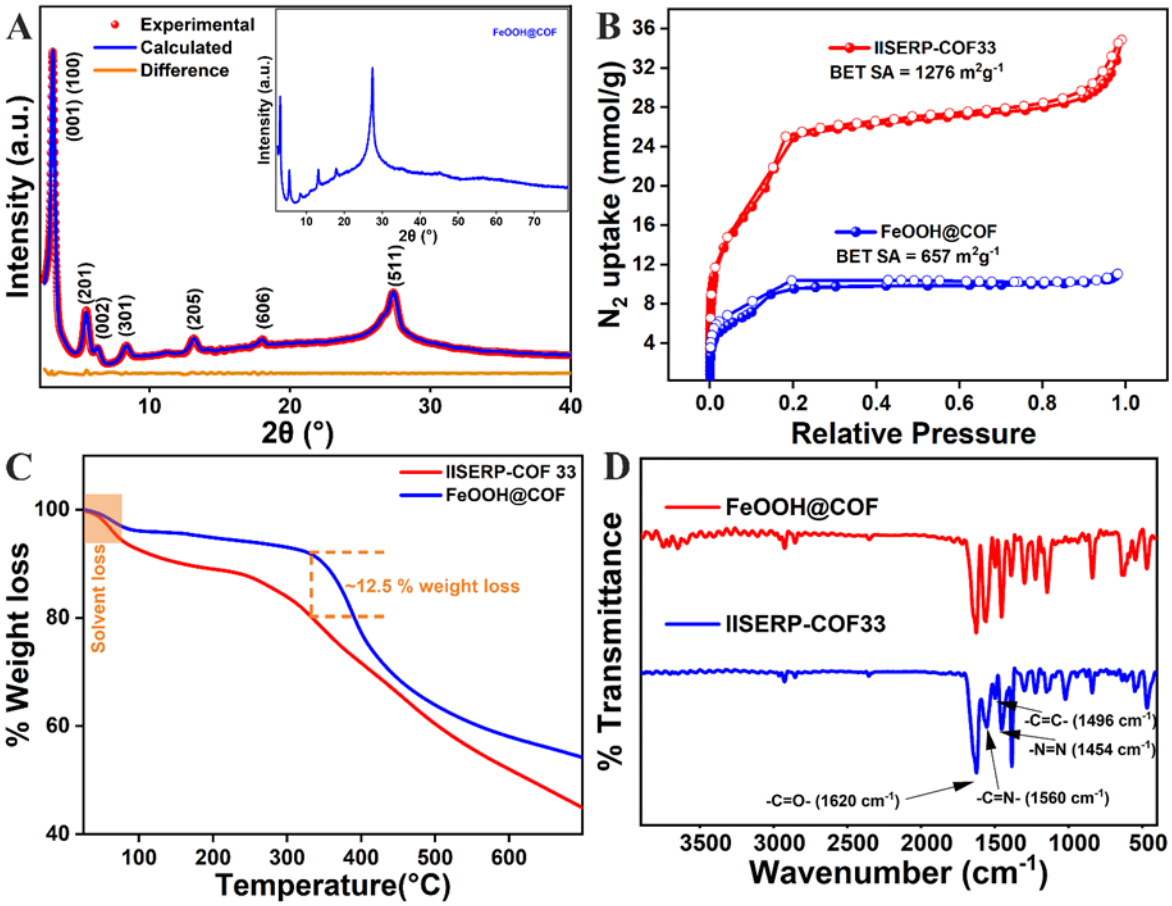

Figure 2.2. (A) Experimental PXRD of IISERP-COF33 and FeOOH@COF. Note that there are no peaks corresponding to the FeOOH in the FeOOH@COF, which indicates their amorphous and nano-sized nature. Also, there is some loss in the COF's crystallinity with the FeOOH loading. (B) N_2 adsorption profile isotherms collected at temperature 77 K and the estimated surface areas. (C) TGA profile of IISERP-COF33 and FeOOH@COF showing that the materials are highly stable up to 300 °C. (D) Fourier Transform Infrared (FTIR) spectra of IISERP-COF33 and FeOOH@COF showing the characteristics stretching frequencies, their match confirm the functional group integrity.

IISERP-COF33's experimental powder x-rays diffraction spectra were refined against this model. The refinement converged extremely well, and several sharp crystalline peaks observed at 2θ = 3.1, 5.4°, 5.6°, 8.3°, 13.1°, 17.8° and 27.4° (Fig. 2.2A) were indexed to the following reflections to (001), (201), (002), (301), (205), (606) and (511) planes. FeOOH@COF maintains this crystallinity, confirming the successful FeOOH loading and COF's stability in this process (Fig A2.1). Using N_2 adsorption at 77 K, the neat COF's permanent porosity was evaluated. A type-I isotherm was produced for the COF (Fig. 2.2B), indicating a saturation N_2 uptake of 28 mmol g^{-1}. According to measurements, the Langmuir and Brunauer-Emmett-Teller (BET) surface areas are 2,798 and 1,276 $m^2 g^{-1}$, respectively (Fig. 2.2B and A2.3). On the other hand, compared to the plain COF (~35% decrease), the N_2 adsorption isotherm of FeOOH@COF showed a reduced saturated N_2 absorption, measuring 10 mmol g^{-1}. This reduction implies a notable loading concentration of iron oxyhydroxide into the COF structure. At the same time ample porosity is left in the FeOOH@COF (Fig. 2.2B and A2.2-A2.4). Note: The samples were washed thoroughly using a hot DMF solution before the porosity studies, which ensured the removal of any weakly held iron particles. Hence, the porosity drop is attributed to FeOOH residing in the COF pores. The thermogravimetric analysis (TGA) reveals that both IISERP-COF33 and FeOOH@COF remain stable up to 300 °C (Fig. 2.2C). The material exhibits porosity as evidenced by the first mass loss that is caused by solvent molecules that have become occluded within the COF pores (Fig. 2.2C). To confirm the linkage formation and stability of this Schiff base COF and the FeOOH@COF, we recorded their Fourier Transform Infrared (FTIR) spectra, which displays all the characteristic stretching vibrations of carbonyl (-C=O-), azo bond (-N=N-) and imine (-C=N-) at 1620, 1560 and 1454 cm^{-1}, respectively (Fig. 2.2D). Chemical shift characteristics are clarified using solid-state magic-angle spinning nuclear magnetic resonance (SS-MAS NMR) spectroscopy. For aromatic carbon atoms, peaks in the δ = 110–120 ppm range have been identified. Notably, the COF's hydroxyl (-OH) groups may have tautomerized to keto (C=O) forms due to the resonance at δ = 183 ppm (Fig. A2.26).

2.3.2 Morphological analysis:

Field emission scanning electron microscopy (FESEM) analysis of IISERP-COF33 and FeOOH@COF revealed a distinctive cotton-like morphology anticipated for this low-density fluffy COF powder (Fig. A2.5). The COF's elemental mapping revealed that iron species were

distributed uniformly throughout (Fig. A2.6). Inductively coupled plasma (ICP) analysis verified a 12.5% iron loading, which was in line with the energy dispersive X-ray analysis (EDAX) of FeOOH@COF that showed 13% iron loading (Fig. A2.7). Important structural insights were revealed by high-resolution transmission electron microscopy (HRTEM) study of pure COF and FeOOH@COF. The COF could be identified as thin platy flakes stacked and bundled up at lower resolution. However, the higher-

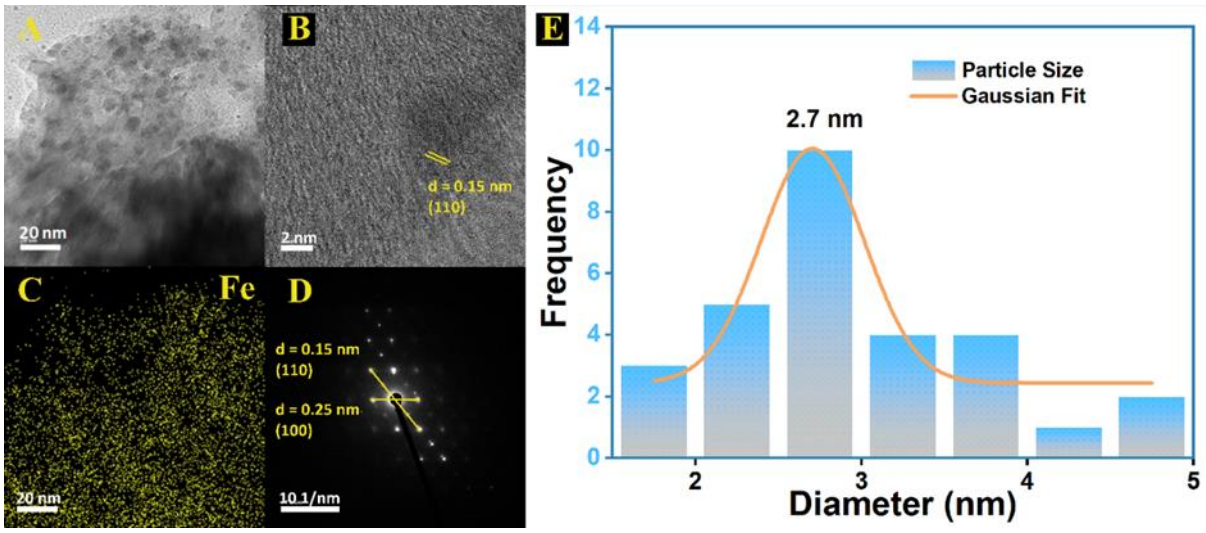

Figure 2.3. (A and B) IISERP-COF33 TEM pictures at various magnifications. Lattice fringes have been observed for FeOOH (110) planes with a d spacing of 0.15 nm. (C) Elemental mapping for FeOOH@COF showing the uniform distribution of Fe in the COF. (D) SAED pattern of FeOOH QDs have been observed which corresponds to planes (100) and (110). (E) Particles distributions of FeOOH QDs on COF collected at different regions which gives average particle size of 2~3 nm.

resolution HRTEM images of the neat COF revealed the presence of large micron-sized flakes with uniform micropores. For FeOOH@COF, similar features were observed. In addition, distinctive diffraction spots from FeOOH QDs with similar particle size of 2.7 nm (Fig. 2.3 and A2.8) were seen. FeOOH QDs are typically amorphous.[40] Interestingly, the FeOOH@COF was crystalline, exhibiting lattice fringes that match the (110) reflections with a d-spacing of 0.15 nm. The COF flakes had multiple domains with similar lattice fringes, which corroborated well with the well-defined diffraction spots observed in the Selected Area Electron Diffraction (SAED) image. These facets are likely the active facets involved in catalytic processes, and they are not usually exposed in bulk FeOOH; these observations suggest structural modifications

induced during the growth of FeOOH in the COF framework and could explain their potential impact on catalytic activity.

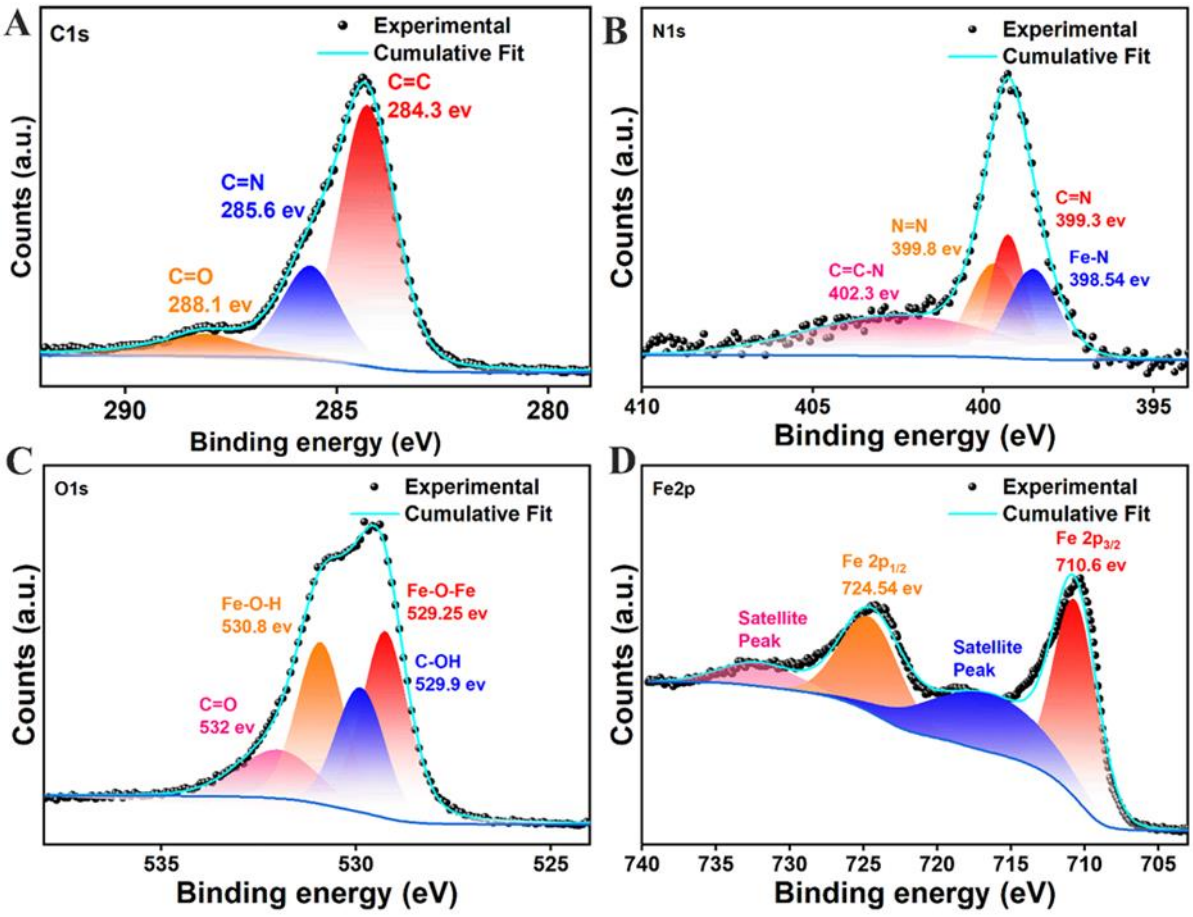

Figure 2.4. High resolution XPS spectra of C1s, N1s, O1s, and Fe 2p for the FeOOH@COF are shown in (A, B, C, and D). FeOOH is suggested to be present by the peaks for Fe-O-H and Fe-O-Fe.

2.3.3 XPS analysis:

Fe 2p's X-ray photoelectron spectroscopy (XPS) spectra, which are shown in Figure 2.4, show clear peaks. To be more precise, the Fe 2p1/2 and Fe 2p3/2 peaks, which were detected at 724.54 and 710.6 eV, respectively, support the idea that the Fe (III) oxidation state is predominant. Additionally, the presence of two satellite peaks provides further evidence supporting the Fe ion's oxidation state of +3.[31] The interaction between the framework atoms and the FeOOH is shown by the peak at 398.54 eV for Fe–N in the deconvoluted N1s spectra (Fig. 2.4B). Additionally, the as-prepared FeOOH@COF's O1s spectra may be deconvoluted into four distinct peaks at 529.25, 529.9, 530.8, and 532 eV (Figure 2.4C). Two of these peaks

correspond to the Fe-O-Fe and Fe-O-H units, consistent with presence of FeOOH as the majority phase. However, these do not rule out the possibility of mixed valence iron oxides, but the lattice spacings observed from HRTEM favour FeOOH. The XPS Spectrum of IISERP-COF33 shows distinct characteristic peaks for Schiff bond formation (Fig. A2.9)

2.3.4 Electrochemical nitrogen reduction:

Recently, there has been a lot of interest in the electrochemical nitrogen reduction process (NRR), which uses renewable energy to create ammonia (NH_3) at room temperature and pressure.[4-8] Whereas iron-based catalysts are used at high temperatures and pressures in the traditional commercial Haber-Bosch process, the electrochemical NRR provides a more environmentally friendly method of producing NH_3. Prior research has investigated a range of materials, such as noble metals, for the generation of NH_3, but obstacles still need to be overcome to achieve high performance and Faradaic efficiency.[10] Extending from prior work on Fe-based catalysts,[30-35] we investigated the catalytic activity of FeOOH@COF with high-density, adequate surface area and finely dispersed FeOOH QDs.

Our investigations focused on electrochemical NRR using the FeOOH@COF electrode at STP in an H-shaped electrochemical cell separated by a Nafion 117 membrane. The NRR activity was assessed through controlled potential electrolysis (CPE) with N_2-saturated electrolytes. Ar- and N_2-saturated electrolytes showed different current densities in linear sweep voltammetry (LSV) curves for FeOOH, suggesting catalytic activity toward N_2 electrochemical reduction. Unless otherwise noted, all potentials provided in this chapter were converted to values versus a reversible hydrogen electrode (RHE). In a 0.1 M $LiClO_4$ solution, the LSV profiles of FeOOH showed fluctuating current densities between 0.2 and -0.8 V. Separate tests were carried out using a nitrogen saturated electrolyte. (Fig. 2.5A). Notably, the current density observed in the nitrogen saturated electrolyte surpassed that in the Argon saturated electrolyte, signifying the catalytic activity of FeOOH@COF towards N_2 electrochemical reduction.

Constant potential electrolysis of FeOOH@COF was conducted under various applied potentials to investigate the resulting products (Fig. 2.5B-C). The indophenol blue technique was used to calculate the NH_3 yield rate[41-44] while N_2H_4 was measured by the Watt Chrisp method (S10-A2.15)[42-44]. The results revealed high selectivity for NH_3 over N_2H_4, with a

maximum NH_3 yield of 77.4 $\mu g h^{-1} mg_{cat.}^{-1}$ and a Faradaic efficiency sharp peak of 46.4% at −0.4 V. Time-dependent current density curves indicated efficient NRR over 2 hours (Figure 2.5B).

2.3.5 Recyclability and control studies:

In the control experiments, utilizing an argon saturated electrolyte and a bare carbon cloth (CC) based electrode, the absence of detectable levels of ammonia through UV–vis analyses substantiated the exclusive generation of NH_3 resulting from the electrocatalytic nitrogen conversion reaction occurring on the FeOOH@COF catalyst (Fig. 2.5D and A2.16). To elucidate the effectiveness of the composite catalyst, FeOOH@COF, for electrocatalytic NRR, bare FeOOH nanoparticles and IISERP-COF33 were studied as control samples, where COF shows slight activity as compared to bare FeOOH (Fig. 2.5D). The outcomes demonstrated that, in ambient settings, the high-density, finely distributed FeOOH quantum dots in FeOOH@COF acted as the real active sites for the electroreduction of N_2. Additionally, COF helps to provide increased surface area with adequate N_2 uptake. Importantly, the optical bandgap measurements and the Tauc plot derived from it suggests lowering of the bandgap of FeOOH when embedded as QDs in the COF's confinement (Figure A2.17). This bandgap lowering would help the electrons to flow better from the current collector to the coated active material, which can positively impact the electrocatalytic activity.

Additionally, the ammonia synthesis's nitrogen-15 isotopic labeling was carried out at a potential of −0.4 V versus the RHE when $^{15}N_2$ and FeOOH@COF were present (Fig. A2.18). With the ^1H NMR spectra of reference samples, $^{14}NH_4Cl$ and $^{15}NH_4Cl$ standard samples, ^1H nuclear magnetic resonance (NMR) spectroscopy was utilized to examine the post-electrolytes produced utilizing $^{14}N_2$ and $^{15}N_2$ as input gases as references (Figure A2.19). Notably, Triplet peaks with a coupling constant of about ≈52 Hz were seen in the ^1H NMR spectra acquired for NH_3 generated in a saturated $^{14}N_2$ environment; these peaks were like those of the reference $^{14}NH_4Cl$ sample. On the other hand, the ^1H NMR spectra of the post-electrolyte of FeOOH@COF with a coupling constant of around ≈72 Hz and commercial $^{15}NH_4Cl$ showed doublet peaks in the presence of $^{15}N_2$ at −0.4 V vs RHE, suggesting the synthesis of $^{15}NH_3$ (Fig. A2.20). Additionally, the measured production yields of ^{14}N-labeled and ^{15}N-labeled NH_3 quantified through ^1H NMR spectroscopy were comparable (78.7

$\mu g h^{-1} mg_{cat.}^{-1}$) (Fig. 2.6A). These findings unequivocally suggest that N_2 gas serves as the sole nitrogen source for electrocatalytic NH_3 synthesis.

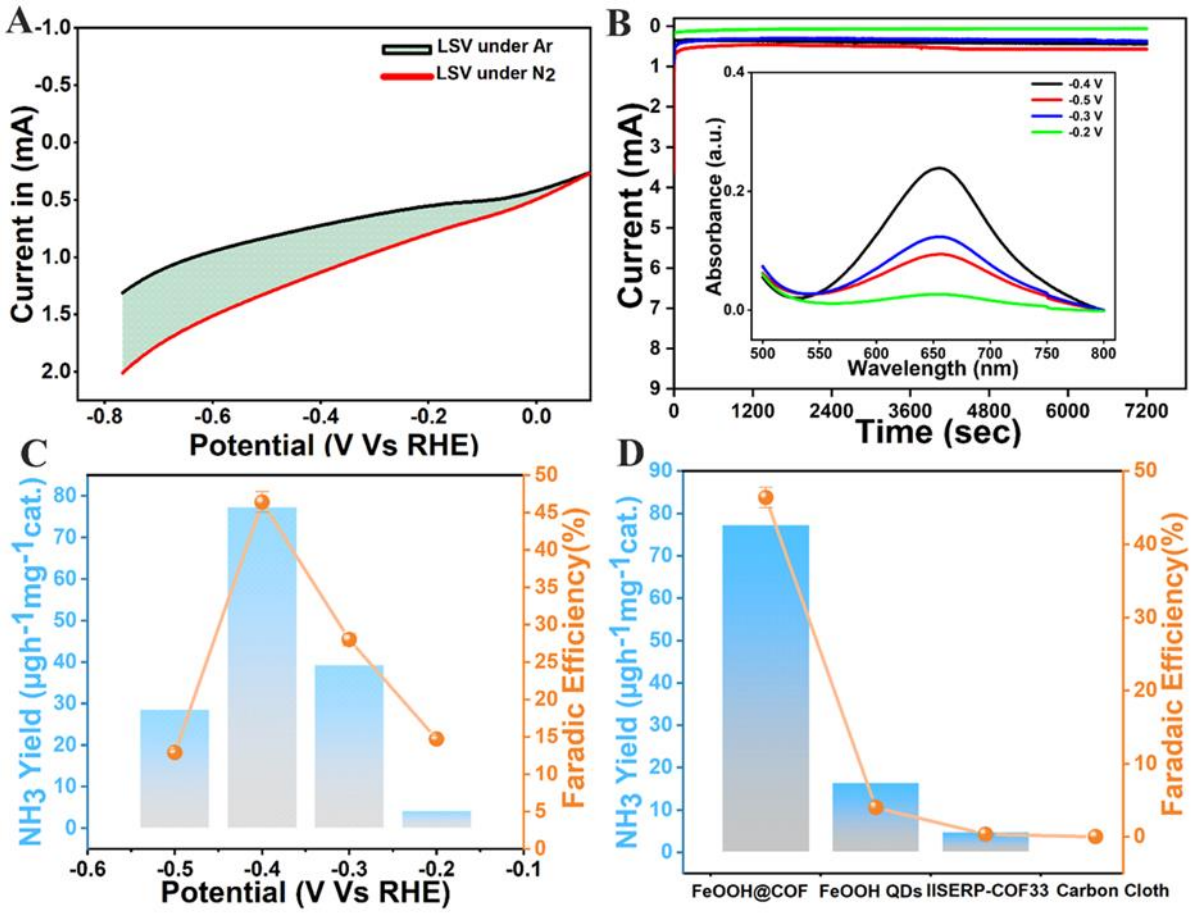

Figure 2.5. (A) LSV curves of the active catalyst under Ar and N_2 gas saturated atmospheres. (B) Constant potential electrolysis curves of the active catalyst at different potentials. (C) NRR performances of the active catalyst at different potentials. (D) NRR performances of FeOOH@COF, FeOOH QDs, IISERP-COF33 and Carbon cloth at −0.4 V vs RHE.

2.3.6 Post Catalytic characterizations:

Following the catalytic process, we characterized the wasted catalyst using a variety of methods. Powder X-ray diffraction reveals that with each cycle, the COF's crystallinity somewhat succumbs (Fig. A2.21). Nonetheless, the intactness of the functional group and covalent connection in the post-catalysis sample are confirmed by IR spectra. The parent material's PXRD peaks were all intact, indicating that the general structure of the COF is still intact despite the crystallinity decline (Fig. A2.22). Notably, no noticeable aldehyde or amine-related peaks, which could have formed due to COF degradation, were observed. The catalyst

is recycled for upto 7 cycles without any appreciable capacity fade, which validates the durability and activity of the catalyst. Additionally, we performed a long-term stability test for 20 hours for CPE measurement to check electrochemical stability in an electrochemical environment (Fig. 2.6B-D.) Fe content (from ICP) stays nearly the same (12.5 %) (Fig. A2.23). To understand the chemical and morphological changes after catalysis, we performed FESEM and XPS studies, which revealed no noticeable changes (Fig. A2.24-A2.25). Additionally, EIS analysis confirmed that the catalyst's electronic properties were retained even after catalysis (Fig. A2.26).

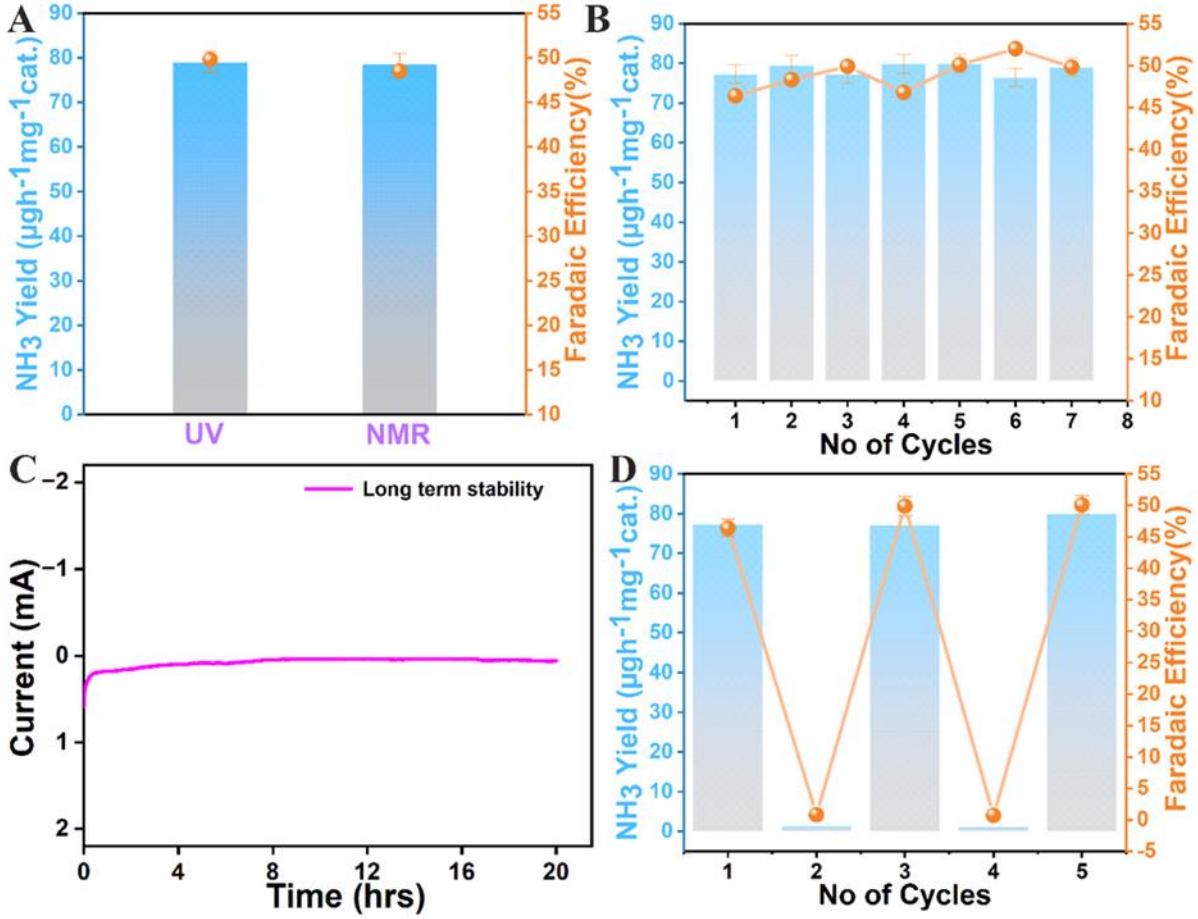

Figure 2.6. (A) NRR performance determined by UV-vis and NMR method. (B) NRR performance of FeOOH@COF for consecutive cycles. (C) Constant potential electrolysis curve of active catalyst for 20 hours. (D) NRR performance of FeOOH@COF under alternate Ar and N_2 saturated atmospheres.

2.3.7 Discussion:

Diverse iron-based nanomaterials and supported FeOOH QDs have been investigated for electrochemical ammonia production. For example, iron has been loaded or anchored into COF[45], and in some cases, such COF has been composted with MXENES[46] or nanocarbon[47,48] and investigated for electrocatalysis. Alternatively, iron vanadate and iron-doped indium vanadates have been explored[49], and more relevantly, FeOOH QDs have been supported on conductive graphene sheets or nanostructured and employed as nitrogen reduction catalysts.[32,50,51] A comparison of the performance of FeOOH@COF with other iron-containing electrocatalysts tested under comparable conditions reveals that achieving simultaneous high Faradaic efficiency and NH_3 yield takes work. Fortunately, our FeOOH@COF exhibits the scores for both efficiency metrics (Table A2.1), opening up many new possibilities to develop cost-effective iron-based electrocatalysts for ammonia production.

2.4. Conclusion

In conclusion, this chapter presents the synthesis and electrocatalytic evaluation of novel heterogeneous catalyst, FeOOH@COF, composed of iron oxyhydroxide (FeOOH) quantum dots integrated into an imine linked COF (IISERP-COF33). The electrocatalyst exhibits structural regularity, stability, and thermal robustness up to 300 °C, as evidenced by PXRD, FTIR, and TGA analyses. The FESEM and HRTEM images confirm the homogeneous distribution of 13 wt.% nano-sized FeOOH quantum dots within the COF matrix. To the best of our knowledge, FeOOH@COF exhibits superior performance compared to other reported COF and iron-based nitrogen reduction electrocatalysts, showing remarkable faradaic efficiency of 46.4% at −0.4 V in 0.1 M $LiClO_4$ aqueous solution and an ammonia production yield of 77.4 μg h^{-1} mg cat^{-1}. This chapter contributes to the systematic design of covalent organic framework-supported aqueous-stable quantum dots, paving the way for an affordable route to electrocatalytic ammonia production. Our FeOOH@COF presents an excellent system for deeper mechanistic studies, diverse operational exploration, and scalability shots. Integration of these affordable systems with renewable energy can materialize sustainable electrocatalysts for ammonia production.

2.5. References

(1) Valera-Medina, A.; Amer-Hatem, F.; Azad, A. K.; Dedoussi, I. C.; de Joannon, M.; Fernandes, R. X.; Glarborg, P.; Hashemi, H.; He, X.; Mashruk, S.; McGowan, J.; Mounaim-Rouselle, C.; Ortiz-Prado, A.; Ortiz-Valera, A.; Rossetti, I.; Shu, B.; Yehia, M.; Xiao, H.; Costa, M. Review on Ammonia as a Potential Fuel: From Synthesis to Economics. *Energy Fuels* 2021, *35* (9), 6964–7029.

(2) Smith, C.; Hill, A. K.; Torrente-Murciano, L. Current and Future Role of Haber–Bosch Ammonia in a Carbon-Free Energy Landscape. *Energy Environ. Sci.* 2020, *13* (2), 331–344.

(3) Humphreys, J.; Lan, R.; Tao, S. Development and Recent Progress on Ammonia Synthesis Catalysts for Haber–Bosch Process. *Adv. Energy Sustain. Res.* 2021, *2* (1), 2000043.

(4) Yang, B.; Ding, W.; Zhang, H.; Zhang, S. Recent Progress in Electrochemical Synthesis of Ammonia from Nitrogen: Strategies to Improve the Catalytic Activity and Selectivity. *Energy Environ. Sci.* 2021, *14* (2), 672–687.

(5) Fu, X.; Zhang, J.; Kang, Y. Recent Advances and Challenges of Electrochemical Ammonia Synthesis. *Chem Catal.* 2022, *2* (10), 2590–2613.

(6) Qing, G.; Ghazfar, R.; Jackowski, S. T.; Habibzadeh, F.; Ashtiani, M. M.; Chen, C.-P.; Smith, M. R. I.; Hamann, T. W. Recent Advances and Challenges of Electrocatalytic N_2 Reduction to Ammonia. *Chem. Rev.* 2020, *120* (12), 5437–5516.

(7) Jin, H.; Kim, S. S.; Venkateshalu, S.; Lee, J.; Lee, K.; Jin, K. Electrochemical Nitrogen Fixation for Green Ammonia: Recent Progress and Challenges. *Adv. Sci.* 2023, *10* (23), 2300951.

(8) Chanda, D.; Xing, R.; Xu, T.; Liu, Q.; Luo, Y.; Liu, S.; Tufa, R. A.; Dolla, T. H.; Montini, T.; Sun, X. Electrochemical Nitrogen Reduction: Recent Progress and Prospects. *Chem. Commun.* 2021, *57* (60), 7335–7349.

(9) Yang, X.; Xu, B.; Chen, J. G.; Yang, X. Recent Progress in Electrochemical Nitrogen Reduction on Transition Metal Nitrides. *ChemSusChem* 2023, *16* (5), e202201715.

(10) Wang, T.; Guo, Z.; Zhang, X.; Li, Q.; Yu, A.; Wu, C.; Sun, C. Recent Progress of Iron-Based Electrocatalysts for Nitrogen Reduction Reaction. *J. Mater. Sci. Technol.* 2023, *140*, 121–134.

(11) Moon, Y. H.; Kim, N. Y.; Kim, S. M.; Jang, Y. J. Recent Advances in Electrochemical Nitrogen Reduction Reaction to Ammonia from the Catalyst to the System. *Catalysts* 2022, *12* (9), 1015.

(12) Chowdhury, I. H.; Gupta, S.; Rao, V. G. Covalent Organic Framework: An Emerging Catalyst for Renewable Ammonia Production. *ChemCatChem* 2023, *15* (11), e202300243.

(13) Chen, S.; Qi, G.; Yin, R.; Liu, Q.; Feng, L.; Feng, X.; Hu, G.; Luo, J.; Liu, X.; Liu, W. Electrocatalytic Nitrate-to-Ammonia Conversion on CoO/CuO Nanoarrays Using Zn–Nitrate Batteries. *Nanoscale* 2023, *15* (48), 19577–19585.

(14) Yang, M.; Wei, T.; He, J.; Liu, Q.; Feng, L.; Li, H.; Luo, J.; Liu, X. Au Nanoclusters Anchored on TiO2 Nanosheets for High-Efficiency Electroreduction of Nitrate to Ammonia. *Nano Res.* 2024, *17* (3), 1209–1216.

(15) Zhang, G.; Wang, G.; Wan, Y.; Liu, X.; Chu, K. Ampere-Level Nitrate Electroreduction to Ammonia over Monodispersed Bi-Doped FeS2. *ACS Nano* 2023.

(16) Côté, A. P.; Benin, A. I.; Ockwig, N. W.; O'Keeffe, M.; Matzger, A. J.; Yaghi, O. M. Porous, Crystalline, Covalent Organic Frameworks. *Science* 2005, *310* (5751), 1166–1170.

(17) Geng, K.; He, T.; Liu, R.; Dalapati, S.; Tan, K. T.; Li, Z.; Tao, S.; Gong, Y.; Jiang, Q.; Jiang, D. Covalent Organic Frameworks: Design, Synthesis, and Functions. *Chem. Rev.* 2020, *120* (16), 8814–8933.

(18) Huang, N.; Wang, P.; Jiang, D. Covalent Organic Frameworks: A Materials Platform for Structural and Functional Designs. *Nat. Rev. Mater.* 2016, *1* (10), 1–19.

(19) Chakraborty, D.; Mullangi, D.; Chandran, C.; Vaidhyanathan, R. Nanopores of a Covalent Organic Framework: A Customizable Vessel for Organocatalysis. *ACS Omega* 2022, *7* (18), 15275–15295.

(20) Pachfule, P.; Panda, M. K.; Kandambeth, S.; Shivaprasad, S. M.; Díaz, D. D.; Banerjee, R. Multifunctional and Robust Covalent Organic Framework–Nanoparticle Hybrids. *J. Mater. Chem. A* 2014, *2* (21), 7944–7952.

(21) Mullangi, D.; Chakraborty, D.; Pradeep, A.; Koshti, V.; Vinod, C. P.; Panja, S.; Nair, S.; Vaidhyanathan, R. Highly Stable COF-Supported Co/$Co(OH)_2$ Nanoparticles Heterogeneous Catalyst for Reduction of Nitrile/Nitro Compounds under Mild Conditions. *Small* 2018, *14* (37), 1801233.

(22) Chakraborty, D.; Shekhar, P.; Singh, H. D.; Kushwaha, R.; Vinod, C. P.; Vaidhyanathan, R. Ag Nanoparticles Supported on a Resorcinol-Phenylenediamine-Based Covalent Organic Framework for Chemical Fixation of CO_2. *Chem. Asian J.* 2019, *14* (24), 4767–4773.

(23) Nandi, S.; Singh, S. K.; Mullangi, D.; Illathvalappil, R.; George, L.; Vinod, C. P.; Kurungot, S.; Vaidhyanathan, R. Low Band Gap Benzimidazole COF Supported Ni_3N as Highly Active OER Catalyst. *Adv. Energy Mater.* 2016, *6* (24), 1601189.

(24) Mullangi, D.; Dhavale, V.; Shalini, S.; Nandi, S.; Collins, S.; Woo, T.; Kurungot, S.; Vaidhyanathan, R. Low-Overpotential Electrocatalytic Water Splitting with Noble-Metal-Free Nanoparticles Supported in a sp^3 N-Rich Flexible COF. *Adv. Energy Mater.* 2016, *6* (13), 1600110.

(25) Guo, J.; Jiang, D. Covalent Organic Frameworks for Heterogeneous Catalysis: Principle, Current Status, and Challenges. *ACS Cent. Sci.* 2020, *6* (6), 869–879.

(26) Chandran, C.; Singh, H. D.; Leo, L. S.; Shekhar, P.; Rase, D.; Chakraborty, D.; Vinod, C. P.; Vaidhyanathan, R. A Covalent Organic Framework with Electrodeposited Copper Nanoparticles – a Desirable Catalyst for the Ullmann Coupling Reaction. *J. Mater. Chem. A* 2022, *10* (29), 15647–15656.

(27) Rao, X.; Liu, M.; Chien, M.; Inoue, C.; Zhang, J.; Liu, Y. Recent Progress in Noble Metal Electrocatalysts for Nitrogen-to-Ammonia Conversion. *Renew. Sustain. Energy Rev.* 2022, *168*, 112845.

(28) Zhang, L.; Fan, Q.; Li, K.; Zhang, S.; Ma, X. First-Row Transition Metal Oxide Oxygen Evolution Electrocatalysts: Regulation Strategies and Mechanistic Understandings. *Sustain. Energy Fuels* 2020, *4* (11), 5417–5432.

(29) Rapson, T. D.; Gregg, C. M.; Allen, R. S.; Ju, H.; Doherty, C. M.; Mulet, X.; Giddey, S.; Wood, C. C. Insights into Nitrogenase Bioelectrocatalysis for Green Ammonia Production. *ChemSusChem* 2020, *13* (18), 4856–4865.

(30) Sun, H.; Yin, H.-Q.; Shi, W.; Yang, L.-L.; Guo, X.-W.; Lin, H.; Zhang, J.; Lu, T.-B.; Zhang, Z.-M. Porous β-FeOOH Nanotube Stabilizing Au Single Atom for High-Efficiency Nitrogen Fixation. *Nano Res.* 2022, *15* (4), 3026–3033.

(31) Tan, J.; He, X.; Yin, F.; Liang, X.; Li, G.; Li, Z. Zr-Doped α-FeOOH with High Faradaic Efficiency for Electrochemical Nitrogen Reduction Reaction. *Appl. Surf. Sci.* 2021, *567*, 150801.

(32) Zhu, X.; Liu, Z.; Wang, H.; Zhao, R.; Chen, H.; Wang, T.; Wang, F.; Luo, Y.; Wu, Y.; Sun, X. Boosting Electrocatalytic N_2 Reduction to NH_3 on β-FeOOH by Fluorine Doping. *Chem. Commun.* 2019, *55* (27), 3987–3990.

(33) Jia, L.; Xue, H.; Xian, F.; Sugahara, Y.; Sakai, N.; Nan, J.; Yamauchi, Y.; Sasaki, T.; Ma, R. Porous and Partially Dehydrogenated Fe^{2+}-Containing Iron Oxyhydroxide Nanosheets for Efficient Electrochemical Nitrogen Reduction Reaction (ENRR). *Small* 2023, *19* (42), 2303221.

(34) Hosseini, M.-S.; Abbasi, A.; Masteri-Farahani, M. Decoration of NH_2-UiO-66 with FeOOH Quantum Dots for Improving Photo-Degradation of Organic Dyes upon Visible Light Irradiation. *Appl. Surf. Sci.* 2022, *604*, 154514.

(35) El Issmaeli, Y.; Lahrichi, A.; Kalanur, S. S.; Natarajan, S. K.; Pollet, B. G. Recent Advances and Prospects of FeOOH-Based Electrode Materials for Supercapacitors. *Batteries* 2023, *9* (5), 259.

(36) Cho, M. K.; Jo, J. H.; Choi, J. U.; Kim, J.; Yashiro, H.; Yuan, S.; Shi, L.; Sun, Y.-K.; Myung, S.-T. Tunnel-Type β-FeOOH Cathode Material for High Rate Sodium Storage via a New Conversion Reaction. *Nano Energy* 2017, *41*, 687–696.

(37) Tomoda, M.; Kondo, M.; Izu, H.; Masaoka, S. Brønsted Acid/Base Site Isolated in a Pentanuclear Scaffold. *Chem. Eur. J.* 2023, *29* (7), e202203253.

(38) Shekhar, P.; Datta Devulapalli, V. S.; Reji, R.; Singh, H. D.; Jose, A.; Singh, P.; Torris, A.; Vinod, C. P.; Tokarz, J. A.; Mahle, J. J.; Peterson, G. W.; Borguet, E.; Vaidhyanathan, R. COF-Supported Zirconium Oxyhydroxide as a Versatile Heterogeneous Catalyst for Knoevenagel Condensation and Nerve Agent Hydrolysis. *iScience* 2023, *26* (11), 108088.

(39) Pei, M.; Lv, S.; Liu, Y.; Si, Z.; Wu, X.; Ran, R.; Weng, D.; Kang, F. Sub-Nano Pt/β-FeOOH Quantum Dots for Photocatalytic Removal of Toluene: Catalyst Design, Preparation, and Benefits. *Front. Mater.* 2022, *9*.

(40) Liu, J.; Zheng, M.; Shi, X.; Zeng, H.; Xia, H. Amorphous FeOOH Quantum Dots Assembled Mesoporous Film Anchored on Graphene Nanosheets with Superior Electrochemical Performance for Supercapacitors. *Adv. Funct. Mater.* 2016, *26* (6), 919–930.

(41) *Colorimetric Determination of Nonmetals*, 2d ed.; Boltz, D. F., Howell, J. A., Eds.; Chemical analysis; Wiley: New York, 1978.

(42) Li, W.; Li, K.; Ye, Y.; Zhang, S.; Liu, Y.; Wang, G.; Liang, C.; Zhang, H.; Zhao, H. Efficient Electrocatalytic Nitrogen Reduction to Ammonia with Aqueous Silver Nanodots. *Commun. Chem.* 2021, *4* (1), 1–11.

(43) Xiong, W.; Guo, Z.; Zhao, S.; Wang, Q.; Xu, Q.; Wang, X. Facile, Cost-Effective Plasma Synthesis of Self-Supportive FeS_x on Fe Foam for Efficient Electrochemical Reduction of N_2 under Ambient Conditions. *J. Mater. Chem. A* 2019, *7* (34), 19977–19983.

(44) He, X.; Ling, Z.; Peng, X.; Yang, X.; Ma, L.; Lu, S. Facile Synthesis of Cu_2SnS_3 Nanocrystals for Efficient Nitrogen Reduction Reaction. *Electrochem. Commun.* 2023, *148*, 107441.

(45) Zhong, H.; Wang, M.; Ghorbani-Asl, M.; Zhang, J.; Ly, K. H.; Liao, Z.; Chen, G.; Wei, Y.; Biswal, B. P.; Zschech, E.; Weidinger, I. M.; Krasheninnikov, A. V.; Dong, R.; Feng, X. Boosting the Electrocatalytic Conversion of Nitrogen to Ammonia on Metal-Phthalocyanine-Based Two-Dimensional Conjugated Covalent Organic Frameworks. *J. Am. Chem. Soc.* 2021, *143* (47), 19992–20000.

(46) He, H.; Wen, H.-M.; Li, H.-K.; Li, P.; Wang, J.; Yang, Y.; Li, C.-P.; Zhang, Z.; Du, M. Hydrophobicity Tailoring of Ferric Covalent Organic Framework/MXene Nanosheets for High-Efficiency Nitrogen Electroreduction to Ammonia. *Adv. Sci.* 2023, *10* (15), 2206933.

(47) Liu, S.; Wang, M.; Qian, T.; Ji, H.; Liu, J.; Yan, C. Facilitating Nitrogen Accessibility to Boron-Rich Covalent Organic Frameworks via Electrochemical Excitation for Efficient Nitrogen Fixation. *Nat. Commun.* 2019, *10* (1), 3898.

(48) Cheng, Y.; Li, X.; Shen, P.; Guo, Y.; Chu, K. MXene Quantum Dots/Copper Nanocomposites for Synergistically Enhanced N_2 Electroreduction. *Energy Environ. Mater.* 2023, *6* (1), e12268.

(49) Li, J.; Zheng, M.; Wei, F.; Dong, C.; Xiu, Z.; Mu, W.; Zhou, X.; Ding, Y.; Han, X. Fe Doped $InVO_4$ Nanosheets with Rich Surface Oxygen Vacancies for Enhanced Electrochemical Nitrogen Fixation. *Chem. Eng. J.* 2022, *431*, 133383.

(50) Zhu, X.; Zhao, J.; Ji, L.; Wu, T.; Wang, T.; Gao, S.; Alshehri, A. A.; Alzahrani, K. A.; Luo, Y.; Xiang, Y.; Zheng, B.; Sun, X. FeOOH Quantum Dots Decorated Graphene Sheet: An Efficient Electrocatalyst for Ambient N_2 Reduction. *Nano Res.* 2020, *13* (1), 209–214.

(51) Zhu, X.; Liu, Z.; Liu, Q.; Luo, Y.; Shi, X.; M. Asiri, A.; Wu, Y.; Sun, X. Efficient and Durable N 2 Reduction Electrocatalysis under Ambient Conditions: β-FeOOH Nanorods as a Non-Noble-Metal Catalyst. *Chem. Commun.* 2018, *54* (80), 11332–11335.

2.6. Appendix of Chapter 2

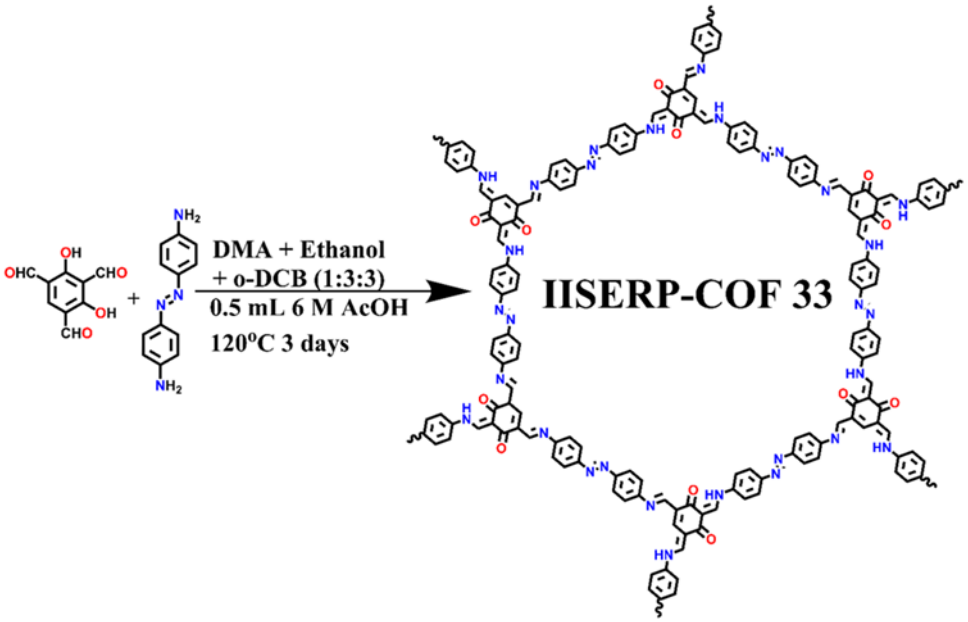

Scheme A2.1. Schematic representation of IISERP-COF33 synthesis.

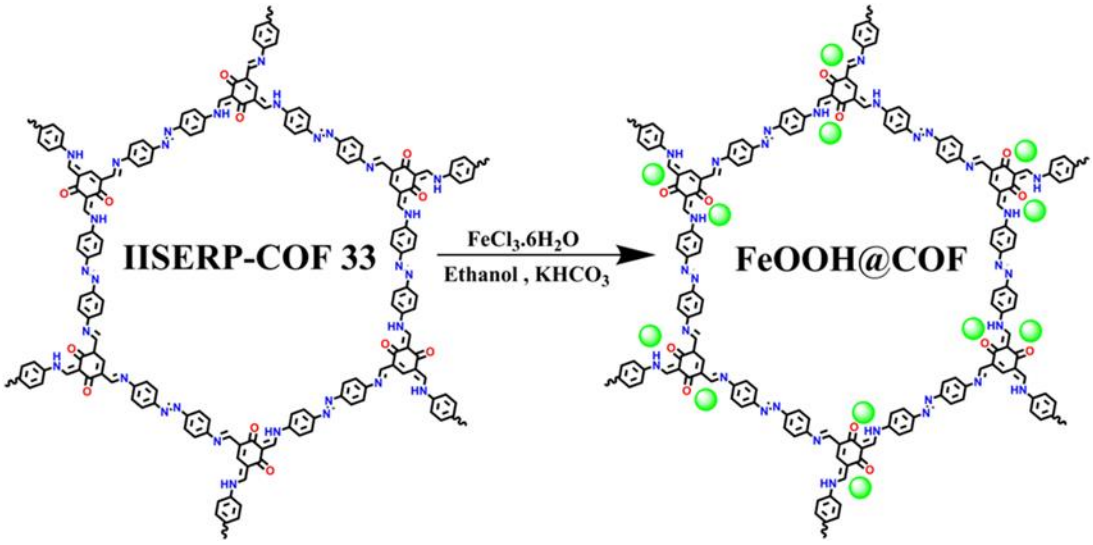

Scheme A2.2. Schematic representation of FeOOH@COF synthesis.

2. Characterizations of IISERP-COF33 and FeOOH@COF

A solvothermal reaction was performed on a bulk scale (gram scale) in which 4,4'-Azodianiline was reacted with triformyl resorcinol in DMA, ethanol and o-DCB in the presence of acetic acid at 120°C for three days in a Teflon liner. The product was obtained as maroon powder by vacuum filtration, and it was washed with an excess of DMF, THF and methanol. The crystalline nature of the COF was confirmed by Powder X-ray diffraction (Fig. A2.1).

Thermogravimetric analysis (TGA) shows that IISERP-COF33 has very good thermal stability up to 300°C (Fig. A2.2).

Powder X-Ray diffraction:

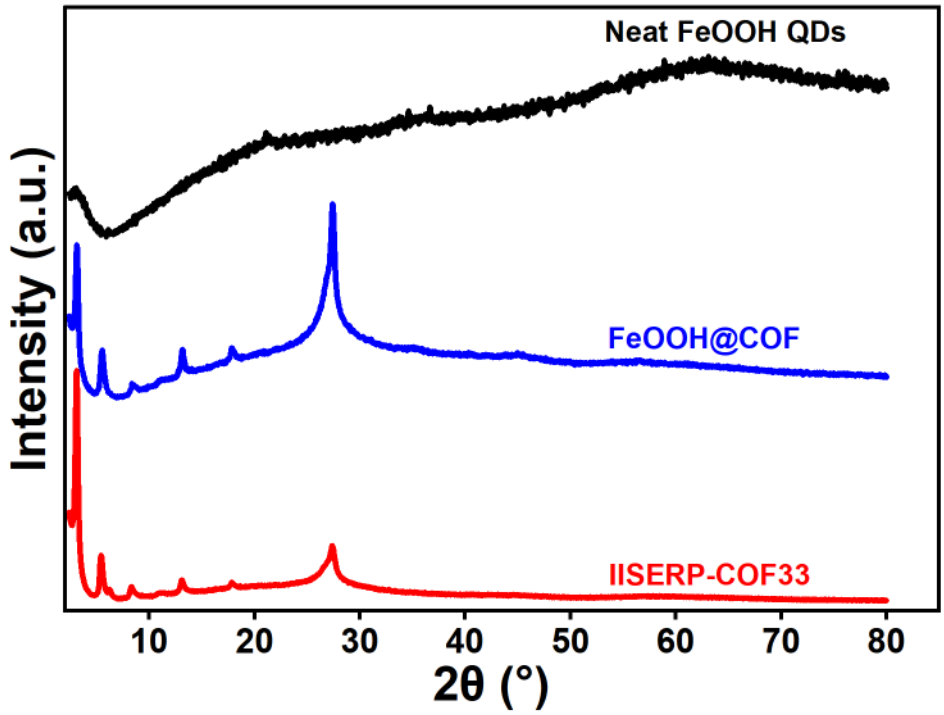

Figure A2.1. PXRD pattern of IISERP-COF33 and FeOOH@COF. The increase in the relative intensity of the (511) reflection (2θ = 28°) has contributions from slightly lowered crystallinity and exfoliation of the COF under the wet reaction conditions.

Adsorption studies:

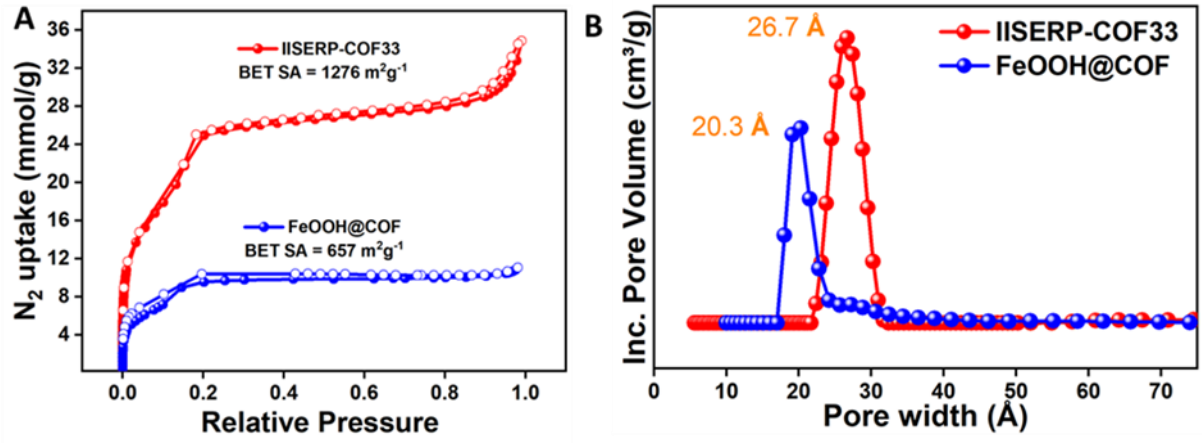

Figure A2.2. Nitrogen adsorption isotherm of IISERP-COF33 and FeOOH@COF measured at 77K. Type I isotherm suggests a microporous structure and shows the pore size distribution of IISERP-COF33 and FeOOH@COF. The narrower pore-size distribution in the FeOOH@COF is seen.

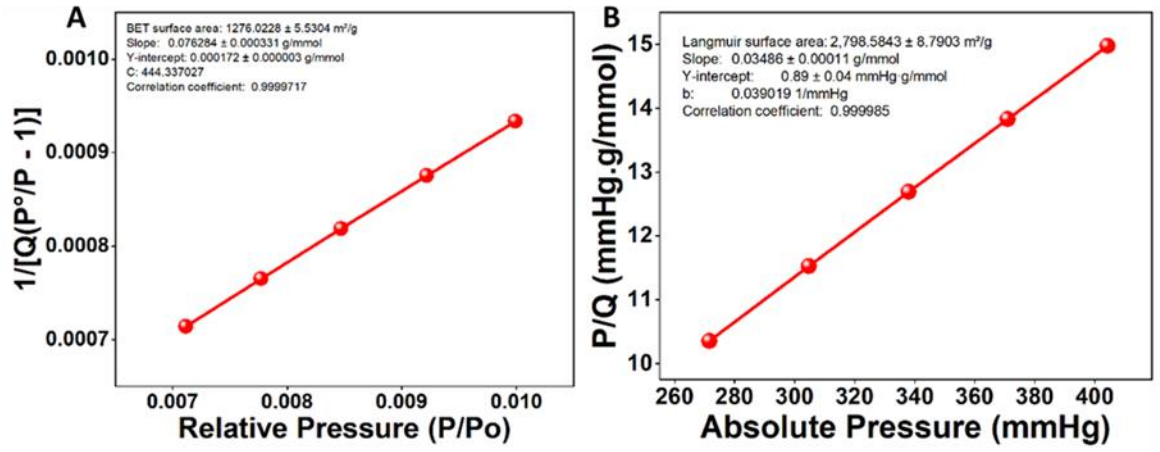

Figure A2.3. (A) Brunauer–Emmett–Teller surface area plot for IISERP-COF33. (B) Langmuir surface area plot for IISERP-COF33.

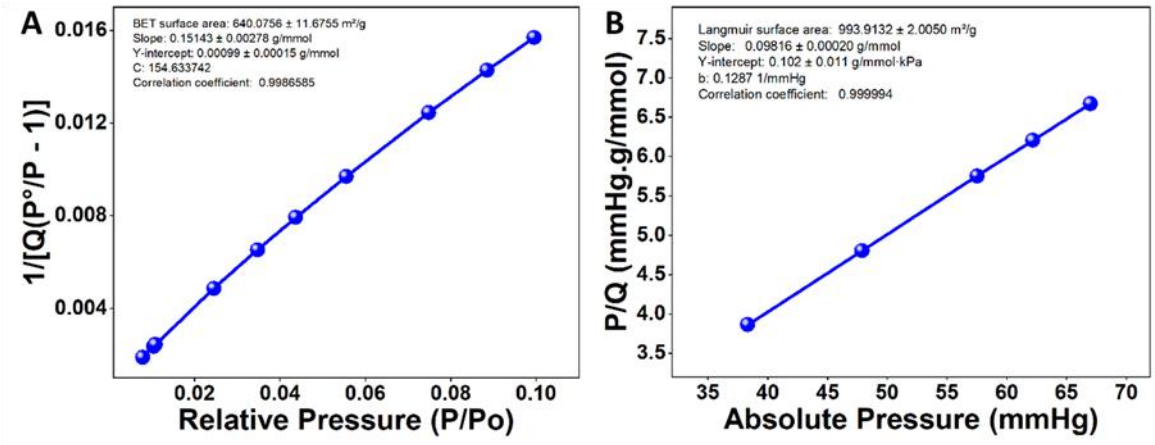

Figure A2.4. (A) Brunauer–Emmett–Teller surface area plot for FeOOH@COF. (B) Langmuir surface area plot for FeOOH@COF.

Microscopy studies:

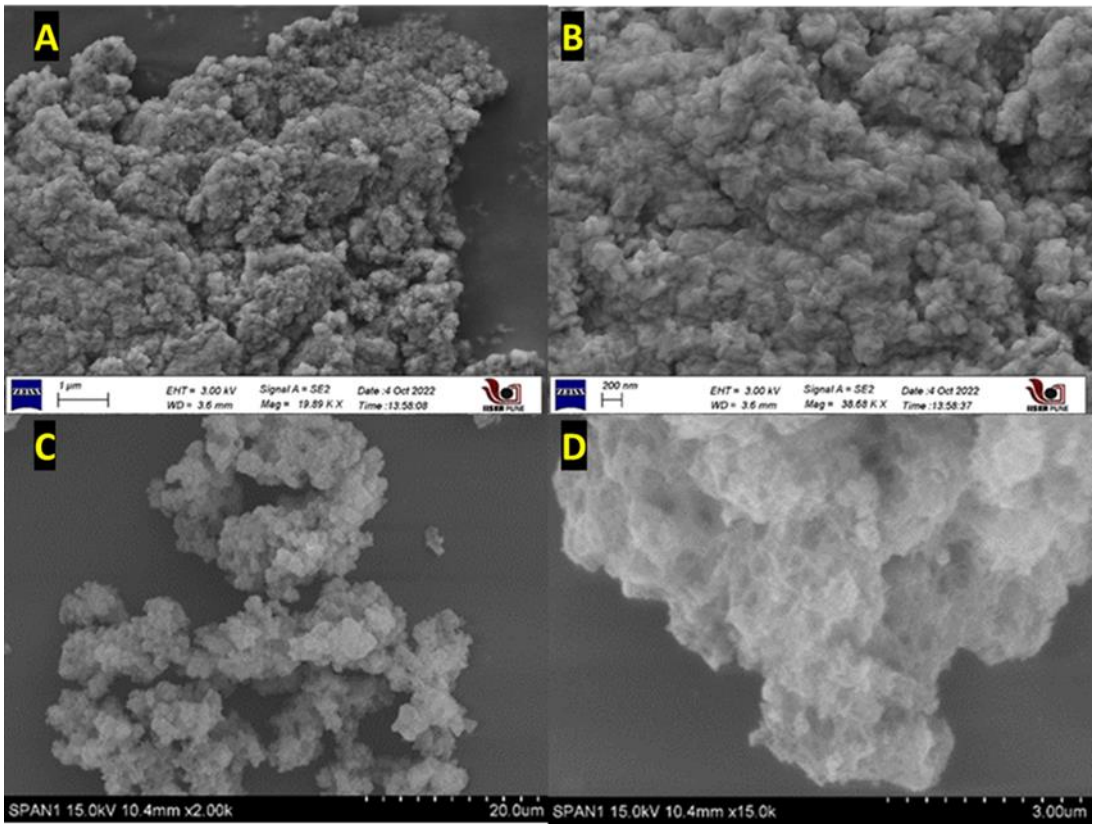

Figure A2.5. (A, B): FESEM images of IISERP-COF33 at different resolutions. (C, D): FESEM images of FeOOH@COF at different resolutions.

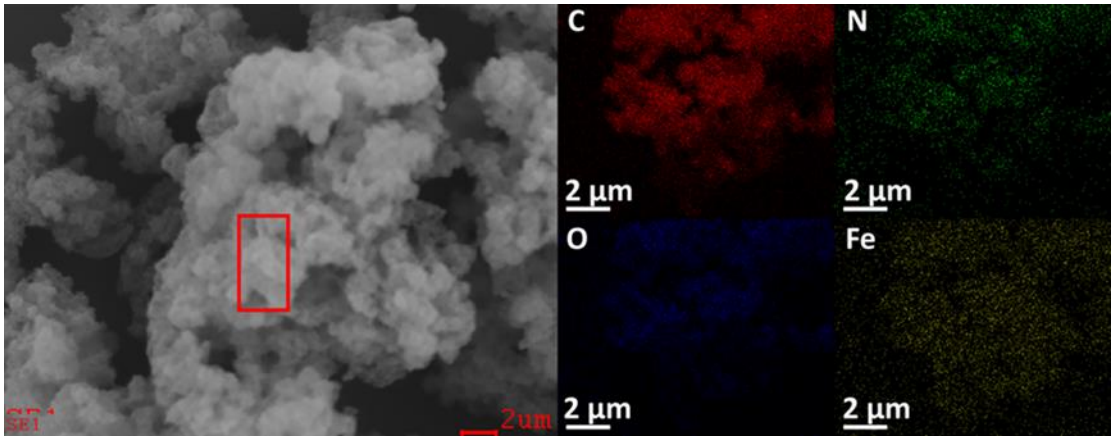

Figure A2.6. The elemental mapping reveals the homogeneous distribution of Fe in FeOOH@COF.

Element	Wt%	At%
CK	59.87	71.09
NK	12.10	12.32
OK	14.83	13.22
FeK	13.20	3.37

Figure A2.7. Elemental percentage calculated from EDX analysis of FeOOH@COF.

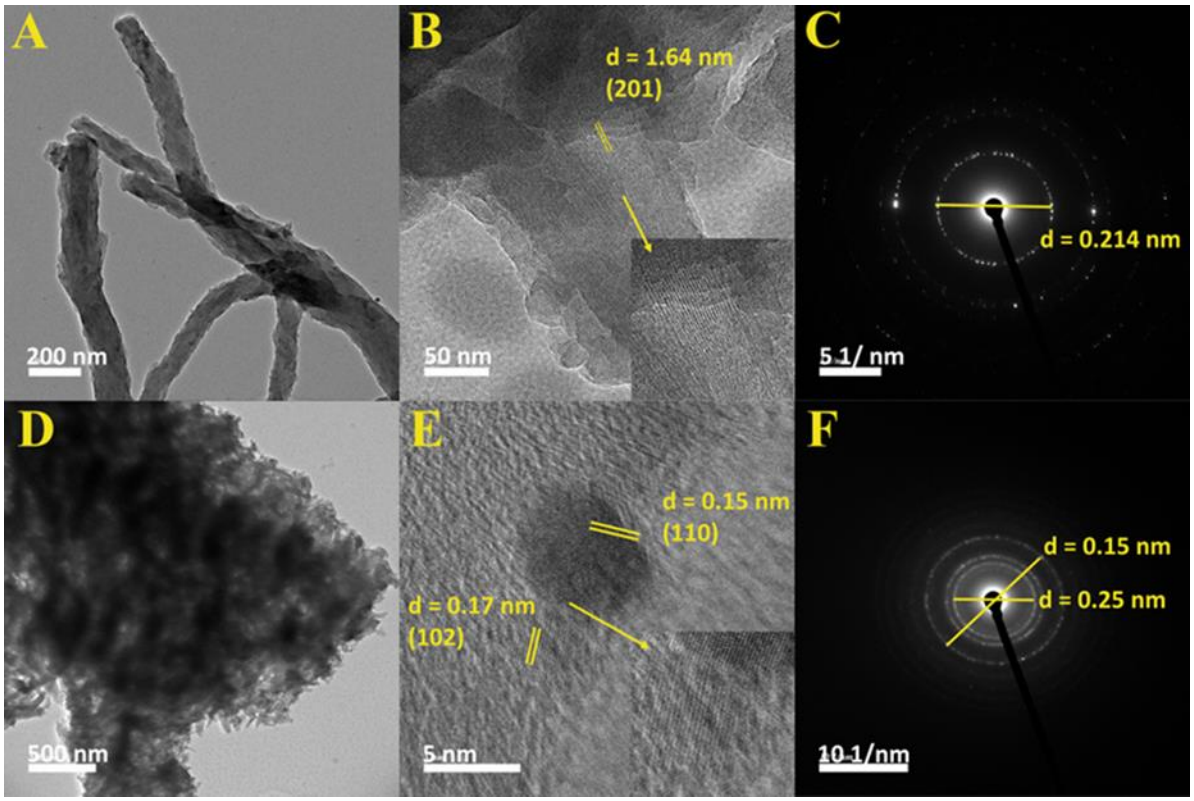

Figure A2.8. (A, B) HRTEM images of IISERP-COF33 at different magnifications. (C) The SAED pattern of IISERP-COF33 showing the diffraction spots from different planes (D,E) HRTEM images of FeOOH@COF at different magnifications. (F) The SAED pattern of FeOOH@COF showing the diffraction spots from different planes, some of them could be indexed to the hkl planes Note: Several other reflections observed in the SAED, especially those situated far from the central beam, remain unindexed. These reflections might originate from another COF flake with a different orientation compared to the flake whose reflections have been successfully indexed.

X-ray photoelectron spectroscopy:

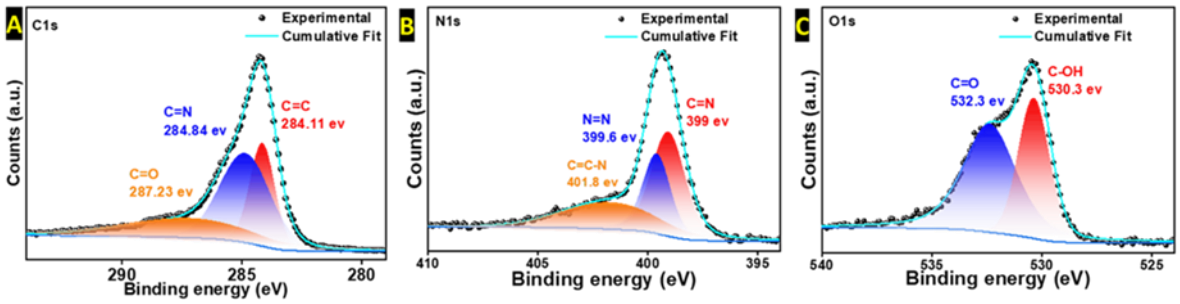

Figure A2.9. Detailed XPS spectra of C1s, N1s and O1s for IISERP-COF33.

3. Ammonia detection and quantification

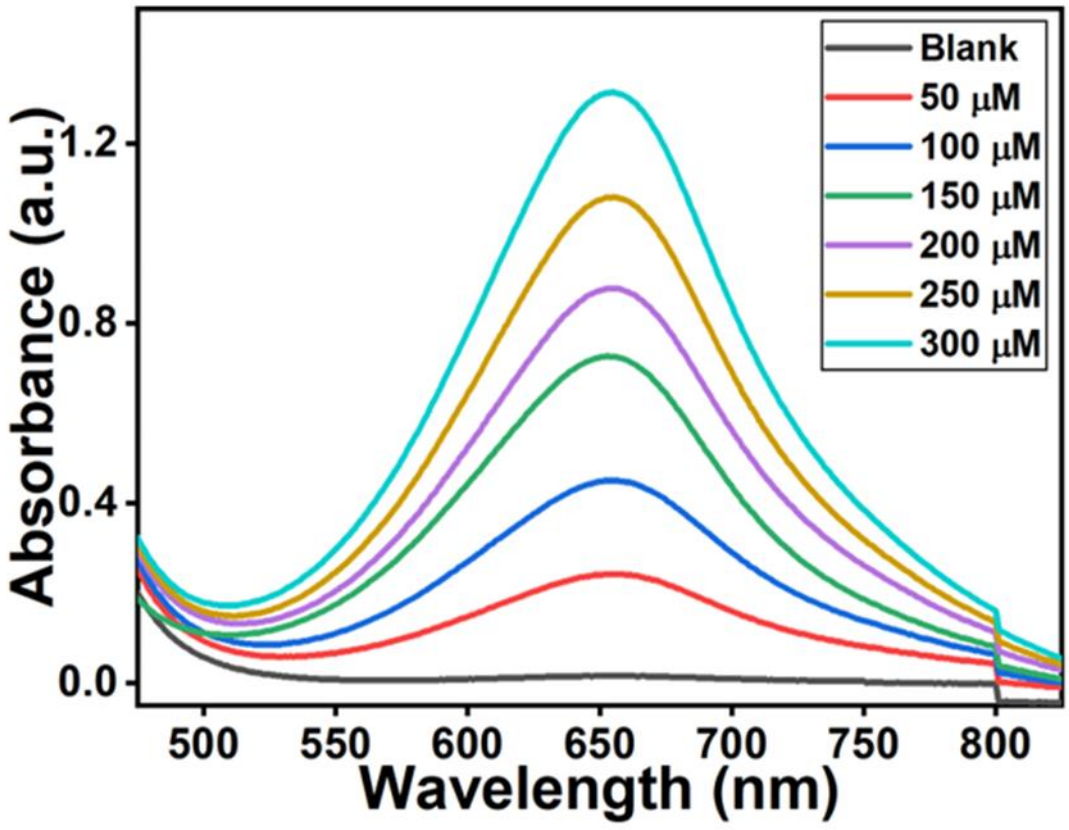

Figure A2.10. UV-vis absorption spectra of indophenol blue solutions of standard NH_4Cl solution.

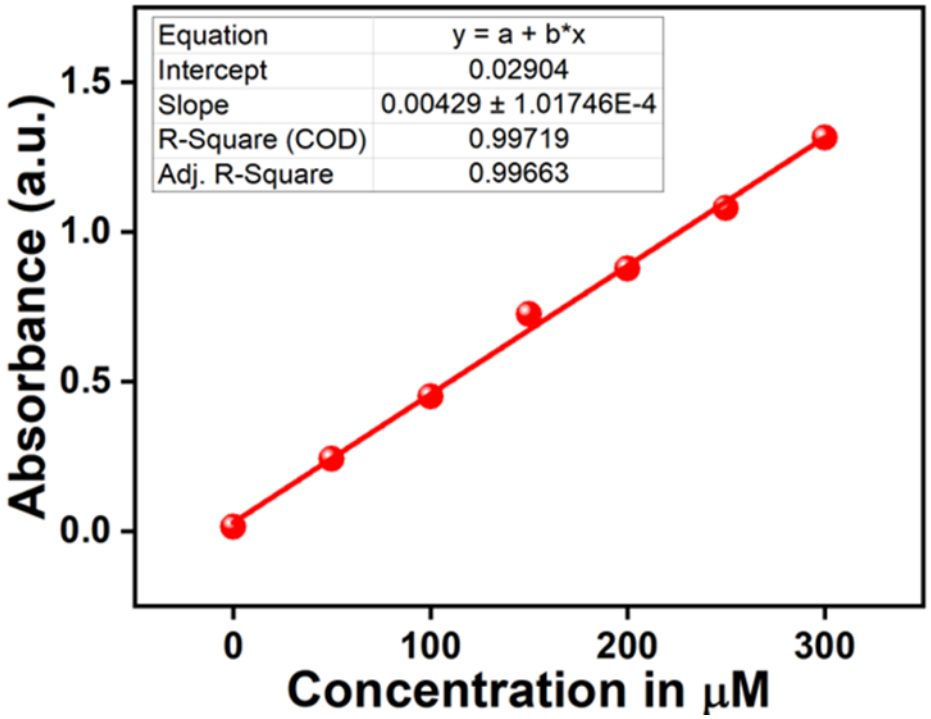

Figure A2.11. Linear fit of known standard NH_4Cl solution.

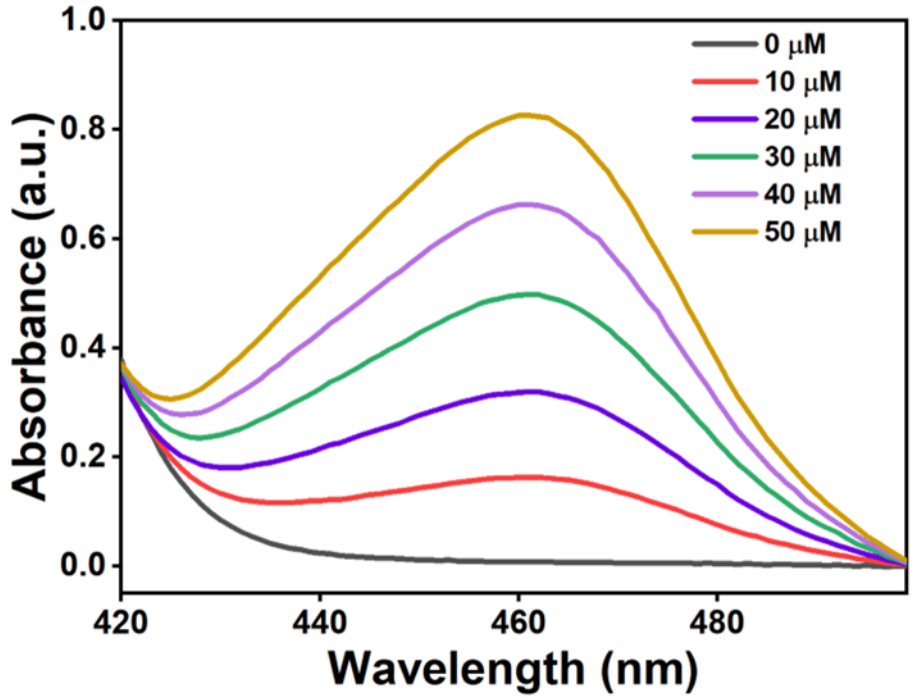

Figure A2.12. UV-vis absorption spectra of standard N_2H_4 solution.

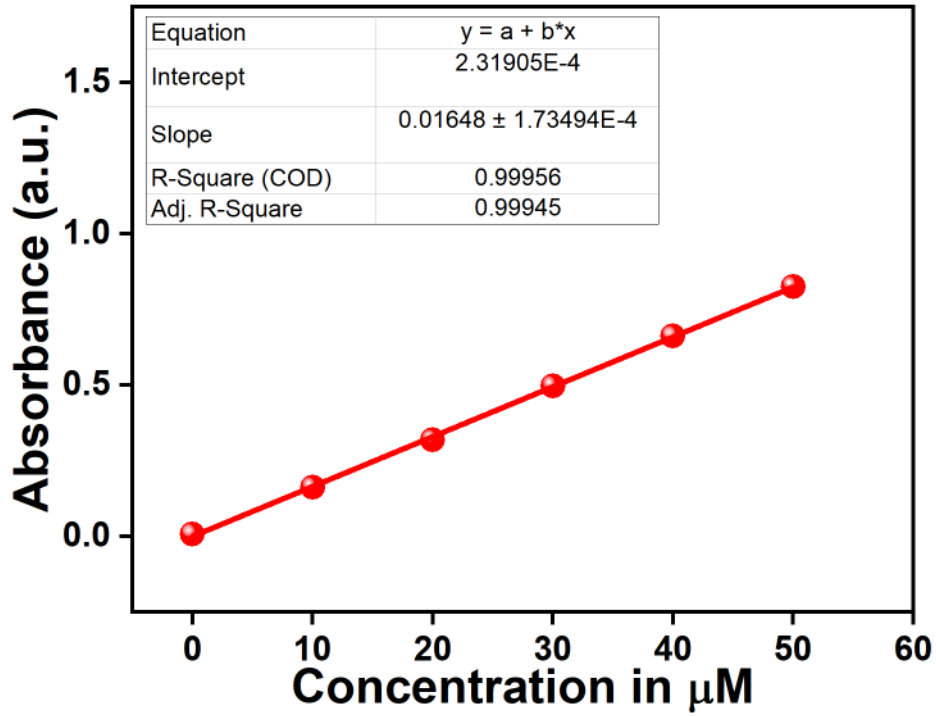

Figure A2.13. Linear fit of known standard N_2H_4 solution.

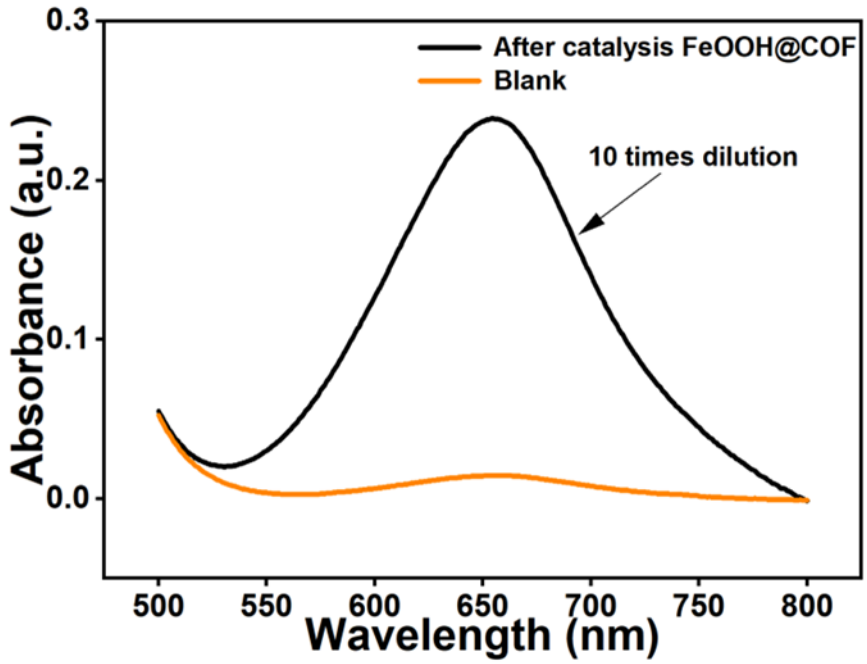

Figure A2.14. UV -vis absorption spectra of N_2-saturated electrolyte solution at –0.4 V versus RHE using the indophenol blue method.

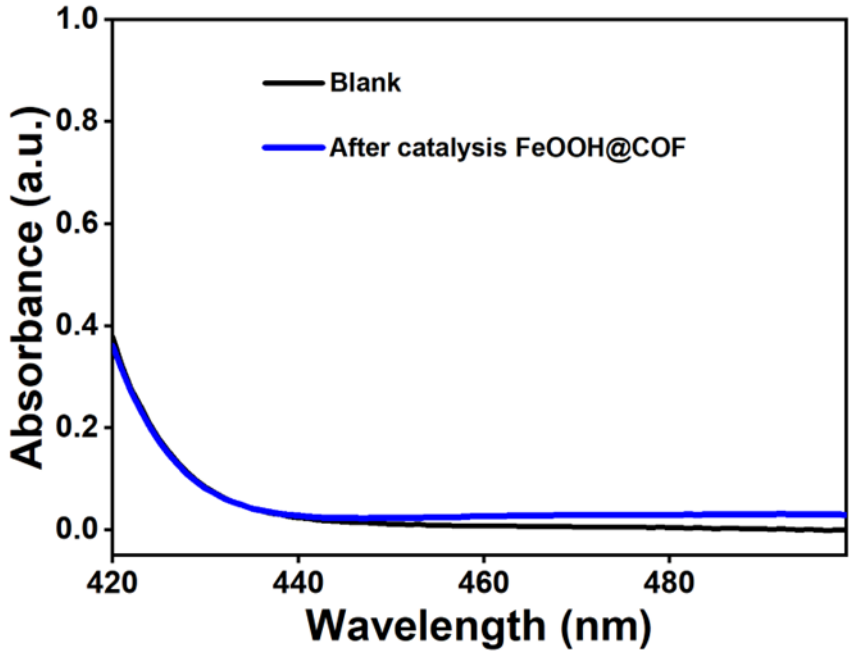

Figure A2.15. UV-vis absorption spectra of N_2 -saturated electrolyte solution at -0.4 V versus RHE for hydrazine detection.

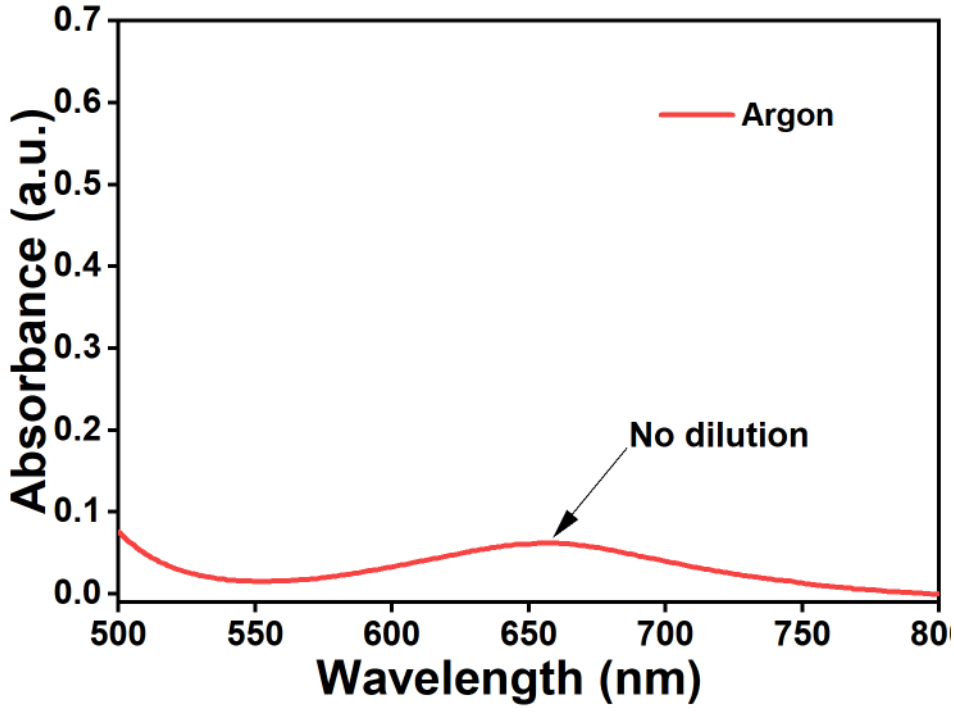

Figure A2.16. UV-vis absorption spectra of Ar-saturated electrolyte solution at -0.4 V versus RHE using the indophenol blue method.

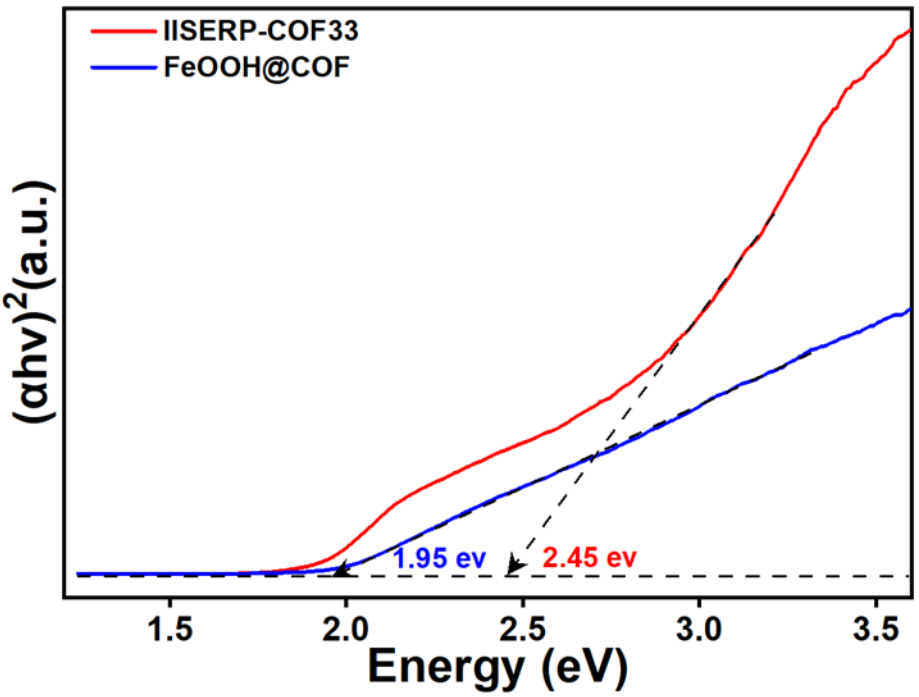

Figure A2.17. A Tauc plot from the UV-Vis spectra of the samples. The plot shows the lowered bandgap of the FeOOH@COF, which is lower than the blank FeOOH QD estimated to be 2.02 eV.

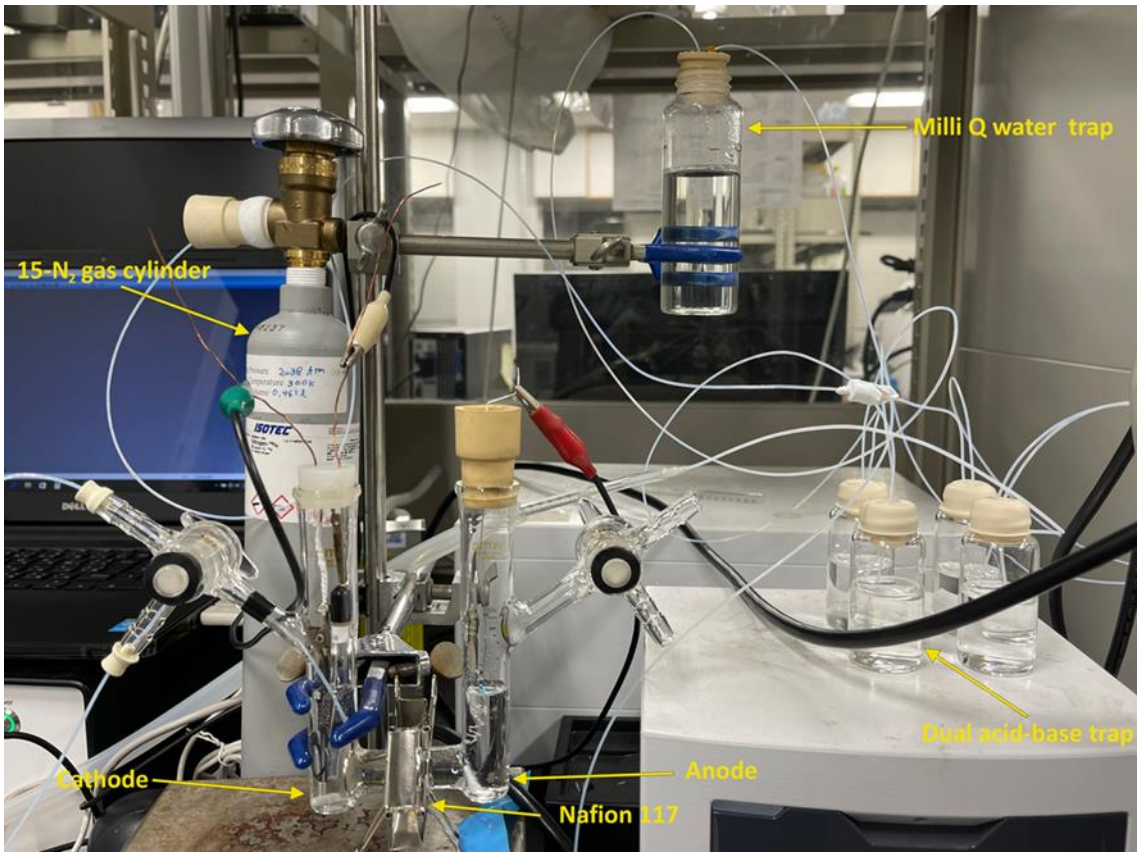

Figure A2.18. Experimental setup for isotopic NRR.

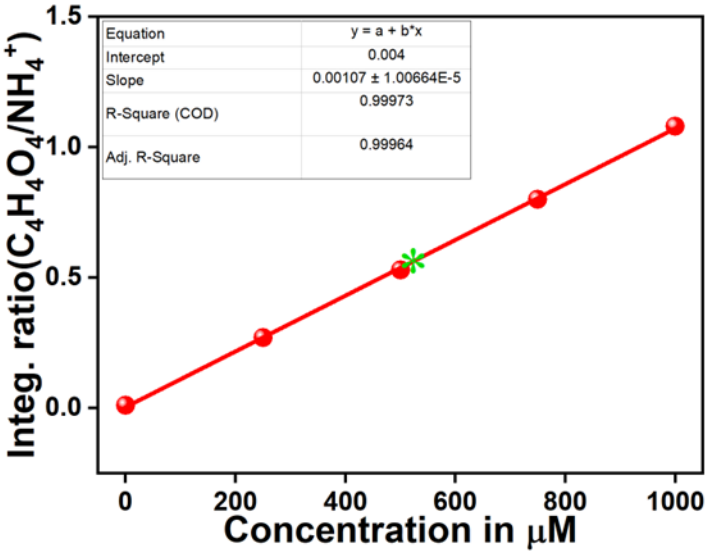

Figure A2.19. Linear fit of standard $^{15}NH_4Cl$ solution for isotopic NRR.

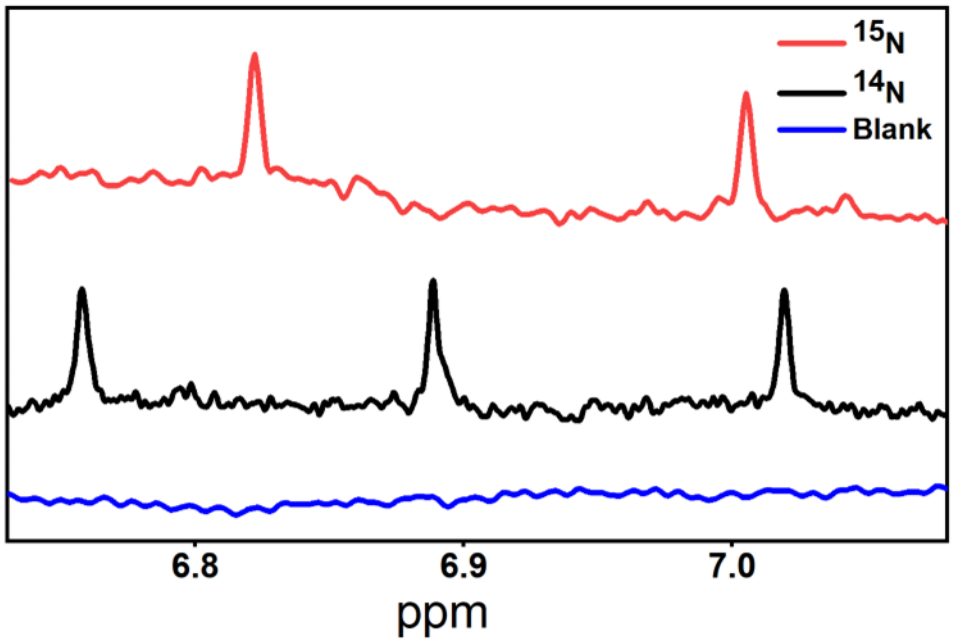

Figure A2.20. ^1H NMR spectra of N_2 -saturated electrolyte solution at -0.4 V versus RHE.

4. Characterizations of the spent catalyst (spent FeOOH@COF)

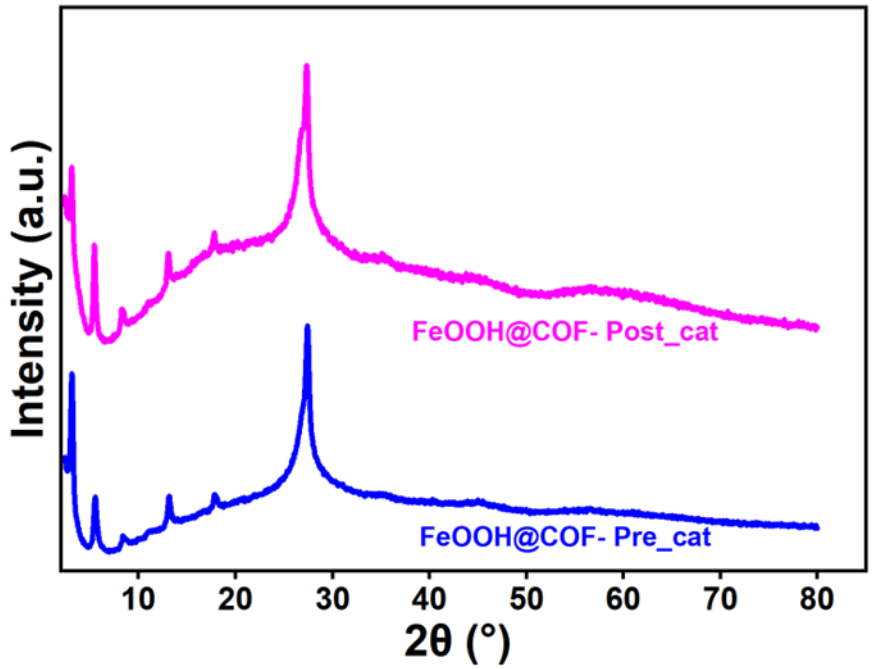

Figure A2.21. PXRD of FeOOH@COF after catalysis.

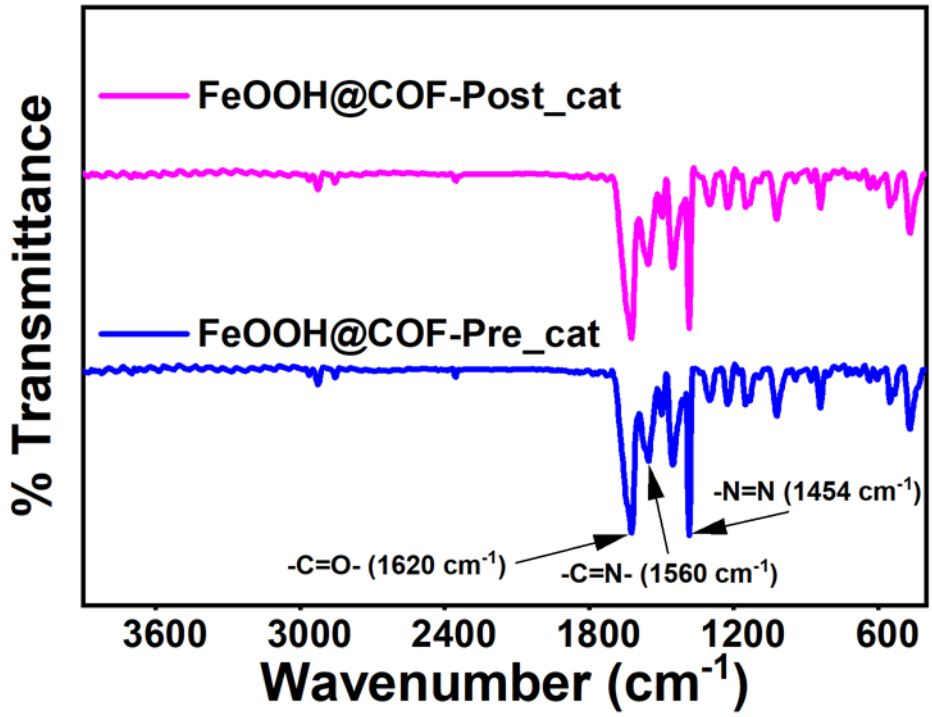

Figure A2.22. FTIR spectra of FeOOH@COF after catalysis.

Sample Name	Fe Wt%
Pre	12.6
Post	12.5

Figure A2.23. Elemental percentage calculated from ICP analysis of pre and post FeOOH@COF.

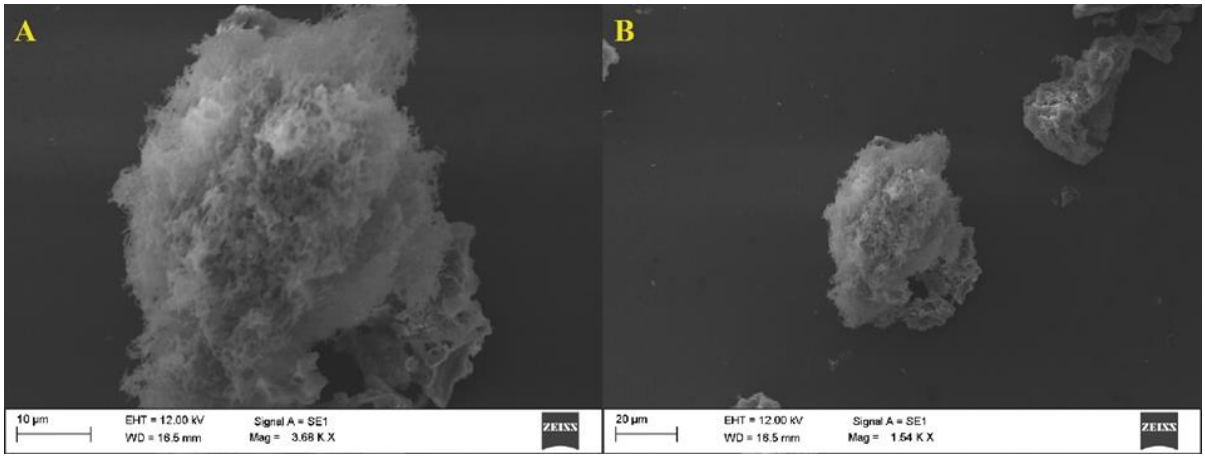

Figure A2.24. (A, B): FESEM images of FeOOH@COF after catalysis at different resolutions.

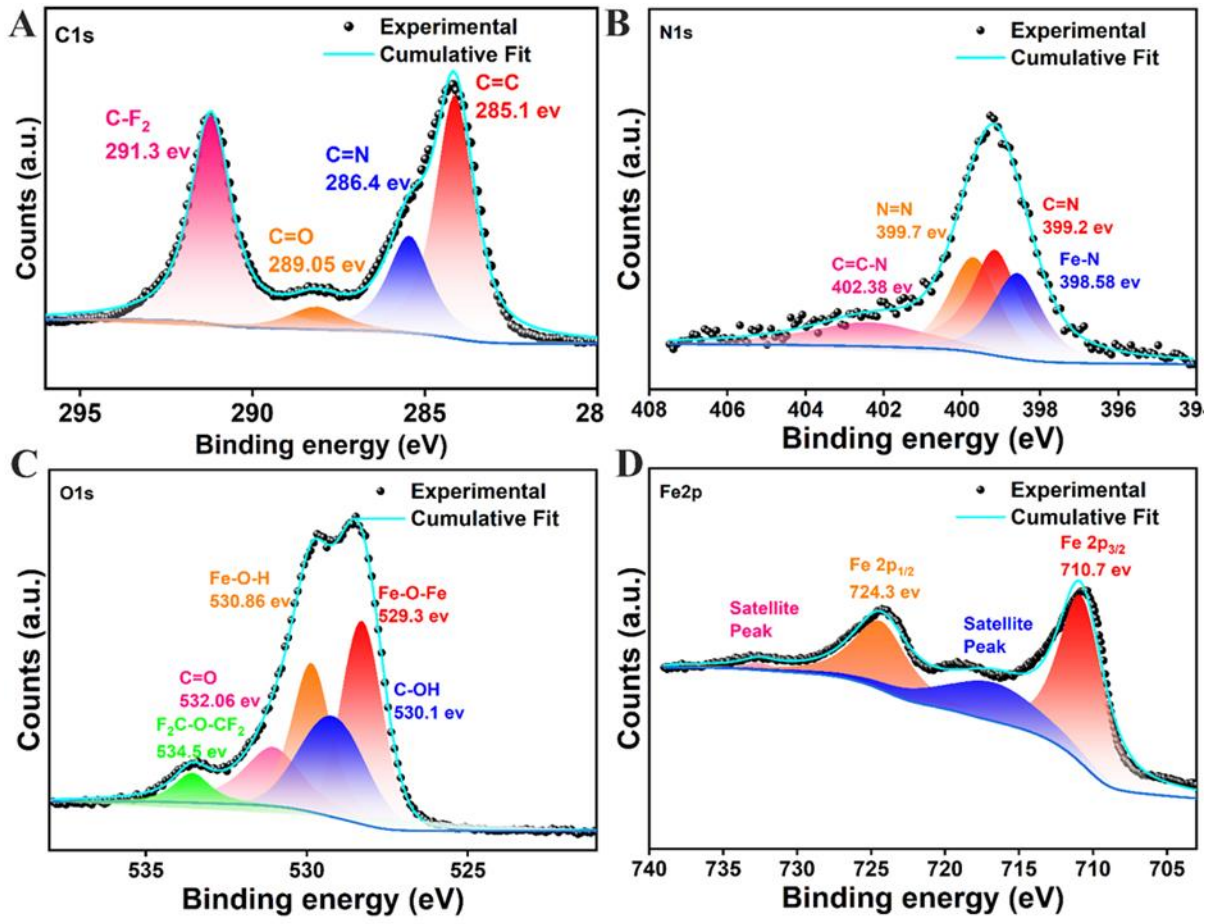

Figure A2.25. Detailed XPS spectra of Fe2p, C1s, N1s and O1s for FeOOH@COF after catalysis.

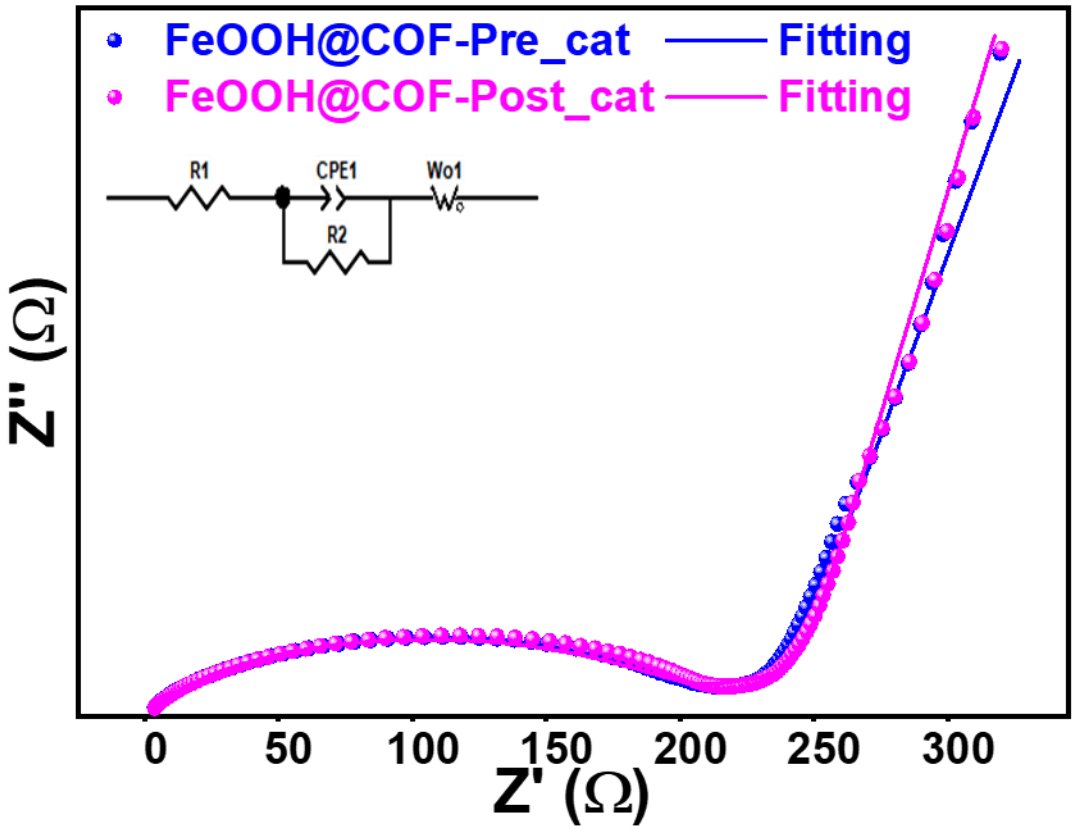

Figure A2.26. EIS of FeOOH@COF before and after catalysis.

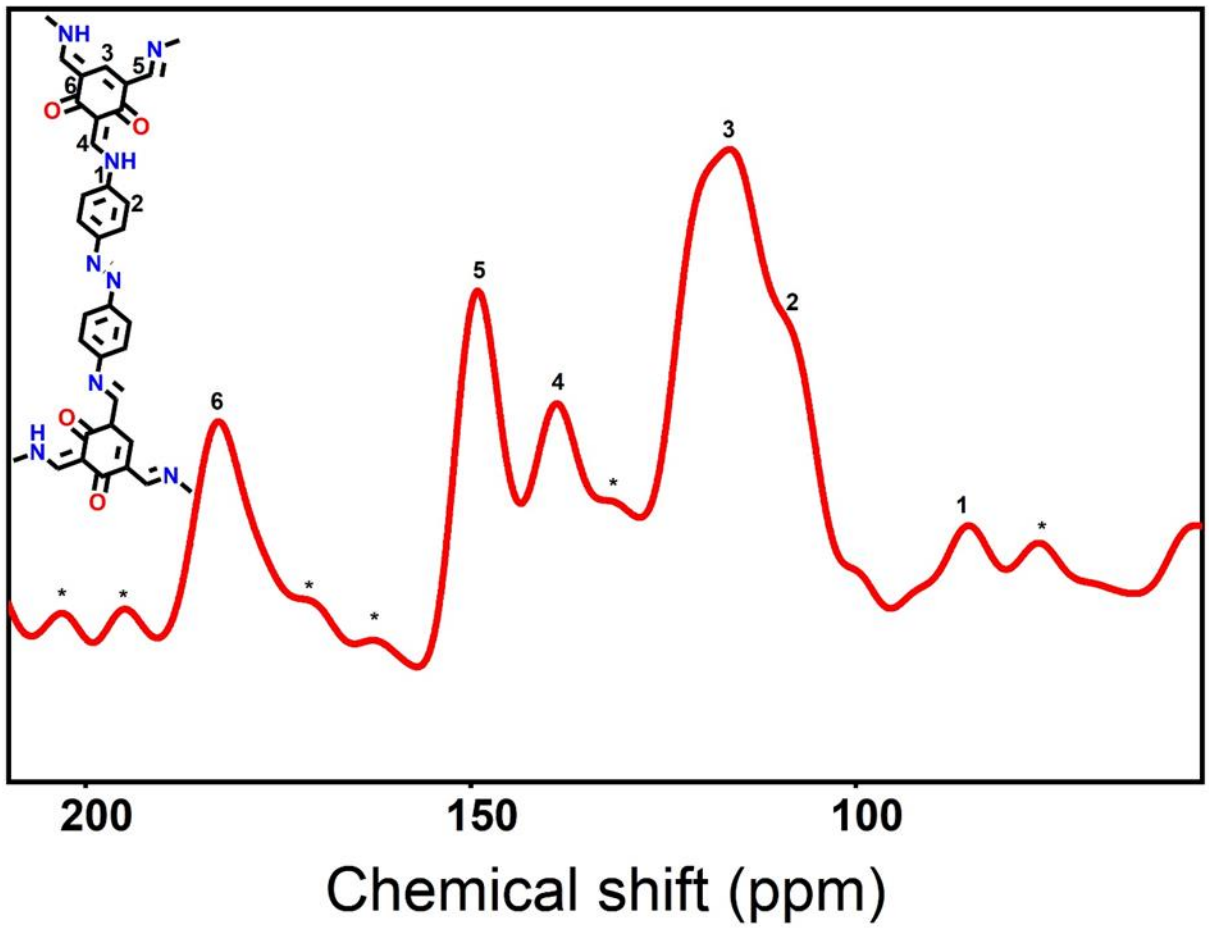

Figure A2.27. ^{13}C-solid state NMR (^{13}C-SSNMR) of the IISERP-COF33. The spectra were recorded at 400 MHz and the chemical shifts have been labelled. Note: * - corresponds to side bands appeared during measurements

Table A2.1: Comparison of performance of COF and Iron-based heterogeneous catalyst for NRR.

Catalyst	Electrolyte	F.E.(%)	NH_3 yield ($\mu g\ h^{-1}mg_{cat}^{-1}$)	References
FeOOH@COF	**0.1 M $LiClO_4$**	**46.4**	**77.4**	**This work**
COF-Fe/MXene - F17	0.1 M Na_2SO_4	43.1	41.8	Ho et al. *Adv. Sci.***2023**,10, 2206933
FePc-pz2Dc-COF	0.01 M H_2SO_4	31.9	33.6	Zhong et al. *J. Am. Chem. Soc.* **2021**,

				143, 47, 19992–20000
Fe_3O_4@rGO	0.1 M Na_2SO_4	11.47	28.01	Wang et al. *Energy Environ. Mater.* **2021**, 4, 88
$FeVO_4$	0.5 M $LiClO_4$	13.8	48.5	Shen et al. *Energy Environ. Mater*. **2021**, 4, 8
Fe-$InVO_4$	0.1 M HCl	14.27	17.23	Li et al. *Chem. Eng. J.* **2022**, 431, 133383
FeOOH QDs-GS	0.1 M $LiClO_4$	14.6	27.3	Zhu et al. *Nano Res.* **2020**, 13, 209
β-FeOOH nanorod	0.5 M $LiClO_4$	6.7	23.32	Zhu et. al. *Chem. Commun.,* **2018**,54, 11332-11335
F- doping on FeOOH	0.5 M $LiClO_4$	9.02	42.38	Zhu et. al. *Chem. Commun.,* **2019**,55, 3987-3990
Eex-COF/NC	0.1 M KOH	45.43	12.53	Liu et. al. *Nat. Commun.* **2019**, 10, 3898
Ti-COF	0.05 M HCl	34.62	26.89	Jiang et. al. *Nano Let.* **2022**, 22, 372

Chapter 3

Pentanuclear Metal Complex-Anchored Covalent Organic Framework for Electrocatalytic Nitrate Reduction Reaction

3.1. Introduction

Nitrogen, a fundamental element for life, is prevalent in various chemical forms including nitrogen oxides (NO, NO_2), nitrates (NO_3^-), nitrites (NO_2^-), and ammonia (NH_3).[1] These nitrogen compounds are crucial in numerous biological, environmental, and industrial processes.[2] The nitrogen cycle, encompassing processes such as nitrification and denitrification, maintains the global nitrogen balance by regulating the transformation of these compounds.[3] Ammonia (NH_3) among these nitrogen based compounds serves as a crucial chemical feedstock with extensive applications in the production of fertilizers, pharmaceuticals, dyes, and in energy storage and carbon-free energy transport.[5-7] The Traditional industrial method for large-scale ammonia synthesis is the Haber-Bosch process, which operates at high temperatures (400-500 °C) and pressures (150-300 atm) using Fe or Ru based catalysts.[8] Despite its effectiveness, this process is a major contributor of global CO_2 emissions and exhibits low energy efficiency, with ammonia conversion rates typically under 15% per cycle.[9] The limitations of the Haber-Bosch process highlight the urgent need to develop more sustainable and efficient ammonia production technologies, particularly through decarbonization and electrification. Electrochemical ammonia synthesis, powered by renewable energy sources, has emerged as a promising alternative to the Haber-Bosch process. The electrochemical nitrogen reduction reaction (ENRR) is a focal point of research for ambient-condition ammonia production. However, ENRR is confronted by low N_2 solubility, struggle with the hydrogen evolution reaction (HER), and the high energy required to break the N≡N bond, resulting in low selectivity and ammonia yields below 200 $\mu g h^{-1} mg^{-1}_{cat}$.[9] Achieving practical ammonia production levels through electrochemical methods remains a significant challenge.

Nitrogenous pollutants, commonly referred to as NOx, are major contributors to environmental pollution and originate from industrial sources such as power stations, factories, and vehicles. Ammonia-selective catalytic reduction (NH_3-SCR) is a widely used technology for NOx mitigation, employing ammonia as a reductant to convert NO_x into inert N_2.[10] However, NH_3-SCR is limited by high energy consumption, substantial ammonia demand, and inefficient utilization of NO_x resources.[11] The extensive use of nitrogen-rich fertilizers and nitrogen-containing chemicals has led to elevated NO_3^- levels in the environment, posing risks to aquatic ecosystems and human health. Therefore, developing improved denitrification

methods that convert NO_3^- into valuable products like ammonia is essential for a more sustainable nitrogen cycle.[12-13] Recent research has focused on electrochemical nitrate reduction (ENO_3RR) as an alternative for waste NO_3^- denitrification into ammonia. ENO_3RR benefits from lower N–O bond energies, higher solubility of NO_3^- in aqueous solutions, and the potential for higher ammonia yields. The nitrate reduction reaction is particularly advantageous due to its significantly lower N–O bond energy (204 kJ/mol) and higher solubility of NO_3^- in water.[14] The larger difference in standard reduction potentials between ENO_3RR and HER (0.69 V) compared to ENRR and HER (0.093 V) allows ENO_3RR to operate over a broader range of potentials, minimizing the impact of competing HER side reactions and resulting in higher selectivity, Faradaic efficiency, and ammonia yield rate.[12,15]

Covalent Organic Frameworks (COFs) are a unique class of crystalline, porous materials formed through the covalent linkage of organic units into ordered polymeric backbones. These frameworks can manifest as two-dimensional (2D) or three-dimensional (3D) structures characterized by intrinsic porosity and a high degree of structural order.[16] The construction of COFs is guided by the careful polymerization of monomers with complementary geometries, which assemble into specific topological configurations, resulting in polygonal backbones that define various skeletal architectures and tailored pore structures.[17] Their unique design flexibility allows for precisely incorporating functional groups and molecular entities, resulting in well-defined architectures with specific local environments.[18] This versatility renders COFs suitable for various applications, including gas sorption, storage, separation, proton conduction, sensing, dye degradation, water remediation, charge storage, and electrocatalysis.[19] The application of COFs in catalysis began in 2011 by introducing a 2D COF material (Pd/COF-LZU1) for the Suzuki-Miyaura coupling reaction.[20] Since then, COFs have been increasingly utilized in electrocatalytic applications, including CO_2 reduction and oxygen reduction reactions. An effective strategy for developing active catalysts or electrocatalysts involves incorporating metal-containing monomers or deposition of catalytically active metal compounds within the COF matrix, typically in the form of nanoparticles (NPs).[21-22] Synthesizing COFs with metalated monomers create open metal sites and maintains structural integrity, offering significant potential. However, their use in electrocatalytic nitrate reduction remains underexplored, presenting opportunities for further research.[23]

In recent years, Pentanuclear complex have garnered significant attention due to their unique structural features and potential in catalysis. These complexes consist of five metal atoms with Quasi-D_3 symmetry.[24-26] This complex core is surrounded by two metal units at the apical positions are hexa-coordinated with distorted octahedral geometries and three metal atoms the triangular are penta-coordinated with a distorted trigonal bipyramidal geometry. This structural design leverages redox flexibility and spatial arrangement to enhance catalytic performance, addressing challenges in multi-electron transfer processes such as water oxidation, CO_2 reduction.[24] Pentanuclear complexes, while advantageous, face challenges with stability and recyclability, including degradation of complex. Addressing these issues is essential for their practical use.

I In this chapter, we present a novel pentanuclear metal complex-anchored covalent organic framework (M_5COF) that uniquely combines Quasi-D_3 symmetric amine and C_3 symmetric anhydride units, linked through polyimide bonds. We explored its application in the electrochemical nitrate reduction reaction (NO_3RR) for ammonia production. The study revealed a trend in catalytic performance based on the metal used, with the Fe-based M_5COF outperforming its Co and Zn counterparts. Specifically, the Fe_5COF achieved a notable nitrate reduction rate of 13.5 $mgh^{-1}mg^{-1}_{cat}$ and an ammonia production efficiency of 88%.

3.2. Experimental details

3.2.1 Synthesis of Fe_5BppNH_2 complex:

The Fe_5BppNH_2 complex was synthesized using a microwave-assisted method. In a microwave tube, 0.5 mmol of $Fe(ClO_4)_2$ and 0.3 mmol of NH_2Bpp were dissolved in 5 mL of DMF. To this mixture, 0.3 mL of 1M NaOH was added, and the solution was heated at 70°C for 30 minutes. After the reaction, the mixture was filtered using a syringe filter, and the filtrate was collected. A saturated aqueous solution of $NaPF_6$ was then added to the filtrate, followed by the addition of water to induce precipitation. The resulting brown solid product was collected by filtration (yield = 78%) (Fig. A3.1).

3.2.2 Synthesis of Co_5BppNH_2 complex:

The Co_5BppNH_2 complex was synthesized using a microwave-assisted method. In a microwave tube, 0.5 mmol of $Co(ClO_4)_2$ and 0.3 mmol of NH_2Bpp were dissolved in 5 mL of MeOH. To this mixture, 0.3 mL of 1M NaOH was added, and the solution was heated at 100°C for 30 minutes. After the reaction, the mixture was filtered using a syringe filter, and the filtrate was collected. A saturated aqueous solution of $NaPF_6$ was then added to the filtrate, followed by the

addition of water to induce precipitation. The resulting light green solid product was collected by filtration (yield = 72%) (Fig. A3.2).

3.2.3 Synthesis of Zn_5BppNH_2 complex:

The Zn_5BppNH_2 complex was synthesized using a microwave-assisted method. In a microwave tube, 0.5 mmol of $Zn(ClO_4)_2$ and 0.3 mmol of NH_2Bpp were dissolved in 5 mL of DMF. To this mixture, 0.3 mL of 1M NaOH was added, and the solution was heated at 100°C for 30 minutes. After the reaction, the mixture was filtered using a syringe filter, and the filtrate was collected. A saturated aqueous solution of $NaPF_6$ was then added to the filtrate, followed by the addition of water to induce precipitation. The resulting yellow solid product was collected by filtration (yield = 82%) (Fig. A3.3).

3.2.4 Synthesis of M_5COF:

The M_5COF was synthesized using a solvothermal method in a Pyrex tube. Initially, 0.03 mmol of M_5BppNH_2 and 0.06 mmol of Mellitic Trianhydride were dissolved in a mixture of 0.5 mL of NMP and 2 mL of mesitylene, stirring until a homogenous dispersion was achieved. Subsequently, 0.5 mL of isoquinoline, serving as a base catalyst, was added to the mixture. The solution was then frozen using liquid nitrogen, sealed, and heated in an oven at 150°C for 5 days. Following the reaction, the mixture was slowly cooled to room temperature over a period of 12 hours. The resulting product was filtered and washed with several organic solvents, including THF, methanol, and acetone. Finally, the product was subjected to Soxhlet extraction in THF, yielding a product with an efficiency of 70-80% (Fig. A3.4).

3.2.5 Working electrode preparation:

The catalyst ink was prepared by mixing 1 mg of the electrocatalyst M_5BppNH_2 and 1 mg of acetylene black with 360 µL of ethanol. Then, 40 µL of a Nafion solution (10 wt.% in ethanol) was added to the mixture, which was then sonicated for at least 15 minutes to achieve a homogeneous dispersion. The resulting catalyst ink was drop-cast onto carbon cloth, achieving a loading of 0.5 mg/cm².

3.2.6 Electrochemical measurements:

The electrochemical H-cell (Fig. A3.9) with Nafion 117 membrane was used for electrocatalysis. Prior to measurement, the Nafion membrane was treated by soaking it in a 5 wt.% H_2O_2 aqueous solution for 5 hours at 100°C and then immersed in ultrapure milliq water. Again, treated in 2M H_2SO_4 solution for 5 hours at 100°C and then immersed in

ultrapure milliq water. Electrochemical measurements were carried in a 0.5M K_2SO_4 with 0.1 M KNO_3 aqueous solution (9 mL) at room temperature and pressure. A carbon cloth coated with the catalyst was performed as the working electrode, while Pt wire work the counter electrode and Ag/AgCl (NaCl 3.0 M) as the reference electrode. Constant potential electrolysis was performed at different potential under constant stirring. Reference electrode measurements were converted to the RHE reference scale using the formula

E(vs RHE) = E(vs Ag/AgCl) + 0.222 + 0.0591 × pH.

3.2.7 Determination of NH_3:

The ammonia concentration in the solution was determined using colourimetry with the indophenol blue method. First, the electrolyte was diluted 100-fold. Specifically, 1 mL of the post-reaction solution was added with 1 mL of a 1 M NaOH solution containing 10% sodium benzoate ($C_7H_5NaO_3$) and 10% sodium citrate ($C_6H_5Na_3O_7{\cdot}2H_2O$). This mixture added 1 mL of an oxidizing solution containing 0.05 M sodium perchlorate ($NaClO_4$) and 0.2 mL of a 1% nitroprusside disodium dihydrate ($C_5FeN_6Na_2O$) solution. UV-Vis absorption spectra were measured after allowing the mixture to stand in the dark for 2 hours. The ammonia concentration was determined based on absorbance at 655 nm. A calibration curve was created using standard NH_4Cl solutions with concentrations of 0, 50, 100, 150, 200, and 250 ppm in a a 0.5M K_2SO_4 with 0.1 M KNO_3 solution. The calibration curve (y = mx + c, R^2 = 0.996) demonstrated a robust linear relationship between absorbance and ammonia concentration.

3.2.8 Determination of N_2H_4:

The concentration of N_2H_4 was determined using the Watt and Chrisp method. The color reagent consisted of a solution with a concentration of 18.15 mg mL^{-1} of para-(dimethylamino) benzaldehyde, $C_9H_{11}NO$, in a mixed solvent of HCl and C_2H_5OH (v/v: 1/10). Specifically, 2 mL of electrolyte was combined with 2 mL of the color reagent and stirred for 15 minutes. The absorbance of the resulting solution was then measured to calculate the hydrazine yields using the standard curve of hydrazine. (y = m x + c , R^2 = 0.999).

3.2.9 Determination of NH_3 yield and FE:

FE = (n$F * C * V$)/Q

YR_{NH3} = (17$C * V$)/($t * m$)

Where n is the number of electrons transferred during NO_3RR, C is the concentration of products, V is the volume of the cathodic electrolyte (9 mL), F is the Faradaic constant (96500

C mol^{-1}), M is the molar mass of products, Q is the total quantity of applied electricity, t is the electrolysis time, and m is the mass of the catalyst.

3.2.10 Isotope-labelled experiments:

The isotopic labelling experiments used $K^{14}NO_3$ and $K^{15}NO_3$ as nitrate sources, both with 99% purity, obtained from Sigma. Before the experiment, the system was purged with Ar gas to eliminate any atmospheric contamination. The nitrate reduction reaction (NO_3RR) was conducted in a closed setup at -1.735 V vs. Ag/AgCl for 2 hours in 9 mL of 0.5 M K_2SO_4 containing 0.1 M KNO_3 aqueous solution. Afterward, 0.5 mL of the resulting solution was combined with 0.1 mL of d_6-DMSO and 0.1 mL of 1 M HCl for analysis via ^1H nuclear magnetic resonance (NMR) spectroscopy using a JEOL 400 MHz instrument.

3.2.11 Powder X-ray diffraction:

Powder XRDs were obtained by using a Rigaku Miniflex-600 instrument and processed using PDXL software.

3.2.12 Nuclear Magnetic Resonance spectroscopy (NMR):

NMR spectra for the catalytic products were performed on a 400 MHz Jeol ECS-400, Bruker 400 MHz.

3.2.13 UV-visible spectroscopy:

Solution state and diffuse-reflectance UV-visible spectra were obtained using a Shimadzu UV-3600 UV-vis-near-IR spectrophotometer. A white standard of $BaSO_4$ served as the reference for diffuse-reflectance spectroscopic measurements.

3.2.14 IR spectroscopy:

The IR Spectra were obtained by using a Bruker Optics ALPHA-E spectrometer with a universal Zn-Se ATR (attenuated total reflection) accessory.

3.2.15 HR-Transmission electron microscopy:

High-resolution transmission electron microscopy (HR-TEM) images were taken using an FEI JEOL FEG 2100F model. This model is equipped with a field emission source operating at 300 keV. The sample, which was well dispersed, was applied to a copper grid using drop-casting for imaging.

3.2.16 Adsorption analysis:

Adsorptions were conducted using a 3-FLEX pore and surface area analyzer and, in a few instances, using Micromeritics ASAP 2020.

3.3. Results and discussion

3.3.1 Characterization:

M_5NH_2Bpp was synthesized under microwave conditions by reaction of metal perchlorate salt and NH_2Bpp ligand. M_5COF was synthesized by solvothermal method by using M_5NH_2Bpp and mellitic trianhydride in presence of base catalyst The detailed synthesis of M_5NH_2Bpp and M_5COF has been outlined in the experimental section (Fig. 3.1, Scheme A3.1-A3.4). This particular COF is unique in its structural design, presenting the first example of Quasi-D3 symmetry and featuring a pentanuclear complex anchored within the framework. This innovative arrangement allows for enhanced coordination and reactivity.

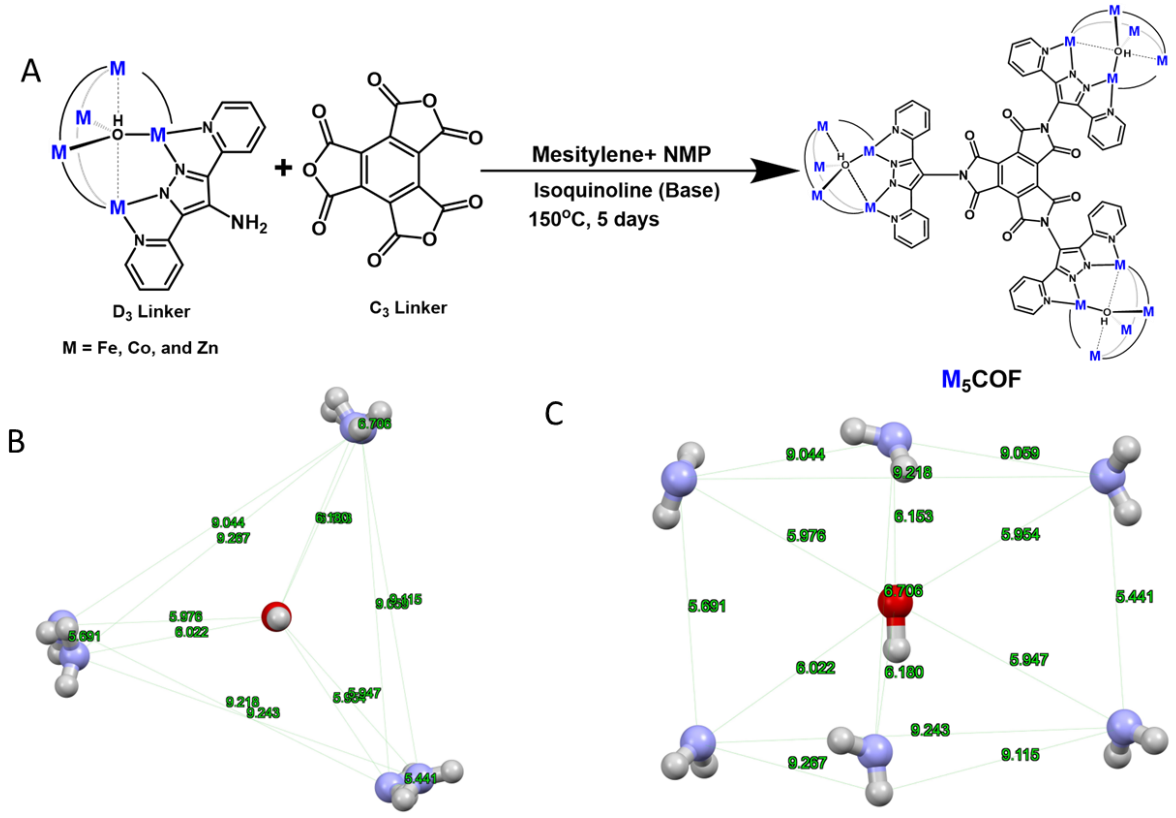

Figure 3.1 (A) Schematic reaction of synthesis of M_5COF (B) Distorted D3 symmetry of M_5 Bpp complex and (C) Distorted hexagonal view of M_5Bpp complex

The PXRD analysis of the M_5COF displayed prominent sharp peaks at 2θ values of 4.4°, 7.1°, 8.8°, and 11.1°, indicating a high degree of crystallinity, a crucial characteristic for the ordered arrangement of COF frameworks. The well-defined diffraction peaks suggest that the M_5COF

exhibits a robust 3D- crystalline structure, reflecting the successful reticular synthesis of the framework (Fig. 3.2). To further assess the material's porosity, nitrogen adsorption-desorption isotherms were measured at 77K. These studies revealed that the M_5COFs are highly microporous, with the Fe_5COF displaying a nitrogen uptake of 6 mmol/g and the Co_5 COF slightly higher at 9.2 mmol/g with BET surface area 271 m^2/g and 291 m^2/g respectively. The average pore sizes were 1.45 nm for Co_5COF and 1.26 nm for Fe_5COF, indicating well-defined, uniform micropores. (Fig. 3.2) To confirm the successful formation and stability of the polyimide bonds, Fourier Transform Infrared (FTIR) spectroscopy was employed. The FTIR spectra revealed characteristic stretching vibrations of the carbonyl group (-C=O-) at 1783 cm^{-1} and 1732 cm^{-1}, along with the C-N stretching vibration at 1368 cm^{-1}, indicative of the polyimide backbone. These distinct vibrational modes provide clear evidence of polyimide linkage formation, confirming both the structural integrity and stability of the COF framework (Fig. A3.1-2).

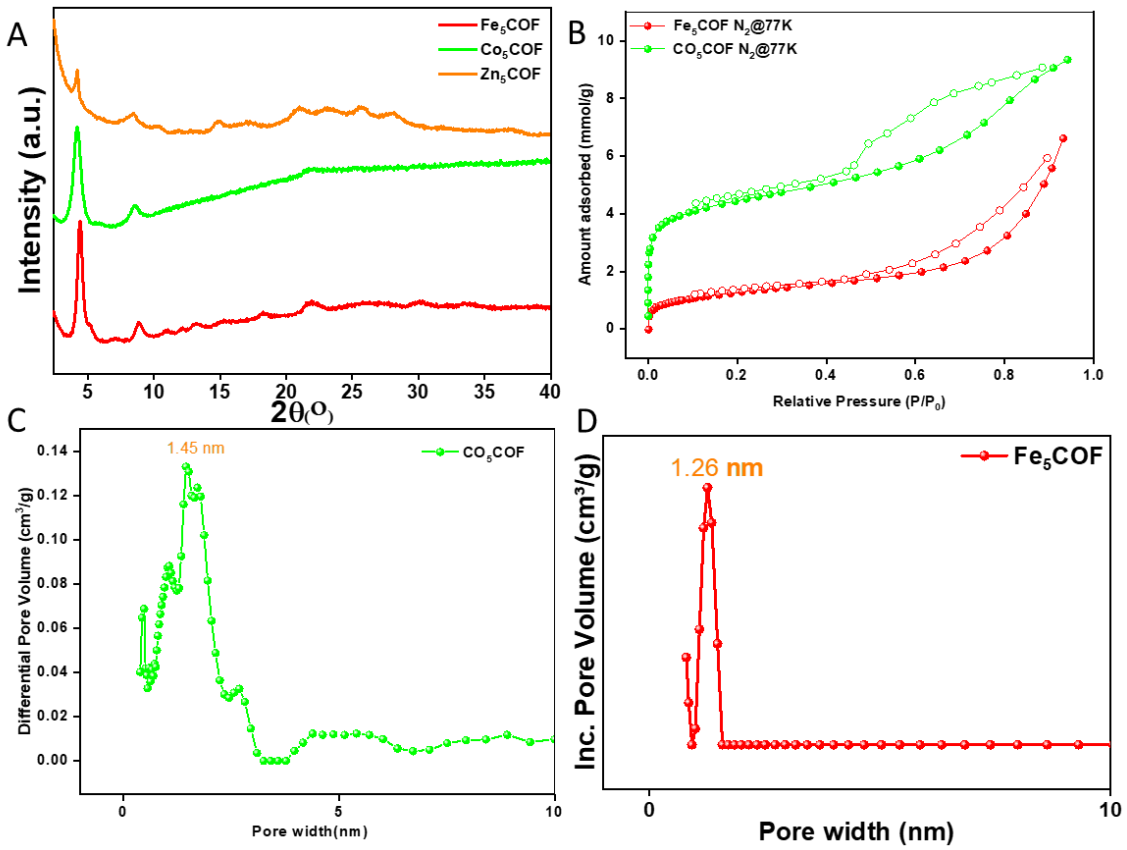

Figure 3.2 (A) Experimental PXRD of M_5COF. Note First peak at 4.4 talks about crystalline nature of COF. (B) Nitrogen isotherm of Fe_5COF and Co_5COF at 77 K (C) Pore size distribution plot of Co_5COF and (D) Pore size distribution plot of Fe_5COF

3.3.2 Morphological analysis:

High-resolution transmission electron microscopy (HRTEM) of M_5COF revealed thin, platy flakes with a fluffy morphology. Detailed imaging showed micron-sized flakes with uniform micropores. The Selected Area Electron Diffraction (SAED) pattern confirmed the crystalline nature of M5COF, with well-defined diffraction spots and lattice fringes indicating structural modifications that may influence catalytic performance. Additionally, Energy-Dispersive X-ray Spectroscopy (EDX) performed using Transmission Electron Microscopy (TEM) confirmed the metal content and demonstrated a homogeneous distribution of atoms, further validating the structural integrity of the COF framework (Fig. A3.3-A3.8).

3.3.3 Electrochemical nitrate reduction reaction:

The electrocatalytic nitrate reduction reaction (NO_3RR) has emerged as a promising method for ammonia (NH_3) production and environmental remediation, but it remains relatively underexplored, particularly within the realm of covalent organic frameworks (COFs).[27-29] This reaction offers a sustainable alternative to traditional ammonia synthesis methods, such as the Haber-Bosch process, by operating under milder conditions.

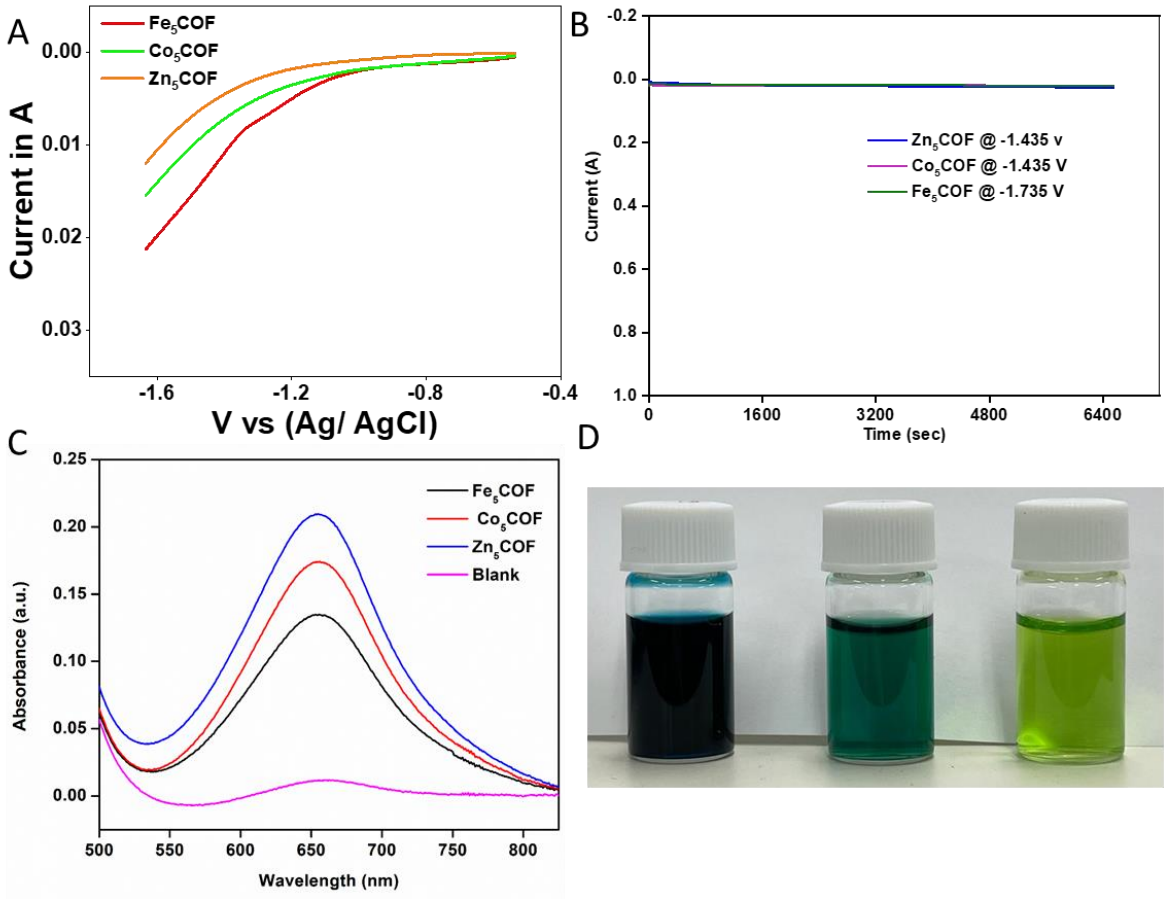

Figure 3.3 (A) LSV profile of M_5COF. (B) LSV profile of M_5COF CPE profile of M_5COF (C) UV abs Spectra for ammonia detection of M_5COF and (D) Dilution of UV solution such as 10, 100, 1000 times for ammonia detection

NO_3RR not only facilitates ammonia production but also provides an effective means for purifying nitrate-contaminated water. This dual functionality highlights the potential of NO_3RR in addressing environmental pollution while simultaneously generating valuable ammonia for industrial and agricultural use.[30-32] Despite these advantages, further investigation is needed to fully exploit the potential of COFs in NO_3RR. Advancing the performance, scalability, and practical applications of COFs for nitrate reduction could significantly impact both environmental management and industrial processes. We tried to explore the catalytic activity of M_5COF for ENO_3RR.

First, we conducted linear sweep voltammetry (LSV) in a 0.5 M K_2SO_4 solution with 0.1 M KNO_3, covering a potential range from -0.535 V to 1.635 V vs Ag/AgCl (equivalent to -0.1 V to -0.9 V vs RHE). The LSV curves demonstrated a significant increase in current with respect to voltage, indicating notable reactivity towards NO_3^- ions. To further investigate the catalytic performance of M_5COF, we performed constant potential electrolysis at various potentials and analyzed the resulting products and their yields (see Fig. 3.3). Ammonia yield was quantified using the indophenol method, while hydrazine (N_2H_4) levels were measured via the Watt and Chrisp method (see Fig. A3.12). The results revealed that Fe_5COF emerged as the most effective catalyst for nitrate reduction, achieving an ammonia production rate of 13.5 mg h^{-1} mg^{-1} cat with a Faradaic efficiency (FE) of 88%.

3.3.4 Isotopic Labelling experiment:

The isotopic labelling experiments utilized $K^{14}NO_3$ and $K^{15}NO_3$, both with 99% purity, procured from Sigma. The system was purged with Ar gas to eliminate atmospheric contamination before the experiments. The nitrate reduction reaction (NO_3RR) was conducted in a closed system at -1.735 V versus Ag/AgCl for 2 hours. The resulting ammonia was analyzed using ^1H NMR spectroscopy. The spectrum for ammonia produced from $^{14}NO_3$ displayed a triplet peak with a coupling constant of 52 Hz, whereas ammonia from $^{15}NO_3$ exhibited a doublet peak with a coupling constant of 72 Hz. These results confirm that ammonia production is attributable to nitrate ions (Fig. A3.13).

3.3.5 Discussion:

Diverse iron-based catalysts and covalent organic framework (COF) systems have been rigorously investigated for their potential in the electrocatalytic nitrate reduction reaction (ENO_3RR). Notably, iron has been incorporated into COF structures, often anchored within porphyrin centers, to leverage its catalytic properties for nitrate reduction. In some studies, both metal centers and organic linkers have been systematically varied to fine-tune the catalytic activity and enhance ENO_3RR performance. Our recent investigations have demonstrated that the COF system developed in our work exhibits comparable, and in certain cases, superior performance relative to previously reported COFs, underscoring its effectiveness as a robust electrocatalyst for nitrate reduction. This pentanuclear COF offers a range of possibilities for tailoring the selectivity of reaction products by varying metal centers.

3.4. Conclusion

In conclusion, this chapter presents the synthesis and electrocatalytic evaluation of a novel heterogeneous covalent organic framework (COF) incorporating a quasi-D_3 symmetry molecule along with a C_3-symmetric monomer, resulting in a three-dimensional structure with an embedded pentanuclear complex for nitrate reduction. Additionally, variations of the COF were synthesized with cobalt and zinc metals, enabling a systematic study of their electrocatalytic performance for the nitrate reduction reaction (NO_3RR). Among the tested materials, the iron-based Fe_5COF demonstrated the highest activity, outperforming the cobalt and zinc counterparts. Comprehensive characterizations, including HRTEM, PXRD, FTIR, and adsorption measurements, confirmed the structural integrity, crystallinity, and porosity of the synthesized COFs. Notably, Fe_5COF exhibited superior catalytic performance, achieving a remarkable ammonia yield of 13.25 $mgh^{-1}mg^{-1}_{cat}$ and a Faradaic efficiency of 88%, establishing it as the most efficient catalyst for NO_3RR within this study.

3.5. References

1. Good, A., Toward nitrogen-fixing plants. *Science* **2018,** *359* (6378), 869-870.
2. Gruber, N.; Galloway, J. N., An Earth-system perspective of the global nitrogen cycle. *Nature* **2008,** *451* (7176), 293-296.
3. Zhang, X.; Ward, B. B.; Sigman, D. M., Global nitrogen cycle: critical enzymes, organisms, and processes for nitrogen budgets and dynamics. *Chem. rev.* **2020,** *120* (12), 5308-5351.
4. Liu, H., Ammonia synthesis catalyst 100 years: Practice, enlightenment and challenge. *Chinese journal of catalysis* **2014,** *35* (10), 1619-1640.
5. Elishav, O.; Mosevitzky Lis, B.; Miller, E. M.; Arent, D. J.; Valera-Medina, A.; Grinberg Dana, A.; Shter, G. E.; Grader, G. S., Progress and prospective of nitrogen-based alternative fuels. *Chem. rev.* **2020,** *120* (12), 5352-5436.
6. Daramola, D. A.; Hatzell, M. C., Energy demand of nitrogen and phosphorus based fertilizers and approaches to circularity. *ACS Energy Lett.* **2023,** *8* (3), 1493-1501.
7. Valera-Medina, A.; Amer-Hatem, F.; Azad, A. K.; Dedoussi, I.; De Joannon, M.; Fernandes, R.; Glarborg, P.; Hashemi, H.; He, X.; Mashruk, S., Review on ammonia as a potential fuel: from synthesis to economics. *Energy & Fuels* **2021,** *35* (9), 6964-7029.
8. Shen, H.; Choi, C.; Masa, J.; Li, X.; Qiu, J.; Jung, Y.; Sun, Z., Electrochemical ammonia synthesis: mechanistic understanding and catalyst design. *Chem* **2021,** *7* (7), 1708-1754.
9. Suryanto, B. H.; Du, H.-L.; Wang, D.; Chen, J.; Simonov, A. N.; MacFarlane, D. R., Challenges and prospects in the catalysis of electroreduction of nitrogen to ammonia. *Nature Catalysis* **2019,** *2* (4), 290-296.
10. Han, L.; Cai, S.; Gao, M.; Hasegawa, J.-y.; Wang, P.; Zhang, J.; Shi, L.; Zhang, D., Selective catalytic reduction of NO x with NH_3 by using novel catalysts: State of the art and future prospects. *Chem. rev.* **2019,** *119* (19), 10916-10976.
11. Shi, Z.; Peng, Q.; Jiaqiang, E.; Xie, B.; Wei, J.; Yin, R.; Fu, G., Mechanism, performance and modification methods for NH_3-SCR catalysts: A review. *Fuel* **2023,** *331*, 125885.
12. Shen, H.; Choi, C.; Masa, J.; Li, X.; Qiu, J.; Jung, Y.; Sun, Z., Electrochemical ammonia synthesis: mechanistic understanding and catalyst design. *Chem* **2021,** *7* (7), 1708-1754.
13. Xiong, Y.; Wang, Y.; Zhou, J.; Liu, F.; Hao, F.; Fan, Z., Electrochemical nitrate reduction: ammonia synthesis and the beyond. *Adv. Mater.* **2024,** *36* (17), 2304021.
14. Chen, W.; Yang, X.; Chen, Z.; Ou, Z.; Hu, J.; Xu, Y.; Li, Y.; Ren, X.; Ye, S.; Qiu, J., Emerging applications, developments, prospects, and challenges of electrochemical nitrate-to-ammonia conversion. *Advanced Functional Materials* **2023,** *33* (29), 2300512.
15. Jiao, F.; Xu, B., Electrochemical ammonia synthesis and ammonia fuel cells. *Adv. Mater.* **2019,** *31* (31), 1805173.
16. El-Kaderi, H. M.; Hunt, J. R.; Mendoza-Cortés, J. L.; Côté, A. P.; Taylor, R. E.; O'Keeffe, M.; Yaghi, O. M., Designed synthesis of 3D covalent organic frameworks. *Science* **2007,** *316* (5822), 268-272.
17. Furukawa, H.; Yaghi, O. M., Storage of hydrogen, methane, and carbon dioxide in highly porous covalent organic frameworks for clean energy applications. *J. Am. Chem. Soc.* **2009,** *131* (25), 8875-8883.
18. Wan, S.; Guo, J.; Kim, J.; Ihee, H.; Jiang, D., A photoconductive covalent organic framework: self-condensed arene cubes composed of eclipsed 2D polypyrene sheets for photocurrent generation. *Angew. Chem. Int. Ed.* **2009,** *48* (30), 5439-5442.
19. Lohse, M. S.; Bein, T., Covalent organic frameworks: structures, synthesis, and applications. *Advanced Functional Materials* **2018,** *28* (33), 1705553.
20. Ding, S.-Y.; Gao, J.; Wang, Q.; Zhang, Y.; Song, W.-G.; Su, C.-Y.; Wang, W., Construction of covalent organic framework for catalysis: Pd/COF-LZU1 in Suzuki–Miyaura coupling reaction. *J. Am. Chem. Soc.* **2011,** *133* (49), 19816-19822.
21. Kushwaha, R.; Kaleeswaran, D.; Haldar, S.; Chakraborty, D.; Mullangi, D.; Borah, A.; Vinod, C. P.; Murugavel, R.; Vaidhyanathan, R., Nanoporous covalent organic framework embedded with Fe/Fe3O4 nanoparticles as air-stable low-density nanomagnets. *ACS Applied Nano Materials* **2020,** *3* (9), 9088-9096.

22. Dong, J.; Han, X.; Liu, Y.; Li, H.; Cui, Y., Metal–covalent organic frameworks (MCOFs): a bridge between metal–organic frameworks and covalent organic frameworks. *Angew. Chem. Int. Ed.* **2020,** *59* (33), 13722-13733.
23. Feng, J.-D.; Zhang, W.-D.; Gu, Z.-G., Covalent Organic Frameworks for Electrocatalysis: Design, Applications, and Perspectives. *ChemPlusChem*, e202400069.
24. Okamura, M.; Kondo, M.; Kuga, R.; Kurashige, Y.; Yanai, T.; Hayami, S.; Praneeth, V. K.; Yoshida, M.; Yoneda, K.; Kawata, S., A pentanuclear iron catalyst designed for water oxidation. *Nature* **2016,** *530* (7591), 465-468.
25. Yoneda, K.; Adachi, K.; Nishio, K.; Yamasaki, M.; Fuyuhiro, A.; Katada, M.; Kaizaki, S.; Kawata, S., An [FeII3O] 4+ core wrapped by two [FeIIL3]− units. *Angew. Chem. Int. Ed.* **2006,** *45* (33), 5459-5461.
26. Praneeth, V. K.; Kondo, M.; Okamura, M.; Akai, T.; Izu, H.; Masaoka, S., Pentanuclear iron catalysts for water oxidation: substituents provide two routes to control onset potentials. *Chem. Sci.* **2019,** *10* (17), 4628-4639.
27. van Langevelde, P. H.; Katsounaros, I.; Koper, M. T., Electrocatalytic nitrate reduction for sustainable ammonia production. *Joule* **2021,** *5* (2), 290-294.
28. Wang, Z.; Richards, D.; Singh, N., Recent discoveries in the reaction mechanism of heterogeneous electrocatalytic nitrate reduction. *Catalysis science & technology* **2021,** *11* (3), 705-725.
29. Lv, F.; Sun, M.; Hu, Y.; Xu, J.; Huang, W.; Han, N.; Huang, B.; Li, Y., Near-unity electrochemical conversion of nitrate to ammonia on crystalline nickel porphyrin-based covalent organic frameworks. *Energy & Environmental Science* **2023,** *16* (1), 201-209.
30. Hu, H.; Miao, R.; Yang, F.; Duan, F.; Zhu, H.; Hu, Y.; Du, M.; Lu, S., Intrinsic Activity of Metalized Porphyrin-based Covalent Organic Frameworks for Electrocatalytic Nitrate Reduction. *Adv. Energy Mater.* **2024,** *14* (6), 2302608.
31. Hu, H.; Miao, R.; Yang, F.; Duan, F.; Zhu, H.; Hu, Y.; Du, M.; Lu, S., Intrinsic Activity of Metalized Porphyrin-based Covalent Organic Frameworks for Electrocatalytic Nitrate Reduction. *Adv. Energy Mater.* **2024,** *14* (6), 2302608.
32. Yuan, S.; Xue, Y.; Ma, R.; Ma, Q.; Chen, Y.; Fan, J., Advances in iron-based electrocatalysts for nitrate reduction. *Science of The Total Environment* **2023,** *866*, 161444.

3.6. Appendix of Chapter 3

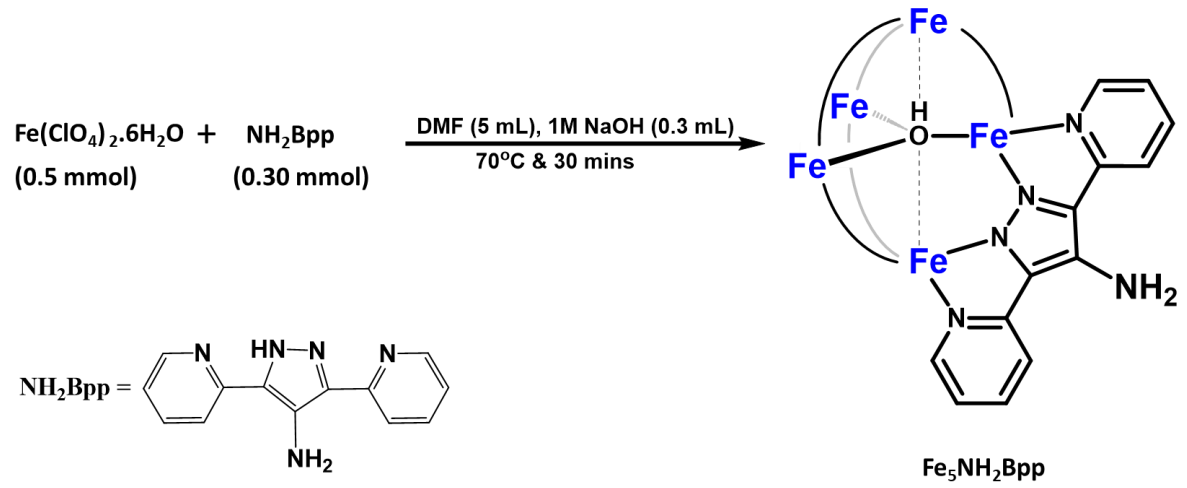

Scheme A3.1. Schematic representation of Fe_5NH_2Bpp synthesis.

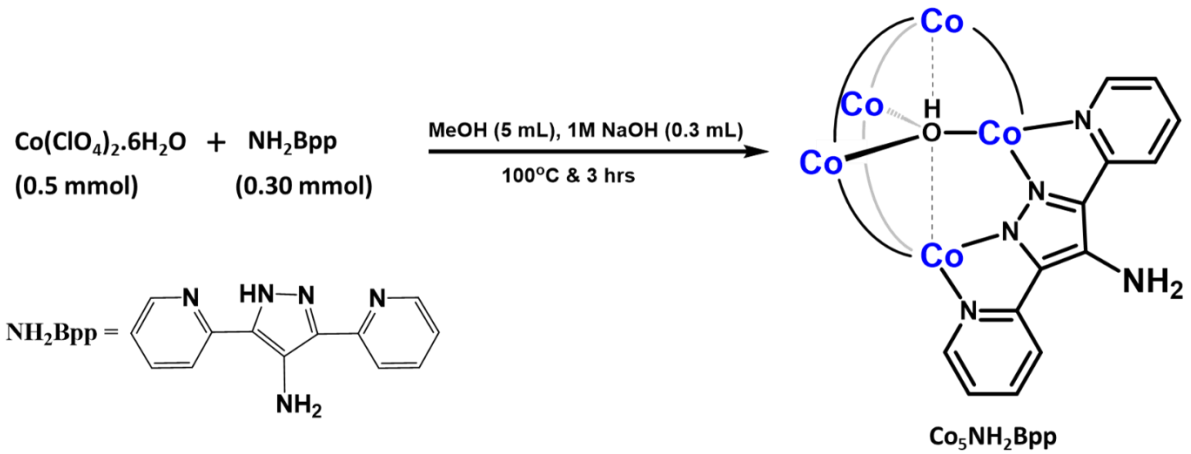

Scheme A3.2. Schematic representation of Co_5NH_2Bpp synthesis.

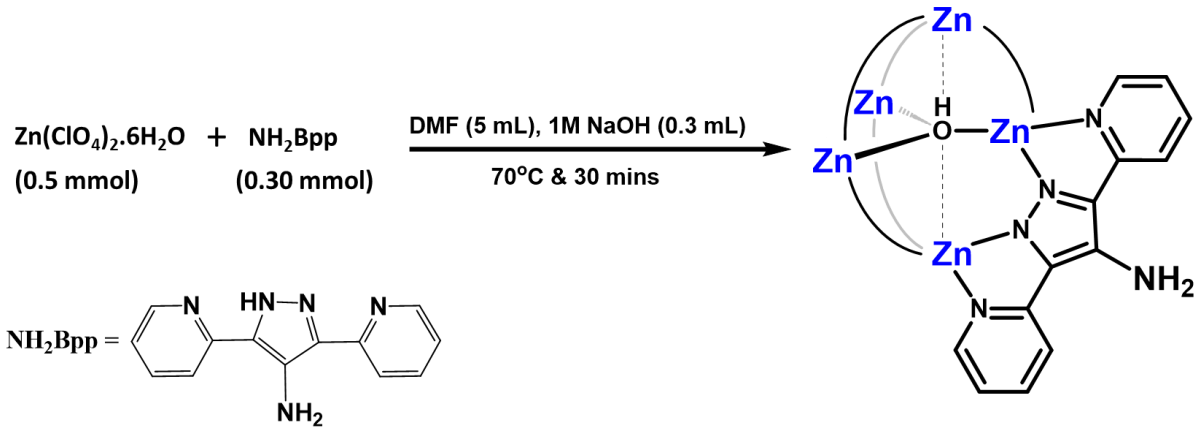

Scheme A3.3. Schematic representation of Zn_5NH_2Bpp synthesis.

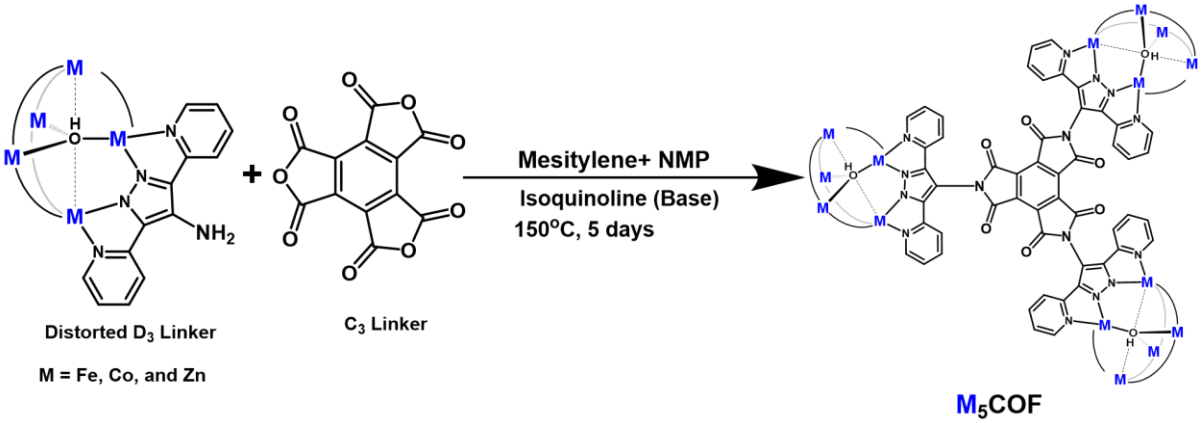

Scheme A3.4. Schematic representation of M_5COF synthesis.

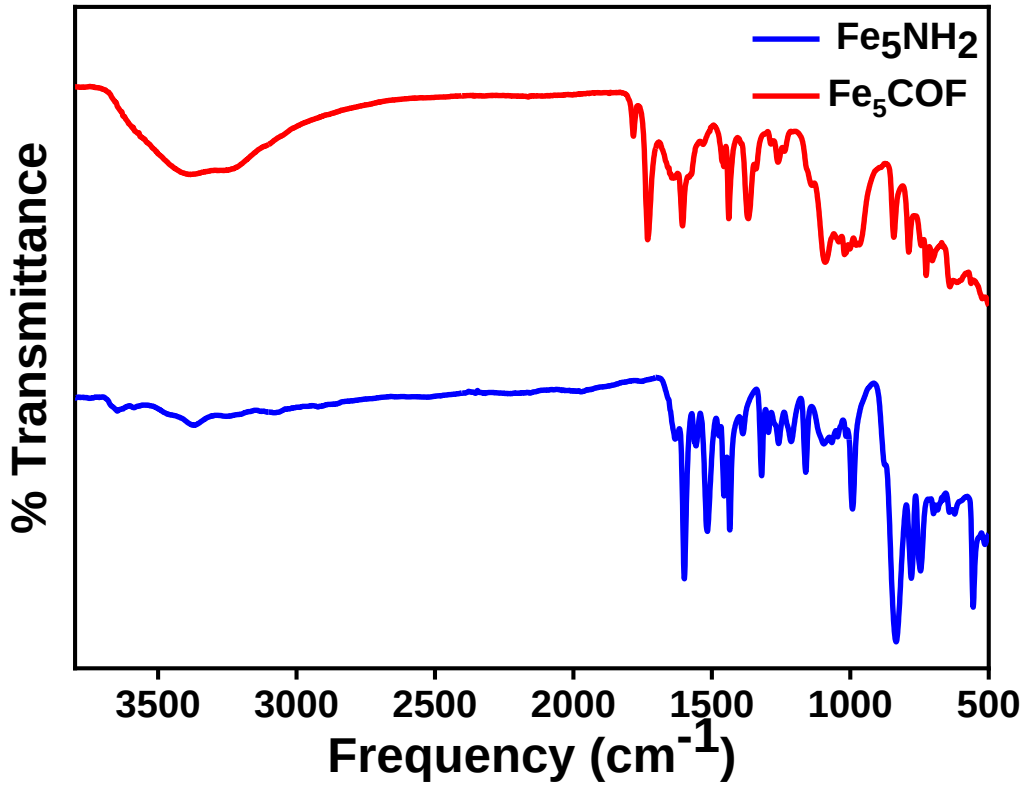

Figure A3.1 FTIR spectra of Fe_5Bpp and Fe_5COF.

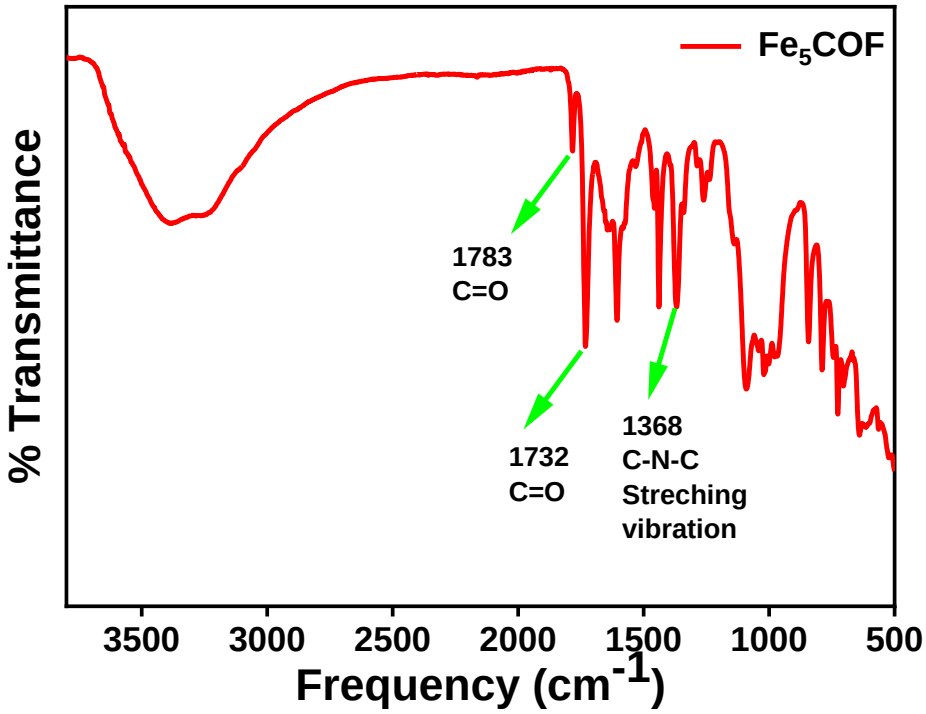

Figure A3.2 Detailed FTIR spectra of Fe_5COF.

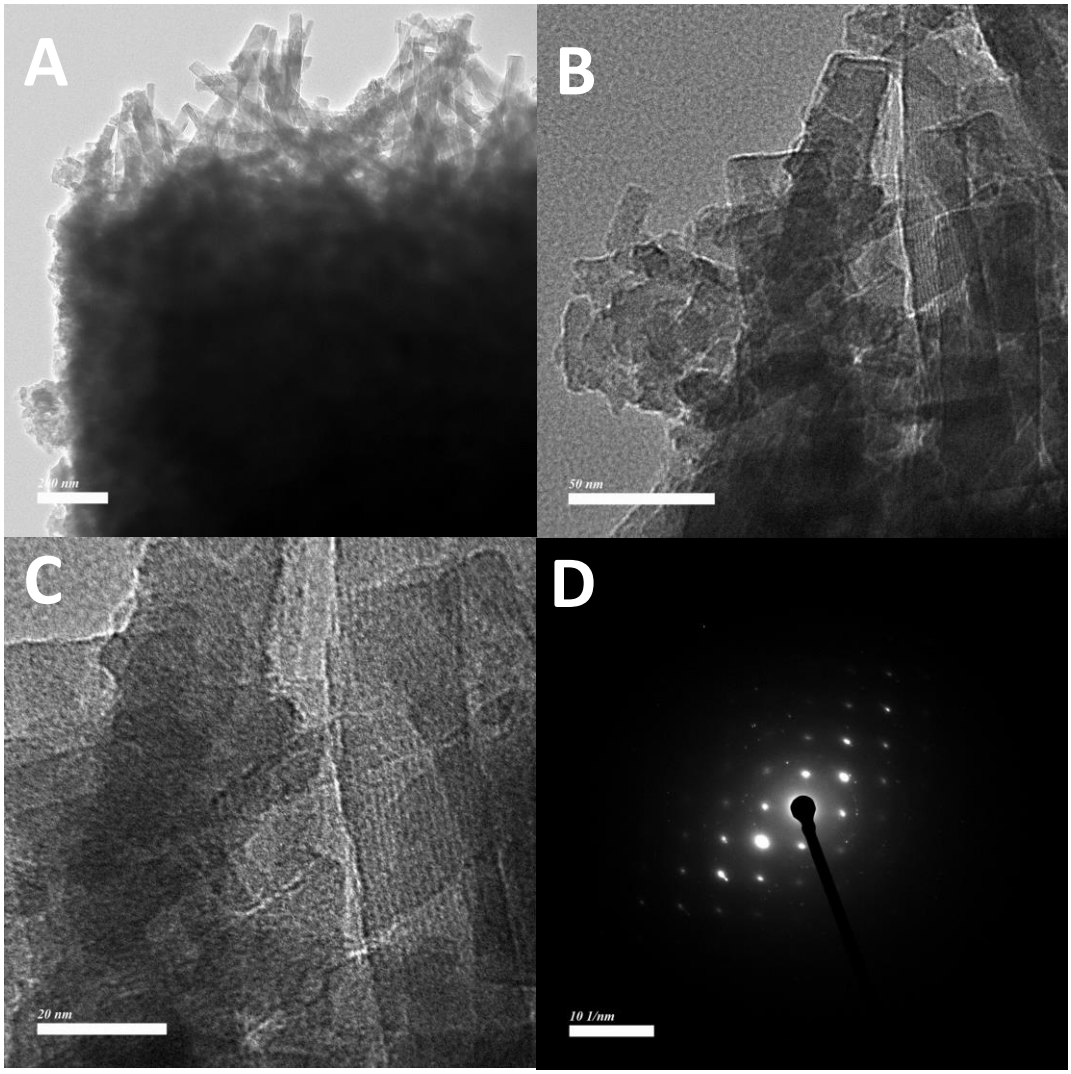

Figure A3.3 HRTEM images having lattice fringes with SAED pattern of Fe_5COF that shows that these COFs are highly crystalline.

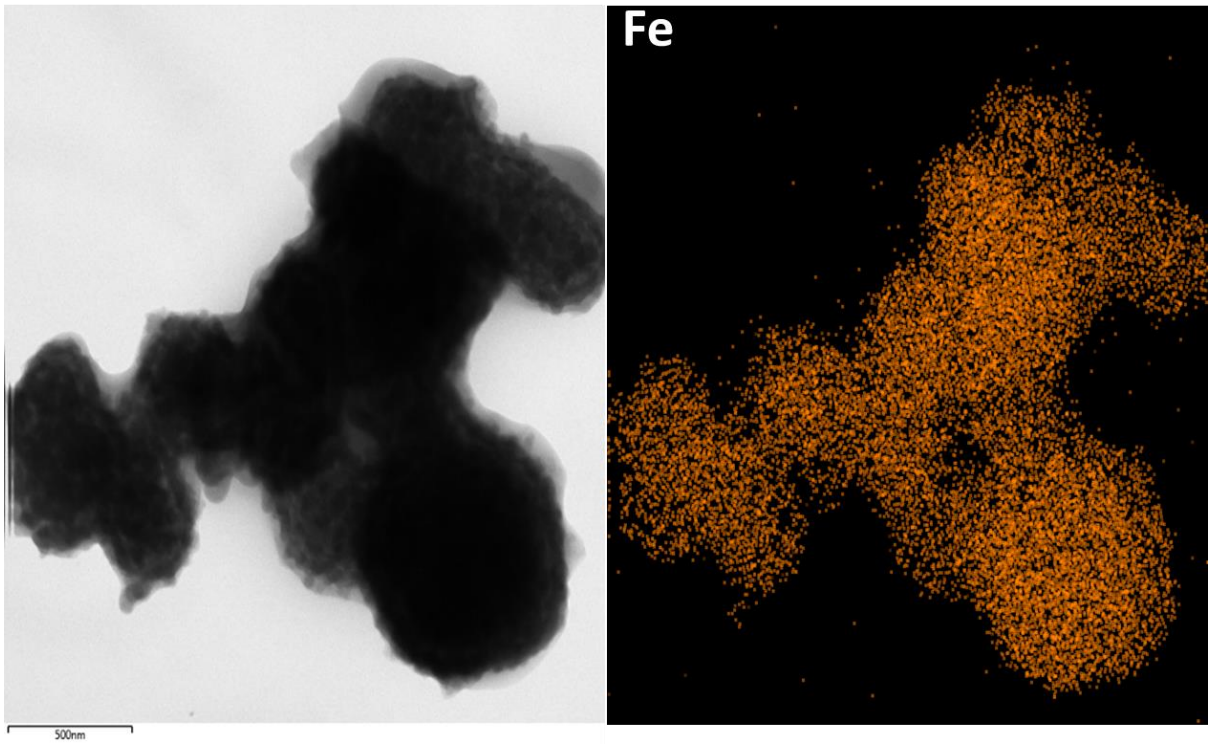

Figure A3.4 The elemental mapping reveals the homogeneous distribution of Fe in Fe_5COF.

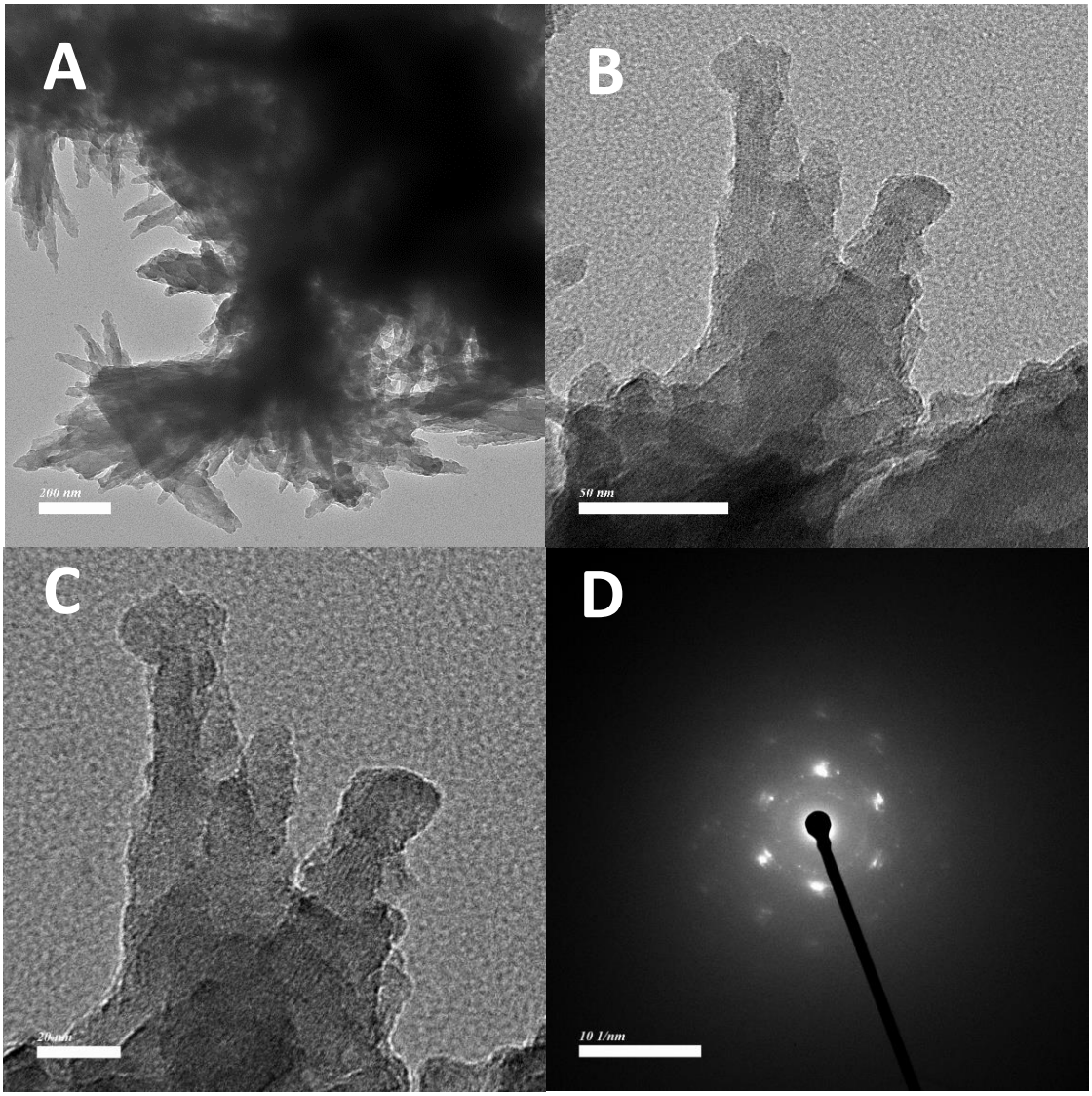

Figure A3.5 HRTEM images having lattice fringes with SAED pattern of Co_5COF that shows that these COFs are highly crystalline.

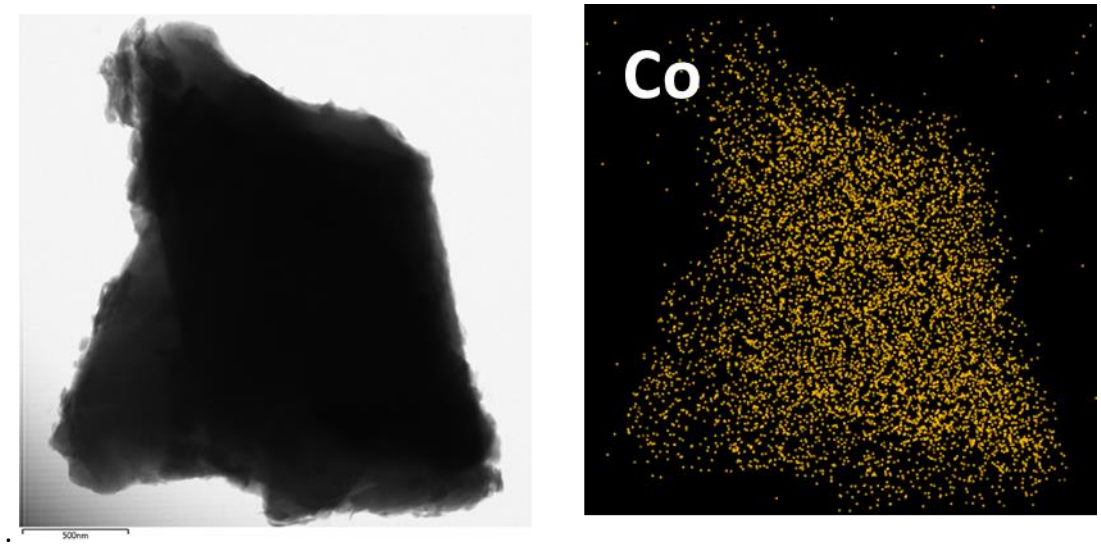

Figure A3.6 The elemental mapping reveals the homogeneous distribution of Co in Co_5COF.

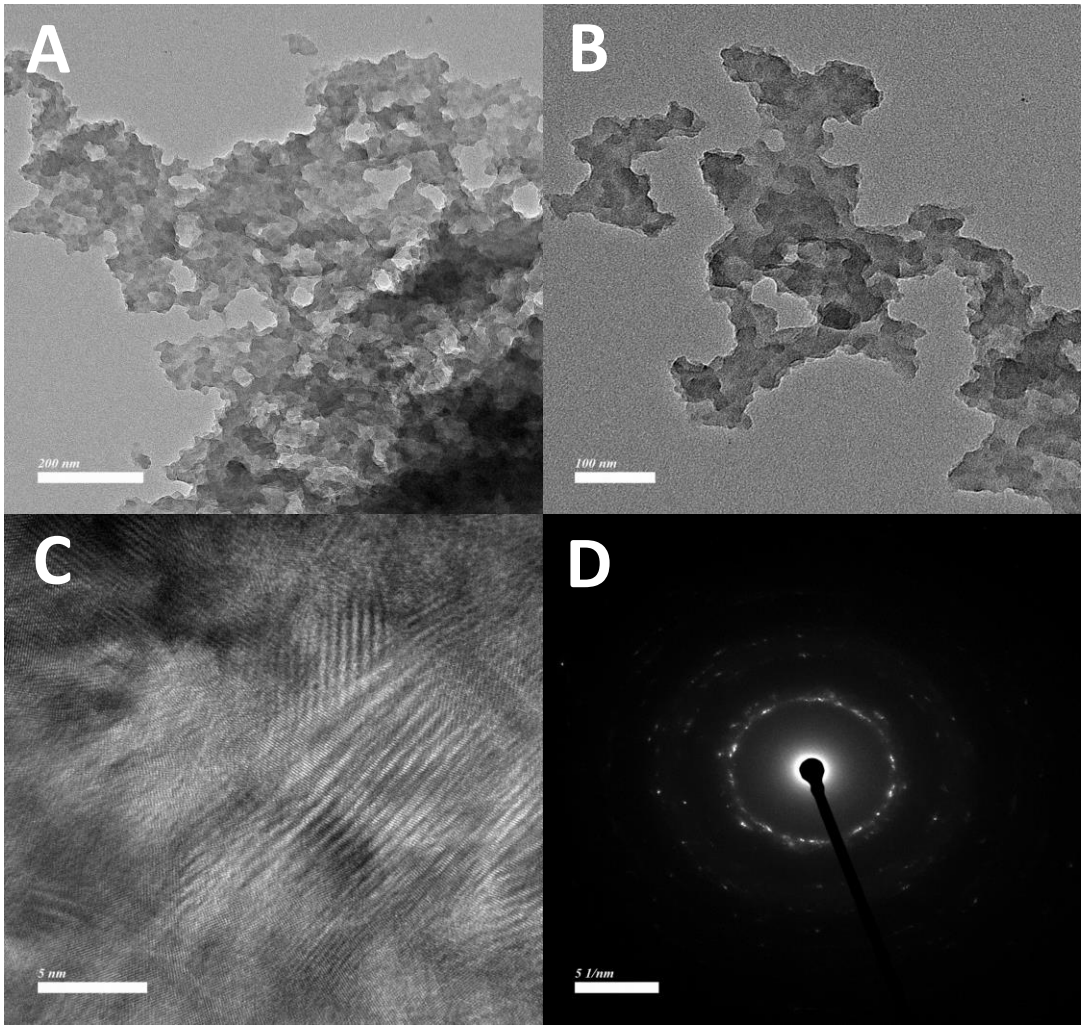

Figure A3.7 HRTEM images having lattice fringes with SAED pattern of Zn_5COF that shows that these COFs are highly crystalline.

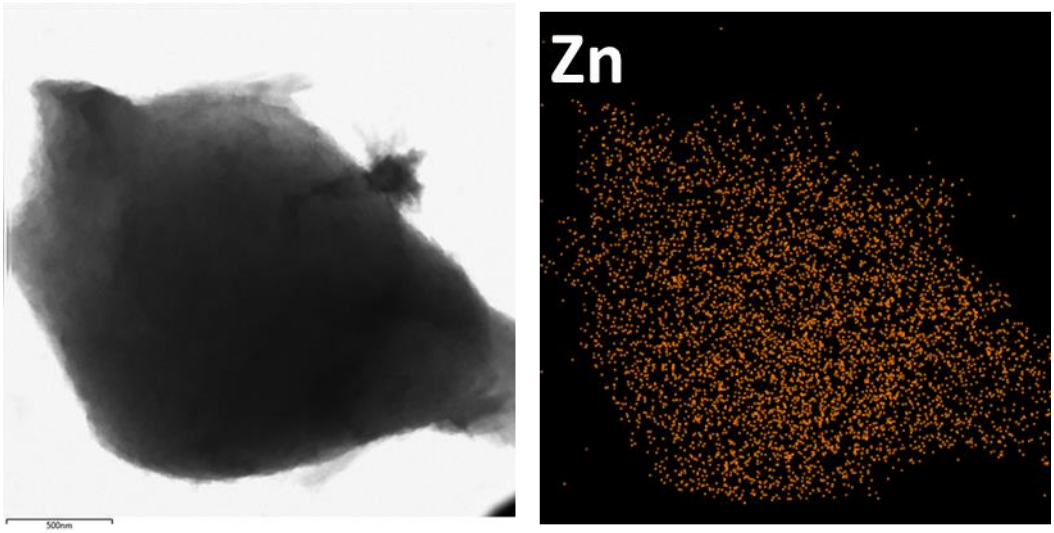

Figure A3.8 The elemental mapping reveals the homogeneous distribution of Zn in Zn_5COF.

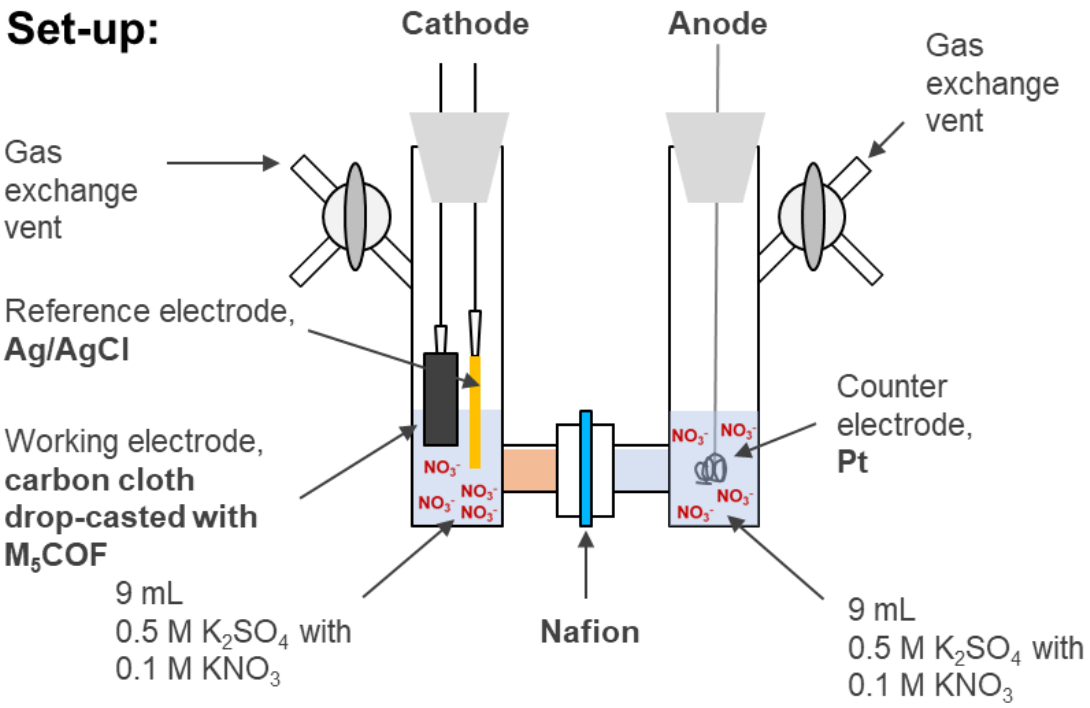

Figure A3.9 Schematic of H-Cell for Nitrate reduction reaction

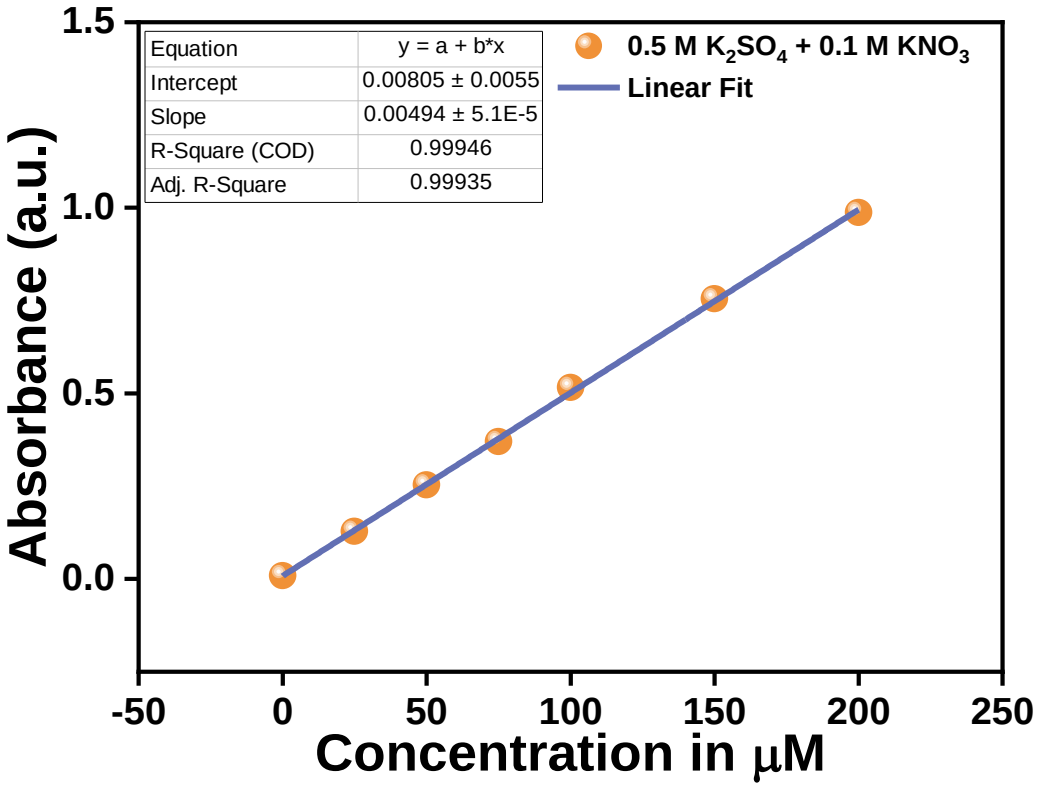

Figure A3.10 Linear fit of known standard NH_4Cl solution.

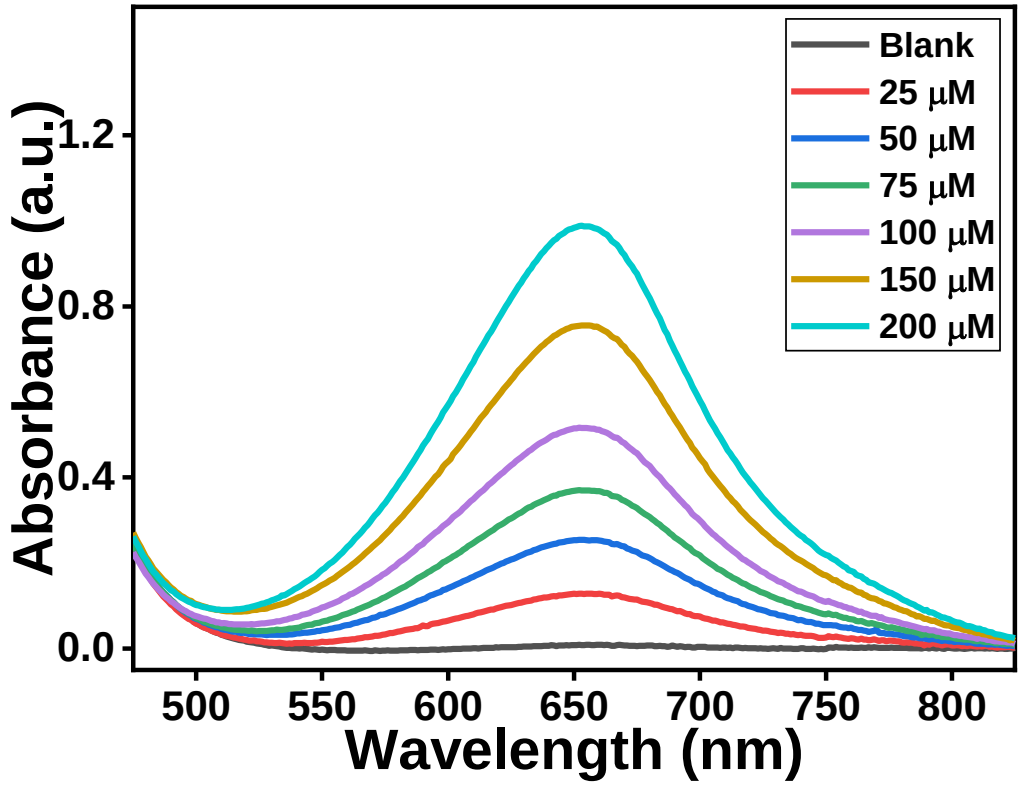

Figure A3.11 UV-vis absorption spectra of indophenol blue solutions of standard NH_4Cl solution.

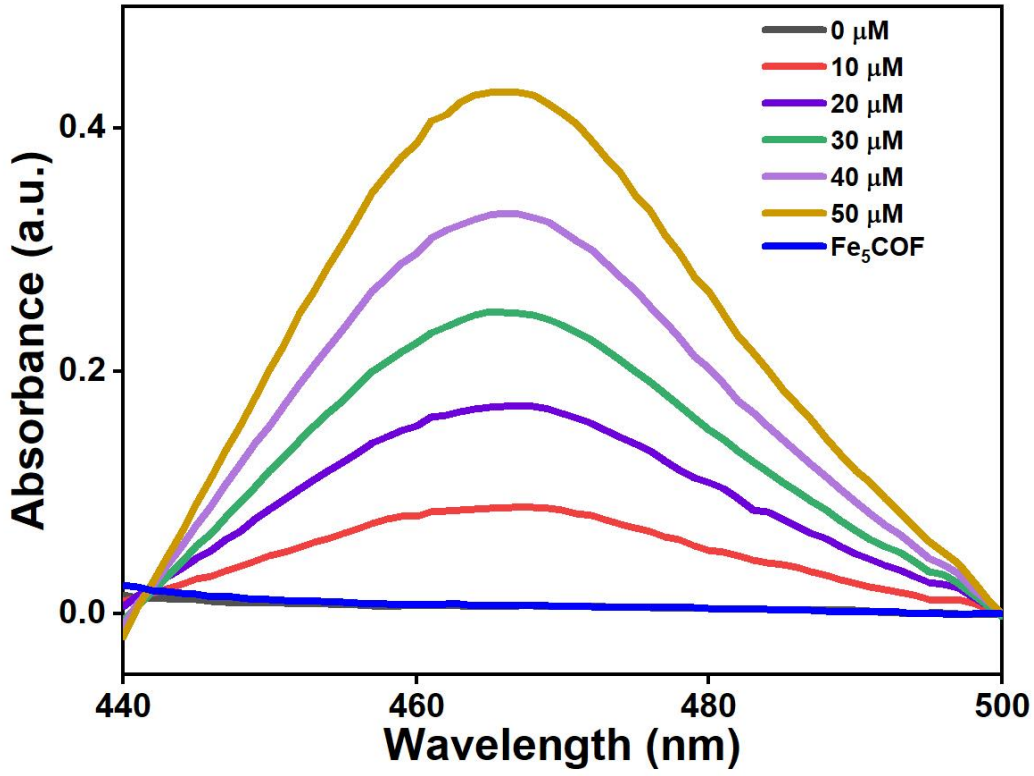

Figure A3.12 UV-vis absorption spectra of standard hydrazine solutions and with catalyst.

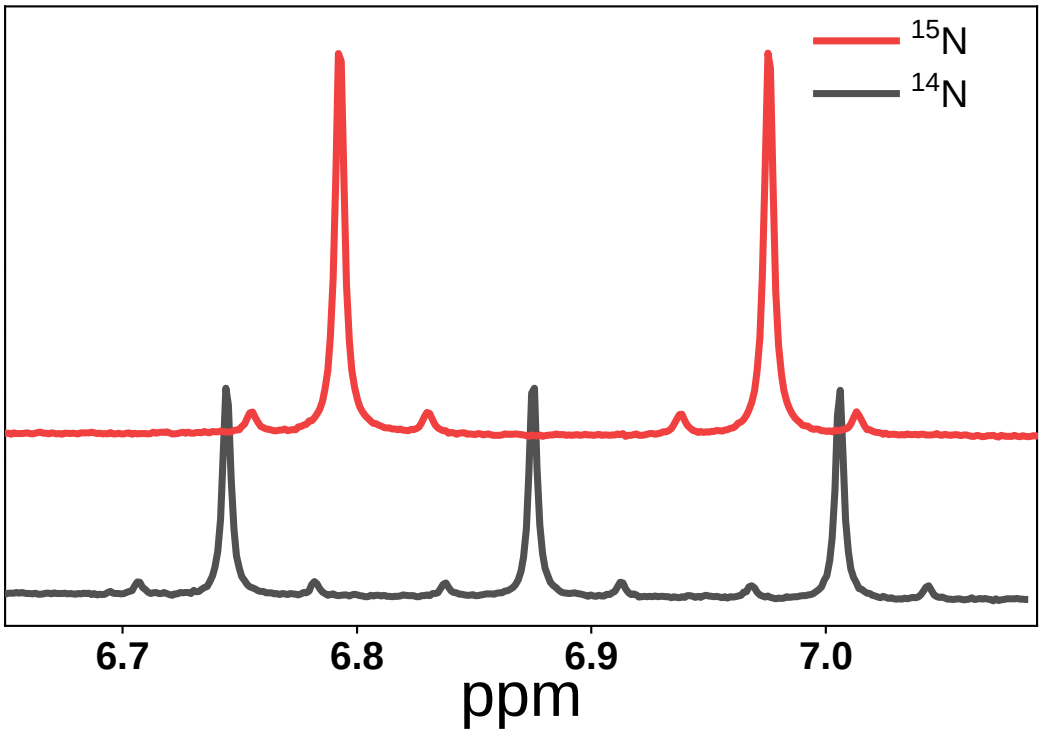

Figure A3.13. ^{1}H NMR spectra of ammonia produced from $K^{14}NO_3$ and $K^{15}NO_3$.

Chapter 4

Pentanuclear Metal Complex-Anchored Covalent Organic Framework for Electrocatalytic Nitrite Reduction Reaction

4.1. Introduction

Ammonia (NH_3) is a fundamental chemical essential for sustaining life on Earth, with significant applications as a feedstock in fertilizers (e.g., urea, ammonium nitrate, ammonium sulfate, ammonium bicarbonate) and as a clean energy carrier.[1-3] Naturally, ammonia is synthesized through nitrogen fixation by bacterial nitrogenase. The Haber-Bosch (HB) process, introduced in 1913, revolutionized industrial ammonia production by increasing crop yields and boosting the global economy by nearly 400%.[4-5] However, the Haber process, one of the significant four industrial contributors to CO_2 emissions alongside cement, steel, and ethylene production, accounts for 1.6% of global emissions annually.[6] To address these challenges, researchers are exploring alternatives to the HB process to reduce energy consumption and CO_2 emissions. Photo/electrocatalytic nitrogen reduction reactions (PNRR/ENRR) under ambient conditions offer a potential green alternative for sustainable ammonia production. This approach utilizes renewable solar or wind energy and water as a green solvent, enabling nitrogen fixation at low temperatures without carbon dioxide emissions. [7-8] Despite its promise, catalytic ENRR faces several challenges, including issues with catalytic selectivity, N_2 adsorption and activation, electron-hole separation, low quantum efficiency, limited visible light harvesting, competition from hydrogen evolution reactions (HER), and the extremely low solubility of N_2 in aqueous media.[9] To overcome the challenges of ENRR, researchers have turned their attention to alternative pathways such as nitrate and nitrite reduction reactions for ammonia production. N-O bonds in these compounds have lower bond dissociation energies than the N≡N bond in nitrogen, facilitating easier cleavage.[11] Their higher water solubility also improves the efficiency of electrochemical reduction. Among these, nitrite (NO_2^-) reduction is particularly notable due to its efficiency and environmental benefits. While nitrite is a hazardous pollutant, its conversion to ammonia can utilize wastewater contaminants, offering a sustainable approach. Furthermore, nitrite reduction can produce value-added chemicals like NO, N_2O, NH_2OH, and NH_3, which are important in various fields.[12] However, achieving high product selectivity remains a significant challenge due to the complexity of the reaction.[13]

Covalent organic frameworks (COFs), first introduced by Yaghi et al. in 2005, represent a new frontier in catalysis due to their unique properties such as modularity, permanent porosity, ultra-stability, and low density.[14] They are a distinctive class of crystalline, porous organic materials characterized by dynamic covalent bonding.[15] These materials are notable for their

unique structural attributes, including high rigidity, tunable configurations, extensive specific surface areas, and highly ordered periodic structures.[16] These attributes make COFs ideal for advanced applications including gas adsorption,[17] molecular trapping,[18] optoelectronics,[19] multiphase catalysis,[20] sensing,[21] and energy storage[22]. Their growing use in electrochemical processes such as N_2 reduction, CO_2 reduction and oxygen reduction reactions highlight their significant potential in enhancing electrocatalytic technologies.[23-24]

In the previous chapter, we examined the performance of pentanuclear metal complex-anchored COFs in nitrate reduction, observing a trend of Fe > Co > Zn. Nitrate reduction typically proceeds through nitrite as an intermediate, and since both nitrate and nitrite are found in polluted waters. In this chapter we investigated nitrite reduction using M_5COF. Our findings reveal that the performance of nitrite reduction varies with the metal type: Co > Fe > Zn, with Co_5COF showing the highest activity. This chapter highlights the exceptional performance of pentanuclear COFs in nitrite reduction by varying metal centers. Notably, the Co_5COF achieved a nitrite reduction rate of 3.9 $mgh^{-1}mg^{-1}_{cat}$ with a Faradaic efficiency (FE) of 99.3%, showcasing its superior catalytic efficiency. Additionally, Fe_5COF demonstrated significant activity with a yield of 3.6 $mgh^{-1}mg^{-1}_{cat}$ and a FE of 100%. These findings underscore the effectiveness of tailored COF systems in optimizing nitrite reduction reactions.

4.2. Experimental details

4.2.1 Synthesis of Fe_5BppNH_2 complex:

The Fe_5BppNH_2 complex was synthesized using a microwave-assisted method. In a microwave tube, 0.5 mmol of $Fe(ClO_4)_2$ and 0.3 mmol of NH_2Bpp were dissolved in 5 mL of DMF. To this mixture, 0.3 mL of 1M NaOH was added, and the solution was heated at 70°C for 30 minutes. After the reaction, the mixture was filtered using a syringe filter, and the filtrate was collected. A saturated aqueous solution of $NaPF_6$ was then added to the filtrate, followed by the addition of water to induce precipitation. The resulting brown solid product was collected by filtration(yield = 78%).

4.2.2 Synthesis of Co_5BppNH_2 complex:

The Co_5BppNH_2 complex was synthesized using a microwave-assisted method. In a microwave tube, 0.5 mmol of $Co(ClO_4)_2$ and 0.3 mmol of NH_2Bpp were dissolved in 5 mL of MeOH. To this mixture, 0.3 mL of 1M NaOH was added, and the solution was heated at 100°C for 30 minutes. After the reaction, the mixture was filtered using a syringe filter, and the filtrate was collected. A saturated aqueous solution of $NaPF_6$ was then added to the filtrate, followed by the

addition of water to induce precipitation. The resulting light green solid product was collected by filtration (yield = 72%).

4.2.3 Synthesis of Zn_5BppNH_2 complex:

The Zn_5BppNH_2 complex was synthesized using a microwave-assisted method. In a microwave tube, 0.5 mmol of $Zn(ClO_4)_2$ and 0.3 mmol of NH_2Bpp were dissolved in 5 mL of DMF. To this mixture, 0.3 mL of 1M NaOH was added, and the solution was heated at 100°C for 30 minutes. After the reaction, the mixture was filtered using a syringe filter, and the filtrate was collected. A saturated aqueous solution of $NaPF_6$ was then added to the filtrate, followed by the addition of water to induce precipitation. The resulting yellow solid product was collected by filtration (yield = 82%).

4.2.4 Synthesis of M_5COF:

The M_5COF was synthesized using a solvothermal method in a Pyrex tube. Initially, 0.03 mmol of M_5BppNH_2 and 0.06 mmol of Mellitic Trianhydride were dissolved in a mixture of 0.5 mL of NMP and 2 mL of mesitylene, stirring until a homogenous dispersion was achieved. Subsequently, 0.5 mL of isoquinoline, serving as a base catalyst, was added to the mixture. The solution was then frozen using liquid nitrogen, sealed, and heated in an oven at 150°C for 5 days. Following the reaction, the mixture was slowly cooled to room temperature over a period of 12 hours. The resulting product was filtered and washed with several organic solvents, including THF, methanol, and acetone. Finally, the product was subjected to Soxhlet extraction in THF, yielding a product with an efficiency of 70-80%.

4.2.5 Working electrode preparation:

A dose of 1 milligram of M_5BppNH_2 and 1 mg of acetylene black, was added to 360 µL of ethanol. 40 µL of Nafion solution (10 wt.% in ethanol) was added to this mixture. To obtain a homogenous catalyst ink, the resulting solution was subjected to ultrasonic agitation for at least 15 minutes. After that, the produced ink was applied using the drop-casting technique to carbon cloth, yielding a final catalyst loading of 0.1 mg cm^{-2}.

4.2.6 Electrochemical measurements:

The electrochemical H-cell with Nafion 117 membrane was used for electrocatalysis. Prior to measurement, the Nafion membrane was treated by soaking it in a 5 wt.% H_2O_2 aqueous solution for 5 hours at 100°C and then immersed in ultrapure milliq water. Again, treated in 2M H_2SO_4 solution for 5 hours at 100°C and then immersed in ultrapure milliq water.

Electrochemical measurements were carried in a 0.1 M NaOH with 0.1 M $NaNO_2$ aqueous solution (9 mL) at room temperature and pressure. A carbon cloth coated with the catalyst was performed as the working electrode, while Pt wire works as the counter electrode and Ag/AgCl (NaCl 3.0 M) as the reference electrode. Constant potential electrolysis was performed at different potential under constant stirring. Reference electrode measurements were converted to the RHE reference scale using the formula

E(vs RHE) = E(vs Ag/AgCl) + 0.222 + 0.0591 × pH.

4.2.7 Determination of NH_3:

The ammonia concentration in the solution was determined using colourimetry with the indophenol blue method. First, the electrolyte was diluted 10-fold. Specifically, 2 mL of the post-reaction solution was added with 2 mL of a 1 M NaOH solution containing 10% sodium benzoate ($C_7H_5NaO_3$) and 10% sodium citrate ($C_6H_5Na_3O_7{\cdot}2H_2O$). This mixture added 1 mL of an oxidizing solution containing 0.05 M sodium perchlorate ($NaClO_4$) and 0.2 mL of a 1% nitroprusside disodium dihydrate ($C_5FeN_6Na_2O$) solution. UV-Vis absorption spectra were measured after allowing the mixture to stand in the dark for 2 hours. The ammonia concentration was determined based on absorbance at 655 nm. A calibration curve was created using standard NH_4Cl solutions with concentrations of 0, 50, 100, 150, 200, and 250 ppm in a a 0.1 M NaOH with 0.1 M $NaNO_2$ solution. The calibration curve (y = mx + c, R^2 = 0.999) demonstrated a robust linear relationship between absorbance and ammonia concentration.

4.2.8 Determination of NH_3 yield and FE:

FE = (n$F * C * V$)/Q

YR_{NH3} = (17$C * V$)/($t * m$)

Where n is the number of electrons transferred during NO_2RR, C is the concentration of products, V is the volume of the cathodic electrolyte (9 mL), F is the Faradaic constant (96500 C mol^{-1}), M is the molar mass of products, Q is the total quantity of applied electricity, t is the electrolysis time, and m is the mass of the catalyst.

4.2.9 Powder X-ray diffraction:

Powder XRDs were performed by using a Rigaku Miniflex-600 instrument and processed using PDXL software.

4.2.10 Nuclear Magnetic Resonance spectroscopy (NMR):

NMR spectra for the catalytic products were performed on a 400 MHz Jeol ECS-400, Bruker 400 MHz.

4.2.11 UV-visible spectroscopy:

Solution state and diffuse-reflectance UV-visible spectra were recorded using a Shimadzu UV-3600 UV-vis-near-IR spectrophotometer. For the diffuse-reflectance measurements, a white BaSO4 standard was used as the reference.

4.2.12 IR spectroscopy:

IR spectra were obtained by using a Bruker Optics ALPHA-E spectrometer equipped with a universal Zn-Se ATR (attenuated total reflection) accessory.

4.2.13 HR-Transmission electron microscopy:

High-resolution transmission electron microscopy (HR-TEM) images were taken using an FEI JEOL FEG 2100F model. This model is equipped with a field emission source operating at 300 keV. The sample, which was well dispersed, was applied to a copper grid using drop-casting for imaging.

4.2.14 Adsorption analysis:

All adsorption measurements were conducted using a 3-FLEX pore and surface area analyzer, and, in some cases, a Micromeritics ASAP 2020.

4.3. Results and discussion

4.3.1 Characterization:

M_5NH_2Bpp was synthesized under microwave conditions by reaction of metal perchlorate salt and NH_2Bpp ligand. M_5COF was synthesized by solvothermal method by using M_5NH_2Bpp and mellitic trianhydride in presence of base catalyst The detailed synthesis of M_5NH_2Bpp and M_5COF has been outlined in the experimental section (Fig. 4.1, Scheme A4.1 and A4.2). This particular COF is unique in its structural design, presenting the first example of Quasi-D_3 symmetry and featuring a pentanuclear complex anchored within the framework. This innovative arrangement allows for enhanced coordination and reactivity. The PXRD analysis

of the M_5COF displayed prominent sharp peaks at 2θ values of 4.4°, 7.1°, 8.8°, and 11.1°, indicating a high degree of crystallinity, a crucial characteristic for the ordered arrangement of COF frameworks. The well-defined diffraction peaks suggest that the M_5COF exhibits a robust 3D- crystalline structure, reflecting the successful reticular synthesis of the framework (Fig. 4.1, SA4.1-SA4.4). To further assess the material's porosity, nitrogen adsorption-desorption isotherms were measured at 77K. These studies revealed that the M_5COF is highly microporous, with the Fe_5COF displaying a nitrogen uptake of 6 mmol/g and the Co_5COF slightly higher at 9.2 mmol/g with BET surface area 271 m^2/g and 291 m^2/g respectively. The average pore sizes were 1.45 nm for Co_5COF and 1.26 nm for Fe_5COF, indicating well-defined, uniform micropores. (Fig. 4.1) To confirm the successful formation and stability of the polyimide bonds, Fourier Transform Infrared (FTIR) spectroscopy was employed. The FTIR spectra revealed characteristic stretching vibrations of the carbonyl group (-C=O-) at 1783 cm^{-1} and 1732 cm^{-1}, along with the C-N stretching vibration at 1368 cm^{-1}, indicative of the polyimide backbone. These distinct vibrational modes provide clear evidence of polyimide linkage formation, confirming both the structural integrity and stability of the COF framework (Fig. 4.1 A4.1-A4.2).

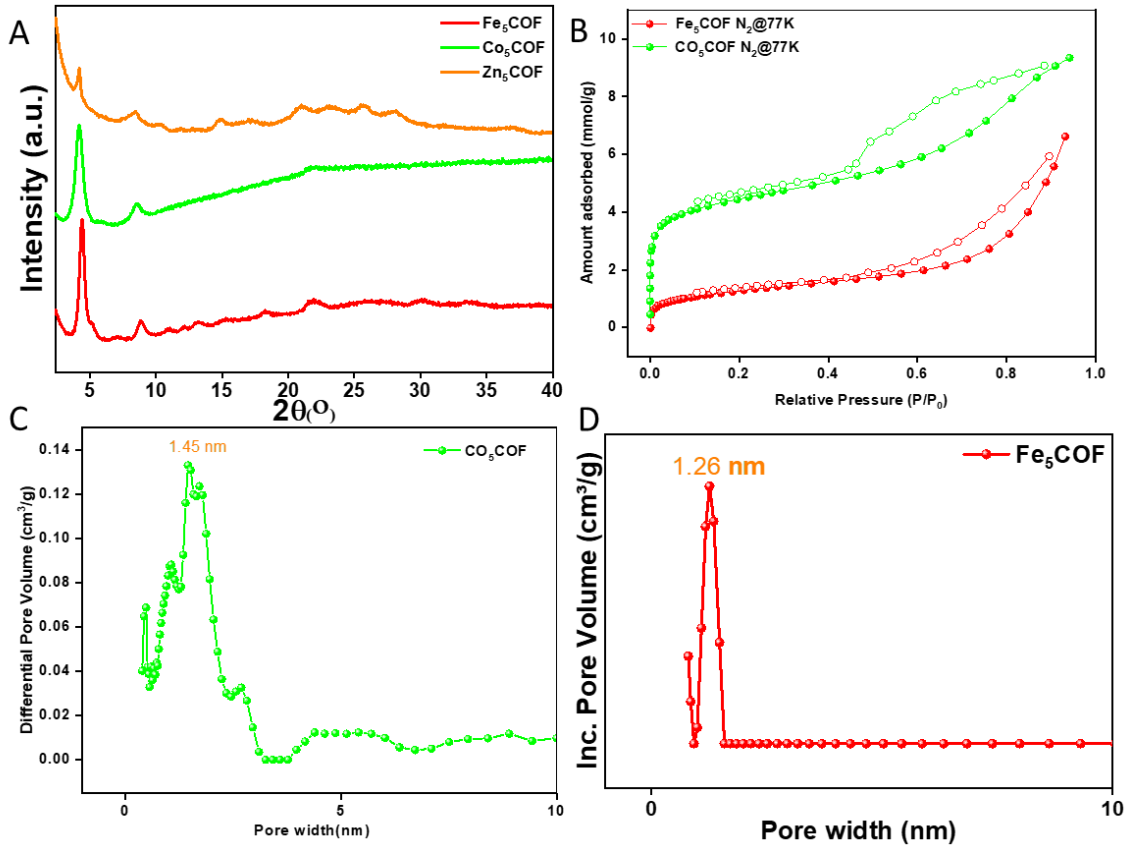

Figure 4.1 (A) Experimental PXRD of M_5COF. Note First peak at 4.4 talks about crystalline nature of COF. (B) Nitrogen isotherm of Fe_5COF and Co_5COF at 77 K (C) Pore size distribution plot of Co_5COF and (D) Pore size distribution plot of Fe_5COF

4.3.2 Morphological analysis:

High-resolution transmission electron microscopy (HRTEM) of M_5COF revealed thin, platy flakes with a fluffy morphology. Detailed imaging showed micron-sized flakes with uniform micropores. The Selected Area Electron Diffraction (SAED) pattern confirmed the crystalline nature of M_5COF, with well-defined diffraction spots and lattice fringes indicating structural modifications that may influence catalytic performance. Additionally, Energy-Dispersive X-ray Spectroscopy (EDX) performed using Transmission Electron Microscopy (TEM) confirmed the metal content and demonstrated a homogeneous distribution of atoms, further validating the structural integrity of the COF framework (Fig. A4.3-A4.7).

4.3.3 Electrochemical nitrite reduction reaction:

Polluted water often contains nitrogen oxides (NO_x), including nitrite (NO_2^-) and nitrate (NO_3^-). While nitrate reduction has been widely studied, nitrite reduction has garnered less attention despite its significance as an intermediate in the nitrogen reduction process. Effective nitrite reduction is crucial for both environmental remediation and ammonia production. Several catalysts have been explored for nitrite reduction, including advanced materials such as Au nanoarrays, ITO@TiO_2 nanoarrays, and CPO-ILBMB/MWCNT-PEI bioconjugates.[25-27] These studies have demonstrated various levels of performance in reducing nitrite to ammonia. However, the development of effective catalysts for nitrite reduction remains a challenging area, with significant opportunities for improvement.

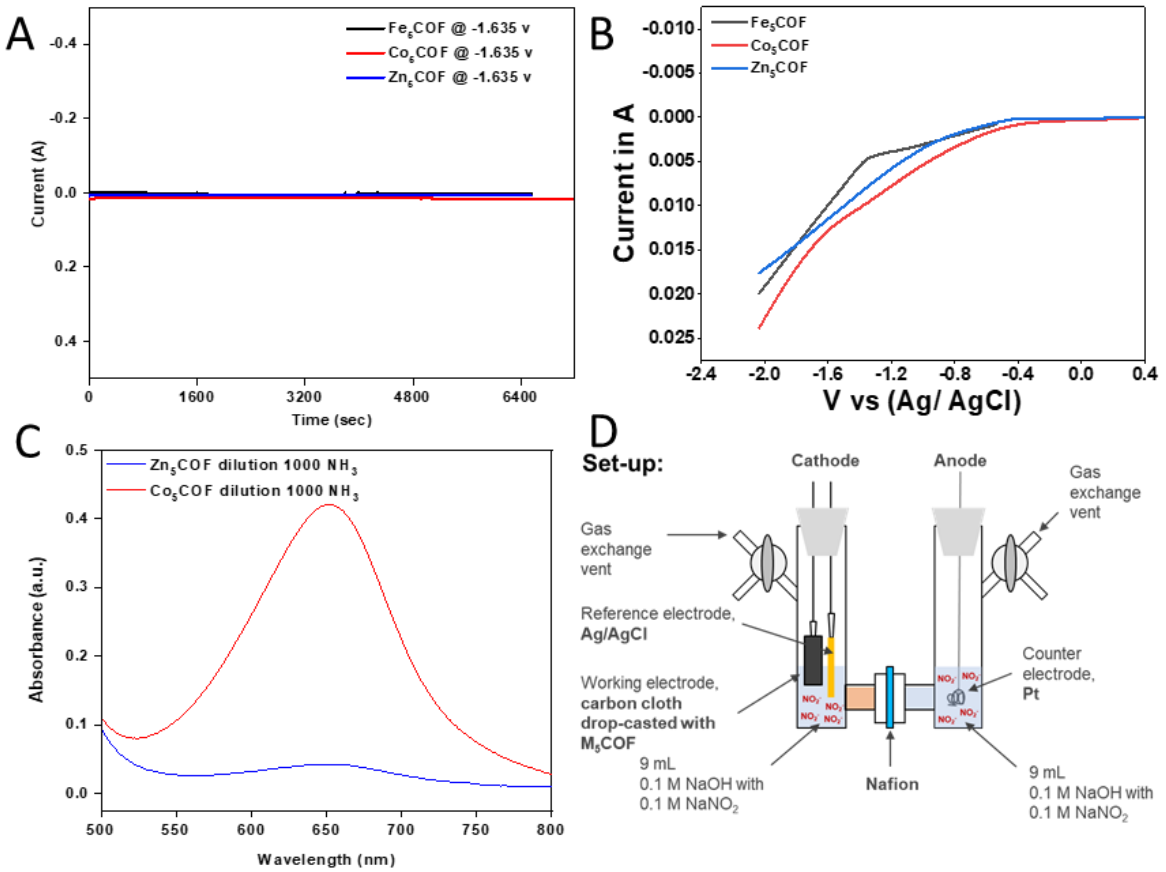

Figure 4.2 (A) LSV profile of M_5COF. (B) LSV profile of M_5COF CPE profile of M_5COF (C) UV abs Spectra for ammonia detection of M_5COF and (D) Schematic of H-Cell for Nitrate reduction reaction

Covalent Organic Frameworks (COFs) represent a novel class of materials that have not yet been extensively explored for nitrite reduction. Their unique structural properties could potentially enhance catalytic performance for nitrite reduction, addressing the dual goals of purifying nitrite-contaminated water and generating valuable ammonia. Given the current lack of reports on COFs for nitrite reduction, it is interesting to explore the catalytic activity of M_5COF for this reaction.

Linear sweep voltammetry (LSV) was first performed in a 0.1 M NaOH solution containing 0.1 M $NaNO_2$, spanning a potential range from -0.535 V to 1.635 V vs. Ag/AgCl (equivalent to -0.1 V to -0.9 V vs. RHE). The LSV curves exhibited a pronounced increase in current as a function of voltage, signifying substantial reactivity towards NO_2^- ions. To further assess the catalytic activity of M_5COF, we conducted constant potential electrolysis across various potentials and analyzed the resultant products and their yields (see Fig. 4.2). Ammonia production was quantified using the indophenol method. The findings indicate that Co_5COF emerged as the

most effective catalyst for nitrite reduction, achieving an ammonia production rate of 3.9 $mgh^{-1}mg^{-1}_{cat}$ and a Faradaic efficiency (FE) of 99.3%. In comparison, Fe_5COF also demonstrated significant catalytic activity, with a yield of 3.6 $mgh^{-1}mg^{-1}_{cat}$ and a Faradaic efficiency of 100%.

4.3.4 Discussion:

Various catalysts have been investigated for their potential in the electrocatalytic nitrite reduction reaction (ENO_2RR). For instance, Au-based nanoarrays, TiO_2 nanoarrays, and CPO-ILBMB/MWCNT-PEI bioconjugates have been explored for this purpose. These studies have demonstrated the capability of such catalysts to facilitate nitrite reduction effectively. Notably, our research reveals that the catalyst system we developed shows performance that is comparable to, and in some cases superior to, these existing systems. This underscores the effectiveness of our approach as a robust electrocatalyst for nitrite reduction. Additionally, the versatility of our catalyst allows for the modulation of reaction product selectivity by varying metal centers and structural components.

4.4. Conclusion

In conclusion, this chapter presents the synthesis and electrocatalytic evaluation of a novel heterogeneous covalent organic framework (COF) incorporating a quasi-D_3 symmetry molecule along with a C_3-symmetric monomer, resulting in a three-dimensional structure with an embedded pentanuclear complex for nitrate reduction. Additionally, variations of the COF were synthesized with cobalt and zinc metals, enabling a systematic study of their electrocatalytic performance for the nitrate reduction reaction (NO_3RR). Among the tested materials, the Co_5COF demonstrated the highest activity, outperforming the iron and zinc counterparts. Comprehensive characterizations, including HRTEM, PXRD, FTIR, and adsorption measurements, confirmed the structural integrity, crystallinity, and porosity of the synthesized COFs. Notably, Co_5COF exhibited exceptional catalytic performance in the electrocatalytic nitrite reduction reaction (ENO_2RR), achieving an impressive ammonia yield of 3.9 $mgh^{-1}mg^{-1}_{cat}$ and a Faradaic efficiency (FE) of 99.3%. This positions Co_5COF as the most effective catalyst for nitrite reduction among those investigated in this study. Additionally, Fe_5COF also demonstrated notable catalytic activity, achieving a yield of 3.6 $mgh^{-1}mg^{-1}_{cat}$ with a Faradaic efficiency of 100%, indicating high selectivity. Both catalysts highlight the potential of COFs in optimizing performance for nitrite reduction reactions.

4.5. References

1. Kim, S.; Dale, B. E., Effects of nitrogen fertilizer application on greenhouse gas emissions and economics of corn production. *Environmental science & technology* **2008,** *42* (16), 6028-6033.
2. Zamfirescu, C.; Dincer, I., Ammonia as a green fuel and hydrogen source for vehicular applications. *Fuel processing technology* **2009,** *90* (5), 729-737.
3. Salmon, N.; Bañares-Alcántara, R., Offshore green ammonia synthesis. *Nature Synthesis* **2023,** *2* (7), 604-611.
4. Pattabathula, V.; Richardson, J., Introduction to ammonia production. *Chem. Eng. Prog* **2016,** *112* (9), 69-75.
5. Travis, A. S.; Travis, A. S., The Direct Synthesis of Ammonia. *Nitrogen Capture: The Growth of an International Industry (1900–1940)* **2018**, 93-127.
6. Moghadam, M. R.; Bazmandegan-Shamili, A.; Bagheri, H., The current methods of ammonia synthesis by Haber-Bosch process. In *Progresses in Ammonia: Science, Technology and Membranes*, Elsevier: 2024; pp 1-32.
7. Jiao, F.; Xu, B., Electrochemical ammonia synthesis and ammonia fuel cells. *Adv. Mater.* **2019,** *31* (31), 1805173.
8. Soloveichik, G., Electrochemical synthesis of ammonia as a potential alternative to the Haber–Bosch process. *Nature Catalysis* **2019,** *2* (5), 377-380.
9. Qing, G.; Ghazfar, R.; Jackowski, S. T.; Habibzadeh, F.; Ashtiani, M. M.; Chen, C.-P.; Smith III, M. R.; Hamann, T. W., Recent advances and challenges of electrocatalytic N2 reduction to ammonia. *Chem. rev.* **2020,** *120* (12), 5437-5516.
10. Hu, J.; Zou, H.; Li, F.; Wei, S.; Cheng, M.; Dai, H.; Song, T.; Duan, L., Review on electrochemical reduction of nitrogen by graphdiyne-based catalysts: recent advances and outlook. *Energy & Fuels* **2023,** *37* (5), 3501-3522.
11. Zhang, X.; Wang, Y.; Wang, Y.; Guo, Y.; Xie, X.; Yu, Y.; Zhang, B., Recent advances in electrocatalytic nitrite reduction. *Chem. Commun.* **2022,** *58* (17), 2777-2787.
12. Zhu, T.; Chen, Q.; Liao, P.; Duan, W.; Liang, S.; Yan, Z.; Feng, C., Single-atom Cu catalysts for enhanced electrocatalytic nitrate reduction with significant alleviation of nitrite production. *Small* **2020,** *16* (49), 2004526.
13. Liang, J.; Li, Z.; Zhang, L.; He, X.; Luo, Y.; Zheng, D.; Wang, Y.; Li, T.; Yan, H.; Ying, B., Advances in ammonia electrosynthesis from ambient nitrate/nitrite reduction. *Chem* **2023,** *9* (7), 1768-1827.
14. Cote, A. P.; Benin, A. I.; Ockwig, N. W.; O'Keeffe, M.; Matzger, A. J.; Yaghi, O. M., Porous, crystalline, covalent organic frameworks. *science* **2005,** *310* (5751), 1166-1170.
15. Waller, P. J.; Lyle, S. J.; Osborn Popp, T. M.; Diercks, C. S.; Reimer, J. A.; Yaghi, O. M., Chemical conversion of linkages in covalent organic frameworks. *J. Am. Chem. Soc.* **2016,** *138* (48), 15519-15522.
16. Ding, S.-Y.; Wang, W., Covalent organic frameworks (COFs): from design to applications. *Chem. Soc. Rev.* **2013,** *42* (2), 548-568.
17. Li, Z.; Feng, X.; Zou, Y.; Zhang, Y.; Xia, H.; Liu, X.; Mu, Y., A 2D azine-linked covalent organic framework for gas storage applications. *Chem. Commun.* **2014,** *50* (89), 13825-13828.
18. Beuerle, F.; Gole, B., Covalent organic frameworks and cage compounds: design and applications of polymeric and discrete organic scaffolds. *Angew. Chem. Int. Ed.* **2018,** *57* (18), 4850-4878.
19. Keller, N.; Bein, T., Optoelectronic processes in covalent organic frameworks. *Chem. Soc. Rev.* **2021,** *50* (3), 1813-1845.
20. Yusran, Y.; Li, H.; Guan, X.; Fang, Q.; Qiu, S., Covalent organic frameworks for catalysis. *EnergyChem* **2020,** *2* (3), 100035.
21. Zhang, X.; Li, G.; Wu, D.; Zhang, B.; Hu, N.; Wang, H.; Liu, J.; Wu, Y., Recent advances in the construction of functionalized covalent organic frameworks and their applications to sensing. *Biosensors and Bioelectronics* **2019,** *145*, 111699.
22. Wang, D.-G.; Qiu, T.; Guo, W.; Liang, Z.; Tabassum, H.; Xia, D.; Zou, R., Covalent organic framework-based materials for energy applications. *Energy & Environmental Science* **2021,** *14* (2), 688-728.
23. Zhao, X.; Pachfule, P.; Thomas, A., Covalent organic frameworks (COFs) for electrochemical applications. *Chem. Soc. Rev.* **2021,** *50* (12), 6871-6913.

24. Lin, C. Y.; Zhang, D.; Zhao, Z.; Xia, Z., Covalent organic framework electrocatalysts for clean energy conversion. *Adv. Mater.* **2018,** *30* (5), 1703646.
25. Liu, Q.; Wen, G.; Zhao, D.; Xie, L.; Sun, S.; Zhang, L.; Luo, Y.; Alshehri, A. A.; Hamdy, M. S.; Kong, Q., Nitrite reduction over Ag nanoarray electrocatalyst for ammonia synthesis. *Journal of Colloid and Interface Science* **2022,** *623*, 513-519.
26. Zhu, X.; Fan, X.; Lin, H.; Li, S.; Zhai, Q.; Jiang, Y.; Chen, Y., Highly efficient electroenzymatic cascade reduction reaction for the conversion of nitrite to ammonia. *Adv. Energy Mater.* **2023,** *13* (20), 2300669.
27. Li, S.; Liang, J.; Wei, P.; Liu, Q.; Xie, L.; Luo, Y.; Sun, X., ITO@ TiO2 nanoarray: An efficient and robust nitrite reduction reaction electrocatalyst toward NH_3 production under ambient conditions. *EScience* **2022,** *2* (4), 382-388.

4.6. Appendix of Chapter 4

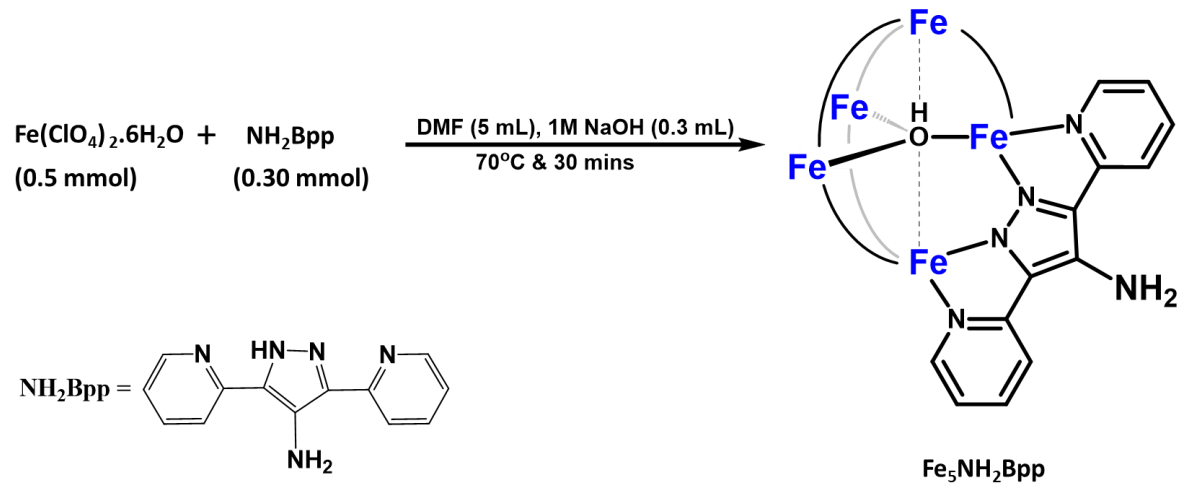

Scheme A4.1. Schematic representation of Fe_5NH_2Bpp synthesis.

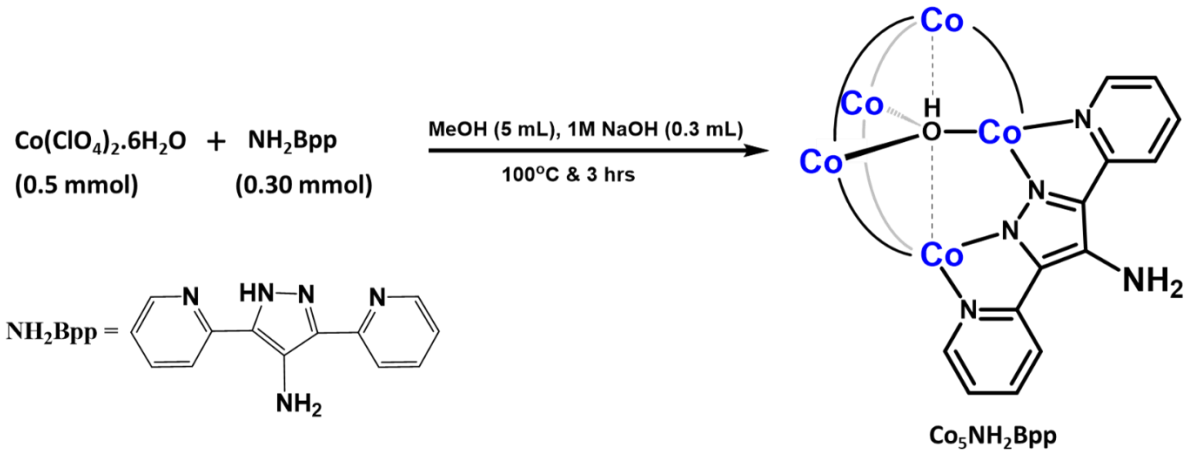

Scheme A4.2. Schematic representation of Co_5NH_2Bpp synthesis.

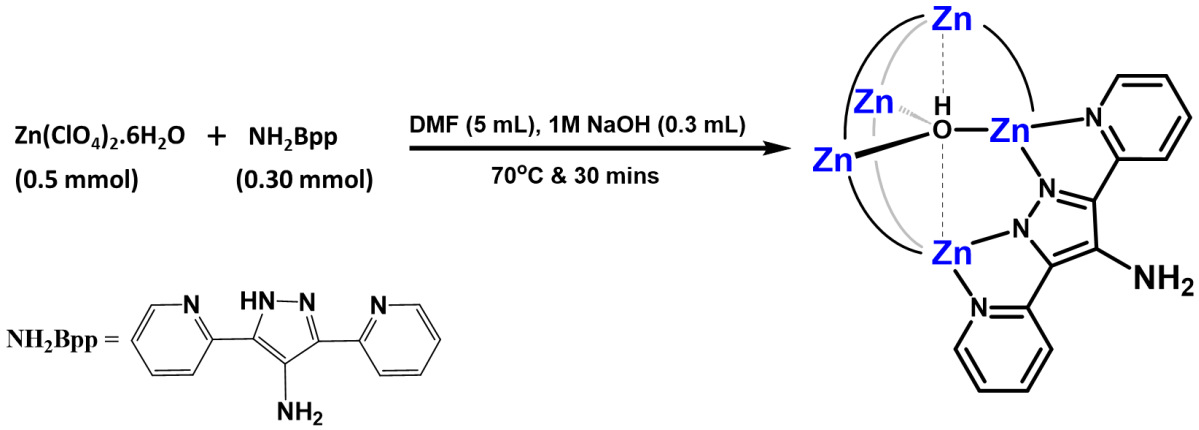

Scheme A4.3. Schematic representation of Zn_5NH_2Bpp synthesis.

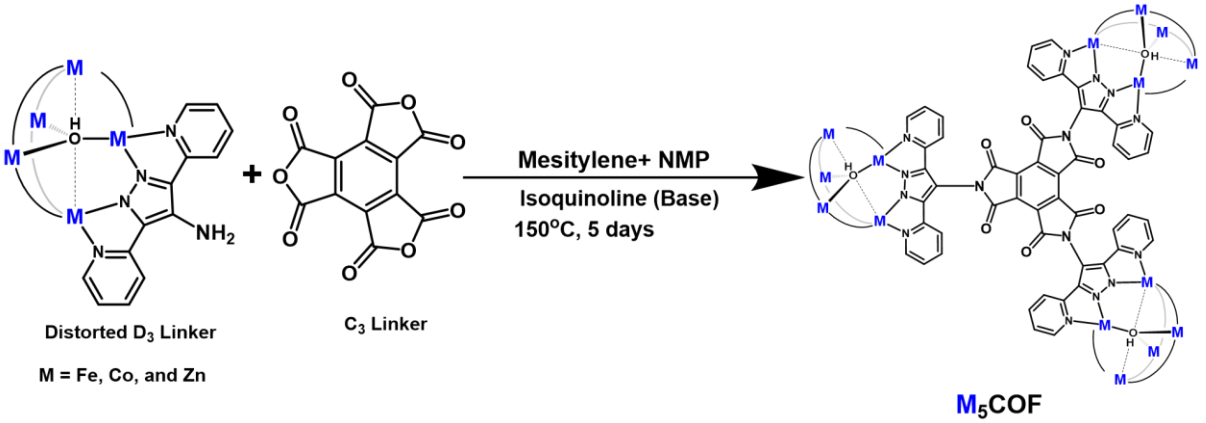

Scheme A4.4. Schematic representation of M_5COF synthesis.

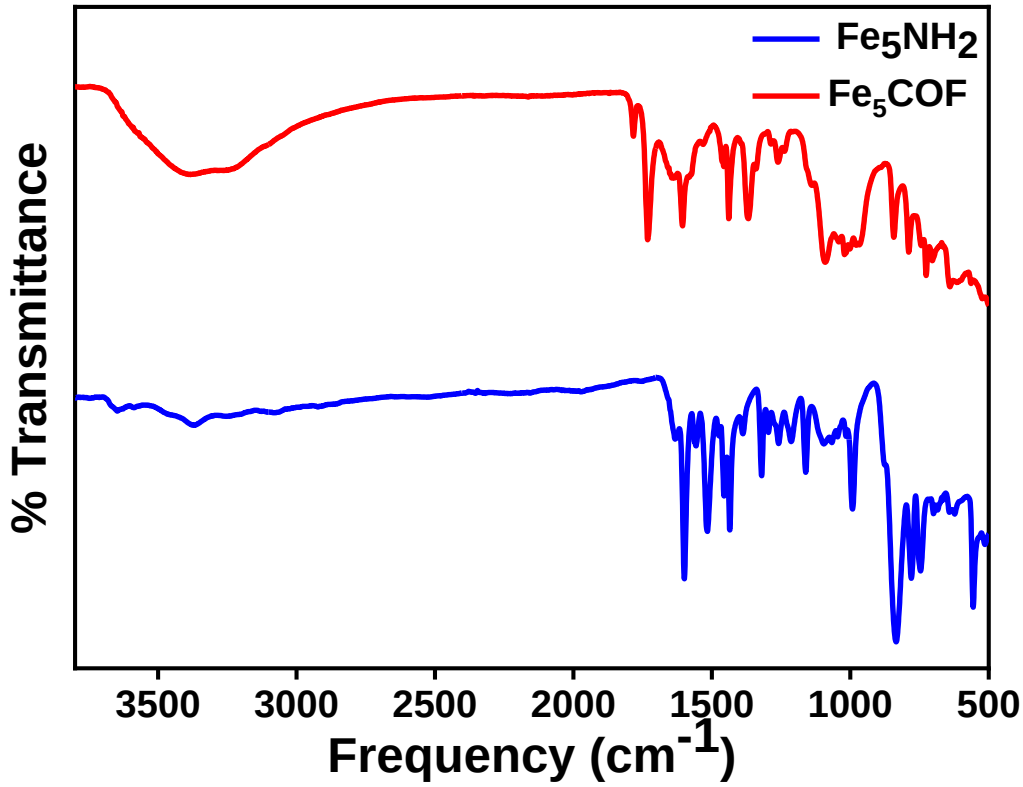

Figure A4.1 FTIR spectra of Fe_5Bpp and Fe_5COF.

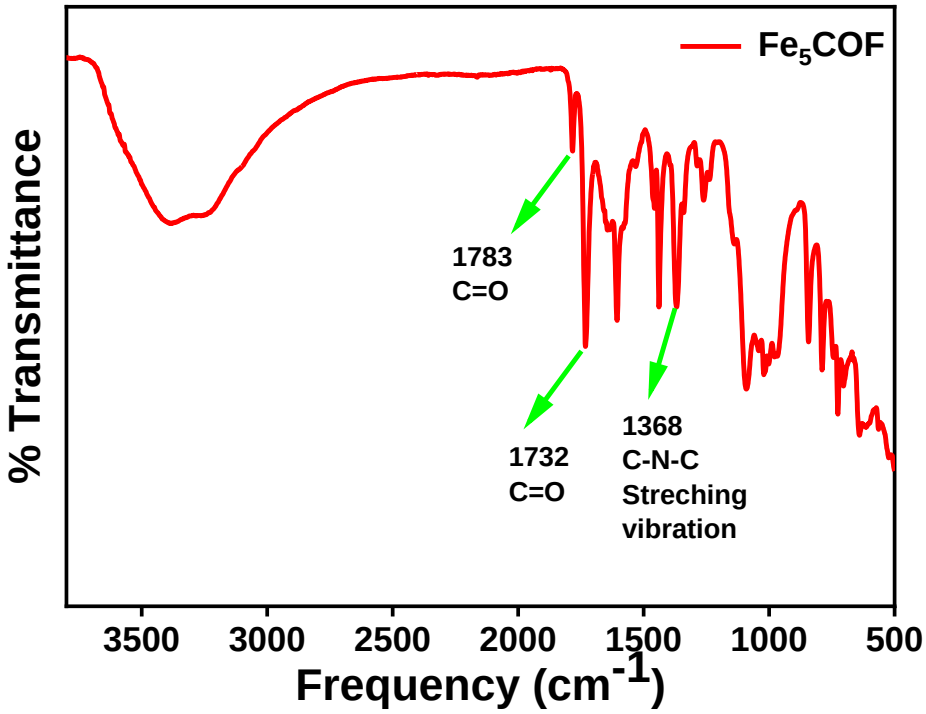

Figure A4.2 Detailed FTIR spectra of Fe_5COF.

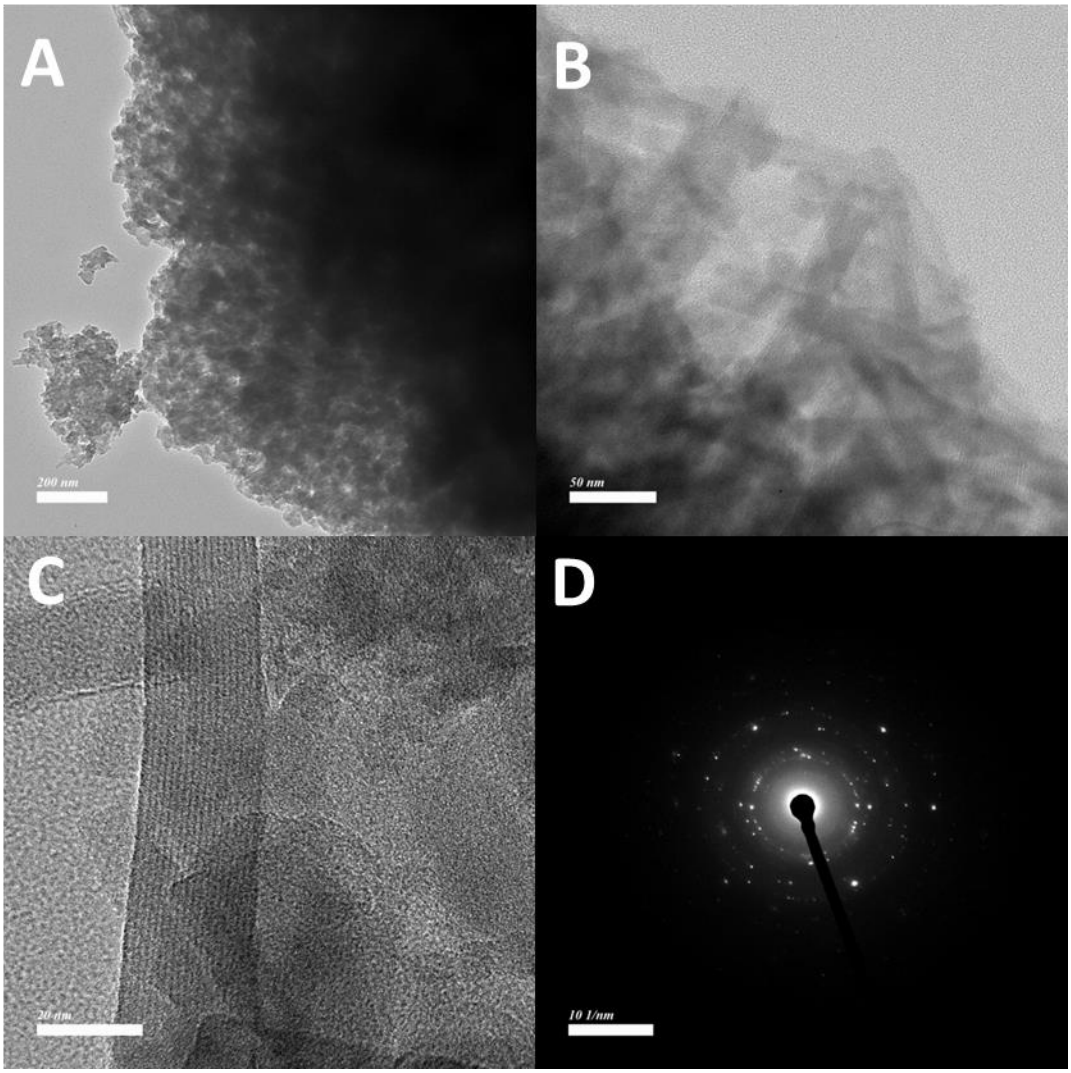

Figure A4.3 HRTEM images having lattice fringes with SAED pattern of Fe_5COF that shows that these COFs are highly crystalline.

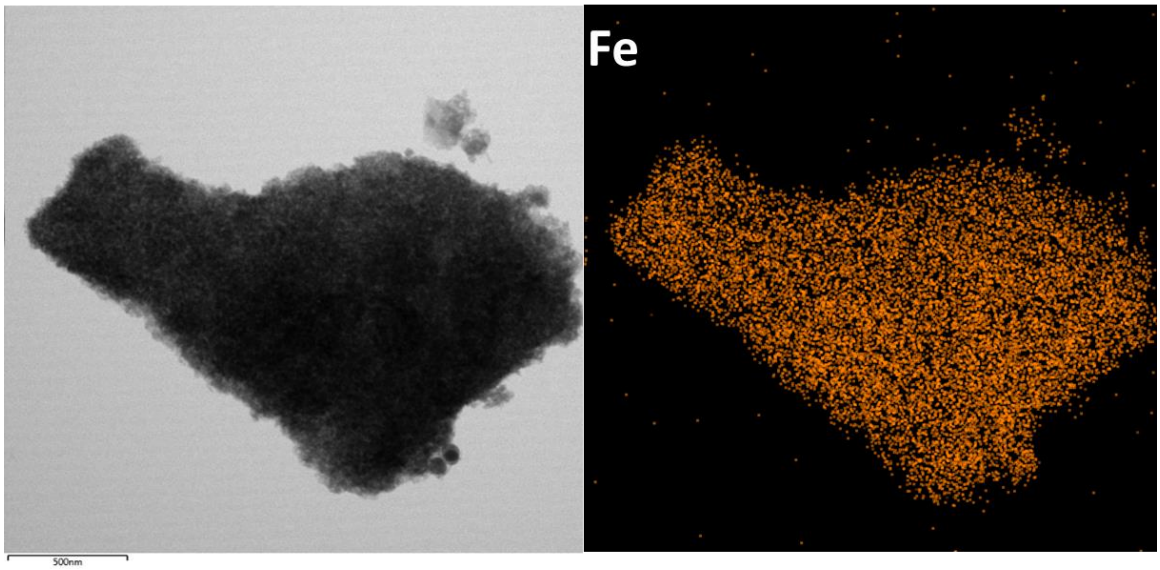

Figure A4.4 The elemental mapping reveals the homogeneous distribution of Fe in Fe_5COF.

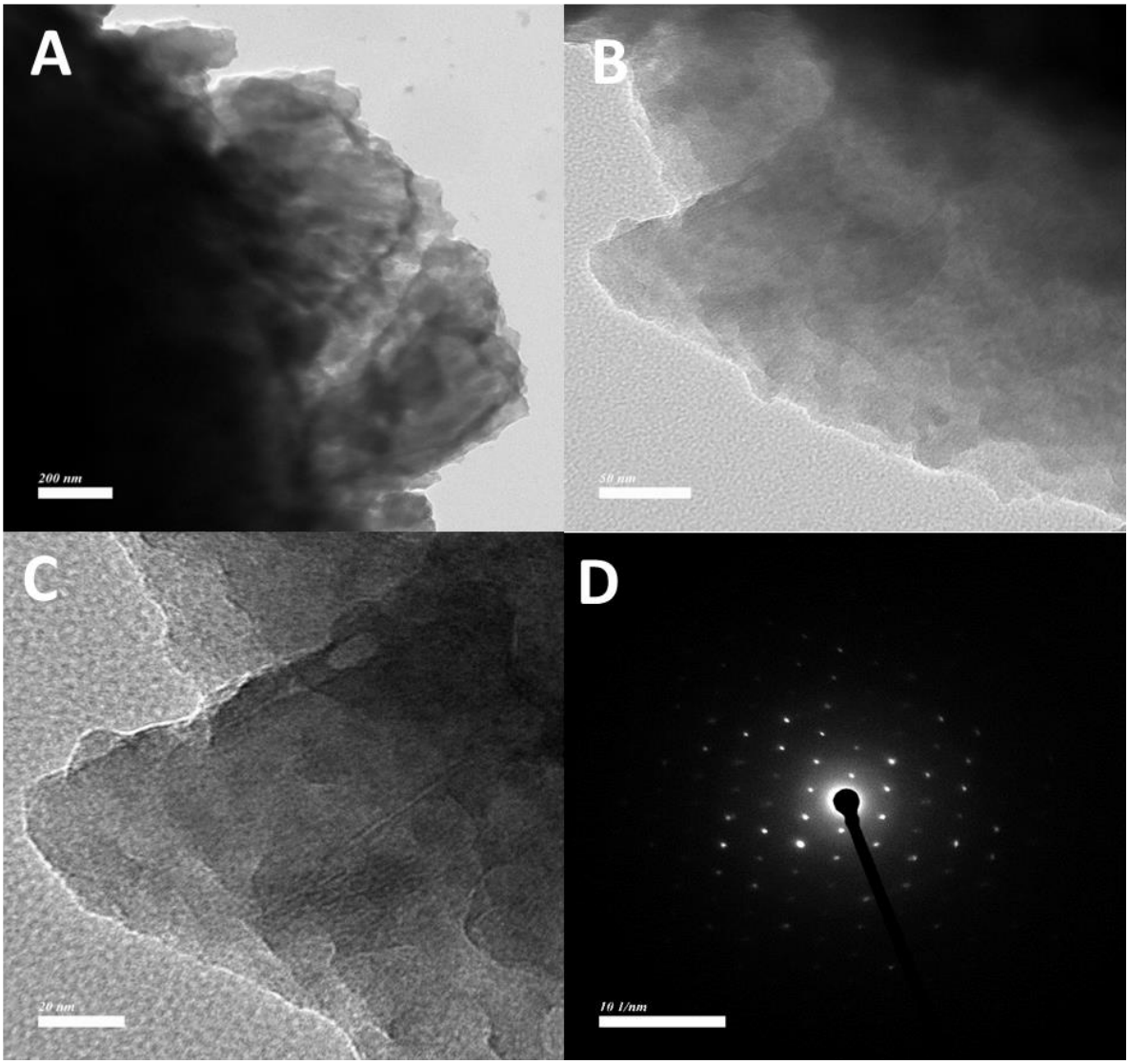

Figure A4.5 HRTEM images having lattice fringes with SAED pattern of Co_5COF that shows that these COFs are highly crystalline.

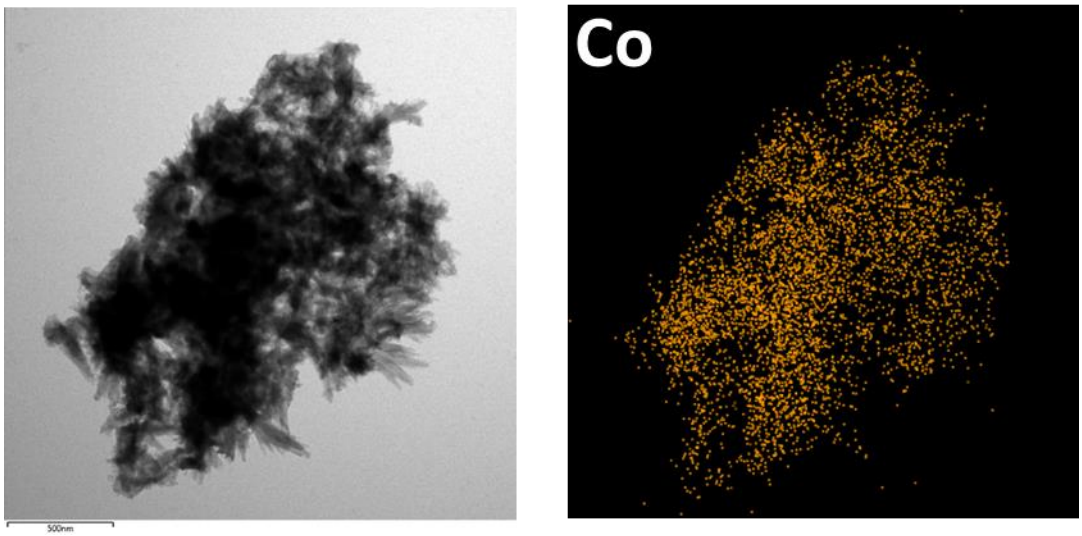

Figure A4.6 The elemental mapping reveals the homogeneous distribution of Co in Co_5COF.

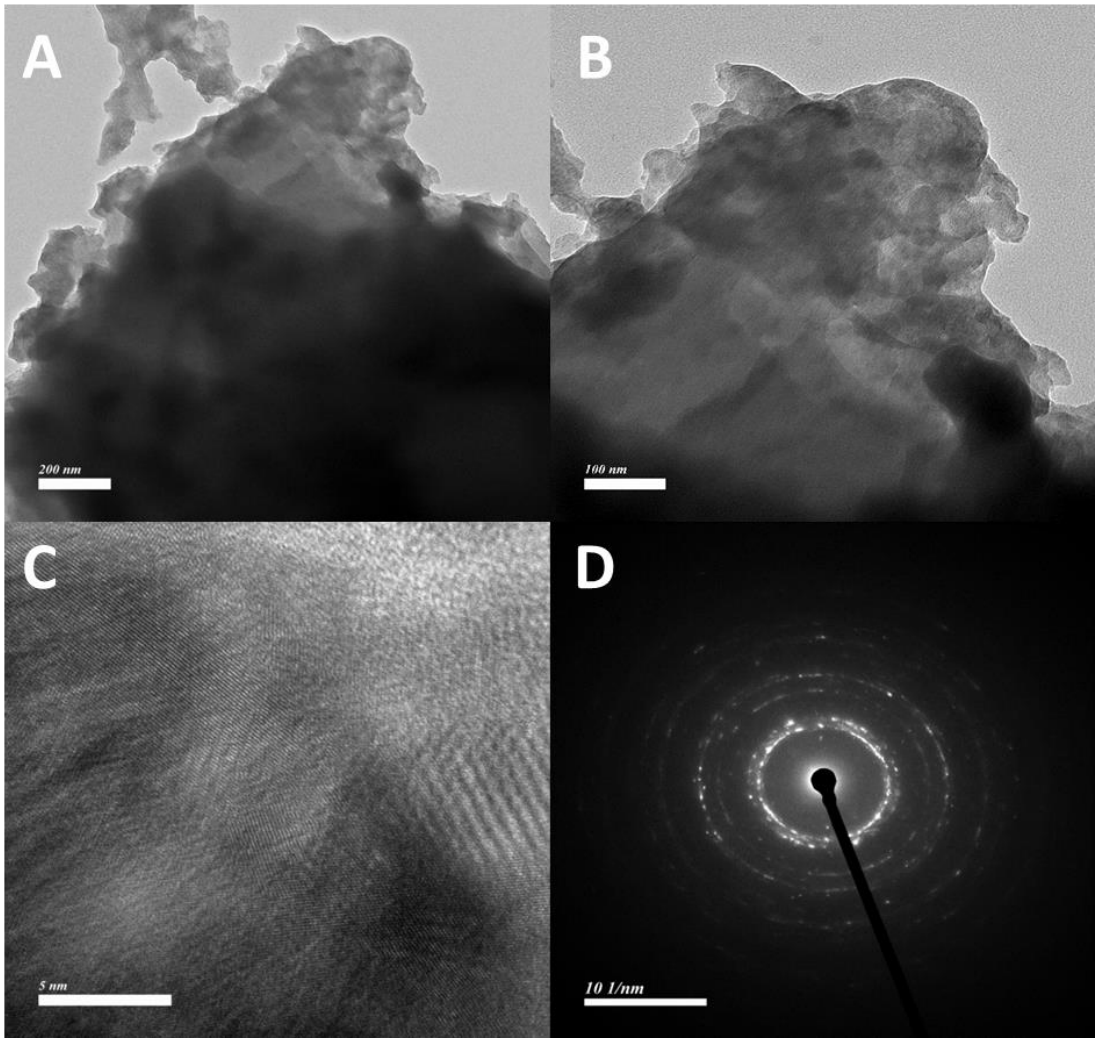

Figure A4.7 HRTEM images having lattice fringes with SAED pattern of Zn_5COF that shows that these COFs are highly crystalline.

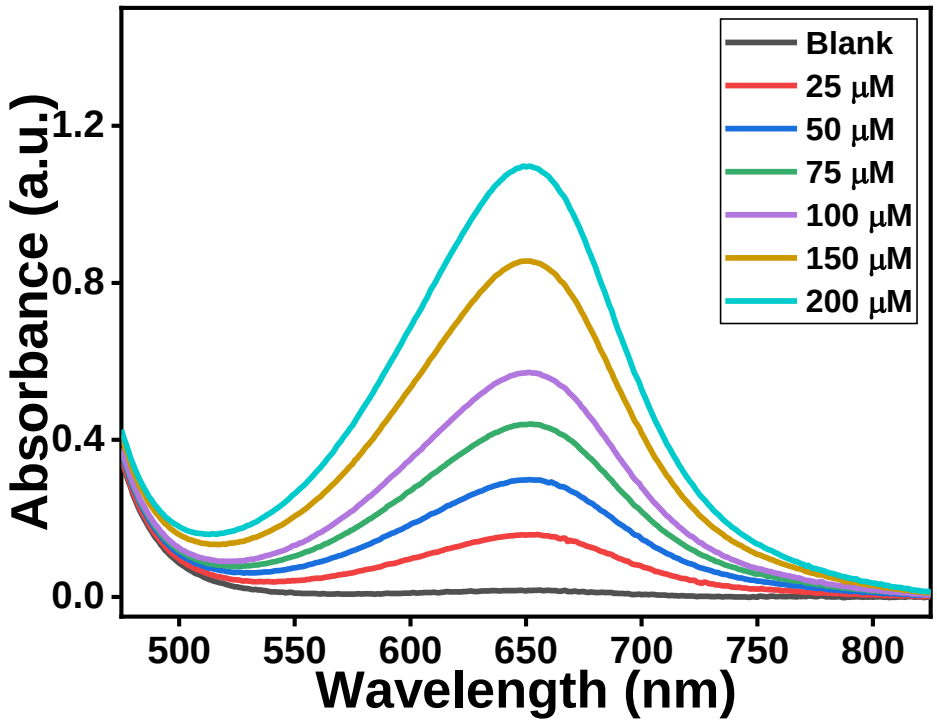

Figure A4.10 Linear fit of known standard NH_4Cl solution.

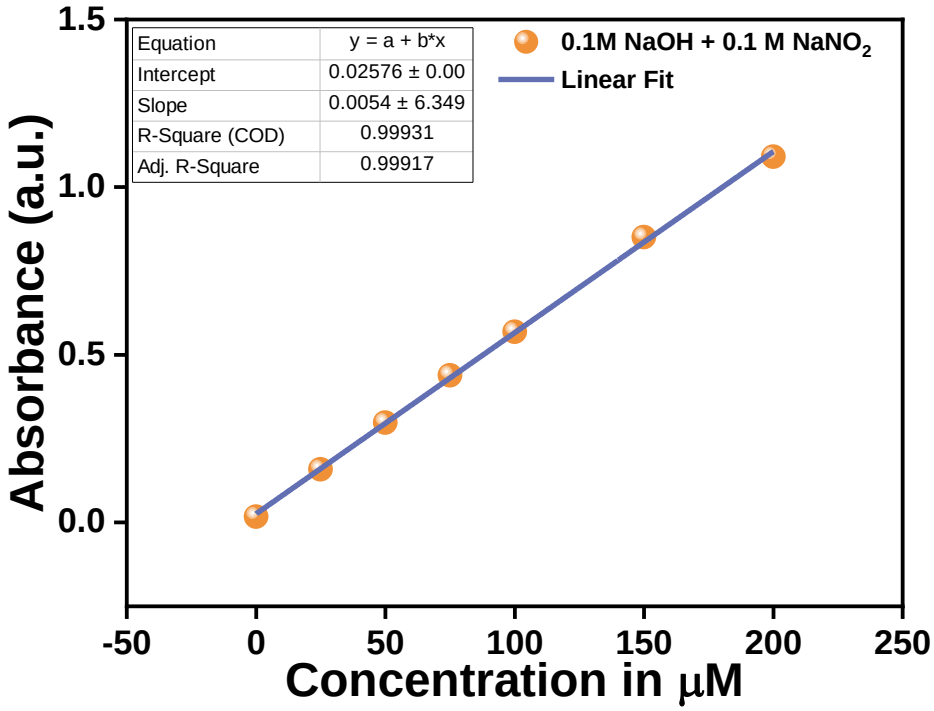

Figure A4.11 UV-vis absorption spectra of indophenol blue solutions of standard NH_4Cl solution.